DEAD-box ATPase Dbp2 participates in a specific mRNP assembly checkpoint during RNA biogenesis in *S. pombe*

Dissertation

zur Erlangung des Doktorgrades der Naturwissenschaften

(Dr. rer. nat.)

am Fachbereich 08 für Biologie und Chemie

der Justus-Liebig-Universität Gießen

Vorgelegt von

Ebru Aydin

Gießen, 2024

Publications

During my PhD studies, I contributed to the following listed publications:

A major part of the work in this thesis is published in:

Published, Nat Commun 15, (2024). doi: 10.1038/s41467-024-51035-z

DEAD-box ATPase Dbp2 is the key enzyme in an mRNP assembly checkpoint at the 3'-end of genes and involved in the recycling of cleavage factors

Ebru Aydin[1], Jacqueline Böhme[1], Birte Keil[1], Silke Schreiner[1], Bojan Žunar[2], Timo Glatter[3], and Cornelia Kilchert[1]

Abstract

mRNA biogenesis in the eukaryotic nucleus is a highly complex process. The numerous RNA processing steps are tightly coordinated to ensure that only fully processed transcripts are released from chromatin for export from the nucleus. Here, we present the hypothesis that fission yeast Dbp2, a ribonucleoprotein complex (RNP) remodelling ATPase of the DEAD-box family, is the key enzyme in an RNP assembly checkpoint at the 3'-end of genes. We show that Dbp2 interacts with the cleavage and polyadenylation complex (CPAC) and localises to cleavage bodies, which are enriched for 3'-end processing factors and proteins involved in nuclear RNA surveillance. Upon loss of Dbp2, 3'-processed, polyadenylated RNAs accumulate on chromatin and in cleavage bodies, and CPAC components are depleted from the soluble pool. Under these conditions, cells display an increased likelihood to skip polyadenylation sites and a delayed transcription termination, suggesting that levels of free CPAC components are insufficient to maintain normal levels of 3'-end processing. Our data support a model in which Dbp2 is the active component of an mRNP remodelling checkpoint that licenses RNA export and is coupled to CPAC release.

Published, Nat Commun 16, 10 (2025). doi: 10.1038/s41467-024-55063-7

DSIF factor Spt5 coordinates transcription, maturation and exoribonucleolysis of RNA polymerase II transcripts

Krzysztof Kuś[1], Loic Carrique[2], Tea Kecman[1], Marjorie Fournier[1], Sarah Sayed Hassanein[1,3], **Ebru Aydin[4]**, Cornelia Kilchert[4], Jonathan M. Grimes[2] and Lidia Vasiljeva[1]

Summary

Precursor messenger RNA (pre-mRNA) is processed into its functional form during RNA polymerase II (Pol II) transcription. Although functional coupling between transcription and pre-mRNA processing is established, the underlying mechanisms are not fully understood. We show that the key transcription termination factor, RNA exonuclease Xrn2 engages with Pol II forming a stable complex. Xrn2 activity is stimulated by Spt5 to ensure efficient degradation of nascent RNA leading to Pol II dislodgement from DNA. Our results support a model where Xrn2 first forms a stable complex with the elongating Pol II to achieve its full activity in degrading nascent RNA revising the current 'torpedo' model of termination, which posits that RNA degradation precedes Xrn2 engagement with Pol II. Spt5 is also a key factor that attenuates the expression of non-coding transcripts, coordinates pre-mRNA splicing and 3'-end processing. Our findings indicate that engagement with the transcribing Pol II is an essential regulatory step modulating the activity of RNA enzymes such as Xrn2, thus advancing our understanding of how RNA maturation is controlled during transcription.

Published, Genome Res. 2020 Jul;30(7):1012-1026. doi: 10.1101/gr.257006.119

System-wide analyses of the fission yeast poly(A)$^+$ RNA interactome reveal insights into organization and function of RNA-protein complexes

Cornelia Kilchert[1], Tea Kecman[2], Emily Priest[2], Svenja Hester[2], **Ebru Aydin[1]**, Krzysztof Kus[2], Oliver Rossbach[1], Alfredo Castello[2], Shabaz Mohammed[2,3], Lidia Vasiljeva[2]

Abstract

Large RNA-binding complexes play a central role in gene expression and orchestrate production, function, and turnover of mRNAs. The accuracy and dynamics of RNA-protein interactions within these molecular machines are essential for their function and are mediated by RNA-binding proteins (RBPs). Here, we show that fission yeast whole-cell poly(A)$^+$ RNA-protein crosslinking data provide information on the organization of RNA-protein complexes. To evaluate the relative enrichment of cellular RBPs on poly(A)$^+$ RNA, we combine poly(A)$^+$ RNA interactome capture with a whole-cell extract normalization procedure. This approach yields estimates of in vivo RNA-binding activities that identify subunits within multiprotein complexes that directly contact RNA. As validation, we trace RNA interactions of different functional modules of the 3'-end processing machinery and reveal additional contacts. Extending our analysis to different mutants of the RNA exosome complex, we explore how substrate channeling through the complex is affected by mutation. Our data highlight the central role of the RNA helicase Mtl1 in regulation of the complex and provide insights into how different components contribute to engagement of the complex with substrate RNA. In addition, we characterize RNA-binding activities of novel RBPs that have been recurrently detected in the RNA interactomes of multiple species. We find that many of these, including cyclophilins and thioredoxins, are substoichiometric RNA interactors *in vivo*. Because RBPomes show very good overall agreement between species, we propose that the RNA-binding characteristics we observe in fission yeast are likely to apply to related proteins in higher eukaryotes as well.

Oral and poster presentations

Ebru Aydin, “DEAD-box ATPase Dbp2 participates in a specific mRNP assembly checkpoint during RNA biogenesis in *S. pombe*”, (Poster Presentation), 2024, the 29th Annual Meeting of the RNA Society, Edinburgh/UK

Ebru Aydin, “DEAD-box ATPase Dbp2 mediates mRNA release after 3’-end formation”, (Oral Presentation), 2024, pombeTalks, Online Seminar Series

Ebru Aydin, “DEAD-box ATPase Dbp2 mediates mRNA release after 3’-end formation”, (Oral Presentation), 2024, Joint symposium with ITN Cell2Cell and RTG / GRK 2355/2, “Dynamics in chromatin organization and RNA regulation: adaptation, infection— and beyond”, Gießen/Germany

Ebru Aydin, “DEAD-box ATPase Dbp2 acts late during transcription and is required for efficient 3’-end formation and RNA release from cleavage bodies”, (Oral Presentation & Poster Presentation), 2023, The 12th Meeting of the GBM Study Section RNA-Biochemistry & Workshop “Advanced RNA Sequencing”, Bonn/Germany

Ebru Aydin, “Release of 3’-end factors that license mRNAs for export requires the DEAD-box ATPase Dbp2”, (Oral Presentation), 2023, Joint Retreat -RTG 2344 & RTG 2355, Bad Dürkheim/Germany

Ebru Aydin, “The essential DEAD-box ATPase Dbp2 functions in nuclear RNA surveillance in *Schizosaccharomyces pombe*”, (Poster Presentation), 2022, The Yeast Transcription Meeting, Gene transcription in yeast: From single molecules to separated phases, CNRS Workshop Conference, Saint Feliu/Spain

Acknowledgments

I would like to express my heartfelt gratitude to my supervisor, Dr. Cornelia Kilchert, for granting me the opportunity to pursue my PhD in her group at Justus-Liebig-Universität Gießen. Your unwavering patience, support, encouragement, and invaluable advice have been instrumental in shaping my academic journey. I deeply appreciate the insights gained through our discussions and the guidance you provided, which have had a profound impact on both my professional and personal growth. I feel truly fortunate to have worked under your mentorship and am especially grateful for the opportunities to contribute to collaborative projects under your leadership. Thank you for your trust and support throughout this journey.

I would like to express my as sincere gratitude to Prof. Dr. Katja Sträßer, for her unwavering kindness and support during my time in the Department of Biochemistry. Your generosity in allowing us to establish our own research group with Dr. Cornelia Kilchert has been instrumental in fostering a supportive and collaborative environment. Moreover, your thoughtful gestures, such as occasionally gifting me plants, have added a personal touch to our professional relationship. The Weeping Fig (*Ficus benjamina*) that you once gave me holds a special place in my heart, and as a lifelong favourite to keep.

I would like to express my appreciation to the PhD examination committee, Dr. Cornelia Kilchert, Apl. Prof. Dr. Elena Evguenieva-Hackenberg, Prof. Dr. Sigurd Braun, and Dr. Oliver Rossbach for taking the time to read, comment and evaluate my work. I also like to express my gratefulness to our collaborators in our publication, for mass spectrometry analysis to Dr. Timo Glatter and AlphaFold predictions to Dr. Bojan Žunar. To all past and present colleagues in the department, I truly value the companionship and friendship you've shared with me over the years. I am also grateful to everyone. I had the privilege of working with, including Prof. Dr. Albrecht Bindereif,

Dr. Wolfgang Wende, and Apl. Prof. Dr. Peter Friedhoff. A special thanks goes to our treasure, Silke Schreiner, the ever-helpful and caring Karina Urbach, and our invaluable RTG coordinator, Vera Bettenworth.

This journey would not have been possible without the financial support provided Emmy Noether Programme and research training group of the RTG/GRK 2355, both funded by the Deutsche Forschungsgemeinschaft (DFG). Being part of RTG/GRK2355 research training group provided me with a very inspiring environment, with many opportunities to learn about the cutting-edge science and research from our joint meetings with other labs as well as through many talks and seminars given by visiting speakers. I was able to gain invaluable insights into science and develop my own ideas, which will help me throughout my career as a scientist. I also like to thank my institution Justus Liebig Universität of Gießen for providing me solid grounds to achieve all these.

Last but not least I would like to thank my family for their full support throughout my life. I would also like to give a final credit to my companions, Sussie, Schatz, Chérie, Aşk, and Santa.

Eidesstattliche Erklärung

Ich, Ebru Aydin, erkläre, dass die in dieser Arbeit vorgestellte Arbeit meine eigene ist. Diese Arbeit wurde im Labor und unter der Betreuung von Dr. Cornelia Kilchert im Fachbereich Biologie und Chemie der Justus-Liebig-Universität am Institut für Biochemie in Gießen durchgeführt. Soweit Informationen aus anderen Quellen übernommen wurden, bestätige ich, dass dies im entsprechenden Text angegeben ist. Bei den von mir durchgeführten und in der Dissertation erwähnten Untersuchungen habe ich die Grundsätze guter wissenschaftlicher Praxis, wie sie in der „Satzung der Justus-Liebig-Universität Gießen zur Sicherung guter wissenschaftlicher Praxis“niedergelegt sind, eingehalten.

Declaration

I, Ebru Aydin, declare that the work presented in this thesis is my own. This thesis was carried out in the laboratory and under the supervision of Dr. Cornelia Kilchert in the Department of Biology and Chemistry of the Justus Liebig University at the Institute of Biochemistry in Gießen. Where information has been derived from other sources, I confirm that this is indicated in the corresponding text. I have abided by the principles of good scientific conduct laid down in the charter of the Justus Liebig University Gießen “Satzung der Justus-Liebig-Universität Gießen zur Sicherung guter wissenschaftlicher Praxis” in carrying out the investigations described in the dissertation”.

Gießen, den/on: ……..... Unterschrift/Signature: …….....

(Vorname/Firstname, Nachname/Lastname)

Submitted on: 20/12/2024

1st Examiner: Dr. Cornelia Kilchert
Department of Biology and Chemistry
Institute of Biochemistry
Justus Liebig University Gießen

2nd Examiner: Apl. Prof. Dr. Elena Evguenieva-Hackenberg
Department of Biology and Chemistry
Institute of Microbiology and Molecular Biology
Justus Liebig University Gießen

List of Figures

List of Tables

Zusammenfassung

Die größte Gruppe von RNA-Helikasen sind die DEAD-Box-Helikasen der Superfamilie 2, welche nicht-prozessive Enzyme sind, die in einer Einzelumdrehungsreaktion an kurzen RNA-Duplexen wirken, um RNA zu entwindern (Helikase-Aktivität) oder Proteine zu verdrängen (RNPase-Aktivität). Diese Aktivitäten ermöglichen es ihnen, Messenger-Ribonukleoproteine (mRNPs) umzugestalten. Die Produktion funktioneller mRNAs ist auf die ko-transkriptionelle mRNP-Assemblierung angewiesen, die hochdynamische und regulierte Prozessereignisse orchestriert. Das Umgestalten von mRNPs, das durch DEAD-Box-ATPasen erleichtert wird, soll die RNA-Reifung fördern, indem es Übergänge zwischen verschiedenen mRNP-Zuständen erleichtert. Ein wesentlicher Schritt in der eukaryotischen mRNA-Biogenese ist die Bildung des 3'-Endes der mRNA durch endonukleolytischen Schnitt gefolgt von Polyadenylierung. Die Rekrutierung des Spalt- und Polyadenylierungs-Komplexes (CPAC) und die anschließende Bildung des 3'-Endes wurden umfassend untersucht. Im Gegensatz dazu ist das Abbau dieser komplexen Proteinassemblierungen, nachdem sie ihre Funktion abgeschlossen haben, weniger gut verstanden. Die hier vorliegende Arbeit zeigt, dass das Spalt-Helikase-Protein Dbp2 in die Nähe des 3'-Endes von Genen rekrutiert wird und sowohl mit CPAC-Komponenten als auch mit Exportfaktoren interagiert. Es lokalisiert sich zu Spaltkörpern, subnuklearen Strukturen im Zellkern, in denen auch CPAC-Faktoren konzentriert sind. Der Verlust von Dbp2 führt zur Akkumulation von 3'-verarbeiteten, polyadenylierten RNAs auf Chromatin und in Spaltkörpern, was mit der Depletion von CPAC-Faktoren aus dem löslichen Pool einhergeht. Diese Beobachtungen deuten darauf hin, dass in Dbp2-depletierten Zellen eine eingeschränkte Verfügbarkeit von CPAC-Faktoren eine optimale 3'-End-Verarbeitung verhindert, was zu erhöhten Mengen an 3'-verlängerten Transkripten und

einer Verzögerung der Transkriptionsbeendigung führt. Der Dbp2-abhängige Umgestaltungs-Checkpoint formt die mRNP-Assemblierung an der Schnittstelle zwischen RNA-3'-End-Bildung und RNA-Export und unterstreicht, dass die Freisetzung von Transkripten nach der 3'-End-Bildung wahrscheinlich ein ATP-abhängiger Prozess ist.

Abstract

The largest group of RNA helicases are the DEAD-box helicases of superfamily 2, which are non-processive enzymes that act in a single turnover reaction on short RNA duplexes to trigger RNA unwinding (helicase activity) or protein displacement (RNPase activity). These activities enable them to remodel messenger ribonucleoproteins (mRNPs). The production of functional mRNAs relies on co-transcriptional mRNP assembly that orchestrates highly dynamic and regulated processing events. Remodelling of mRNPs, facilitated by DEAD-box ATPases, is thought to promote RNA maturation by facilitating transitions between different mRNP states.

An essential step in eukaryotic mRNA biogenesis is the formation of the 3'-end of the mRNA by endonucleolytic cleavage followed by polyadenylation. The recruitment of cleavage and polyadenylation complex (CPAC) and the subsequent formation of the 3'-end have been extensively investigated. On the contrary, the dismantling of these complex protein assemblies once they have completed their functions is less thoroughly understood. The work here shows that fission yeast Dbp2 is recruited to the 3'-end of genes and interacts with both CPAC components and export factors. It localises to cleavage bodies, subnuclear structures in the nucleus where CPAC factors are also concentrated. Loss of Dbp2 results in the accumulation of 3'-processed, polyadenylated RNAs on chromatin and in cleavage bodies, coinciding with the depletion of CPAC factors from the soluble pool. These observations suggest that in Dbp2-depleted cells, restricted availability of CPAC factors prevents optimal 3'-end processing, resulting in elevated levels of 3′-extended transcripts, along with a delay in transcription termination. Dbp2-dependent remodelling checkpoint shape mRNP assembly at the intersection between RNA 3'-end formation and RNA export, highlighting that transcript release after 3'-end formation as likely an ATP-dependent process.

Abbreviations

aa	amino acid
as RNAs	antisense RNAs
bp	base pair
CBC	cap-binding complex
CBCA	Ars2-associated cap-binding complex
CBCN	CBC-NEXT
CF	cleavage factor
CFIA	mRNA cleavage stimulating factor complex 1A
CPAC	cleavage and polyadenylation complex
CPF	cleavage and polyadenylation factor
CPSF	cleavage and polyadenylation specificity factor
CTD	carboxyl-terminal domain of Rpb1 in RNAPII
CUTs	cryptic unstable transcripts
DMSO	dimethyl sulfoxide
DNA	deoxyribonucleic acid
dNTP	deoxyribonucleoside triphosphate
DSE	downstream sequence elements
DSR	determinant of selective removal
dsRNA	double-stranded RNA
DTT	dithiothreitol
E. coli	*Escherichia coli*
EDTA	ethylenediaminetetraacetic acid
EMMG	Edinburgh complete minimal media Edinburgh + glutamate
EMMG -URA	Edinburgh minimal medium + glutamate – Uracil amino acid
eRNA	enhancer RNA
GTF	general transcription factors
H. s./ H. sapiens	*Homo sapiens* (human)
HA	hemagglutinin
HEPES	N-2-Hydroxyethylpiperazine-N'-2-Ethanesulfonic Acid.
h/hr(s)	hour(s)
HRP	horse radish peroxidase
HTP	His_6-TEV-ProteinA
IP	immunoprecipitation
IDR	intrinsically disordered region
kb	kilobase
kDa	kilodalton
LB	Lysogeny broth
LLPS	liquid-liquid phase separation
lncRNA	long noncoding RNA
m7G	5’-methylguanosine
µg	microgram
µL	microliter

µM	micromolar
mg	milligram
min	minute
miRNA	microRNA
ml	millilitre
mM	millimolar
MQ H_2O	Milli-Q water
mRNA	messenger RNA
mRNP	messenger ribonucleoprotein
MTREC	Mtl1-Red1core
ncRNA	noncoding RNA
NDR	nucleosome depleted regions
NEXT	nuclear exosome targeting
ng	nanogram
Ni-NTA	nickel-nitrilotriacetic acid
NNS	Nrd1-Nab3-Sen1
NMD	nonsense-mediated mRNA decay
nt(s)	nucleotide(s)
OD_{600}	optical density measured at 600 nm
ORF	open reading frame
PAGE	polyacrylamide gel electrophoresis
PAS	poly(A) signal sequence
PAXT	poly(A)-tail exosome targeting connection
PBS	phosphate buffered saline
PCI	phenol:chloroform:isomyl alcohol
PCR	polymerase chain reaction
PEG	polyethylene glycol
PIC	pre-initiation complex
PMSF	phenylmethylsulfonyl fluoride
pre-mRNA	precursor mRNA
PROMPTs	PROMoter uPstream transcripts
PTMs	post-translational modifications
ptRNAs	prematurely terminated RNAs
PVDF	polyvinyllidene fluoride
qPCR	quantitative-PCR
RITS	RNA-induced transcriptional silencing complex
RNA	ribonucleic acid
RNAPII	RNA polymerase II
RNA-seq	RNA sequencing
RNP	ribonucleoprotein complex
rpm	revolutions per minute
RRM	RNA recognition motif
rRNA	ribosomal RNA
RT	room temperature

s/sec(s)	second(s)
S. c. / S. cerevisiae	*Saccharomyces cerevisiae* (budding yeast)
S. p. / S. pombe	*Schizosaccharomyces pombe* (fission yeast)
SDS-PAGE	sodium dodecyl sulfate–polyacrylamide gel electrophoresis
Seq	sequencing
Ser2	Serine 2 of the CTD heptapeptide YSPTSPS
Ser5	Serine 5 of the CTD heptapeptide YSPTSPS
Ser2P	phosphorylated Serine 2 of the CTD heptapeptide YSPTSPS
Ser5P	phosphorylated Serine 5 of the CTD heptapeptide YSPTSPS
SNHG	snoRNA host gene
snoRNA	small nucleolar RNA
snRNA	small nuclear RNA
snRNP	small nuclear ribonucleoprotein
sRNAs	small RNAs
ssRNA	single-stranded RNA
TBE	Tris-buffered EDTA
TBST	Tris-buffered saline + Tween
TE	Tris EDTA
TEC	transcription elongation complex
TF	transcription factor
TRAMP	Trf4/5-Air1/2-Mtr4 polyadenylation
Tris	Tris(hydroxymethyl)aminomethane
tRNA	transfer RNA
TSS	transcription start site
TTS	transcription termination site
uaRNAs	upstream antisense RNAs
Ubi	ubiquitin
UTR	untranslated region
WB	Western blot
WT	wild type
YES	yeast extract broth + supplements

Table of Contents

Chapter1 Introduction

1.1 RNA helicases – general biochemical features and functions

RNA helicases are ubiquitously expressed in all three domains of life and are frequently present in viral genomes. RNA helicases are central regulators of RNA metabolism, participating in nearly all aspects of RNA processing including ribosome biogenesis, transcription, splicing, RNA export, and translation (Fairman-Williams et al., 2010; Jankowsky & Fairman, 2007). They form a large group among RNA-binding proteins, having more than 70 members in humans and more than 40 in *Saccharomyces cerevisiae.* Most RNA helicases show high conservation from yeast to humans and many are essential for cell function (Bohnsack et al., 2023). RNA helicases require nucleoside triphosphates to bind or remodel nucleic acids, nucleic acid–protein complexes, or both (Fairman-Williams et al., 2010; Pyle, 2008). While some RNA helicases have the ability to processively translocate through RNA substrates and unwind double-stranded regions, and subsequently displace proteins, others do not exhibit translocation along their substrate but instead unwind local secondary structures (Bourgeois et al., 2016; Jarmoskaite & Russell, 2014).

Helicases, in general, have been classified into six different superfamilies (SF) based on sequence, function, and structural similarities. These superfamilies are further divided into two primary subgroups: monomer helicases (SF1-SF2) and hexamer helicases (SF3-SF6) (Sami et al., 2021; Tanner & Linder, 2001) (Figure 1.1A). Eukaryotic RNA helicases belong to the superfamilies SF1 and SF2, and fall into six families, namely DEAD-box, RIG-I-like, DEAH-box/RNA helicase A-like (DEAH/RHA), Ski2-like, NS3/NPH-II, and Upf1-like, based on amino acid sequence identity (Figure 1.1B) (Fairman-Williams et al., 2010; Jankowsky & Fairman, 2007; Jia et al., 2011).

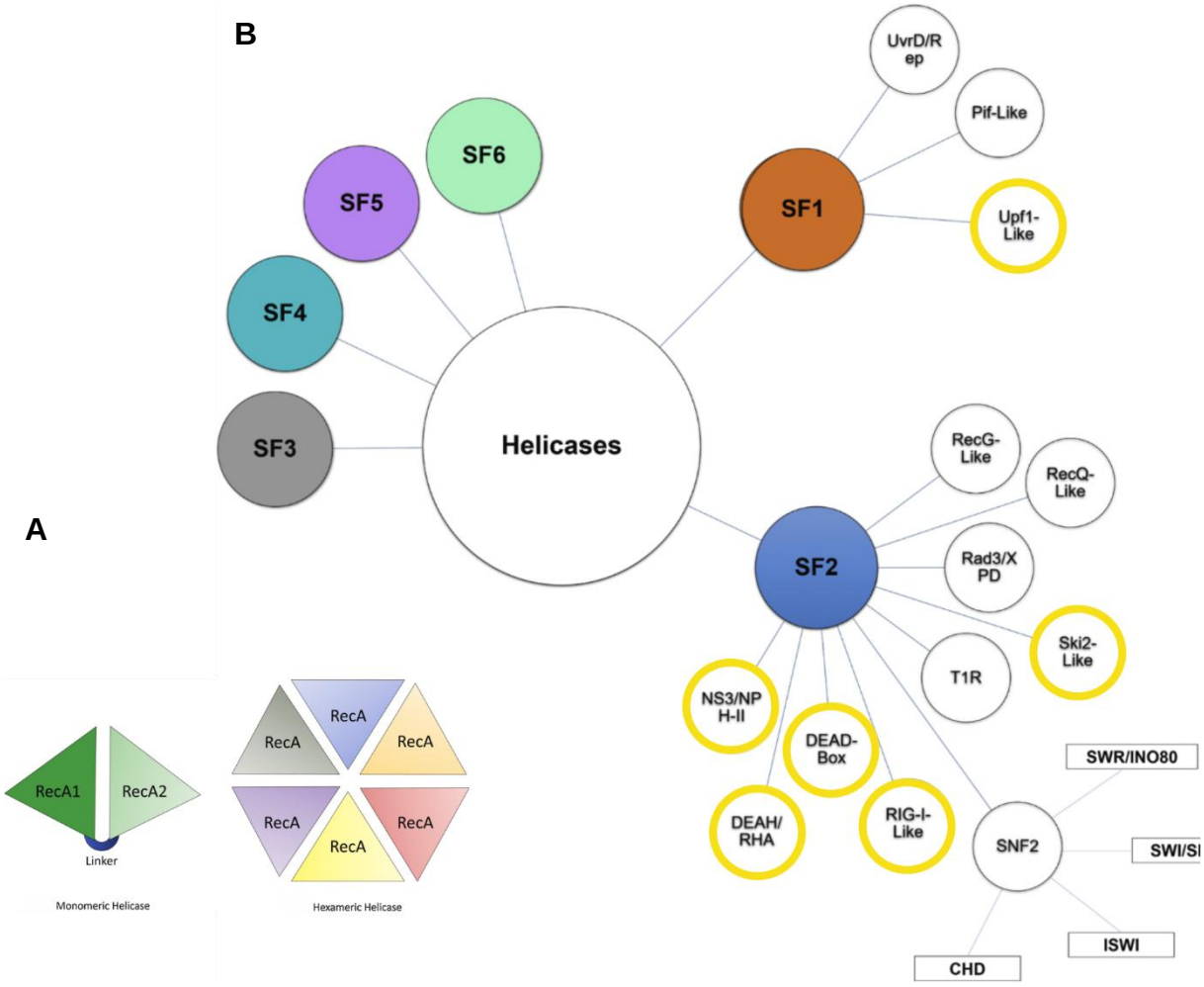

Figure 1.1 | Classification of helicase families

A. Schematic diagram showing the structural arrangement of helicases. Left: a monomeric helicase with two identical RecA domains joined by a linker sequence (SF1 and SF2). Right: Six helicase monomers assemble together forming a hexameric structure in which each monomer is consisted of a single RecA domain (SF3-SF6). Adopted from (Sami et al., 2021). **B.** Unrooted cladogram showing the three identified families of the SF1 (upper right), and the 9 families and one group (viral SF2 helicases related to NS3/NPH-II proposed as a group) of the SF2 (lower right). Branch lengths are not to scale. The oval indicates significant uncertainty in cladogram topology in this region. Yellow circles to specify families harbouring RNA helicases (Fairman-Williams et al., 2010; Leitão et al., 2015). Helicases are categorised into six superfamilies from SF1 to SF6. SF1 and SF2 are further grouped into different families. While monomeric SF1, SF2 and hexameric SF6 encompass eukaryotic members, Superfamilies SF3, SF4 and SF5 helicases are mainly hexameric from viral or bacterial origin. Adapted and modified after (Sami et al., 2021).

1.1.1 General overview of the SF2 RNA helicases

Superfamily 2 helicase proteins are abundant in RNA metabolism and exhibit a wide range of functional roles (Jarmoskaite & Russell, 2014). SF2 helicases typically have a helicase core comprising two RecA-like domains. The helicase core is variably

flanked by N- and C- terminal extensions among different members of the superfamily (Jankowsky & Fairman, 2007). The two RecA-like domains are composed of 13 characteristic sequence motifs at specific positions. Nucleoside triphosphate (NTP) binding and hydrolysis executed by four motifs, namely Q, I, II, and VI. The nucleic acid binding is accomplished by seven motifs, namely Ia, Ib, Ic, IV, IVa, V, and Vb. The two intervening motifs, namely III and Va play a role in coupling nucleic acid and NTP binding (Figure 1.1.1A) (Bohnsack et al., 2023; Fairman-Williams et al., 2010).

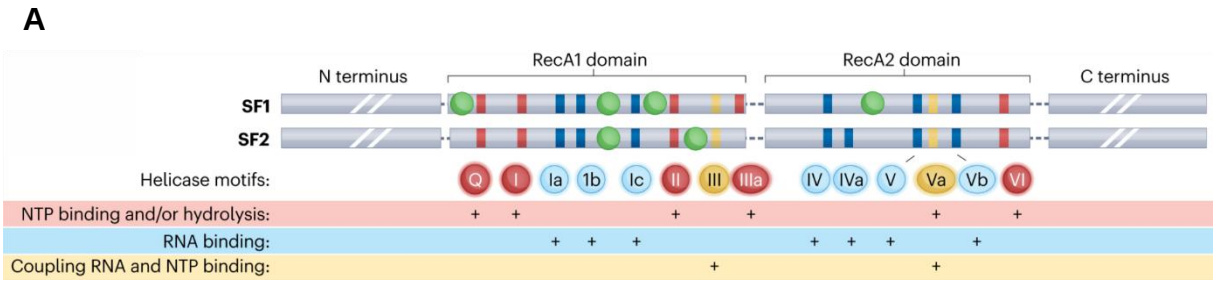

Figure 1.1.1 | Domain organisation and characteristics of SF2 and SF1 helicase families and groups

A. The indicated positions correspond to the characteristic helicase sequence motifs Q, I, Ia, Ib, Ic, II, III, IIIa, IV, IVa, V, Va, Vb, and VI. The motifs are colour-coded based on their functions, with red denoting involvement in nucleoside triphosphate (NTP) binding and/or hydrolysis, blue indicating RNA binding, and gold signifying the coupling of these activities. Green circles highlight positions where specific helicases possess additional domains. Adopted from (Bohnsack et al., 2023).

The SF2 superfamily is further divided into five different subfamilies comprising DEAD-box helicases, DEAH-RHA helicases, RIG-I like proteins, Ski2-like proteins and the NS3/NPH-II subfamily; the latter is only found in proteins of viral origin (Leitão et al., 2015). This sub-division in the SF2 superfamily is based on the differences in the sequence motifs, structural and mechanistic characteristics of its constituents (Leitão et al., 2015). SF2 RNA helicases use their helicase activity to unwind RNA secondary structures. This can happen either i) “non-processive” unwinding of short duplexes, acting for example as mechanical switches (e.g., DEAD-box); ii) “processive” unwinding via translocating along the unwound single strand (e.g., DEAH/RHA,

NS3/NPH-II); or iii) binding or translocating along a duplex without unwinding (e.g., RIG-I-like) (Jarmoskaite & Russell, 2014; Mallam et al., 2014; Singleton et al., 2007) (Table 1.1).

		Number of protein members			Nucleic acid preference		NTP preference	Unwinding polarity		Substrate	Mechanism	Function
		H.s.	*S.c.*	*E.c.*	DNA	RNA	A/G/C/U	3'→5'	5'→3'			
SF2												
	DEAD-box	37	26	9	-	+	ATP	+	+	Double-stranded	Local-strand separation	RNA/RNP remodelling
	DEAH/RHA	15	7	2	+	+	ATP/GTP/CTP/UTP	+	+	Single-stranded	Translocation-based unwinding	Transcription regulation
	Ski2-like	7	5	2	+	+	ATP	+	-	Single-stranded	Translocation-based unwinding	Coupling of unwinding and degradation
	RIG-I-like	5	1	-	+	+	ATP	+	-	Double-stranded	Translocation on double-substrates, no unwinding	Innate immune response
	NS3/NPHII	-	-	-	+	+	ATP/GTP/CTP/UTP	+	-	Single-stranded	Translocation-based unwinding	Viral replication
SF1												
	Upf1-like	11	5	2	+	+	ATP	-	+	Single-/Double-stranded	Translocation-based unwinding	mRNA decay

Table 1.1 | Enzymatic properties of individual SF1 and SF2 RNA helicase families

The properties of SF1 and SF2 RNA helicases based on the information in the following publications Fairman-Williams et al., 2010; Jarmoskaite & Russell, 2014; Linder & Jankowsky, 2011; López-Ramírez et al., 2011; Mallam et al., 2014.

In addition to the characteristic helicase domains, many SF1 and SF2 RNA helicases possess N-terminal and C-terminal auxiliary domains with functions that range from RNA or protein binding to oligomerisation, and may also contain intrinsically disordered regions (IDRs), which can promote liquid–liquid phase separation (LLPS) (Bohnsack et al., 2023; Fairman-Williams et al., 2010; Hondele et al., 2019; Leitão et al., 2015).

1.1.1.1 General structure and functions of DEAD-Box helicases

DEAD-box RNA helicases are essential for RNA metabolism and have versatile functions including roles in ribosome biogenesis, RNA export, RNA decay, RNA storage, pre-mRNA splicing, snRNP biogenesis, organelle-specific RNA metabolism, and translation. They are involved in general transcription as well as in the co-transcriptional and post-transcriptional regulation of gene expression (Sarkar & Ghosh, 2016). DEAD-box helicases are evolutionary conserved and constitute the largest class of the superfamily 2 (SF2) helicase family; having 37 members in humans, 26 in budding yeast and 9 in bacteria (Linder & Fuller-Pace, 2013; Linder & Jankowsky, 2011; López-Ramírez et al., 2011).

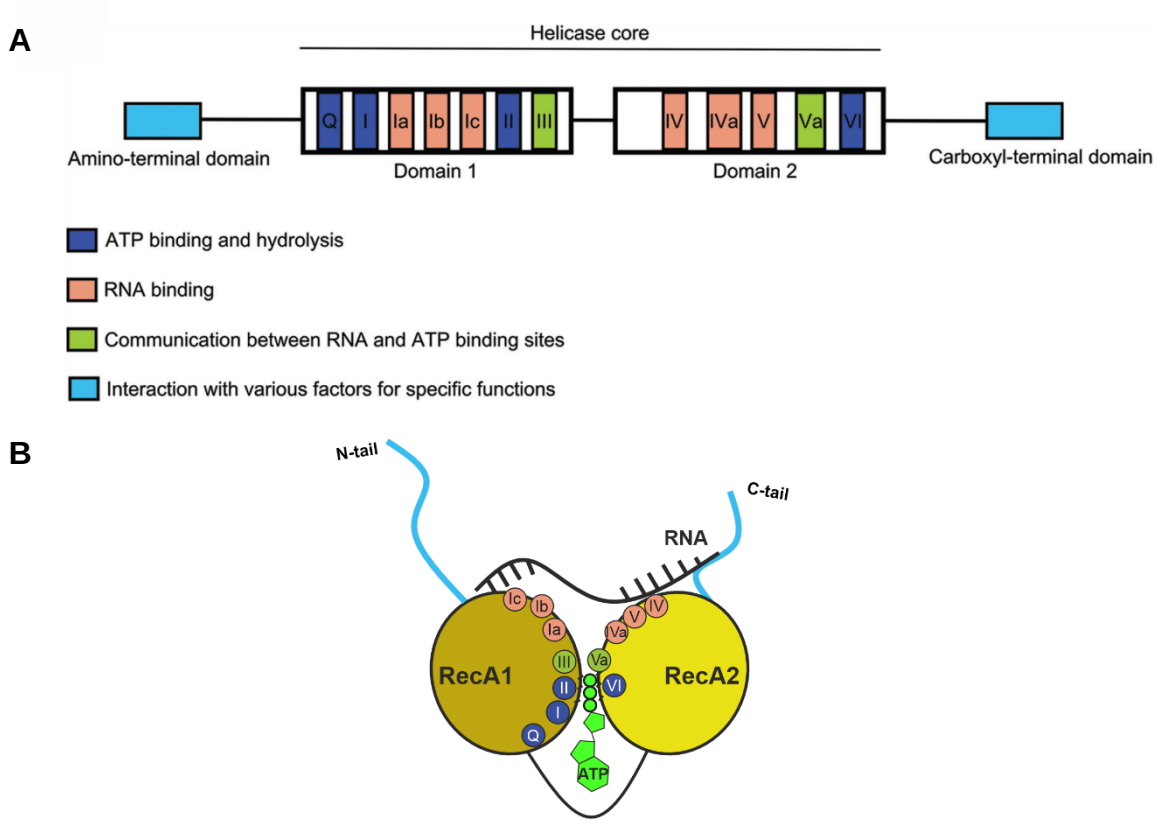

Figure 1.1.1.1 | Structure of DEAD box RNA helicases

A. The helicase core of DEAD box helicases is composed of two covalently linked identical globular domains (RecA-like); each contains five beta-strands surrounded by five alpha-helices domains, where the conserved twelve motifs are embedded in. These motifs play roles in ATP binding and hydrolysis, RNA binding, and facilitating communication between ATP and RNA binding sites. DEAD box helicases feature auxiliary amino-terminal and carboxyl-terminal domains, contributing to the specificity of function through interactions with other factors. Adopted from (Sarkar & Ghosh, 2016). **B.** Depiction of a DEAD-box helicase with conserved motifs bound to ATP and RNA.

DEAD-box helicases are characterised by two highly conserved globular helicase core domains tethered to one another by a linker region, which are homologous to the bacterial recombination protein, recombinase A (RecA), namely N-terminal RecA-like domain 1 (RecA1) and C-terminal RecA-like domain 2 (RecA2) (Patrick Linder & Jankowsky, 2011; Ballut et al., 2005; Ozgur et al., 2015). DEAD-box helicases have at least 12 highly conserved motifs within the helicase core (Figure 1.1.1.1A). There is a gap between the RecA1 and RecA2 domains, which houses the ATP-binding site. The closure of this gap is essential for efficient ATP binding and hydrolysis. RNA binds in a position opposite to that of the ATP-binding site (Figure 1.1.1.1B) (Sarkar & Ghosh, 2016). RecA1 encompasses the ATP-binding and hydrolysing motifs Q, I, and II, the RNA-binding motifs Ia, Ib, and Ic, as well as motif III, which coordinates ATP and RNA binding (Cordin et al., 2006; Linder & Jankowsky, 2011). The name “DEAD-box” is derived from the single letter amino acid code of Asp-Glu-Ala-Asp (D-E-A-D) in motif II (Walker B) within the RecA1 helicase core domain (Linder et al., 1989; Linder & Jankowsky, 2011). DEAD-box helicases also possess a unique and characteristic Q-motif approximately 17 amino acids (aa) upstream of motif I (Tanner et al., 2003). While motifs I and II bind the triphosphate moiety of NTP directly or through a Mg^{2+}, the Q motif recognises the adenine moiety, and is also important for RNA binding , therefore regulating the helicase activity (Tanner, 2003; Tanner et al., 2003; Cordin et al., 2004).

The RecA2 domain, on the other hand, comprises the RNA-binding motifs IV, IVa, and V, along with motif VI responsible for the interaction with RNA during unwinding and ATP hydrolysis. Motif Va, which might coordinate ATPase and unwinding activities, is also present. Overall, motifs Q, I, II, III, and VI are critical for both helicase and ATPase activities. In addition to the RecA-like domains, DEAD box helicases possess auxiliary amino-terminal and carboxyl-terminal domains. These additional domains contribute

to diverse functions by facilitating interactions with other proteins and RNAs (Cordin et al., 2006; Linder & Jankowsky, 2011).

A total of 26 DEAD-box proteins are encoded in *S. cerevisiae* genome. A total of 14 (Dbp3, Dbp4, Dbp6, Dbp7, Dbp8, Dbp9, Dbp10, Drs1, Fal1, Has1, Mak5, Rok1, Rrp3, Spb4) are involved in ribosome assembly, constituting the largest group. Others have been shown to take part in transcription (Dbp2), splicing (Prp5, Prp28 and Sub2), RNA export (Sub2, Dbp5), and translation [eIF4A (two isoforms), Ded1 (two isoforms), Dhh1] (Karbstein, 2022; Stewart, 2019).

1.1.1.2 Biochemical properties and activities of the DEAD-Box helicases

The basic biochemical activities of DEAD-box helicases encompass RNA, nucleotide, and protein binding. The biochemical characteristics allow them to carry out diverse RNA-stimulated activities including RNA-dependent ATP hydrolysis, RNA binding & unwinding, protein displacement from RNA, RNA clamping, RNA chaperone, strand annealing, and conversion in RNA structure (Figure 1.1.1.2). It remains elusive if DEAD-box helicases have functions within cellular contexts that are achieved solely from protein binding without involving RNA (Putnam & Jankowsky, 2013b). In contrast, it is very well evidenced that RNA, nucleotide, and protein binding influence one another (Putnam & Jankowsky, 2013b). While protein binding regulates both ATP and RNA binding, likewise RNA and nucleotide can also affect protein binding (Ballut et al., 2005; Montpetit et al., 2011; Rogers et al., 2001). Notably, DEAD-box helicases have two primary characteristics: they are RNA-binding and ATP-binding proteins. Additionally, they can link these functions with ATP hydrolysis and conformational changes, which ultimately lead to RNA unwinding or the displacement of proteins (Cordin et al., 2006; Linder & Jankowsky, 2011).

A

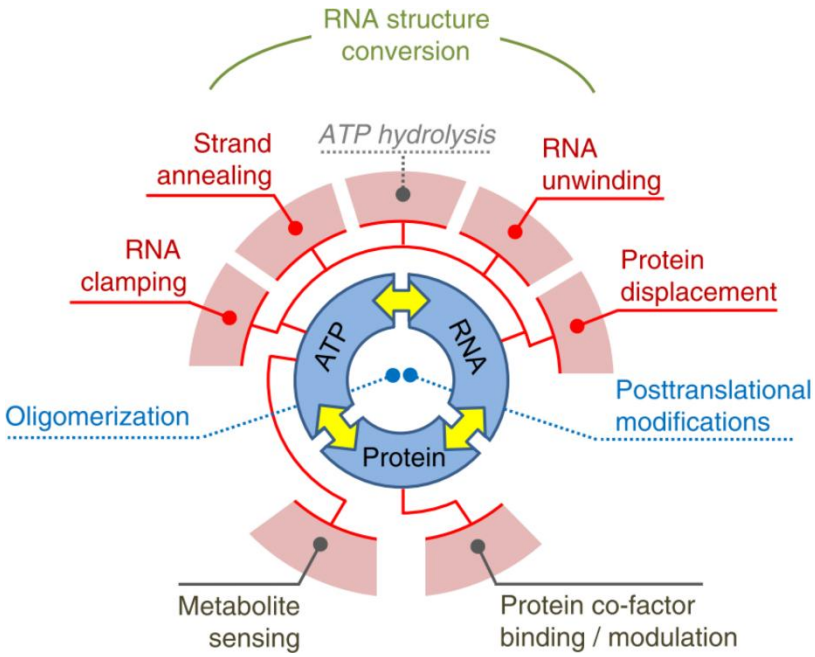

Figure 1.1.1.2 | Biochemical features and activities of DEAD-box helicases depicted under a single schematic

A. The inner circle coloured blue is for the basic biochemical features that are RNA, nucleotide (ATP) and protein binding and the yellow arrows within is to show the connection between the activities. The outer circle sections coloured red show the activities resulting from either one or two-coordinated biochemical features and the revolving red lines is to point which biochemical features is responsible for a given activity. RNA structure conversion depends on the orchestrated activities of strand annealing and RNA unwinding. Adopted from (Putnam & Jankowsky, 2013b).

Some DEAD-box helicases exhibit strand-annealing activity, which is influenced by factors such as protein oligomerisation state, ATP and ADP concentrations, and the presence of an annealing domain (Sarkar & Ghosh, 2016). These factors regulate the balance between unwinding and annealing activities in helicases that exhibit annealing, which is largely ATP-independent (Song et al., 2023). This characteristic of DEAD box helicases is critical in RNA remodelling reactions and RNA chaperoning (Jankowsky, 2011; Jarmoskaite & Russell, 2014; Linder & Jankowsky, 2011). Additionally, DEAD-box helicases were also shown to be biosensors for metabolites, allowing them to adjust RNA metabolism to adenosine monophosphate (AMP) concentrations. While AMP was shown to inhibit RNA binding and unwinding functions

of *S. cerevisiae* Ded1, Mss116, and eIF4A, it had no such an effect on the budding yeast DEAD-box helicases Sub2 and Dbp5 (Putnam & Jankowsky, 2013a).

Importantly, DEAD-box helicases possess no sequence-specificity with regards to their RNA substrate, and structural studies of various members of the family have illustrated that DEAD-box helicases interact with the ribose phosphate backbone and not with the nucleobases of RNA (Hilbert et al., 2009; Singleton et al., 2007). Despite the strong conservation of the helicase core, DEAD-box helicases differ in their cellular localisation, catalytic activity, and regulation by accessory factors. Their apparent lack of sequence-specificity, along with the high expression and strong enzymatic activity of DEAD-box proteins *in vitro*, makes it particularly interesting to understand their regulation in the cellular context (Bowers et al., 2006).

Many DEAD-box helicases have been shown to unwind short double-stranded RNAs and/or displace RNA-bound proteins in an ATP-dependent fashion *in vitro*, such as budding yeast eIF4A, DDX5 (p68) in humans, and *Drosophila* Vasa (Blum et al., 1992; Hirling et al., 1989; Liang et al., 1994; Rozen et al., 1990). Some members of this family exhibit weak RNA-dependent ATPase and ATP-dependent RNA unwinding activities *in vitro* (Ballut et al., 2005; Tseng et al., 1998; Weirich et al., 2006), possibly due to the absence of cellular cofactors, accessory proteins, or specific RNA substrates, which would otherwise enhance their activities in cellular contexts (Daugeron & Linder, 1998; Weirich et al., 2006).

1.1.1.3 DEAD-box helicases act in a single turnover reaction on short RNA duplexes

The RNA unwinding mechanism of DEAD-box helicases is distinctive. They are non-processive enzymes that act in a single-turnover reaction on short RNA duplexes. Because the processivity is very low, unwinding becomes inefficient when the length of the RNA substrate exceeds 10 to 15 base pairs. They utilise a local strand separation mechanism through tethering interactions that keep the helicase core in close proximity to the targeted RNA duplexes. DEAD-box helicases bind to the duplex region of RNA, assisted by single-stranded or structured nucleic acid regions (Sarkar & Ghosh, 2016).

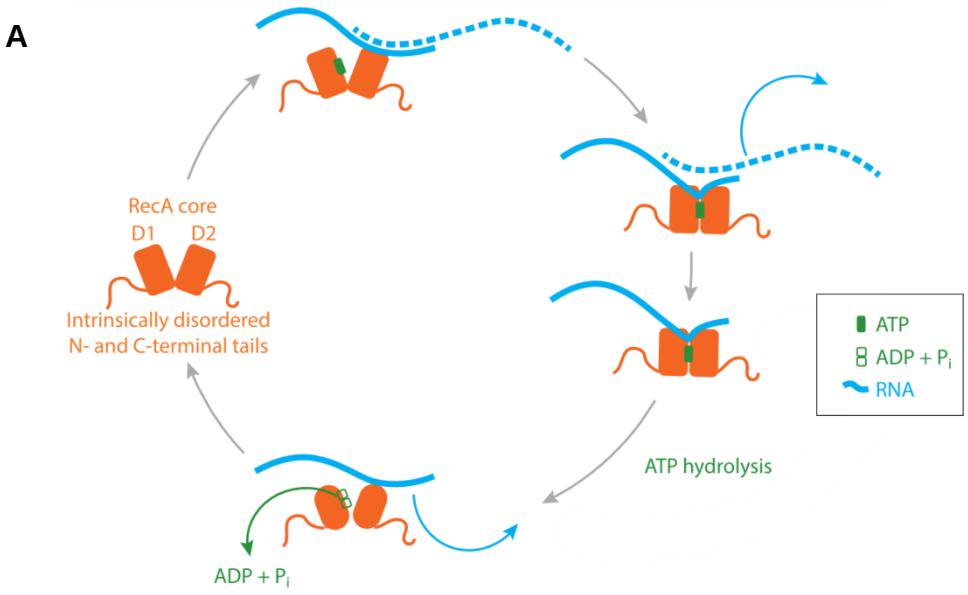

Figure 1.1.1.3 | Model of the DEAD-box ATPase cycle

A. DEAD-box ATPases are non-processive and act in a single-turnover reaction on short RNA duplexes. ATP binding induces a closed conformation in the two RecA domains (D1 and D2) of the DEAD-box ATPase, forming an elongated RNA-binding surface that facilitates interactions with the RNA phosphate backbone of a single strand. This binding results in the bending of the RNA strand into an arch, making it incompatible for interaction with another RNA strand as a duplex and potentially displacing associated proteins. Subsequent ATP hydrolysis disrupts the interdomain contacts between the D1 and D2 RecA domains, leading to the release of RNA and ADP + Pi, thus allowing the cycle to restart. If the release of inorganic phosphate after ATP hydrolysis is inhibited or the protein is locked in the ATP-bound state, DEAD-box ATPases can form stable clamps on RNAs. Adopted from (Weis and Hondele, 2022).

In detail, a single ATPase cycle by DEAD-box helicases involves, first, the rearrangement of the two RecA-like domains (RecA1 and RecA2) of the DEAD-box protein into a closed conformation upon binding to ATP in the presence of RNA. This conformational rearrangement results in an extended RNA-binding surface permitting interactions with the RNA phosphate backbone of one strand. This extended RNA binding causes bending of the RNA strand into a pronounced kink, which prohibits its interaction with another RNA strand as a secondary structure. Following ATP hydrolysis, interdomain contacts between the RecA1 and RecA2 domains are disrupted, which leads to the release of RNA and ADP+P_i (Figure 1.1.1.3A). Through repeated ATPase cycles, DEAD-box helicases can disrupt RNA-RNA and protein-RNA complexes (Andersen et al., 2006; Bono et al., 2006; Y. Chen et al., 2008; Cheng et al., 2005; Hilbert et al., 2009; Linder & Lasko, 2006; Sengoku et al., 2006; Ozgur et al., 2015; Theissen et al., 2008; Weis & Hondele, 2022).

ATP binding is a prerequisite for the RNA binding of DEAD box helicases. Importantly, ATP binding, but not ATP hydrolysis, is required for the process of RNA duplex unwinding. However, ATP hydrolysis is necessary for the recycling of DEAD-box helicases (Liu et al., 2008). The order of ATP and RNA binding by DEAD-box helicases is not sequential. RNA and ATP binding occurs rapidly (Lorsch & Herschlag, 1998), but the release of substrate RNA and ADP+Pi is considered the rate-limiting step before starting another ATPase cycle. Overall, the ATPase cycle comprises ATP binding, ATP hydrolysis, strand separation, the generation of a segment of single-stranded RNA, and finally, the release of single-stranded RNA from the helicase core. Each unwinding event involves a single ATP molecule. (Andersen et al., 2006; Bono et al., 2006; Cheng et al., 2005; Hilbert et al., 2009; Sengoku et al., 2006; Ozgur et al., 2015; Theissen et al., 2008; Weis & Hondele, 2022). The DEAD-box ATPase cycle is

crucial for regulating DEAD-box helicases functions in RNA binding and processing, with many known regulators blocking the cycle at specific processing steps. Since their enzymatic activity is driven by ATP hydrolysis, they are referred to as DEAD-box ATPases in the following sections.

1.1.2 The cellular acts of DEAD-box ATPases

DEAD-box ATPases are among the most abundant cellular proteins, with levels of expression similar to ribosomal proteins (Weis & Hondele, 2022). Due to their biochemical properties, DEAD-box ATPases can act as (a) ATP-dependent RNA helicases (Figure 1.1.2A), (b) RNA clamps (Figure 1.1.2B) facilitating the recruitment of protein complexes to RNA, or (c) RNPases (Figure 1.1.3C) removing proteins from RNA, allowing other proteins to bind (Weis & Hondele, 2022). In the following sections, the current state of knowledge about the cellular functions of DEAD-box ATPases and the mechanisms involved will be summarised, and their crucial contributions to the regulation of gene expression will be highlighted.

1.1.2.1 DEAD-box ATPases as clamping platforms

An important function of the DEAD-box ATPases is to form stable clamps on RNA serving as a scaffold for the assembly of higher-order RNP complexes (Leitão et al., 2015; Linder & Jankowsky, 2011). The term 'RNA clamp' refers to the persistent binding of RNA by the helicase, where the dissociation of DEAD-box ATPases from RNA is inhibited either by blocking the release of inorganic phosphate after ATP hydrolysis or by locking the protein in the ATP-bound conformation, which prevents progression through the ATPase cycle (Liu et al., 2014). These mechanistic details suggest that DEAD-box ATPases use their ATP hydrolysis cycle as a regulatory mechanism, controlling their binding to and release from RNA in a manner that is essential for proper RNA processing.

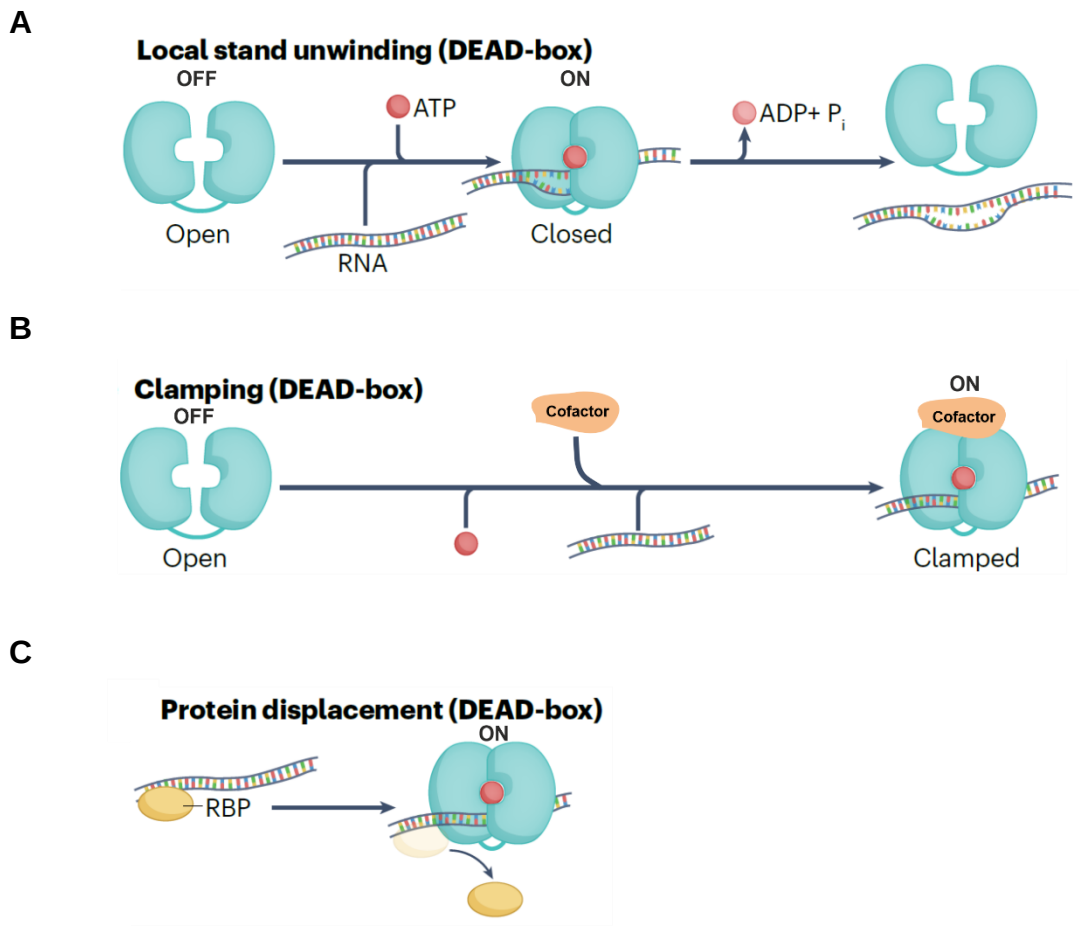

Figure 1.1.2 | Mechanisms of function of DEAD-box ATPases

A. DEAD-box ATPases can perform local strand unwinding, or **B.** when their ATPase activity is blocked, can function as clamps within RNPs, or **C.** displace RNA-binding proteins (RBP) from their substrate. Adapted and modified after (Bohnsack et al., 2023).

The first ever characterised DEAD-box ATPases acting as a clamp was eIF4A-III. eIF4A-III functions as part of the exon junction complex (EJC), which is a multiprotein complex deposited at a conserved position located upstream of exon junctions upon pre-mRNA splicing. The EJC maintains this association during export to the cytoplasm and remains attached until it is removed during the initial cycle of translation (Nielsen et al., 2009). The EJC is composed of a heterotetrameric core containing the proteins eIF4A-III, MLN51, MAGOH, and Y14. Within EJC, eIF4A-III acts as an adaptor for the other EJC components by remaining stably bound to mRNA following splicing, which secures the stable association of other EJC components with the RNA (Andersen et

al., 2006; Ballut et al., 2005; Bono et al., 2006). Structural studies have shown that the stable binding of eIF4A-III to the RNA is achieved through an arrest in the ATP hydrolysis cycle (Andersen et al., 2006; Ballut et al., 2005; Bono et al., 2006). This is accomplished by the associated protein factors within the EJC, the MAGOH-Y14 heterodimer, which interacts with eIF4A-III and traps the helicase core in the RNA-bound state by stabilising eIF4A-III in the ADP-Pi-bound state (Nielsen et al., 2009).

In addition to eIF4A-III, the ability to form stable, long-lived complexes with RNA has been demonstrated *in vitro* for several other DEAD-box ATPases, such as *S. cerevisiae* Mss116, Ded1 and Sub2. They were shown to form complexes lasting several hours with the non-hydrolysable ATP analogue ADP-BeF_x, suggesting that DEAD-box ATPases may have an intrinsic ability to act as RNA clamps (Liu et al., 2014).

1.1.2.2 DEAD-box ATPases as RNPases

DEAD box ATPases can also remove proteins from RNA in an ATP-dependent manner but independent of unwinding, a property commonly referred to as RNPase activity (Sarkar & Ghosh, 2016; B. Schwer, 2001; Weis & Hondele, 2022). The processing and fate of mRNA rely on its packaging into an mRNP (messenger ribonucleoprotein), which undergoes continuous remodelling throughout its lifespan (Bourgeois et al., 2016) (Bourgeois et al., 2016). DEAD-box ATPases, acting as RNPases, drive these compositional changes, a key function for RNA maturation and processing (Bowers et al., 2006; Rocak & Linder, 2004; Beate Schwer & Shuman, 2011). As one of the few protein classes capable of mediating RNP remodelling, DEAD-box ATPases are crucial for preventing RNA processing stalls. Examples of RNPase activity executed by DEAD-box ATPases have been shown in the context of pre-mRNA splicing and

mRNA export (Jankowsky & Bowers, 2006; Jarmoskaite & Russell, 2014; B. Schwer, 2001).

The early examples of DEAD-box proteins destabilising RNA–protein interactions were discovered in *S. cerevisiae* with Prp28 (DDX23 in humans), Sub2 (UAP56/DDX39B in humans, Uap56 in *S. pombe*), Prp5 (DDX46 in humans, Prp11 in *S. pombe*), and Dbp5 (DDX19 in humans) (Chen et al., 2001; Kistler & Guthrie, 2001; Lund & Guthrie, 2005; Perriman et al., 2003; Tseng et al., 1998). The DEAD-box protein Prp28 plays a role in exchanging U1 snRNA with U6 snRNA on the 5' splice site and has been specifically implicated in the removal of the U1 snRNP from the 5' splice site (J. Y. F. Chen et al., 2001; Staley & Guthrie, 1999). Alongside Sub2's other functions, such as playing a role in RNA export, it also contributes to early spliceosome assembly and was shown to remove budding yeast Mud2 during pre-mRNA splicing (Kistler & Guthrie, 2001). Finally, another example for such regulatory mechanism involves Dbp5, which binds to the mRNP in the nucleus and shuttles together with it through the nuclear pore complex (NPC). Dbp5 becomes activated at the cytoplasmic face of the NPC by interaction with Gle1 and inositol hexaphosphate (IP_6) and releases mRNA export factor Mex67 from the freshly exported mRNP. This action prevents the re-entry of the mRNP into the nucleus (Ledoux & Guthrie, 2011b; Lund & Guthrie, 2005; Tran et al., 2007). The RNPase function of DEAD-box ATPases can be instrumental in implementing checkpoints during RNA biogenesis and contributes to the directionality of the process.

1.1.3 DEAD-Box ATPases as global regulators of condensates

DEAD-box ATPases regulate diverse facets of RNA biology (Jarmoskaite & Russell, 2014). A recently described phenomenon is the dynamic and reversible condensation of cellular proteins and nucleic acids into membraneless organelles such as the

nucleolus, processing bodies (P-bodies) or stress granules (SG). DEAD-box ATPases have been proposed to be the global regulators of RNA-containing phase-separated organelles from bacteria to man (Hondele et al., 2019).

A

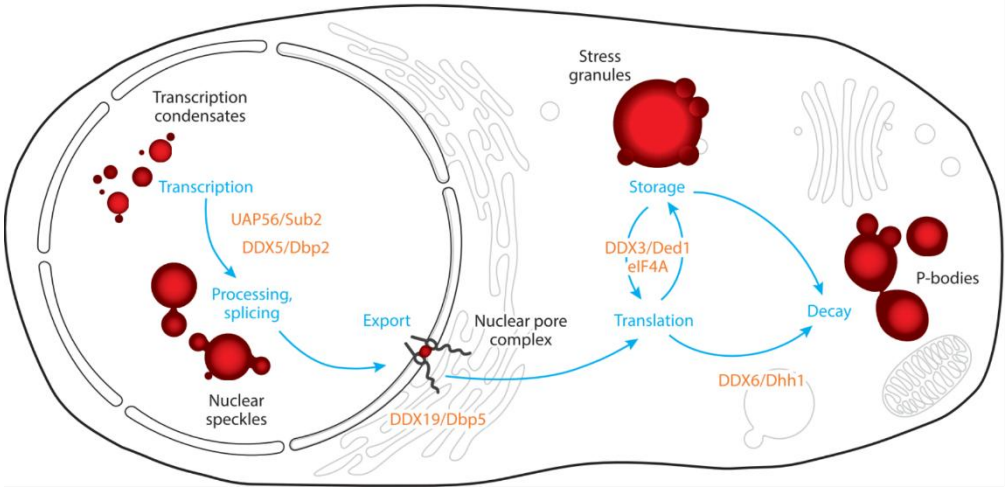

Figure 1.1.3 | DEAD-box ATPases and their association with distinct biomolecular condensates and membraneless organelles

RNP-containing membraneless organelles form during transcription, pre-mRNA splicing, nuclear pore transport, translation, and mRNA degradation, processes in which DEAD-box ATPases are involved and may regulate liquid–liquid phase separation of RNP condensates (Weis & Hondele, 2022).

Biomolecular condensates are enriched in multivalent molecules (Banani et al., 2017). Many DEAD-box ATPases have N- and C- terminal extensions, which often exhibit a low amino acid complexity, a characteristic associated with protein domains capable of liquid–liquid phase separation. For example, DDX5/Dbp2 possesses N- and C-terminal extensions surrounding its two RecA domains. The ability of *S. cerevisiae* Dbp2 to undergo phase separation in the presence of ATP and RNA was demonstrated *in vitro* (Hondele et al., 2019). DDX6/Dhh1, a key regulator of mRNA turnover, is crucial for processing body (P-body) formation, which occurs when untranslated mRNAs

accumulate in the cytoplasm. Notably, recombinant Dhh1 undergoes dynamic phase separation in the presence of RNA and ATP, and these condensates disperse when Dhh1's ATPase activity is stimulated by its activator Not1, which contains an MIF4G-like domain. Yet another abundant DEAD-box ATPase, the cytoplasmic DDX3/Ded1 is implicated in translational repression and localises to stress granules, membraneless organelles that form through the condensation of mRNA-protein complexes during stress when overall translation is reduced (Figure 1.1.3A) (Weis & Hondele, 2022).

1.1.4 DEAD-box ATPase Dbp2 (*H.s*. DDX5)

Dbp2 (*H.s.* DDX5) is a member of the DEAD-box ATPase family that has been implicated in many different processes, including transcription, pre-mRNA splicing, nuclear RNA export, RNA decay, RNA-DNA hybrid homeostasis, regulation of liquid-liquid phase-separated compartments, gene looping, RNA silencing, and ribosome biogenesis (Figure 1.1.4) (Terrone et al., 2022; Weis & Hondele, 2022; Xing, 2018). *H.s.* DDX5 was initially called p68, a name derived from the molecular size of a host protein that was immunologically cross-reacting with an antibody (DL 3C4, also named PAb204) generated against the eukaryotic viral DNA helicase, simian virus 40 (SV40) large T (Lane & Hoeffler, 1980). Later studies revealed that p68 shared extensive homology with the murine translation initiation factor known to exhibit an ATP-dependent RNA helicase activity, eIF-4A (Ford et al., 1988). By 1989, a new family of proteins, D-E-A-D box, was first described after collectively analysing the homology of five other genes from organisms ranging from bacteria to humans, to eIF-4A (Linder et al., 1989). Iggo et al., 1991 cloned and named the yeast genes related to *H. s. DDX5* DEAD-box protein 2 (*dbp2* in *S. pombe* and *DBP2* in *S. cerevisiae*) and showed that *H. s. DDX5*, *S. c. DBP2*, and *S. p. dbp2* genes all have an intron precisely at the same position in motif V (the ARGID motif). The intron is 699 bp long in *S. pombe*, 1 kb long

in *S. cerevisiae*, and 1.2 kb long in humans. Later, the same lab demonstrated that this particular intron mediates a negative feedback loop autoregulating the expression of *S. c. DBP2* (Barta et al., 1995). The autoregulation mechanism in *S. pombe dbp2* involves rapid splicing of intron 1, while intron 2 has low splicing efficiency. Splicing variants that retain intron 2 are targeted for nuclear decay through a Pab2-dependent pathway. This decay is initiated when Mmi1 recognises multiple copies of the hexanucleotide motif U(U/C/G)AAAC within intron 2 of *dbp2*, marking the transcript for degradation by the exosome. Efficient co-transcriptional splicing removes decay-promoting features of the intron, preventing Mmi1 recruitment and promoting Dbp2 expression (Kilchert et al., 2015; Lemieux et al., 2011). Loss of *S. c. DBP2* can be complemented by expressing the human DDX5 protein, suggesting that the function of the protein is conserved (Barta and Iggo, 1995; Xing et al., 2017). *In vitro*, it functions as a highly efficient RNA-duplex unwinding helicase in the presence of ATP (Cloutier et al., 2012, 2013, 2016; Ma et al., 2013). Under ATP-limited conditions, *S. cerevisiae* Dbp2 promotes RNA strand annealing, an activity that is dependent on its disordered C-terminal tail (Ma et al., 2013; Song et al., 2023). Additionally, the N- and C-terminal tails were shown to be essential for RNA substrate binding, ATP hydrolysis, and RNA unwinding, such that the helicase core is completely inactive in isolation (Song et al., 2023). Using iCLIP (individual-nucleotide resolution crossLinking and immunoprecipitation), *S. c.* Dbp2 was found to interact with RNA *in vivo* with a preference for transcripts targeted by the Nrd1-Nab3-Sen1 (NNS) complex, a specialised transcription termination pathway for snRNAs, snoRNAs, cryptic unstable transcripts (CUTs), and some mRNAs (Lai et al., 2019; Tedeschi et al., 2018). Here, crosslinking sites often coincide with regions known to form R-loops. In *S. cerevisiae,* Dbp2 facilitates co-transcriptional mRNP assembly, represses cryptic transcription initiation, and antagonises long noncoding RNA activity and has been proposed to act

as a co-transcriptional chaperone (Xing et al., 2019). In line with its chaperone function, a recent study suggested that *S. cerevisiae Dbp2* induces double-stranded RNA (dsRNA) formation via antisense RNAs (asRNAs) annealing with sense counterparts, thereby accelerating mRNA export to the cytoplasm (Coban et al., 2024). Dbp2 is required for proper mRNA export in the budding yeast (Ma et al., 2013). Accordingly, the observation of a synthetic growth defect between *DBP2 and YRA1* (an export adaptor) in *S. cerevisiae* suggests that both genes function in a closely related pathway or complex involved in RNA metabolism, and their combined dysfunction leads to severe cellular consequences, particularly in the crucial process of mRNA export. It was proposed that Yra1 inhibits the single-stranded RNA (ssRNA) binding and unwinding activity of Dbp2 *in vitro*, thereby terminating mRNP rearrangements by Dbp2 (Ma et al., 2013, 2016). Furthermore, the expression of a C-terminal truncation of Yra1 unable to interact with Dbp2 leads to the accumulation of Dbp2 on mRNA, suggesting that interaction with Yra1 induces release of Dbp2 from mRNA *in vivo* (Ma et al., 2016). Conversely, the formation of the Yra1–Mex67–Nab2 complex (the nuclear poly(A) binding protein Nab2, and the mRNA export receptor Mex67) on the mRNP is promoted by the RNA unwinding activity of the Dbp2 (Ma et al., 2013).

Extensive research over the past decades have advanced our understanding in the cellular roles of the human orthologue DDX5 as well. DDX5 is involved in many aspects of RNA metabolism including pre-mRNA splicing, alternative splicing, microRNA processing, and ribosomal RNA processing (Jalal et al., 2007; Kar et al., 2011; Salzman et al., 2007; Zonta et al., 2013). In addition to its functions in RNA metabolism, DDX5 is also implicated in DNA conformational changes through its interaction with different topoisomerases. It is also involved in DNA repair processes by interacting with protein complexes associated with non-homologous end joining (NHEJ), as well as

with DNA replication factors in nucleotide excision repair (NER) pathways, thereby contributing to maintaining genome stability (Li et al., 2023). In HeLa cells, the reduction of DDX5 levels leads to the accumulation of unspliced pre-mRNA, and the levels of DDX5 and its paralogue DDX17 impact alternative splicing patterns (Dardenne et al., 2014; Kar et al., 2011; Lin et al., 2005).

A

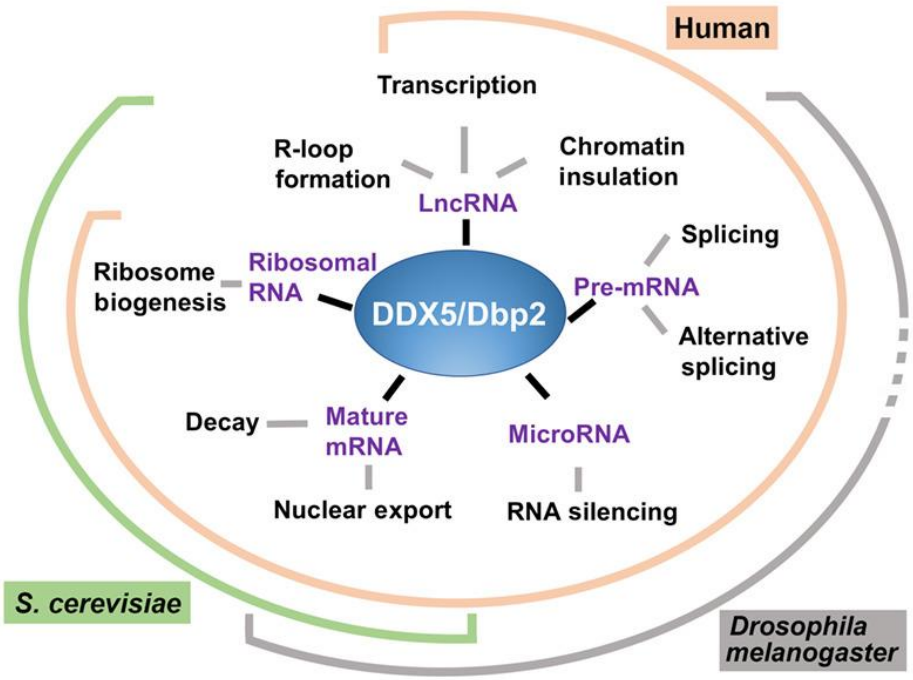

Figure 1.1.4 | Characterised functions of Dbp2/DDX5 across budding yeast, flies, and humans

The DDX5/Dbp2 subfamily of RNA helicases act on various RNA substrates in numerous cellular pathways. Adopted from (Xing Z. et al., 2019).

DDX5 has also been shown to have the ability to regulate transcription through various mechanisms. It binds to multiple transcription factors, acting as a transcriptional co-activator or co-repressor (Fuller-Pace, 2013). Human DDX5 regulates transcription by interacting with the histone acetyltransferase p300/CBP, of which it is also a substrate both *in vitro* and *in vivo* (Mooney et al., 2010; Rossow & Janknecht, 2003). DDX5 was shown to resolve a DNA G-quadruplex structure in the Myc proximal promoter region

that functions as a transcriptional silencer, thereby activating the expression of the Myc oncogene in breast and prostate cancer. G-quadruplexes are non-conventional secondary structures formed in guanine-rich DNA and RNA sequences (Guanhui Wu et al., 2019). In *S. pombe,* the ability to bind and destabilise both DNA and RNA G-quadruplexes was mapped to the arginine-glycine-glycine (RGG) domain in its C-terminal tail and was shown to be independent of ATP (Yan et al., 2021). *H. s.* DDX5 is predominantly located in the nucleus but shuttles between the nucleus and the cytoplasm. Shuttling depends on two nuclear localisation signals (NLS) and two nuclear export signals (NES), mapping to amino acids 282–308 and 446–461 and 351–363 and 482–502, respectively, and utilises the canonical Ran-GTPase-dependent pathway (H. Wang et al., 2009).

1.1.5 DEAD-box RNA helicases and their relation to diseases

Due to their pivotal roles in various crucial cellular processes, RNA helicases have been implicated in a wide array of diseases, including viral infections, neurological disorders, and cancer (Steimer & Klostermeier, 2012). RNA helicases play essential roles in the life cycles of viruses, contributing to various aspects of host-pathogen interactions. While many RNA viruses possess their own RNA helicases, retroviruses do not have helicases of their own. Instead, they exploit cellular RNA helicases to assist in their life cycle processes (Steimer & Klostermeier, 2012). For instance, during HIV-I infection, DDX1 is recruited to support viral replication (Edgcomb et al., 2012; Krishnan & Zeichner, 2004). Various DEAD-box ATPases act as viral sensors, restrict viral replication, or activate innate immunity, while others serve as negative regulators by inhibiting interferon production during viral infection (Ali, 2021; Bonaventure & Goujon, 2022). Additionally, RNA interference screening revealed an antiviral role for DDX56 (Dbp9 in *S. pombe* and *S. cerevisiae*), with its depletion enhancing infection in

Drosophila and human cells (Taschuk et al., 2020). The supporting role of DEAD-box ATPases in the viral replication makes them attractive therapeutic targets for antiviral treatments. For instance, several inhibitors have been developed against DDX3, which was shown to promote life cycle progression of various virus types and has also been implicated in the nuclear export of viral RNAs (Abdelkrim et al., 2021; Kukhanova et al., 2020; Yedavalli et al., 2004).

DEAD-box RNA ATPases may contribute to cancer development through their involvement in other processes like alternative pre-mRNA splicing, miRNA regulation, ribosome biogenesis, and apoptosis (Clark et al., 2008; Fuller-Pace, 2013; Suzuki et al., 2009). Translation initiation helicases, such as eIF4A, mediate the translation of oncogenic mRNAs with complex 5'-UTR structures and are frequently upregulated in cancer (Heerma van Voss et al., 2017). Notably, DDX5 serves as a co-activator for various cancer-related transcription factors, including the tumour suppressor p53, Oestrogen Receptor α (ERα), and β-Catenin. These proteins are central to the regulation of cell growth and survival, and their dysregulation can contribute to cancer development by either promoting tumorigenesis or preventing proper tumour suppression (Caretti et al., 2007; Fuller-Pace, 2006; Janknecht, 2010). Furthermore, DDX5 induces a large number of circular RNAs (circRNAs), a novel group of noncoding RNAs (ncRNAs) generated by back-splicing that can be associated with pathological processes such as tumour formation (Wang et al., 2023). m⁶A (N6-methyladenosine) is a common RNA modification, and YTHDC1 helps interpret this modification, influencing RNA splicing, export, and gene expression regulation. DDX5 and the m⁶A reader YTHDC1 interact to promote the production of certain circRNAs in rhabdomyosarcoma (RMS), with DDX5 mediating the back-splicing of circRNAs and functioning as a co-factor in the m⁶A regulatory network. m⁶A modification of circRNAs

regulates RMS cell proliferation (Dattilo et al., 2023). The levels of DDX5 are upregulated in various types of cancer, for example in breast cancer, colon cancer, prostate cancers, and acute myeloid leukaemia (Fuller-Pace, 2013; Xu et al., 2022). Studies indicate that DDX5 acts as a master regulator of tumorigenesis, proliferation, and metastasis, and have also linked it to resistance to cancer therapy (Li et al., 2023).

Moreover, proper RNA processing is crucial for the nervous system, and mutations in RNA helicases involved in pre-mRNA splicing and nuclear export of mRNAs, such as UAP56 (Sub2) and DDX19 (Dbp5), are associated with neurodegenerative diseases (Steimer & Klostermeier, 2012). Given the extensive connections between RNA helicases and different pathological conditions, these enzymes emerge as potential targets for therapeutic applications.

1.2 mRNA biogenesis in eukaryotes

In eukaryotes, the expression of protein-coding genes requires transcription of the DNA template into a messenger RNA (mRNA) by RNA polymerase II (RNAPII) (Inada, 2018). In addition to protein-coding mRNAs, RNAPII is responsible for transcribing small nuclear RNAs (snRNAs), microRNAs (miRNAs), and other noncoding RNAs (Hsin & Manley, 2012). The activity of RNAPII is tightly regulated to facilitate both the continuous expression of essential "housekeeping" genes and the dynamic transcription of regulatory genes in response to signals. Transcriptional control is indispensable for all cellular processes including development, growth, and stress responses (Rodríguez-Molina et al., 2023).

In the nucleus of eukaryotic cells, primary transcripts, or precursor mRNAs (pre-mRNAs), go through extensive coordinated co-transcriptional and post-transcriptional processing to ultimately form a mature message (Figure 1.2) (Bird et al., 2004; Darnell, 1982). These processes include transcription, capping, splicing, polyadenylation, and mRNA export, each playing a vital role in generating mature, translatable mRNA. Dysregulation of mRNA biogenesis can lead to various cellular dysfunctions and is implicated in numerous diseases, highlighting the importance of understanding the

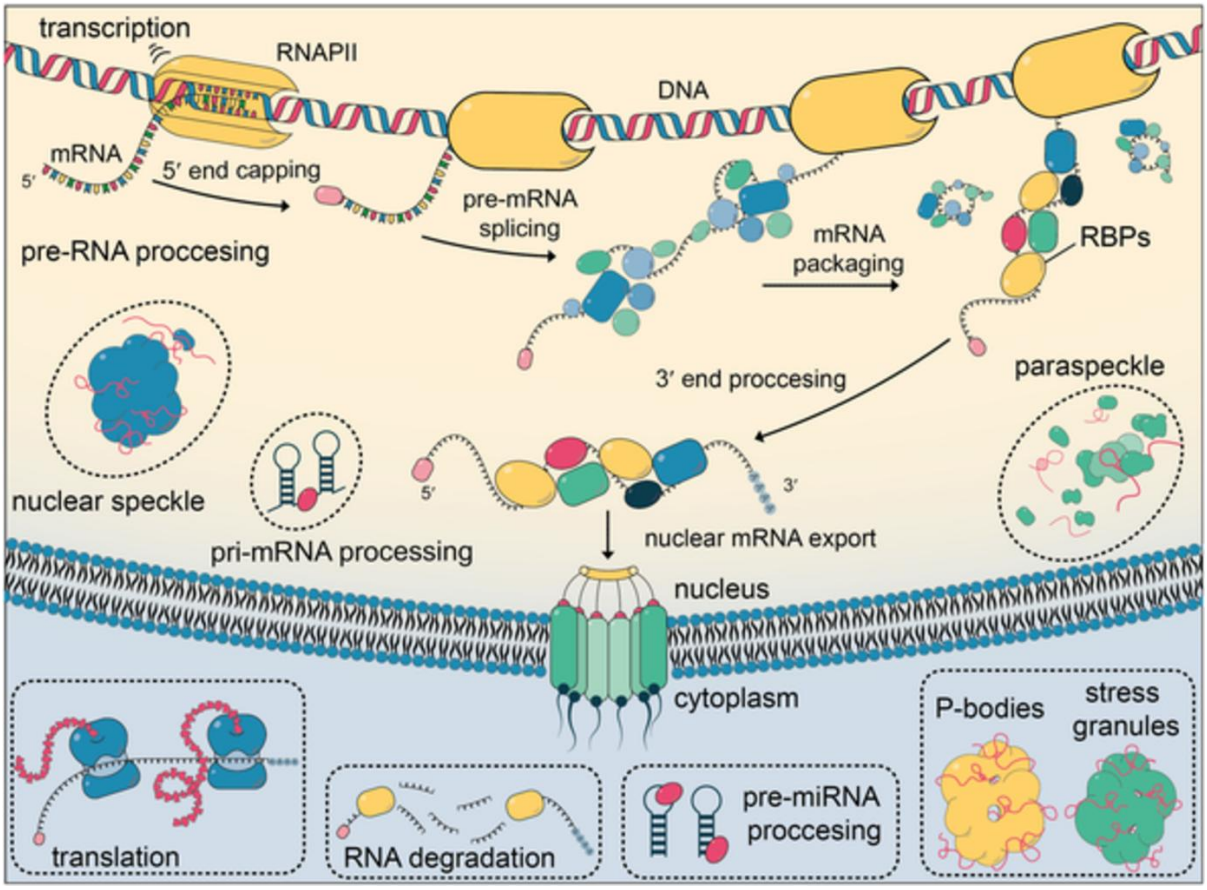

Figure 1.2 | mRNA biogenesis in eukaryotes

RNA-binding proteins (RBPs) facilitate every step of RNA biogenesis in RNA polymerase II (RNAPII)-dependent gene expression. Each step of RNA processing is carried out by a dedicated core complex during biogenesis: capping with a 7-methylguanosine cap at the 5'-end, excision of introns followed by exon ligation (splicing), and formation of the 3'-end through cleavage and addition of a non-templated poly(A)-tail. Messenger RNA (mRNA) processing steps are tightly coupled with each other and with RNAPII transcription. Abbreviations, pre-miRNA: precursor microRNA, pri-mRNA: hairpin-containing primary transcripts. P-bodies: processing bodies. Adopted from (Kilchert et al., 2019).

molecular mechanisms that govern this complex process (Bentley, 2014; Cáceres & Kornblihtt, 2002; Mitchell & Parker, 2014).

RNA processing occurs co-transcriptionally, with nascent transcripts from elongating RNAPII being immediately recognised by processing factors and incorporated into RNA-protein particles (RNPs), allowing transcription and processing to happen simultaneously, rather than sequentially (Bentley, 2014; Gregory Bird et al., 2004; Dreyfuss et al., 1993; Zhang et al., 2021). The capping, splicing, and 3′-end processing machineries all physically interact with RNAPII, thereby coupling mRNA processing with transcription (Zhao et al., 1999). These mRNPs are then exported to the cytoplasm through nuclear pores in the nuclear envelope, which mediate the movement of macromolecules between the cytoplasm and nucleus (Kelly & Corbett, 2009; Singh et al., 2015).

1.2.1 The transcription cycle of RNAPII and the CTD code

The RNAPII transcription cycle in eukaryotic cells is divided into three major stages: initiation, elongation, and termination. These stages are intricately linked to the processing of the nascent RNA transcript (Shandilya & Roberts, 2012). The C-terminal domain (CTD), a key feature of RNAPII's largest subunit, Rpb1, consists of highly conserved heptad repeats (Y1-S2-P3-T4-S5-P6-S7) that are extensively modified during transcription (Corden, 1990). The cyclin-dependent kinase (CDK) complexes (Table 1.2) are involved in phosphorylation of the RNAPII-CTD, which in turn assist in the CDK-dependent transcription cycle (Figure 1.2.1.1). These modifications, particularly phosphorylation of Ser 2, Ser 5, and Ser 7, govern the transcription cycle by recruiting RNA processing factors (Bentley, 2014; Buratowski, 2009).

The phosphorylation patterns of the CTD serve as a "code" that coordinates transcription with co-transcriptional RNA processing, including capping, splicing, and polyadenylation (Eick & Geyer, 2013). Phosphorylation of Ser 5 marks the early stages of transcription and facilitates the recruitment of capping and splicing factors (McCracken et al., 1997). As transcription proceeds, Ser 2 phosphorylation predominates, marking the transition to productive elongation (Porrua & Libri, 2015). These phosphorylation events are dynamically regulated by kinases such as CDK7, which initiates Ser 5 and Ser 7 phosphorylation, and CDK9, which promotes Ser 2 phosphorylation during elongation (Hsin & Manley, 2012; Yamaguchi et al., 1999). Phosphorylation of Ser 2 at the 3′-end is crucial for the recruitment of termination factors, while dephosphorylation of Ser 2 by CTD phosphatases signals the end of transcription. This cycle ensures that RNAPII is properly processed and can be recycled for subsequent rounds of transcription (Hsin & Manley, 2012).

S. pombe	***S. cerevisiae***	***H. sapiens***		
			Complex	**CTD Residue(s)**
Mcs6/Mcs2	Kin28	CDK7	TFIIH	Ser5P, Ser7P
Lsk1	Ctk1	CDK12, CDK13	CTDK1	Ser2P
Cdk9/Pch1	Bur1	CDK9	P-TEFb	Ser2P, Ser5P, Ser7P
Cdk8	Srb10	CDK8	Mediator	Ser5P

Table 1.2 | CTD kinases in *S. pombe* and the corresponding homologues in *S. cerevisiae* and *H. sapiens* and their complex together with CTD residues they phosphorylate.

1.2.1.1 Transcription initiation

During transcription initiation, the preinitiation complex (PIC) assembles at the promoter, including RNAPII and general transcription factors (GTFs) like TFIIB, TFIID, TFIIE, TFIIF, and TFIIH.

The PIC unwinds the DNA to form a transcription bubble, and transcription begins with the synthesis of the first RNA nucleotides at the transcription start site (TSS) (Hantsche & Cramer, 2017; Nechaev & Adelman, 2011). This process progresses through the formation of the closed promoter complex, DNA opening to form the open promoter complex, and RNA chain initiation, leading to the initiation complex (ITC) (Osman & Cramer, 2020). Once RNA surpasses a critical length, the initiation complex dissociates, and the elongation complex forms (Hantsche & Cramer, 2017).

The Mediator complex, a key regulator of transcription, bridges transcriptional activators with the PIC, activating the kinase Kin28 of TFIIH, which phosphorylates Ser5 in the RNAPII-CTD, facilitating promoter escape (Buratowski, 2009). Additionally, transcription initiation can be regulated by both activators and repressors, with factors like enhancers contributing to the efficiency of transcription (Allen & Taatjes, 2015).

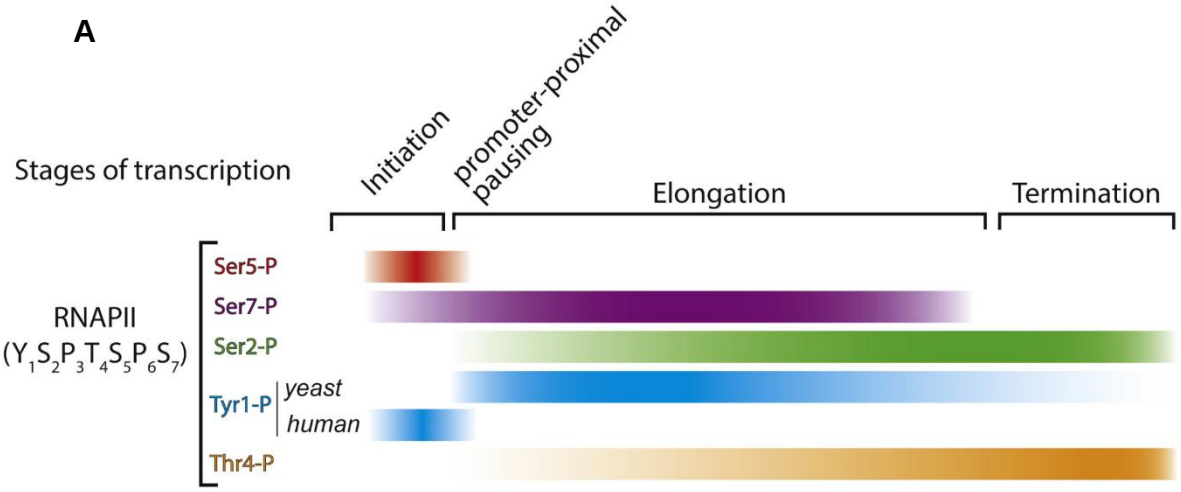

Figure 1.2.1.1 | CTD phosphorylation cycle during transcription

A. Three stages of transcription: initiation, elongation, and termination, are influenced by differential phosphorylation of the residues in the C-terminal domain (CTD) of the largest RNAPII subunit, Rpb1. The phosphorylation pattern acts as a signal for recruitment and exchange of stage-specific transcription and RNA processing factors, while the CTD itself serves as a binding platform for these factors (Rodríguez-Molina et al., 2023).

1.2.1.2 Transcription elongation

During elongation, RNAPII progresses along the DNA, synthesising the RNA transcript. However, in many metazoan genes, elongation is often paused shortly after initiation due to the action of negative elongation factors like DSIF and NELF (Yamaguchi et al., 1999). The release from this paused state requires the kinase P-TEFb, which phosphorylates both DSIF and NELF, switching DSIF to a positive elongation factor and enabling productive elongation (Peng et al., 1998; Yamaguchi et al., 2013).

In budding yeast and metazoans, elongation can also be influenced by chromatin remodellers and elongation factors such as FACT and PAF1C, which facilitate transcription through nucleosomes and stabilise the elongation complex (Ehara et al., 2022; Michl-Holzinger et al., 2022). Furthermore, RNAPII can undergo backtracking, a phenomenon in which the enzyme reverses along the DNA template, potentially leading to transcriptional arrest. This backtracking can be resolved by the RNA cleavage factor TFIIS, which helps RNAPII resume transcription (Martinez-Rucobo & Cramer, 2013).

Simultaneously with elongation, the nascent RNA undergoes co-transcriptional splicing and polyadenylation, processes crucial for generating mature mRNA (Figure 1.2.1.2) (M. J. Moore & Proudfoot, 2009). The rate of elongation can influence the formation of the spliceosome and the selection of polyadenylation sites, adding an additional layer of regulation to gene expression (Pinto et al., 2011; Saldi et al., 2016).

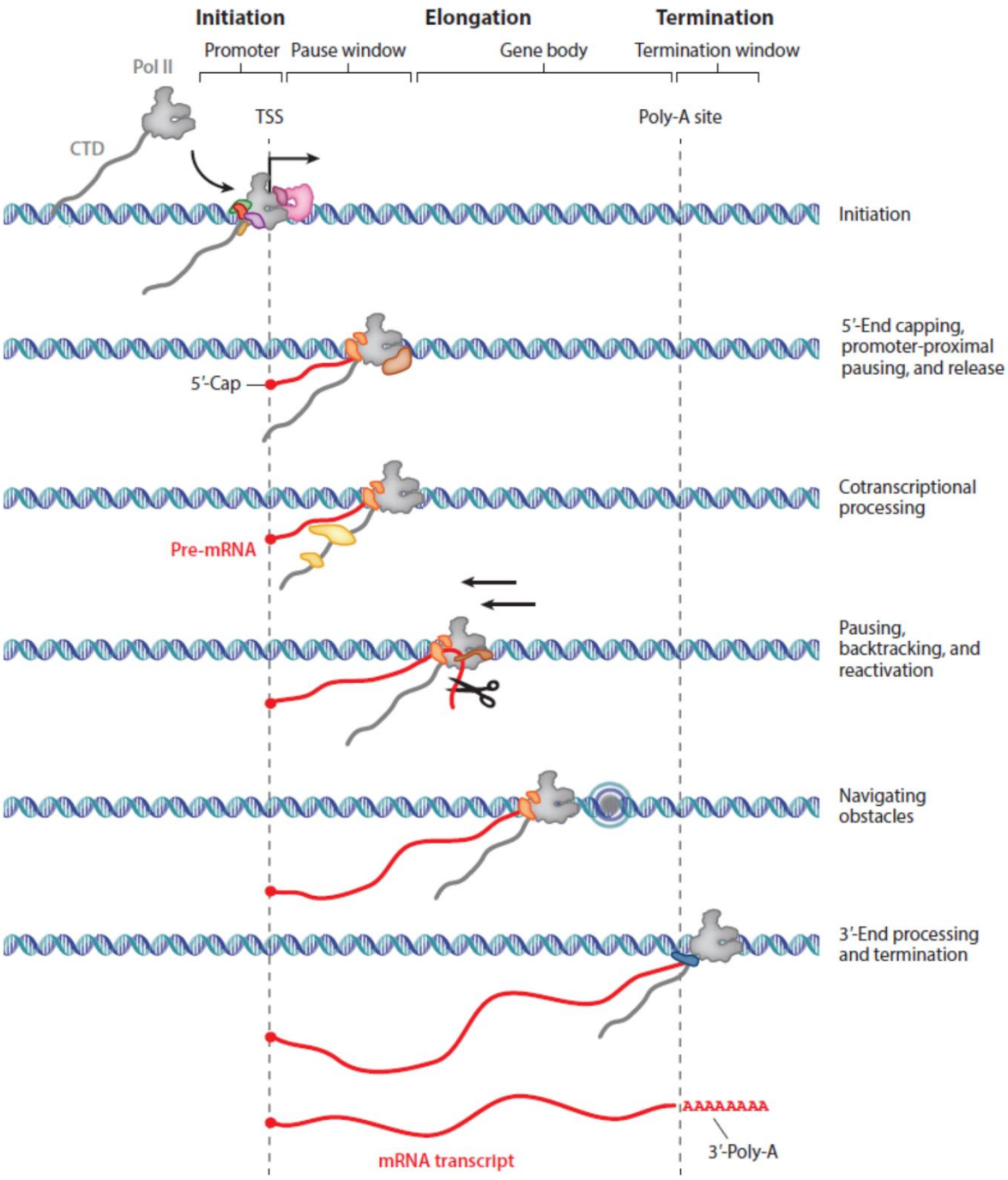

Figure 1.2.1.2 | RNAPII transcription cycle

RNAPII transcription involves initiation at promoters, assembly with general transcription factors (GTFs) (TBP, TFIIA, TFIIB, TFIIE, and TFIIH), unwinding of the DNA duplex, and RNA chain synthesis. After initiation, RNAPII extends its RNA product, undergoing co-transcriptional processes like promoter-proximal pausing, pause release, backtracking, reactivation, and navigating obstacles during elongation. The transcription cycle ends with RNAPII termination, releasing a mature mRNA transcript. Adopted from (Osman & Cramer, 2020).

1.2.1.3 Transcription termination

The termination of RNAPII transcription at gene ends ensures its release from the DNA template, enabling efficient recycling for future cycles. This process, closely linked to 3'-end mRNA processing, will be discussed in section 1.2.2.3.

1.2.2 mRNP assembly

During mRNA synthesis, it is quickly bound by mRNA-binding proteins, forming a messenger ribonucleoprotein particle (mRNP). This packaging is essential for mRNA stability, nuclear export, and regulating its functions in the cytoplasm, including translation and degradation. Specific proteins involved in this process and their assembly are crucial for proper gene expression (Wende et al., 2019). Proteins involved in nuclear mRNP formation listed below:

S. pombe	***S. cerevisiae***	***H. sapiens***	**Protein complex**	**Function(s)**
Cbc1 Cbp2 Cbc3	Cbc1/Cbp80/Sto1 Cbc2/Cbp20	Cbp80/NCBP1 Cbp20/NCBP2 NCBP3	CBC	Cap-binding complex, 5’-cap binding
Tho1 Tho2 Tho3 Tho5 Tho7	Hpr1 Tho2 Tex1 Mft1 Thp2 Gbp2	THOC1 THOC2 THOC3 THOC5 THOC6 THOC7	TREX/THO	Transcription elongation, prevention of hyper-recombination, transcription-coupled DNA repair (TCR), nuclear mRNA export
Uap56	Sub2	UAP56/ DDX39A/B	TREX	TREX
		UIF LUZP4 CHTOP POLDIP3 ZC3H11A		Additional human TREX subunits
Mlo3 Tho4	Yra1	ALYREF/ THOC4	TREX	

Nab2	Nab2	ZC3H14		Poly(A) binding, nuclear mRNA export
Srp2	Npl3	SRSF4/5/6		Transcription elongation, 3'-end formation, nuclear mRNA export
Mlo1	Tho1	CIP29/SARNP		Nuclear mRNA export; in humans classified as TREX subunit
Iss9 Pci2 Cdc31 Sus1 Dss1	Sac3 Thp1 Cdc31 Sus1 Sem1	GANP PCID2 Centrin/CENP ENY1 DSS1	THSC/TREX2	Nuclear mRNA export, chromatin modification
	Pab1	PABPN		Poly(A) binding
Mex67/Nxt1	Mex67/Mtr2	NXF1/NXT1 (TAP/p15)	mRNA exporter	mRNA exporter

Proteins involved in nuclear mRNP formation. Adapted from (Wende el. al., 2019).

1.2.2.1 5'-end processing

During early elongation, 20-25nt long emerging RNAPII transcript is co-transcriptionally capped at the 5'-end. Caps pinpoint to the start sites of gene transcription, and also critically influence mRNA maturation, translation and stability (Shatkin & Manley, 2000).

During capping, a 7-methylguanosine moiety is attached to the 5′ terminus of the RNA transcript via a 5′-5′ linkage, requiring three enzymatic activities: a triphosphatase (Cet1 in *S. cerevisiae*, Pct1 in *S. pombe*), a guanylyltransferase (Ceg1 in *S. cerevisiae* and *S. pombe*; RNGTT in humans), and a methyltransferase (Abd1 in *S. cerevisiae*, Pcm1 in *S. pombe*; RNMT in humans) (Harris et al., 2022; Osman & Cramer, 2020). The 5'-triphosphatase removes the γ-phosphate from the 5′-end of the RNA substrate leaving a diphosphate end. The guanylyltransferase then transfers GMP from GTP to form the structure GpppN1. Lastly, the methyltransferase adds a methyl group to the

N-7 position of the guanine cap to form the mature m^7GpppN1 structure, where N signifies the first amino acid of the nascent transcript (Shatkin & Manley, 2000; Shuman, 2000).

The cap structure of mRNA is recognised by the cap-binding complex (CBC), which protects nascent transcripts against 5′-3′ exonucleolysis (Izaurralde et al., 1994; Moteki & Price, 2002; Ramanathan et al., 2016). The CBC complex remains bound to the mRNA until it is transported to the cytoplasm, where it is exchanged for the translation initiation factor, eIF4E (Jeong et al., 2019). It plays a crucial role in several stages of mRNP biogenesis, highlighting the significance of functional coupling in this process. Studies in budding yeast have shown that the CBC complex can promote the formation of the transcription pre-initiation complex on active genes (Lahudkar et al., 2011). Furthermore, it is essential for co-transcriptional spliceosome assembly and for proper transcription termination, as the complex prevents the recognition of weak polyadenylation sites (Görnemann et al., 2005; Wong et al., 2007). The CBC complex generally has a productive effect on nuclear RNAs by stimulating the splicing, RNA 3′-end formation, and the packaging of export-competent ribonucleoprotein particles. However, it is also linked to destructive factors, interacting with those that target RNA for degradation and establishing a direct link between the capped 5'-ends of RNAPII transcripts and degradation processes (H. Cheng et al., 2006; Giacometti et al., 2017; Izaurralde et al., 1994; Lubas et al., 2015; Meola et al., 2016; Narita et al., 2007; Vasiljeva & Buratowski, 2006; Guifen Wu et al., 2020).

1.2.2.2 Splicing

Following transcription, emerging nascent pre-RNA contains both noncoding introns and coding exons. The spliceosome, a large protein-RNA complex, facilitates the removal of introns, guided by short consensus sequences found at the intron-exon boundaries (Hoskins & Moore, 2012; M. S. J. and M. J. Moore, 2003; Staley & Guthrie, 1998). These sequences include the 5' splice site, the branch point sequence within the intron, and the 3' splice site (Wahl et al., 2009). The spliceosome plays a vital role in folding the mRNA transcript, bringing these sequences into proximity to facilitate the excision of the targeted intron (Wahl et al., 2009). RNAPII^{Ser5P} levels have been demonstrated to reach peak at actively spliced exons, aiding in the recruitment of the spliceosome and splicing regulation (Harlen et al., 2016; Nojima et al., 2015). As elongation progresses, RNAPII^{Ser5P} phosphorylation levels decrease, and RNAPII^{Ser2P} starts to increase. This shift in phosphorylation dynamics is crucial for the ongoing regulation of splicing, as well as the recruitment of downstream factors, including transcription termination factors and proteins involved in 3'-end processing and polyadenylation of the nascent RNA (Ahn et al., 2004; Davidson et al., 2014).

In *S. cerevisiae*, the spliceosome comprises five small nuclear RNAs (snRNAs), namely U1, U2, U4, U5, and U6 snRNAs, along with over 100 various proteins (Fabrizio et al., 2009). The human spliceosome is more intricate, with the major spliceosome complex containing the same snRNAs but involving over 300 diverse proteins. Additionally, humans possess a secondary spliceosome unit known as the minor spliceosome, which includes U11, U12, U4atac, U5, and U6atac snRNAs (J. A. Steitz et al., 2008). Various other proteins are involved in the process as splicing factors. Human UAP56, a 56-kDa U2AF-associated protein, and its budding yeast counterpart Sub2 are crucial DECD-box splicing factors (Fleckner et al., 1997; Kistler & Guthrie,

2001; Libri et al., 2001; M. Zhang & Green, 2001). UAP56 plays an essential role in the association of U2 small nuclear ribonucleoprotein with pre-mRNA (Fleckner et al., 1997), while Sub2 is implicated in both ATP-independent and ATP-dependent steps of pre-spliceosome assembly (Kistler & Guthrie, 2001; Libri et al., 2001). The proposed function of Sub2 is to displace Mud2 from pre-mRNA before the binding of U2 small nuclear ribonucleoprotein (Kistler & Guthrie, 2001). The deletion of Mud2, the budding yeast homologue of U2AF2, can circumvent the requirement for Sub2 for this step (Kistler & Guthrie, 2001). Splicing of pre-mRNAs has been shown to promote their nucleus export, suggesting that the two processes may be coupled (M. J. Luo & Reed, 1999).

The consensus for RNA helicases to function as spatial and temporal checkpoints mostly derives from studies with the pre-mRNA splicing machinery (Jankowsky & Fairman, 2007). The splicing process of pre-mRNAs alone requires the activities of several SF2 RNA helicases, which modulate conformational changes within the spliceosome (Cordin et al., 2012). Specifically, early steps of spliceosome assembly and activation involve the DEAD-box RNA helicases, Prp5, Sub2 (UAP56), and Prp28 as well as the Ski2-like RNA helicase Brr2. The DEAH-box subfamily RNA helicases Prp2, Prp16, Prp22, and Prp43 on the other hand act on the late stages of the splicing cycle during disassembly of the spliceosomal complex (De Bortoli et al., 2021).

1.2.2.3 3’-end formation

A fundamental step in eukaryotic mRNA biogenesis is the formation and processing of the 3’-end of the mRNA by endonucleolytic cleavage and subsequent polyadenylation (CPA). 3’-end processing is essential for the export of mRNAs from the nucleus into the cytoplasm for their translation into functional proteins (Boreikaitė & Passmore, 2023; Rodríguez-Molina et al., 2023). Over the past decades, extensive research both

in vivo and *in vitro* has expanded our understanding of the mechanism of 3′-end cleavage and polyadenylation of transcripts and termination of transcription.

3’-end processing and transcription termination are two distinct but tightly coupled processes (Connelly & Manley, 1988; Yonaha & Proudfoot, 2000). The complement of *trans*-regulatory proteins involved in 3’-end processing and *cis*-regulatory RNA sequences have been extensively studied in *S. cerevisiae* and human systems but are less well studied in *S. pombe*. Although there are variations in complex organisation and the presence of divergent accessory factors, the core components and the overall mechanism of CPA are highly conserved (Boreikaitė & Passmore, 2023). In the following section, the eukaryotic 3’-end processing machinery and transcription termination, based on the current knowledge from studies with *S. cerevisiae* and humans, will be discussed in detail.

There are three principle mechanisms for the 3’-end processing, determined by the type of RNA that is being transcribed. These are namely, the poly(A)-dependent pathway for pre-mRNAs and many long noncoding RNAs (ncRNA), the poly(A)-independent pathway for snoRNAs (small-nucleolar RNAs) and cryptic unstable transcripts (CUTs), and the Integrator-dependent processing-termination pathway for small nuclear RNAs (snRNAs) (Eick & Geyer, 2013).

CPA is executed by the cleavage and polyadenylation complex, which comprises cleavage and polyadenylation factor (CPF) and cleavage factors IA (CFIA) and cleavage factor IB (CFIB) in budding yeast, and cleavage and polyadenylation specificity factor (CPSF), cleavage stimulatory factor (CstF), and the mammalian cleavage factors I (CFIm) and the cleavage factors II (CFIIm) in mammals (Table 1.3) (Boreikaitė & Passmore, 2023). The 3'-end processing in eukaryotic mRNAs is achieved in a three-steps process namely, recognition of polyadenylation signal (PAS)

sequences on the precursor RNA, cleavage at a distinct site, and addition of a poly(A)-tail to the newly formed 3'-end (Figure 1.2.2.1A & B) (J. Chen & Moore, 1992).

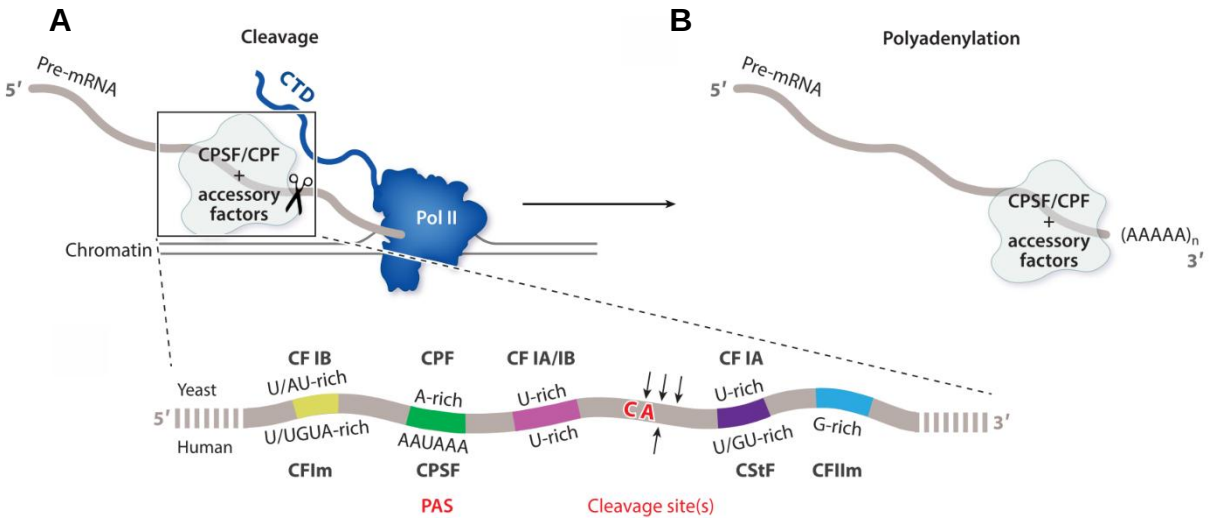

Figure 1.2.2.1 | 3′-end processing executed by multiple protein complexes and *cis*-regulatory elements

A. Schematic representation of co-transcriptional cleavage. The pre-mRNA region encompassing the cis-regulatory elements required for 3′-end processing. **B.** Polyadenylation reaction is catalysed by CPSF/CPF and regulated by accessory factors. Adopted from (Boreikaite & Passmore 2023).

The phosphorylation of the RNAPII^{Ser2P}, just like it is for the splicing processing step, is also crucial for 3'-end processing events (Cho et al., 2001; Komarnitsky et al., 2000; Richard & Manley, 2009). However, a recent study challenges this view, suggesting that RNAPII^{Ser2P} does not directly promote co-transcriptional mRNA 3'-end processing. Instead, it may serve to repress noncoding cryptic transcription (Boulanger et al., 2024). Genome-wide chromatin immunoprecipitation (ChIP) experiments have revealed that peaks of 3'-end processing factors align with RNAPII^{Ser2P} peaks, indicating that both poly(A) sites and RNAPII^{Ser2P} are essential for the subsequent recruitment and assembly of the cleavage and polyadenylation factors onto the newly transcribed RNAs (Mayer et al., 2010; Mayer, Heidemann, et al., 2012; Wittmann et al., 2017).

		H. sapiens		*S. cerevisiae*	*S. pombe*
Complex	**Module**	**Subunit**	**Complex**	**Subunit**	**Subunit**
CPSF	Nuclease	CPSF100	CPF	Cft2	Cft2
		CPSF73		Ysh1	Ysh1
		RBBP6		Mpe1	Mpe1
	Poly(A) polymerase	CPSF160		Cft1	Cft1
		WDR33		Pfs2	Pfs2
		hFip1/CPSF		Fip1	Iss1
		CPSF30		Yth1	Yth1
		PAPOLA/PAP		Pap1	Pla1
	Phosphatase	Symplekin		Pta1	Pta1
		PP1α/β		Glc7	Dis2
		-		-	Ppn1
		Ssu72		Ssu72	Ssu72
		WDR82		Swd2	Swd22
		-		Pti1	-
		-		Ref2	-
		-		Syc1	-
CstF		CstF77	CF1A	Rna14	Rna14
		CstF64		Rna15	Rna15
		CstF50		-	-
CFIIm		hPcf11		Pcf11	Pcf11
		hClp1		Clp1	Clp1
CFIm		CFIm68	CF1B	-	-
		CFIm59		-	-
		CFIm 25		-	-
		-		Hrp1	Msi2

Table 1.3 | RNA 3'-end processing machinery subunits in *H. sapiens*, *S. cerevisiae*, and *S. pombe*

CF: cleavage factor, CPF: cleavage and polyadenylation factor, PF: polyadenylation factor, CPSF: cleavage and polyadenylation specificity factor, CstF: cleavage stimulation factor. CFIA: cleavage factor complex 1A, CFIB: cleavage factor 1B. The table is based on Roguev et al. (2004), Shi et al. (2009), Wood et al. (2011), and Chan et al. (2011) and Pombase (Ramírez et al., 2023).

Cleavage and polyadenylation complex is recruited to elongating RNAPII (Ahn et al., 2004; Cho et al., 2001; Komarnitsky et al., 2000). In the poly(A)-dependent pathway, CFIA and CFIB, and CPF factors recognise consensus elements in the nascent transcript that define the polyadenylation site (PAS), including the canonical AAUAAA signal upstream of the cleavage site, as well as various accessory elements that can be positioned either up- or downstream of the PAS sequence (Bienroth et al., 1991; Dichtl & Keller, 2001; Mischo & Proudfoot, 2013; Murthy & Manley, 1992; Porrua & Libri, 2015; Y. Shi, Di Giammartino, et al., 2009; Y. Shi & Manley, 2015). The key cis-

regulatory elements involved in PAS selection, particularly the AAUAAA signal and U-rich elements upstream of the cleavage site, share similarities across eukaryotes; however, other accessory elements are less well conserved tail (Figure 1.2.2.1A). (Schlackow et al., 2013; Zhao et al., 1999). Recognition of the PAS triggers RNA cleavage by the endonuclease, Ysh1 in budding yeast and CPSF-73/CPSF3 in humans (Zhao et al., 1999). The polymerase module then adds a stretch of non-templated adenosines to the newly generated RNA 3'-end to generate the poly(A)-tail, a process controlled by poly(A)-binding proteins that associate with the synthesised poly(A)-tail (Figure 1.2.2.1B). This addition of poly(A) chain protects the nascent transcript from 3'-5'-end exonucleolysis (Boreikaitė & Passmore, 2023; Zhao et al., 1999). Whether the cleavage and polyadenylation complex engages with RNAPII as a pre-established complete complex or through co-transcriptional assembly, remains to be elucidated (Sara A. Johnson et al., 2010).

Several cleavage and polyadenylation complex components, including CPSF1 (Cft1), CstF50, Pta1, and Pcf11 interact with the CTD of RNAPII (Barillà et al., 2001; Meinhart & Cramer, 2004; Shi et al., 2009; McCracken et al., 1997). Pcf11, for example, contains an N-terminal CTD interaction domain (CID) and binds the CTD in a RNAPII^{Ser2P}-dependent manner (Barillà et al., 2001; Donny D. Licatalosi et al., 2002; Meinhart & Cramer, 2004). Pcf11-CID also interacts with the emerging RNA. Pcf11 is a bifunctional protein that contributes to transcription termination by promoting the release of RNAPII from DNA *in vitro* and *in vivo* as well as to cleavage activity (Birse et al., 1998; Hollingworth et al., 2006; Sadowski et al., 2003; Zhang et al., 2005; Zhang & Gilmour, 2006). ChIP experiments and mutational analyses of Pcf11, have demonstrated its presence at both protein-coding and noncoding genes. Its absence leads to the generation of read-through transcripts due to inefficient cleavage. Human Pcf11 was

shown to augment the degradation of RNAPII-associated nascent RNA product and transcription termination. Collectively, this evidence suggests that Pcf11 potentially has a key role in termination in addition to its 3'-end processing function of coding and noncoding genes (Donny D. Licatalosi, Gabrielle Geiger et al., 2002; Meinhart & Cramer, 2004; Sadowski et al., 2003; West & Proudfoot, 2008; Zhang et al., 2005; Zhang & Gilmour, 2006).

3'-end processing occurs on the ternary complex (nascent RNA, DNA and RNAPII). A critical step in the termination of RNAPII transcription is the disengagement of RNAPII from the DNA template (Yonaha & Proudfoot, 2000). Transcription termination by RNAPII is tightly coupled to the 3'-end processing. Originally, two models have been put forward to explain how transcription termination occurs at protein coding genes, namely the allosteric/anti-terminator model and the torpedo model (Figure 1.2.2.2). The allosteric model posits that upon transcribing the PAS sequence, RNAPII undergoes conformational changes that lead to an exchange of the elongation complex with termination factors (Logan et al., 1987). The torpedo model, on the other hand, proposes that cleavage of the nascent transcript at the cleavage site (C/S) creates an entry site for the 5'-3' exonuclease Xrn2 (Dhp1 in *S. pombe*, Rat1 *S. cerevisiae*) which degrades the accessible 5'-PO_4 end of the downstream RNAPII-associated nascent RNA product and triggers RNAPII disengagement by chasing the complex until it catches up with RNAPII (Connelly & Manley, 1988; Fong et al., 2015; Richard & Manley, 2009). A combination of both models best describes the process: as per "allosteric model" part of this joint model, the cleavage and polyadenylation complex-associated phosphatase Dis2/PNUTS-PP1 is activated during PAS recognition. Dis2/PNUTS-PP1 dephosphorylates the elongation factor Spt5, causing a deceleration in transcription within the termination zone, termed as ''Sitting Duck Torpedo". This

deliberate slowdown grants an advantage to the torpedo nuclease over RNAPII, as per “torpedo model” part of the joint model (Cortazar et al., 2019; Kecman, Kuś, et al., 2018; Parua et al., 2018).

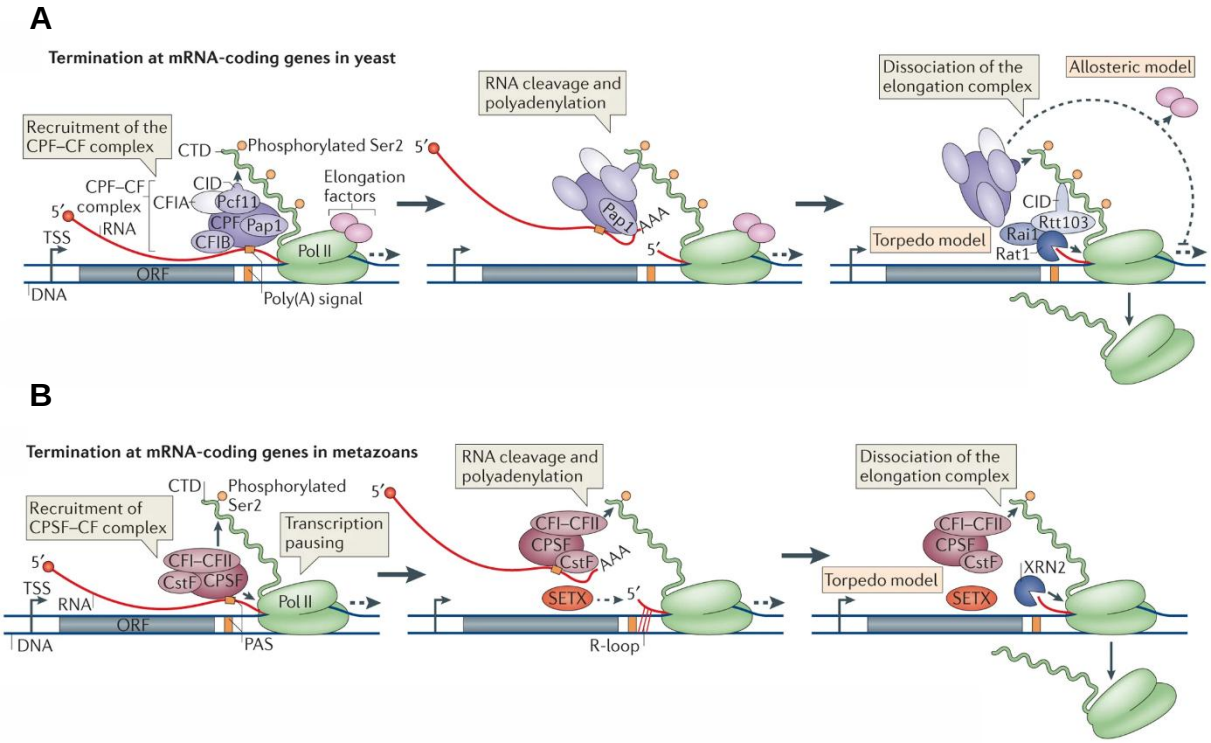

Figure 1.2.2.2 | Transcription termination mechanisms at protein-coding genes in budding yeast and metazoans

A. Both models shown for budding yeast. Allosteric model: Loss of elongation factors or polymerase conformational changes destabilise the elongation complex and Torpedo model: Rat1/Dhp1/Xrn2 degrades the nascent RNA post-cleavage, leading to dissociation of the elongation complex. **B.** For simplicity reasons only the torpedo model shown for metazoan system, the allosteric model as shown in (A). Notably, the budding yeast Sen1 homologue, senataxin (SETX), is believed to play a role in the termination of certain mRNA genes, potentially by resolving R-loops, which facilitates the access of the 5′–3′ exoribonuclease XRN2, the counterpart of Rat1. Adopted from (Porrua & Libri, 2015).

In mammalian cells, mRNA 3’-end processing tends to proceed at a relatively slow pace, with reaction times spanning 1–5 minutes (Boireau et al., 2007). As a result, the speed of poly(A) site processing becomes a crucial factor in determining whether there is sufficient time for splicing to be fully completed in a co-transcriptional manner (Bentley, 2014). The facilitation of the splicing process for the last intron is influenced

by the recognition of the poly(A) site, and contrarywise, the recognition of the last intron aids in the cleavage and polyadenylation steps (Niwa et al., 1990; Niwa & Berget, 1991). There is significant interplay between 3'-end formation and various other RNA processing reactions, including splicing (Kyburz et al., 2006; K. M. W. and J. A. Steitz, 1993). For example, interactions between 3'-end processing factors and the U2 snRNP stimulate the cleavage activity (Kyburz et al., 2006). In mammals, binding of U1 small nuclear ribonucleoprotein (snRNP) protects pre-mRNAs from premature cleavage and polyadenylation upstream of canonical cleavage sites (Kaida et al., 2010). Moreover, the canonical poly(A) polymerase responsible for polyadenylation of RNAPII transcripts as part of the cleavage and polyadenylation factor complex can also promote the decay of nuclear RNAs through hyperadenylation (Bresson et al., 2015; Bresson & Conrad, 2013), connecting 3'-end processing with nuclear RNA surveillance. Polyadenylated RNAs that successfully pass the quality control steps are rapidly transported to the cytoplasm (Mouaikel et al., 2013; Zenklusen et al., 2008). A physical link between mRNA 3'-end processing complex and the mRNP export adaptor has been established (Sara A. Johnson et al., 2010; Sara Ann Johnson et al., 2009; Li et al., 2023). In budding yeast, mutations affecting the cleavage and polyadenylation pathway can result in the retention of poly(A)-RNA within the nucleus due to a defect in coordinating transcription termination and mRNA export (Amberg et al., 1992; Custódio et al., 1999; Hammell et al., 2002). The termination process is highly dynamic, allowing it to take place at various locations within a single gene and it is closely linked to the export of mRNPs (Gilbert & Guthrie, 2004; Sara Ann Johnson et al., 2009; W. Luo et al., 2006). Intriguingly, mRNA maturation factors, in particular packaging and export factors, are required for the efficient release of the 3'-end processing complex from the transcript after polyadenylation (Qu et al., 2009).

Short stable noncoding RNAs rely on polyadenylation-independent termination mechanisms. In budding yeast, the NNS complex targets short nucleolar RNAs (snoRNAs) and CUTs (also known as the Nrd1-Sen1-Nab3 pathway, Nrd1-dependent termination, Sen1-dependent termination). The NNS complex consists of the RNA-binding proteins Nrd1 and Nab3 and the DNA/RNA helicase Sen1 (Arigo, Carroll, et al., 2006; Arigo, Eyler, et al., 2006; Kim et al., 2006; Porrua & Libri, 2015; Steinmetz et al., 2001). This complex interacts with RNAPII-CTD via the CTD-interacting domain (CID) of Nrd1, which preferentially binds the RNAPII^{Ser5P} of the CTD, a predominantly early mark in transcription. This results in the recruitment of NNS to the 5'-ends of both noncoding and coding genes, consistent with its role in terminating short RNAPII-transcribed genes such as sn/snoRNAs and CUTs (Steinmetz et al., 2001; Vasiljeva et al., 2008). In consequence, the decision between torpedo- and NNS-dependent transcription termination appears to be, in part, influenced by the phosphorylation status of the CTD of RNAPII (Porrua et al., 2016). The phosphorylation of RNAPII^{Ser2P} has been suggested to repress the use of the Nrd1-Sen1-Nab3 termination pathway downstream (Gudipati et al., 2008). The Nrd1-Nab3 heterodimer binds to RNAPII near the RNA exit channel and interacts with the emerging transcript in a sequence-specific manner, with Nrd1 and Nab3 recognising GUAA/G and UCUUG, respectively. The dimer then recruits the DNA and RNA helicase Sen1, which is presumed to terminate RNAPII by moving along the RNA and dissociating the nascent RNA from the DNA template once it reaches the polymerase (Heo et al., 2013; Porrua & Libri, 2015; Tudek et al., 2014). In comparison to protein-coding genes, there is no cleavage of the primary transcript and release of the polymerase occurs by a mechanism that strictly requires the action of the helicase Sen1 (Porrua & Libri, 2015). Nrd1 also connects transcription and 3'-end formation with surveillance by interacting with the exosome, resulting in 3'-end trimming or transcript degradation as part of a quality control process (Vasiljeva &

Buratowski, 2006). Following transcription termination, Nrd1 and Nab3 are proposed to remain bound to the RNA and subsequently recruit the Trf4-Air1/2-Mtr4 (TRAMP) complex through a direct interaction between Nrd1 and Trf4 (Tudek et al., 2014; Vasiljeva & Buratowski, 2006). TRAMP appends a short (~40 nt) poly(A)-tail to the RNA. In contrast to the adenylation of pre-mRNAs by Pap1, this particular adenosine addition by TRAMP, destabilises the transcript through the recruitment of the exosome complex (LaCava et al., 2005; Wyers et al., 2005). CUTs are as a result entirely degraded, while sn/snoRNAs undergo only partial trimming as a part of their maturation (Vasiljeva & Buratowski, 2006).

In *S. pombe* a functional analogue of the *S. cerevisiae* NNS complex does not exist (Lemay et al., 2016; Wittmann et al., 2017). The Mtr4 paralogue Mtl1 associates with the zinc finger protein Red1 to form the major exosome cofactor in the nucleoplasm, MTREC. MTREC targets meiosis-specific transcripts in mitotically growing *S. pombe* cells as well as other RNAPII-derived transcripts, such as cryptic unstable RNAs, and unspliced pre-mRNAs to the nuclear exosome (H. M. Chen et al., 2011; Egan et al., 2014; Harigaya et al., 2006; N. N. Lee et al., 2013; Vo et al., 2019; Yamashita et al., 2012; Zhou et al., 2015).The central Mtl1-Red1 core module associates with at least four additional sub-modules: the Cbc1–Cbc2–Ars2 complex (CBCA), the Iss10-Mmi1-Erh1 complex that targets meiotic RNAs, the Pab2-Rmn1-Red5 complex likely recognising poly(A) sequences, and the canonical poly(A) polymerase Pla1, which hyperadenylates MTREC substrates (Egan et al., 2014; Foucher et al., 2022; N. N. Lee et al., 2013; Soni et al., 2023; Zhou et al., 2015). MTREC is the *S. pombe* orthologue of the human PAXT connection (Foucher et al., 2022; Soni et al., 2023) and all its components have human homologues, namely the zinc-finger protein Red5 (ZC3H3), the RNA-binding protein Rmn1 (RBM26/RBM27), the canonical poly(A) polymerase

Pla1 (PAPOLA/G/B), the YTH-family RNA-binding protein Mmi1 (YTHDF1/2/3) (Foucher et al., 2022; Soni et al., 2023).

Metazoans employ a mechanism for processing and terminating their noncoding RNAs that is distinct from budding yeast, and no functional homologue of the NNS complex has been identified (O'Reilly et al., 2014; Porrua & Libri, 2013). Here, the integrator (INT) complex is responsible for terminating transcription of small nuclear RNA (snRNA) (Lykke-Andersen et al., 2021), which is recruited to snRNA-encoding genes through Serine 2 and Serine 7 phosphorylation (Baillat et al., 2005; Egloff et al., 2010). The Integrator complex contains orthologues of several CPSF proteins, including INT11 –the endonuclease for Integrator, which shares sequence homology with CPSF-73, recognises RNA sequences, and cleaves the nascent transcript (Baillat et al., 2005; Ezzeddine et al., 2011). Xrn2 appears to play a minor role in terminating such genes; instead, a nucleosome-free region spanning the entire transcription unit, combined with NELF action, is believed to terminate transcription (Fong et al., 2015; O'Reilly et al., 2014; Yamamoto et al., 2014).

1.2.2.4 Export

Nuclear export of mRNAs is a fundamental step in eukaryotic gene expression that is physically and functionally coupled to transcription and pre-mRNA processing steps (Y. Huang et al., 2003; Sara Ann Johnson et al., 2009; M. J. Luo & Reed, 1999; Sträßer et al., 2002). The TREX (TRanscription-EXport) complex exhibits evolutionary conservation and holds a crucial function in linking transcription to the export of mRNA (H. Cheng et al., 2006; Jimeno et al., 2002; Katahira et al., 2009; Köhler & Hurt, 2007; Masuda et al., 2005; Reed & Cheng, 2005; Reed & Hurt, 2002; Sträßer et al., 2002).

Consisting of the THO complex, the DEXD-box RNA helicase UAP56/DDX39B (Sub2 in *S. cerevisiae*, Uap56 in *S. pombe*), and an RNA export adaptor like ALYREF (Yra1

in *S. cerevisiae*, Mlo3 in *S. pombe*), TREX is conserved across all eukaryotes. The human THO complex comprises six subunits, with known counterparts in yeast *Saccharomyces cerevisiae*, namely THOC1 (Hpr1 in *S cerevisiae*, Tho1 in *S. pombe*), THOC2 (Tho2 in both yeasts), THOC3 (Tex1 in *S. cerevisiae*, Tho3 in *S. pombe*), THOC7 (Mft1 in *S. cerevisiae* and Tho7 in *S. pombe*), and THOC5 (Tho5 in *S. pombe*) and the metazoan-specific THOC6. Additional TREX interactors in humans include SARNP/CIP29 (Tho1 in *S. cerevisiae*, Mlo1 in *S. pombe*), ZC3H11A, and ALYREF-like proteins UIF, LUZP4, POLDIP3, and CHTOP (Dufu et al., 2010; Heath et al., 2016; A. L. Mitchell et al., 2019; Sträßer et al., 2002; Xie & Ren, 2019).

mRNA export is thought to be coupled to transcription in budding yeast and directly coupled to splicing in metazoans, necessitating an alternative splicing-independent pathway for intron-less transcripts (M. Shi et al., 2017). Importantly, ALYREF as part of the TREX complex acts as a key mRNA export adaptor that facilitates the loading of the global mRNA export factor NXF1–NXT1 (Mex67-Mtr2 in budding yeast) in order to licence mRNAs for export pathway (Hautbergue et al., 2008; Köhler & Hurt, 2007; Sträßer et al., 2002; Sträßer & Hurt, 2001; Taniguchi & Ohno, 2008). By playing a crucial role in co-transcriptional mRNA packaging into export-competent mRNPs, the TREX complex has also been shown to prevent the formation of harmful DNA-RNA hybrids, known as R-loops, thus protecting genome integrity (Luna et al., 2019; Pérez-Calero et al., 2020).

The DEXD-box RNA helicase is essential across species, indicating a crucial role for the helicase in mRNA export (UAP56/DDX39B in humans, Uap56 in *S. pombe*, Sub2 in *S. cerevisiae*, UAP56 in *C. elegans*, and Hel25E in *D. melanogaster*). In humans, URH49, a paralogue of UAP56 (with 90% amino acid identity and 96% amino acid similarity), is suggested to form a distinct alternative mRNA export (AREX) complex,

which is involved in a selective mRNA export pathway (Fujita et al., 2024; Pryor et al., 2004; Yamazaki, et al., 2010). Chromatin immunoprecipitation experiments in budding yeast have shown that the THO components, along with the RNA export adaptors Sub2 and Yra1, associate with active chromatin during transcription elongation (Peña et al., 2012; Zenklusen et al., 2002). Based on the current understanding, the THO complex is recruited to the mRNP and delivers UAP56, which then ‘clamps’ onto the mRNA. THO–UAP56 binds the export adaptor ALYREF and collaboratively they facilitate the loading of the export factor NXF1–NXT1 onto the mRNA (Hautbergue et al., 2008; Köhler & Hurt, 2007; Pühringer et al., 2020; Sträßer & Hurt, 2001; Taniguchi & Ohno, 2008). The human TREX complex is recruited to the 5′-cap end of the mRNA via an interaction between ALYREF and the cap-binding complex (CBC; CBP80 and CBP20) during splicing to facilitate mRNA export to the cytoplasm in a 5′-to-3′ direction (H. Cheng et al., 2006; Nojima et al., 2007). The mRNA–protein complex (mRNP) exits through the nuclear pore complex (Katahira et al., 2009; M. J. Luo et al., 2001; Rodrigues, 2001; Sträßer & Hurt, 2001). In addition to ALYREF, SR proteins, known regulators of pre-mRNA splicing, also serve as adaptor proteins to facilitate the recruitment of NXF1/TAP onto mRNA (Y. Huang et al., 2003; Müller-McNicoll et al., 2016; Walsh et al., 2010). NXF1/TAP is thought to occupy a pivotal position in the final step of the mRNA export pathway for the majority of mRNAs, playing an integrating role in various mRNA export pathways (Figure 1.2.3) (Katahira et al., 1999; Stutz & Izaurralde, 2003).

Another highly conserved DEAD-box ATPase Dbp5 provides directionality to the export process (Alcázar-Román et al. 2006; Weirich et al. 2006; Bolger et al. 2008; Wente and Rout 2010). Dbp5 is activated at the cytoplasmic face of the nuclear pore complex (NPC) by Gle1 and inositol hexaphosphate (IP6) and releases mRNA export

factor Mex67 from the freshly exported mRNP (Figure 1.2.3). The spatially controlled remodelling of mRNP composition by the removal of the export receptor dimer Mex67–Mtr2 prevents the re-entry of the mRNA into the nucleus (Ledoux & Guthrie, 2011b; Lund & Guthrie, 2005; Tran et al., 2007). However, recent findings challenge the conventionally known recruitment of Mext67/NXF1 and propose that Mex67/NXF1 is generally not assembled into an mRNP within the nucleoplasm but is instead recruited independently to the NPC to assist in mRNP export (Ben-Yishay et al., 2019; Derrer et al., 2019).

1.2.3 mRNPs are remodelled by several different mechanisms

As mRNA matures, it undergoes several processing steps, as outlined in the previous sections. The transition in between RNA processing steps requires mRNP remodelling (Mitchell & Parker, 2014). One mechanism for compositional changes in mRNPs was shown to be through posttranslational modifications (PTMs), which can impact the binding or function of RNA-binding proteins. Such an example involves the budding yeast SR protein Npl3, which is phosphorylated by the cytoplasmic kinase Sky1 only after export from the nucleus, promoting the dissociation of Npl3-RNA complexes and reimport back into the nucleus (Gilbert et al., 2001).

Notably, mRNP remodelling can be driven by DEAD-box ATPases – ATPases that use ATP hydrolysis to unwind duplex-RNA structure which can lead to destabilise RNA-protein interactions. In the context of mRNP remodelling, a well-known example is the essential DEAD-box ATPase Dbp5 (DDX19A/B), which mediates nuclear mRNP export (Figure 1.2.3). After being activated by Gle1 and inositol hexaphosphate (IP_6) on the cytoplasmic side of the NPC, Dbp5 facilitates the release of export factors and mRNA into the cytoplasm (Ledoux & Guthrie, 2011a; Lund & Guthrie, 2005; Tran et al., 2007).

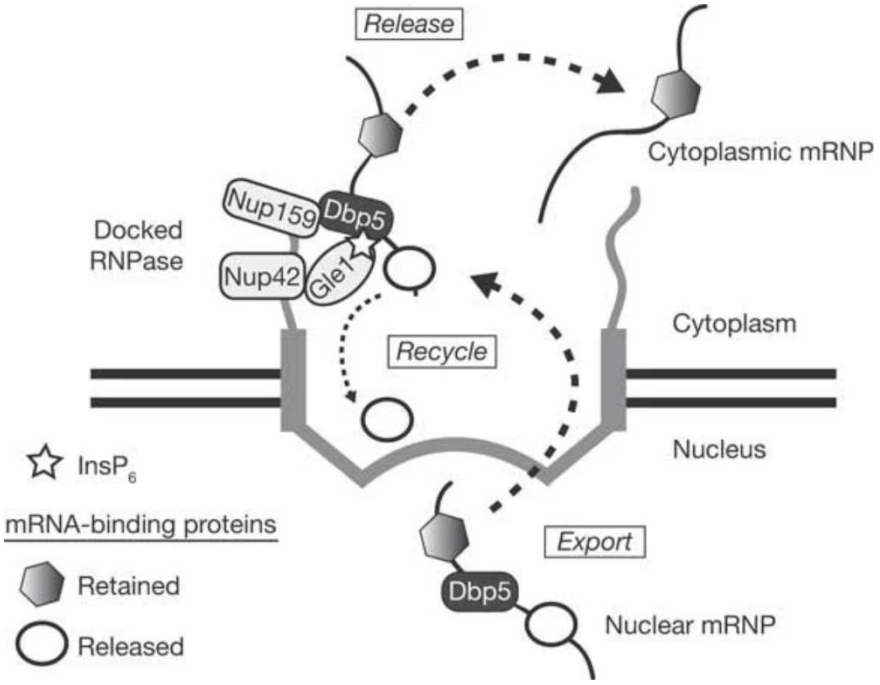

Figure 1.2.3 | A DEAD-box ATPase-mediated mRNP remodelling at the cytoplasmic side

DEAD-box RNA ATPase, Dbp5, associates with nascent transcripts in the nucleus and is recruited to the cytoplasmic NPC fibrils through interaction with Nup159. This positions Dbp5 in close proximity to Gle1 — which is docked to the NPC via Nup42 — enabling optimal $InsP_6$ binding and activation of Dbp5's ATPase activity. Using its ATPase cycle, Dbp5 remodels mRNPs during export, promoting the dissociation of the export receptor Mex67-Mtr2 through ATP hydrolysis. Afterward, Dbp5-ADP is recycled at the NPC by nucleoporin Nup159. The release and recycling of specific mRNA-binding proteins gives a directionality to the process. Adopted from (Alcázar-Román et al., 2006).

1.3 *Schizosaccharomyces pombe* as a key model organism

Two yeasts commonly used as eukaryotic model organisms in molecular and cellular biology are *Saccharomyces cerevisiae* (budding yeast) and *Schizosaccharomyces pombe* (fission yeast), with *S. cerevisiae* being the most widely studied. However, there are marked differences between the two yeasts at the molecular level. *S. pombe* and *S. cerevisiae* are only distantly related, having diverged about 370 million years ago, following the split from metazoans more than 1,000 million years ago; however, *S. pombe* appears to have evolved less rapidly than *S. cerevisiae* (Ast, 2004; Hoffman et al., 2015), retaining many characteristics of the common ancient yeast ancestor and,

by extension, sharing common features with metazoans. Thus, the fission yeast *S. pombe* has been termed a "micro-mammal", exhibiting greater similarities to complex eukaryotes than the budding yeast *S. cerevisiae* (Forsburg & Rhind, 2006; Vyas et al., 2021).

The whole genome sequence of *S. pombe* was completed in 2001 by initiative teams at the Imperial Cancer Research Fund (now called Cancer Research UK) in London and at the Wellcome Trust Sanger Institute in Hinxton, UK. The results and insights into key characteristics of the *S. pombe* genome were published in 2002 as a milestone paper by Nature (Wood et al., 2003; Yanagida, 2002). The initial research in *S. pombe* was focussed on chromosome biology, mitosis, cytokinesis, meiosis and cell-shape control but its scope has gradually expanded over the years (Yanagida, 2002).

The following characteristics have added to this trend: For instance, *S. pombe* was found to have a mitochondrial genome architecture similar to that of humans. While mitochondria are essential in fission yeast, they are dispensable in budding yeast as *S. cerevisiae* can grow under anaerobic conditions. Furthermore, *S. pombe* has the smallest eukaryotic genome in terms of chromosome number, with only three chromosomes (Yanagida, 2002). In the following, other important molecular differences to *S. cerevisiae* are briefly discussed, highlighting the importance of *S. pombe* as an alternative model organism for studying fundamental cellular processes such as transcription, translation, DNA replication, cell cycle control, and signal transduction (Hoffman et al., 2015).

Introns. In *S. pombe*, 43% of genes contain introns (Wood et al., 2003), compared to only 4% of protein-coding genes in *S. cerevisiae* (Goffeau et al., 1996). In *S. cerevisiae*, intron-containing genes use a UACUAAC box as the consensus branch-site sequence (Ast, 2004; Parker et al., 1987), which differs from the consensus in higher eukaryotes.

Consequently, mammalian introns are not spliced in *S. cerevisiae* (Russell & Nurse, 1986). In contrast, *S. pombe* has a CURAY consensus branch-site sequence (where R is a purine and Y is a pyrimidine), similar to that in mammalian genes (Ast, 2004; Russell & Nurse, 1986).

The exon junction complex (EJC). The EJC is a multiprotein complex that is deposited 20–24 nucleotides upstream of exon-exon junctions following pre-mRNA splicing (Le Hir et al., 2000). Its deposition marks the splice sites in mRNA transcripts and is thought to serve as a memory of the introns contained in their precursor mRNAs (Bannerman et al., 2018). A trimeric complex of Magoh, Y14 and eIF4A3 forms the core of the EJC, with a fourth protein MLN51 identified only in animals (Bannerman et al., 2018; Kervestin & Jacobson, 2012). The EJC travels with an mRNA into the cytoplasm, where its impact on mRNA metabolism, including mRNA export, translation activation as well as quality control via nonsense-mediated mRNA decay (NMD), have been intensively studied (Kervestin & Jacobson, 2012). While all three core components of the EJC, marking the splice sites, are preserved in *S. pombe*, eIF4A3 is the only component found in *S. cerevisiae* (encoded by the FAL1 gene). Magoh and Y14 are selectively absent in organisms with low intron densities, such as *S. cerevisiae*, consistent with the loss of the EJC during the evolution of budding yeast (Bannerman et al., 2018; Boisramé et al., 2019).

H3K9me/Heterochromatin. In eukaryotes, heterochromatin is the product of assembly of DNA into inaccessible regions, and is also referred to as silent chromatin (Moazed, 2001). It is associated with transcriptional silencing and repression of recombination and therefore implicated in the regulation of gene expression as well as maintenance of chromosome stability (Grewal & Jia, 2007; Moazed, 2001). Heterochromatin often forms in regions with a high density of repetitive DNA elements,

for example centromeric, telomeric, ribosomal DNA (rDNA) loci, and the mating-type regions of *S. pombe* chromosomes (Allshire & Ekwall, 2015; Grewal & Jia, 2007). The formation of heterochromatin, also known as heterochromatinization, is specified by the methylation of lysine 9 of histone H3 (H3K9me), a modification recognised by the chromodomain of heterochromatin protein 1 (HP1) (Grewal & Jia, 2007). This epigenetic mark is self-sustaining and preserves a heritable silent state (Bhattacharjee et al., 2019). Similar to metazoans, fission yeast uses H3K9 methyltransferase (*S. p.* Clr4; H. s. SUV39H1) and heterochromatin proteins (*S. p.* Swi6 and Chp2; *H. s.* HP1) for heterochromatin formation and silencing (Hirai & Ohta, 2023; Nakayama et al., 2001). In contrast, budding yeast relies on histone deacetylases (HDAC) and Sir proteins (Grunstein & Gasser, 2013). The conservation of the heterochromatin formation machinery with higher eukaryotes makes fission yeast the unicellular model organism of choice for heterochromatin analyses (Shimada et al., 2009).

RNAi. The RNA interference (RNAi) machinery also contributes to the formation and maintenance of transcriptionally silent heterochromatin in fission yeast (Allshire & Ekwall, 2015; Grewal, 2010; Verdel, 2013; Volpe et al., 2002). The mechanisms of heterochromatin establishment in *S. pombe* are distinct from *S. cerevisiae* and more similar to plants and metazoans (Allshire & Ekwall, 2015). *S. pombe* and *S. cerevisiae* have silent chromatin at telomeres, the mating-type loci, and rDNA regions (Allshire et al., 1995; Briggs et al., 2001; Egel et al., 1984); however, only *S. pombe* exhibits silencing at centromeric regions (Allshire et al., 1995; Volpe et al., 2002). Studies revealed that small interfering RNA (siRNA) molecules (~21 to 24 nucleotides) and components of the RNAi pathway play an important role in the establishment of transcriptional gene silencing at fission yeast centromeres (Volpe et al., 2002). The key effector complex of the RNAi pathway in *S. pombe* is the RNA-induced Initiation of

Transcriptional Gene Silencing (RITS) complex. RITS contains a chromodomain protein (Chp1), Argonaute 1 (Ago1), and Tas3, as well as siRNA (Motamedi & Andre Verdel, 2004). In addition to the Argonaute-containing complex RITS, siRNA-directed centromeric heterochromatin formation in fission yeast requires the endonuclease Dicer (Dcr1) and an RNA-dependent RNA polymerase complex (RDRC) (Barrales et al., 2016; Motamedi & Andre Verdel, 2004). Studies in *S. pombe* have shown that the RNAi machinery and small RNAs are crucial for centromeric heterochromatin assembly and function (Creamer & Partridge, 2011; Motamedi & Andre Verdel, 2004).

1.4 Objectives of this work

mRNA biogenesis is a vital cellular process in eukaryotic organisms, where precursor RNA (pre-mRNA) is synthesised and undergoes a series of dynamic and tightly regulated processing events. These steps include 5' capping, splicing, and 3' polyadenylation, which collectively contribute to the maturation of the transcript, enabling its competence for the export pathway. Extensive studies across various model organisms have highlighted the existence of specific regulatory checkpoints during mRNA biogenesis. These checkpoints ensure efficient assembly of the messenger ribonucleoprotein (mRNP) complex, a process crucial for maintaining mRNA stability, facilitating nuclear export, and regulating downstream cytoplasmic events such as translation, mRNA localisation, and decay.

DEAD-box RNA helicases, a family of ATP-dependent RNA helicases and RNA-dependent ATPases, are key molecular players in these processes. Their helicase and RNPase activities allow them to remodel RNA-protein complexes, enabling structural and compositional rearrangements necessary for mRNA biogenesis. The objective of this study is to investigate the biological role of Dbp2, a DEAD-box ATPase, in the remodelling of mRNPs in *Schizosaccharomyces pombe* (fission yeast). Specifically, this study aims to:

1. Investigate the biological function of Dbp2: characterise its role in mRNP remodelling during mRNA biogenesis in *S. pombe*.
2. Explore Dbp2's role at early checkpoints of mRNA biogenesis: determine its contribution to regulatory processes that ensure accurate RNA processing prior to nuclear export and translation.
3. Examine the mechanisms of mRNP remodelling: assess how the ATPase activity of Dbp2 facilitate structural and compositional changes in mRNPs.

By addressing these objectives, this study seeks to provide new insights into the role of Dbp2 in RNA biogenesis and its broader implications for the regulation of gene expression.

Chapter2 Structural and biochemical analysis of Dbp2

2.1 DEAD-box ATPase 2 has disordered regions at N- and C-terminal

To lay the groundwork for understanding its *in vivo* functions, analyses were conducted to explore the biochemical properties and structural composition of Dbp2. Like other DEAD-box ATPases, *S. pombe* Dbp2 was found to contain a conserved helicase core comprising two structured helicase domains connected by a short linker sequence (Figure 2.1A). Disorder prediction analysis indicated that the amino (N)- and carboxy (C)-terminal tails of Dbp2 are disordered and exhibit low amino acid sequence complexity (Figure 2.1B), a characteristic commonly associated with proteins capable of liquid–liquid phase separation and the formation of biomolecular condensates or membrane-less organelles (Weis & Hondele, 2022). Within these disordered regions, a diRGG-box motif in the N-terminal tail and four RGG-box motifs in the C-terminal tail were identified (Figure 2.1A). These motifs, which are enriched in arginine and glycine residues, have been linked to RNA binding, protein–protein interactions, and subcellular localisation, and are known to be regulated by arginine methylation (Banroques et al., 2011; Gilman et al., 2017; Hondele et al., 2019; Thandapani et al., 2013). Notably, the strong biochemical affinity of these motifs for RNA has been reported (Thandapani et al., 2013), and their presence in Dbp2 suggests potential involvement in RNA-related processes and participation in phase-separated condensates.

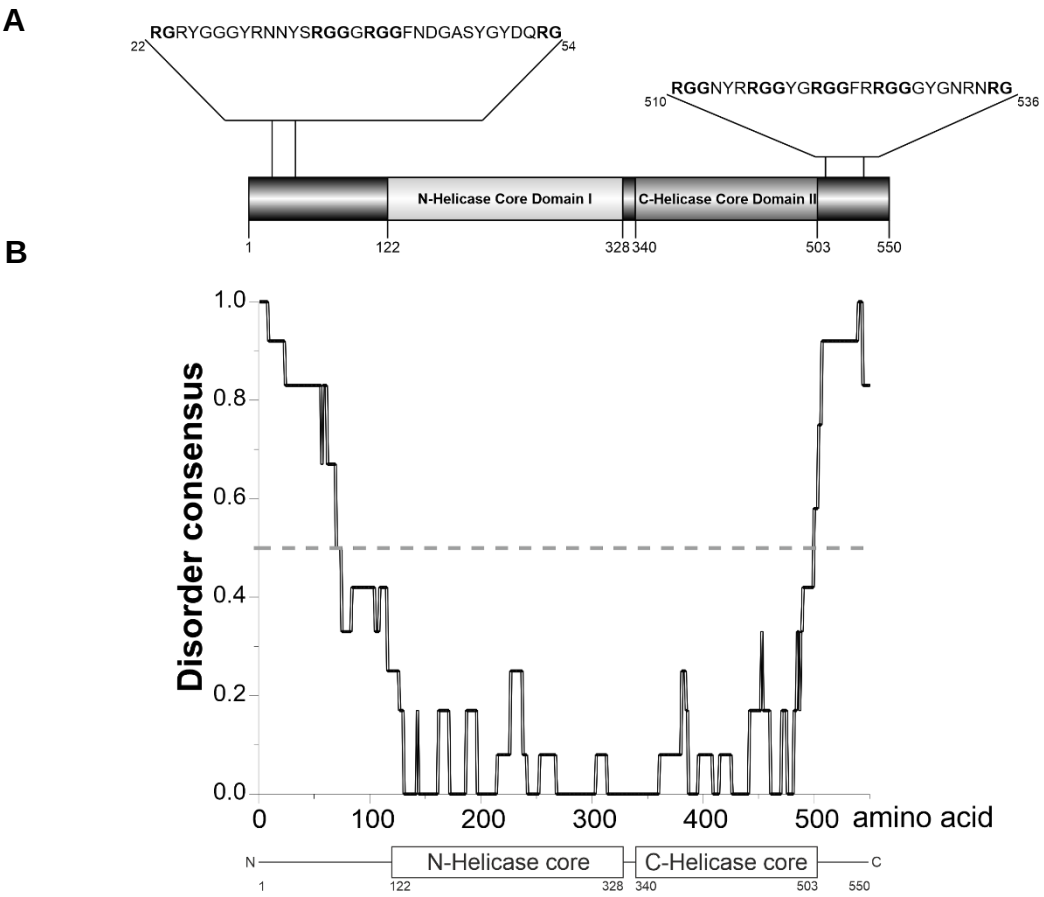

Figure 2.1 | Dbp2 protein has disordered regions both at the N- and C- terminus, surrounding two highly conserved DEAD-box helicase core

A. A schematic of the domain architecture of the Dbp2 protein, is drawn to scale, and provided for the bottom plot. **B.** Disorder prediction of the full-length Dbp2 protein. The prediction was performed using the Disorder Prediction MetaServer (DisMeta) (Huang et al., 2014). The Dismeta server defines consensus disorder prediction results of a given protein, and any disorder consensus above 0.5 as an indicator for disorder, which is exhibited by dashed line in the plot. The boundaries of two helicase core domains are shown as annotated in the uniprot P24782 accession number. N-helicase core domain: RecA-like domain 1 (containing conserved Q-motif and DEAD-box motif II) and C-helicase core domain: RecA-like domain 2 (containing conserved helicase C terminal motif). The Dismeta analysis also predicts that the region between 87-107 amino acids is in the form of coils.

2.2 *S. pombe* DEAD-box ATPase 2 is evolutionary conserved

To assess the evolutionary conservation of *S. pombe* Dbp2 with its orthologues, multiple sequence alignment was performed (Figure 2.2.1). This analysis revealed a high degree of conservation among the amino acid sequences of *S. pombe* Dbp2, *S. cerevisiae* Dbp2, human DDX5 and its paralogue DDX17, as well as *D. melanogaster*

Rm62. All 12 conserved DEAD-box motifs were identified within the helicase core of these proteins, consistent with their classification within the DEAD-box family. Motifs Q, I, Ia, Ib, II, and III were found in the first RecA-like domain (DEAD domain or RecA1), while motifs IV, IVa, V, Va, and VI were located in the second RecA-like domain (cHelicase or RecA2). These motifs are known to be involved in RNA binding, ATP binding, and hydrolysis (Linder & Fuller-Pace, 2013; Sengoku et al., 2006). A percent identity table was generated to provide an overview of orthologue similarity (Table 2.2). Human DDX5 and its paralogue DDX17 were found to share 70.48% identity. *S. pombe* Dbp2 was shown to share 65.03% identity with *S. cerevisiae* Dbp2 and 53.21% similarity with *D. melanogaster* Rm62.

Despite the highly conserved helicase core, variations were observed in the N- and C-terminal regions among these orthologues. Variable N-terminal extensions were identified in DDX17 and Rm62, which are partially present in *S. pombe* and *S. cerevisiae* Dbp2 but entirely absent in DDX5. Additionally, mammalian-specific yet uncharacterised C-terminal extensions (CTEs) were noted in DDX5 and DDX17, with limited sequence similarity between them. Within the CTE of DDX17, a unique proline-rich region was identified, which is noteworthy as such regions are typically associated with facilitating protein–protein interactions (Brian K. Kay, Michael P. Williamson, 2000). Nonetheless, the N- and C-terminal regions of DEAD-box ATPases are known to play a role in modulating helicase core activity (Hilbert et al., 2009; Ma et al., 2013; Song et al., 2023).

Both *S. cerevisiae* Dbp2 and human DDX5 have been shown to exhibit highly efficient RNA duplex unwinding *in vitro* (Ma et al., 2013; Xing et al., 2017). Given the conservation of all motifs within the helicase core across these orthologues, it is likely that *S. pombe* Dbp2 also functions as an active ATPase and RNA helicase *in vivo*.

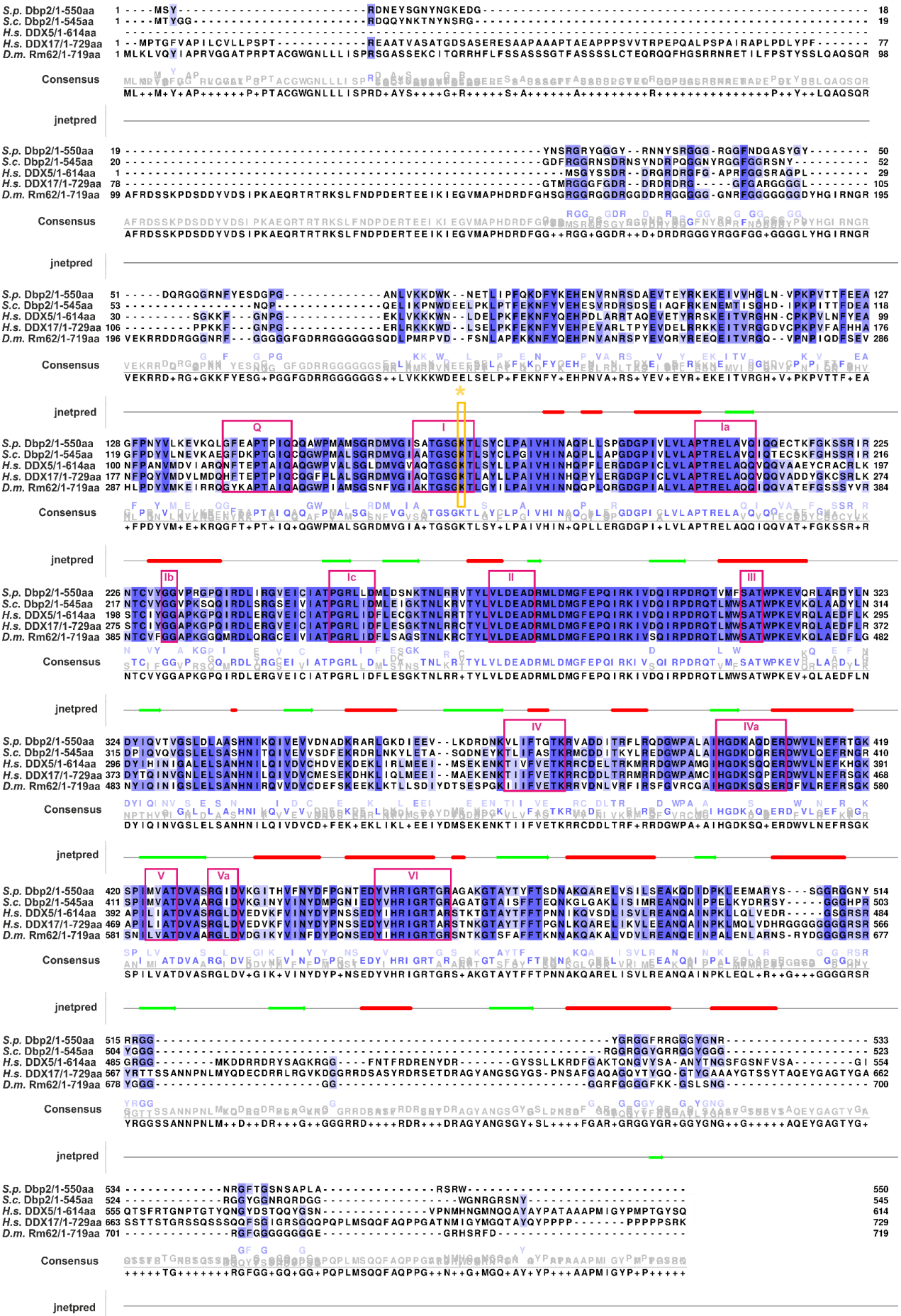
S.p. Dbp2/1-550aa
S.c. Dbp2/1-545aa
H.s. DDX5/1-614aa
H.s. DDX17/1-729aa
D.m. Rm62/1-719aa
Consensus
jnetpred
Q
I
Ia
Ib
Ic
II
III
IV
IVa
V
Va
VI

Figure 2.2.1 | DEAD-box ATPase 2 is evolutionary conserved

Multiple sequence alignment of *S. pombe* Dbp2, *S. cerevisiae* Dbp2, human DDX5 and its paralogue DDX17, and *D. melanogaster* Rm62 was conducted using the Clustal Omega web interface (McWilliam et al., 2013). The sequence alignment was visualized using JalView (Version: 2.11.3.2) (Waterhouse et al., 2009) using MUSCLE (Edgar et al., 2004). Conserved residues are highlighted with blue, with darker shades indicating higher conservation. The consensus sequence is indicated below. Secondary structure prediction was carried out with Jnetpred (Drozdetskiy, 2015) for *S. pombe* Dbp2, with helices marked as red tubes, and sheets as green arrows. Twelve conserved domains in the helicase core are highlighted in pink boxes. An orange box is to highlight the conserved lysine ('K') residue within motif I of the ATP-binding domain, where a point mutation was introduced for subsequent analysis.

| Percent identity matrix between *S. pombe* Dbp2 and orthologues

	***S. p.* Dbp2**	***S. c.* Dbp2**	***H. s.* DDX5**	***H. s.* DDX17**	***D. m.* Rm62**
***S. p.* Dbp2**	**100.00**	65.03	56.25	57.23	53.21
***S. c.* Dbp2**	65.03	**100.00**	54.33	55.86	54.70
***H. s.* DDX5**	56.25	54.33	**100.00**	70.48	58.03
***H. s.* DX17**	57.23	55.86	70.48	**100.00**	55.37
***D. m.* Rm62**	53.21	54.70	58.03	55.37	**100.00**

Table 2.2 | Percent identity matrix between *S. pombe* Dbp2 and orthologues

Percent Identity Matrix between *S. pombe* Dbp2, *S. cerevisiae* Dbp2, human DDX5 and its paralogue DDX17, and *D. melanogaster* Rm62. The percent identity matrix was created by Clustal2.1.

To further investigate the structural conservation of Dbp2 across species, AlphaFold 3 was used to predict the secondary structure of *S. pombe* Dbp2, *S. cerevisiae* Dbp2, human DDX5 and DDX17, and *D. melanogaster* Rm62, with the predicted alignment error (PAE) matrix providing additional insight. The predicted models revealed remarkable conservation of the helicase core across these orthologues, with high structural similarity observed in all species (Figure 2.2.2). This conservation is consistent with the functional roles of these proteins, suggesting that nucleotide binding, hydrolysis, and RNA interaction mechanisms are likely preserved. However, the N- and C-terminal regions exhibit greater variability among the orthologues, hinting at the possibility of species-specific adaptations.

In support of the structural quality, the predicted template modelling (pTM) scores were calculated for each orthologue, which measure the accuracy of the predicted overall fold. A pTM score above 0.5 suggests that the predicted fold is likely to be similar to the true structure. Individual pTM scores for the proteins are as follows: 0.75 for *S. pombe* Dbp2, 0.74 for *S. cerevisiae* Dbp2, 0.65 for DDX5, 0.61 for DDX17, and 0.62 for Rm62. This further suggests that the overall fold of the helicase core is well-conserved across species. Taken together, these findings underscore the evolutionary conservation of the helicase core and provide valuable insights into the structural and functional adaptations of Dbp2 across species.

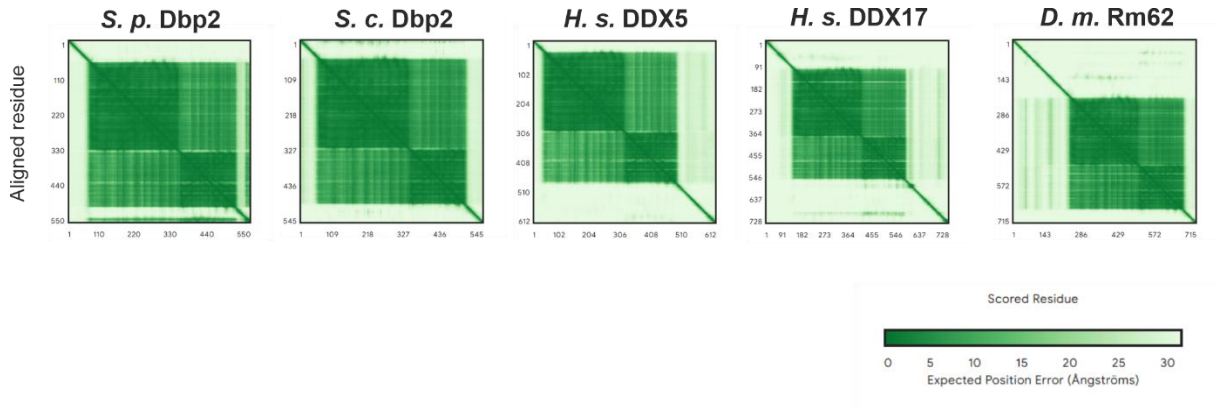

Figure 2.2.2 | Predicted alignment error (PAE) matrices between *S. pombe* Dbp2, *S. cerevisiae* Dbp2, human DDX5 and DDX17, and *D. melanogaster* Rm62

The predicted alignment error (PAE) matrices, generated by AlphaFold 3, provide estimates of the relative positional errors between aligned amino acids across the sequences of the respective orthologues. Strongly structured regions have lower alignment errors (Abramson et al., 2024).

2.3 *S. pombe* full-length Dbp2 is an efficient RNA-duplex unwinding helicase *in vitro*

Both the human DDX5 and *S. cerevisiae* Dbp2 orthologues have been shown to possess high RNA duplex unwinding activity *in vitro* (Ma et al., 2013; Xing et al., 2017). To biochemically characterise *S. pombe* Dbp2 and to assess whether it is a functional

ATP-dependent RNA helicase, an *in vitro* assay was established to quantify RNA duplex unwinding with recombinant purified full-length wild type Dbp2 ($Dbp2^{WT}$) and mutant Dbp2 ($Dbp2^{K172R}$) from *S. pombe*. In $Dbp2^{K172R}$, the conserved lysine residue in motif I, G-(K)-T, which coordinates the triphosphate moiety of ATP, is substituted by arginine (R), which is expected to disrupt ATP binding, impair ATPase activity and consequently hinder RNA unwinding activity (Figure 2.2.1, orange asterisk box).

The constructs for $Dbp2^{WT}$ and $Dbp2^{K172R}$ were expressed with an N-terminal His_6-small ubiquitin-like modifier (SUMO)-tag, followed by a 3C cleavage site (Figure 2.3.1). To circumvent potential solubility issues, the SUMO tag was used, as it is known to enhance protein solubility (Marblestone et al., 2006). The His_6-SUMO tag facilitated affinity purification, and it was cleavable due to the presence of a 3C protease recognition site. Successfully purified $Dbp2^{WT}$ and $Dbp2^{K172R}$ were subsequently used in *in vitro* RNA unwinding assays (Figure 2.3.1B & C).

Given that most RNA molecules function through interactions with proteins or as components of ribonucleoprotein complexes, and hypothesising that Dbp2 may regulate these RNA-protein interactions or influence complex assembly and/or disassembly via its enzymatic activity, a helicase assay was conducted to assess its efficiency as an RNA helicase *in vitro* and to determine whether it exhibits substrate preference based on RNA duplex-length.

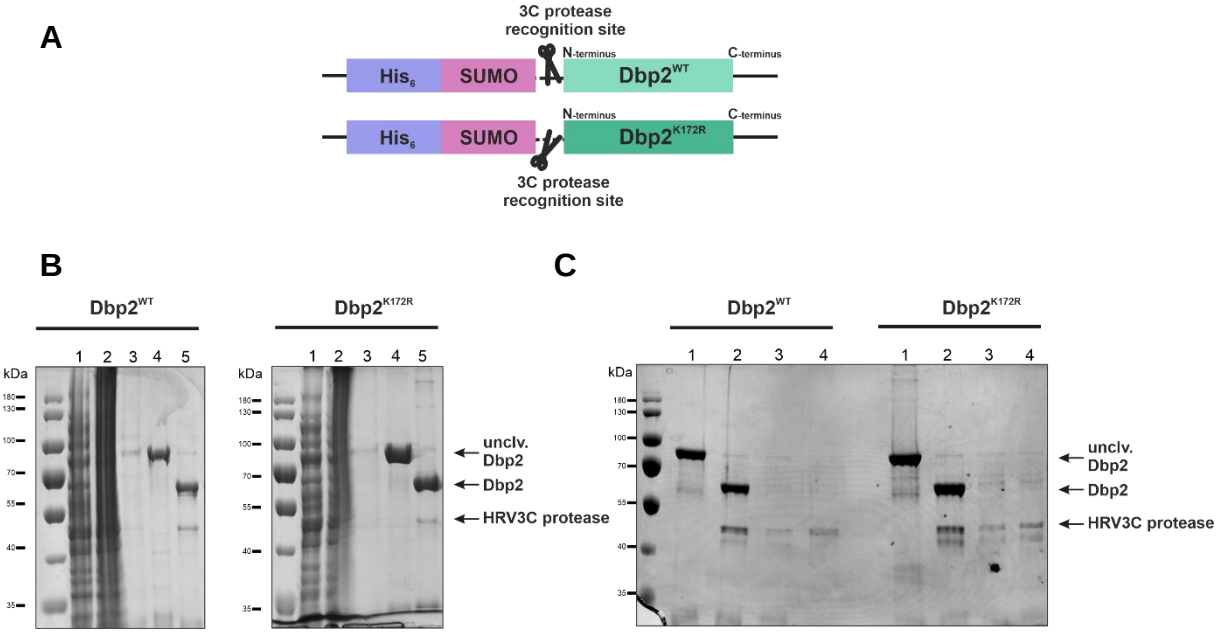

Figure 2.3.1 | *S. pombe* full-length (WT) and ATP-binding mutant (K172R) recombinant Dbp2 purifications from *E. coli*

A. Schematic view of Dbp2 constructs for affinity purification. Dbp2^{WT} and Dbp2^{K172R} are N-terminally His$_6$-SUMO-tagged, the tag is cleavable through a 3C protease recognition site. The mutant was generated by a site-directed mutagenesis to incorporate amino acid substitution, and validated by sequencing. **B.** Representative Coomassie-stained 10% SDS gel following the purification procedure for full-length His$_6$-SUMO-3C$_{site}$-Dbp2^{WT} (left) and ATP-binding mutant His$_6$-SUMO-3C$_{site}$-Dbp2^{K172R} (right) shown isolated from *E. coli* strain BL21(DE3)pLysS. Expression is induced at OD$_{600}$ ~0.8/ml with 0.2 mM IPTG and temperature reduced to 25 °C for 3 h and harvested. Upon lysing cells with sonication, the lysate (Lane #1) was cleared by centrifugation yielding to pellet and supernatant. The supernatant was subjected to affinity purification using Ni-NTA agarose beads. The flow-through (Lane #2) was discarded. The resin was washed six times with wash buffer (Lane #3), and bound protein was eluted with the elution buffer containing 300 mM imidazole (Lane #4) and samples were then subjected to buffer exchange via dialysis with 40 mM Tris/HCl pH 8.0, 50 mM NaCl, and 5 mM ß-mer and cleavage reaction with 1:50 dilution factor of 3C protease overnight at 4 °C (Lane #5). Human Rhinovirus 3C-His$_6$ tagged protease has molecular weight of 47.8 kDa. (WT Dbp2 on the left, K172R mutant Dbp2 on the right). **C.** Purification and cleavage of Dbp2 constructs. Representative Coomassie-stained 10% SDS-PAGE gel showing purified Dbp2 proteins. Lanes #1 and #2 correspond to Lanes #4 and #5 in panel **B**, representing the protein before and after cleavage, respectively. At this point (Lane #2), the solution contains the uncleaved Dbp2 construct, His$_6$-tagged 3C protease, and the cleaved Dbp2 fraction. The cleaved Dbp2 constructs kept in the flow-through (data not shown) after reverse Ni-NTA approach. Clearance is shown in lanes #3 and #4. Lane #3 represents the wash fractions obtained after incubating with Ni-NTA agarose beads for 1 hour at 4 °C, following the reverse Ni-NTA strategy. This indicates that all cleaved Dbp2 constructs were successfully collected in the flow-through during the previous step. Lane #4: Liberated fractions using 300 mM imidazole containing elution buffer after reverse Ni-NTA purification. (WT Dbp2 on the left, K172R mutant Dbp2 on the right).

In vitro strand unwinding (helicase assay) was conducted under room temperature using different lengths of single-stranded overhang duplex-RNA substrates and 2 mM ATP:Mg^{2+} in the presence of both recombinant, purified $Dbp2^{WT}$ and $Dbp2^{K172R}$ proteins. Two different partial RNA duplexes were used as substrates, using either a 13 nt dsRNA duplex with a 25 nt single-stranded overhang, or a 16 nt duplex with a 21 nt single-stranded overhang (Figure 2.3.2A). Both substrates carried at one end a Cy5 fluorophore on one strand and a quencher, BHQ2 on the other, leading to an increase in fluorescence as the strands are unwound (Figure 2.3.2B). The assays were conducted with either 600 nM $Dbp2^{WT}$ and $Dbp2^{K172R}$ proteins over a 2-minute time course, with measurements taken every second (Figure 2.3.2C).

For $Dbp2^{WT}$, the fluorescence signal gradually increased and reached saturation within two minutes when the shorter RNA duplex (Putnam 13bp RNA) was used as a substrate, with a total 3-fold fluorescence increase, indicating complete unwinding of the duplex RNA. In contrast, when the longer RNA duplex (Ma 16bp RNA) was used, the fluorescence signal increased more slowly and inefficiently, deviating from the gradual trend observed with the shorter duplex, thereby suggesting that Dbp2 unwinds shorter RNA duplexes more efficiently than longer ones. Notably, the ATP-binding mutant $Dbp2^{K172R}$ completely abolished unwinding activity *in vitro*, regardless of the duplex RNA substrate length. This suggests that the mutation of the residue within motif I disrupts its ATP-binding, and thereby impair its enzymatic activity.

Recombinant $Dbp2^{WT}$ demonstrated robust RNA unwinding activity, suggesting that it may play a role in destabilising RNA-protein complexes, potentially acting as an RNPase at *in vivo* setting. However, the intricate nature of cellular environments cannot be overruled as its ATPase activity may be subject to regulation by additional interacting factors present within the cells.

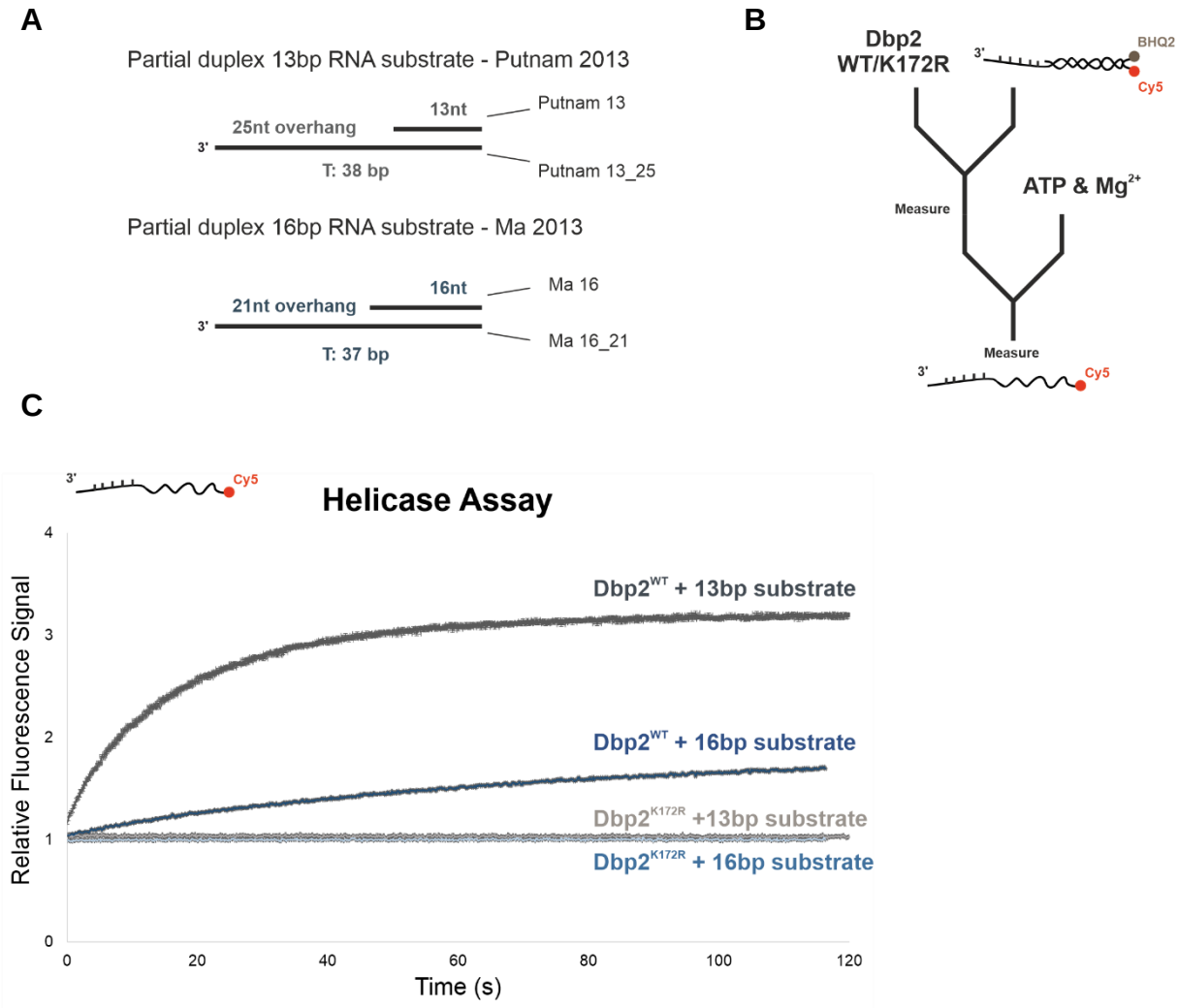

Figure 2.3.2 | *S. pombe* Dbp2 is a highly efficient DEAD-box RNA helicase *in vitro*

A. Depiction of partial RNA duplex substrates used in the dsRNA unwinding assay. In both cases, the single strands were annealed *in vitro* prior to use (see sub-section 9.4.4) (Ma et al., 2013; Putnam & Jankowsky, 2013a). **B.** A diagram illustrating the order of component addition for the real-time unwinding/helicase assay is shown. In each reaction, 600 nM of $Dbp2^{WT}$ or $Dbp2^{K172R}$ was incubated with 10 nM BHQ2-Cy5 pre-annealed partial RNA-duplex substrates. The signal was recorded every second for a total duration of 2 minutes, with excitation at 620 nm and emission at 670 nm, following the addition of 2 mM ATP and 2 mM $MgCl_2$ by spraying. The signal was measured using a Tecan Infinite F200 Pro plate reader. **C.** Time course of Cy5 fluorescence signal in the helicase assay for $Dbp2^{WT}$ and $Dbp2^{K172R}$ using both shorter and longer RNA duplex substrates. The Cy5 fluorescence signal for each reaction was normalised to the signal measured for the protein + substrate mix before the addition of $ATP:Mg^{2+}$ to each reaction. Error bars represent the SD, the experiments with Putnam 13bp RNA, n = 4 and the experiments with Ma 16bp RNA, n = 3 independent experiments.

2.4 Discussion

This chapter provides a detailed structural and biochemical characterisation of *S. pombe* Dbp2, a DEAD-box ATPase, focusing on its disordered regions, evolutionary conservation, and functional roles in RNA metabolism. The biochemical and structural (*in silico*) analyses suggest that the N- and C-terminal regions of *S. pombe* Dbp2 are disordered, as predicted by disorder analysis and supported by RGG/RG-rich motifs (Figure 2.1). These findings are consistent with the disordered regions found in other DEAD-box ATPases, which are thought to mediate phase separation and interactions with RNA and other macromolecules (Weis & Hondele, 2022). The presence of these motifs suggests that *S. pombe* Dbp2 might participate in forming biomolecular condensates, a hypothesis that aligns with the known roles of such proteins in regulating RNA-protein interactions and phase transitions. In fact, *S. cerevisiae* Dbp2 was shown to have the ability to induce phase separation (Hondele et al., 2019). Nonetheless, these motifs being present in Dbp2 supports the hypothesis that this protein participates in RNA-related processes, potentially through interactions with RNA or in the formation of RNA-protein condensates in *S. pombe*.

The sequence alignment and structural predictions revealed a high degree of conservation of the helicase core of Dbp2 across species, including *S. pombe*, *S. cerevisiae*, human DDX5, and *D. melanogaster* Rm62. This conservation suggests that the core functional mechanisms of Dbp2, including ATP and RNA binding, hydrolysis, and unwinding, are preserved across species. The conservation of the DEAD-box motifs in the helicase core of Dbp2, along with the unique properties of the N- and C-terminal regions, further suggests that *S. pombe* Dbp2 may operate in a similar manner to other DEAD-box ATPases, but with potential regulatory adaptations specific to its role in *S. pombe* cells.

Notably, among different species, the N- and C-terminal regions showed significant variability, particularly in mammalian orthologues like DDX5 and DDX17. This variability could indicate species-specific adaptations that fine-tune the helicase's interactions with RNA or other cellular components, potentially influencing their involvement in distinct cellular pathways or regulatory mechanisms (Hilbert et al., 2009; Ma et al., 2013). This opens avenues for further investigations into how the structural diversity of DEAD-box ATPases contributes to their specialised roles in different species.

Previous studies have reported that recombinant expression of *S. cerevisiae* Dbp2 in *E. coli* cells was highly toxic, even at low levels, which hindered successful protein purification (Banroques et al., 2008, 2011). Similar difficulties were encountered by others (W. K. M. and E. J. Tran, 2015). In initial attempts using either Rosetta or BL21(DE3) expression cells, induction of wild type Dbp2 protein expression was very low, resulting in poor purification (data not shown). However, strong induction of Dbp2 expression was achieved in the BL21(DE3)pLysS expression strain, enabled successful purification of the recombinant proteins (Figure 2.3.1), which were subsequently used for *in vitro* helicase activity assays. The *in vitro* RNA unwinding assays with recombinant wild type Dbp2 showed that the protein is an efficient RNA helicase, with strong activity observed particularly with shorter RNA duplexes. The fact that Dbp2 can efficiently unwind RNA *in vitro* also supports the hypothesis that it may act as an RNPase *in vivo*, playing a role in destabilising RNA-protein complexes or facilitating their assembly/disassembly. On contrary, the ATP-binding mutant, which harbours a substitution in motif I that disrupts ATP binding, completely abolished unwinding activity, highlighting the critical role of ATP hydrolysis in Dbp2's biochemical function. These observations align with findings in other DEAD-box ATPases, such as

S. cerevisiae Dbp2 and human DDX5 (Ma et al., 2013; Xing, 2018), suggesting that *S. pombe* Dbp2 likely shares similar RNA duplex unwinding mechanisms. Moreover, the observation that Dbp2 unwinds shorter RNA duplexes more efficiently than longer ones suggests a preference for certain RNA substrates (Figure 2.3.2). The observed preference for shorter RNA substrates may reflect the functional context of Dbp2 *in vivo*, and may be linked to its involvement in specific RNA-protein complexes or its regulation by cellular cofactors. However, the regulation of Dbp2's ATPase activity in the cell may be influenced by other cofactors, signalling events, or post-translational modifications. A more extensive analysis of the *in vivo* characterisation of Dbp2 in the context of RNA-protein complex remodelling and RNA processing was conducted and will be discussed in the following chapters.

Chapter3 Requirement for Dbp2 *in vivo*

3.1 *S. pombe* Dbp2 is essential for cell viability

In order to evaluate transcription-related cellular functions of Dbp2 in fission yeast, a conditional *P.nmt-dbp2* strain was used where the expression of endogenous genomic *dbp2* is under the control of the strong thiamine-repressible promoter (*P.nmt*) (Figure 3.1A). The *nmt1* gene of *S. pombe* is part of the thiamine biosynthetic pathway and highly expressed under thiamine-limiting conditions; in the presence of thiamine, transcription is repressed (Maundrell, 1990). Replacement of endogenous gene promoters with the *nmt* promoter allows to conditionally induce transcriptional shut-off of genes of interest to study the *in vivo* functions of their protein products.

To monitor Dbp2 protein levels, both endogenous and *nmt*-controlled *dbp2* were C-terminally tagged with a myc epitope (Figure 3.1A). To determine the optimal depletion time, Dbp2 levels were examined over a time course following the switch to thiamine-containing rich media and the addition of 15 µM thiamine. Five hours was selected as the time point for downstream analyses, as more than 90% of Dbp2 protein was effectively depleted in whole cell lysates (Figure 3.1B). This confirms that the *nmt* expression system works as expected and can be utilised for further analyses. The effectiveness of the thiamine-induced transcriptional shut-down was also confirmed by gene expression analysis at the global scale, ChIP-seq (RNAPII) (Figure 3.1C) and RNA-seq (transcriptome) (Figure 3.1D). The occupancy of RNAPII at the *dbp2* locus and *dbp2* transcript levels were dramatically reduced upon 9 h and 5 h growth at thiamine-containing conditions, respectively (Figure 3.1C & D). The essentiality of Dbp2 was confirmed in a plate-based growth assay (Figure 3.1E), where metabolic depletion of Dbp2 or Dbp2-3myc under the *P.nmt* promoter led to poor growth on

thiamine-containing medium, confirming that Dbp2 is an essential protein. The poor growth phenotype was rescued when an additional copy of *dbp2-flag* under its endogenous promoter was inserted at an ectopic locus (*leu1*).

Figure 3.1 | Targeting cellular Dbp2 levels by promoter shut-down upon thiamine repression

A. Schematic depiction of the gene structure of *dbp2* in the wild type as well as expressed under the thiamine-sensitive *nmt1* promoter (*P.nmt-dbp2*). C-terminally 3xmyc-tagged versions was used for protein detection. **B.** Western blot for determining Dbp2 protein levels upon a time-course (in hours) after switching the cells to thiamine-containing rich media. Myc antibody is used for detecting Dbp2 levels. GAPDH is used as a loading control. **C.** Genome-wide RNAPII occupancy profiles in the presence and absence of Dbp2, showing the RNAPII recruitment at the *dbp2* gene locus for both wild type and *P.nmt-dbp2* upon growing cells with thiamine-containing rich media for 9 h. ChIP was carried out by Cornelia Kilchert. **D.** RNA-seq transcriptome data for wild type cells and *P.nmt-dbp2* confirms the shut-off of expression of *dbp2*; no transcripts of *dbp2* are detected after a 5 h depletion period. **E.** Ten-fold serial dilutions of the indicated strains were spotted on thiamine-free (EMMG-minimal agar medium) or thiamine-containing (YES-rich agar medium) and incubated at 30 °C for three days. The image is a representative of three independent experiments. Note: Abbreviations are based on suggested nomenclature by the PomBase curators (Ramírez et al., 2023), *P: promoter*

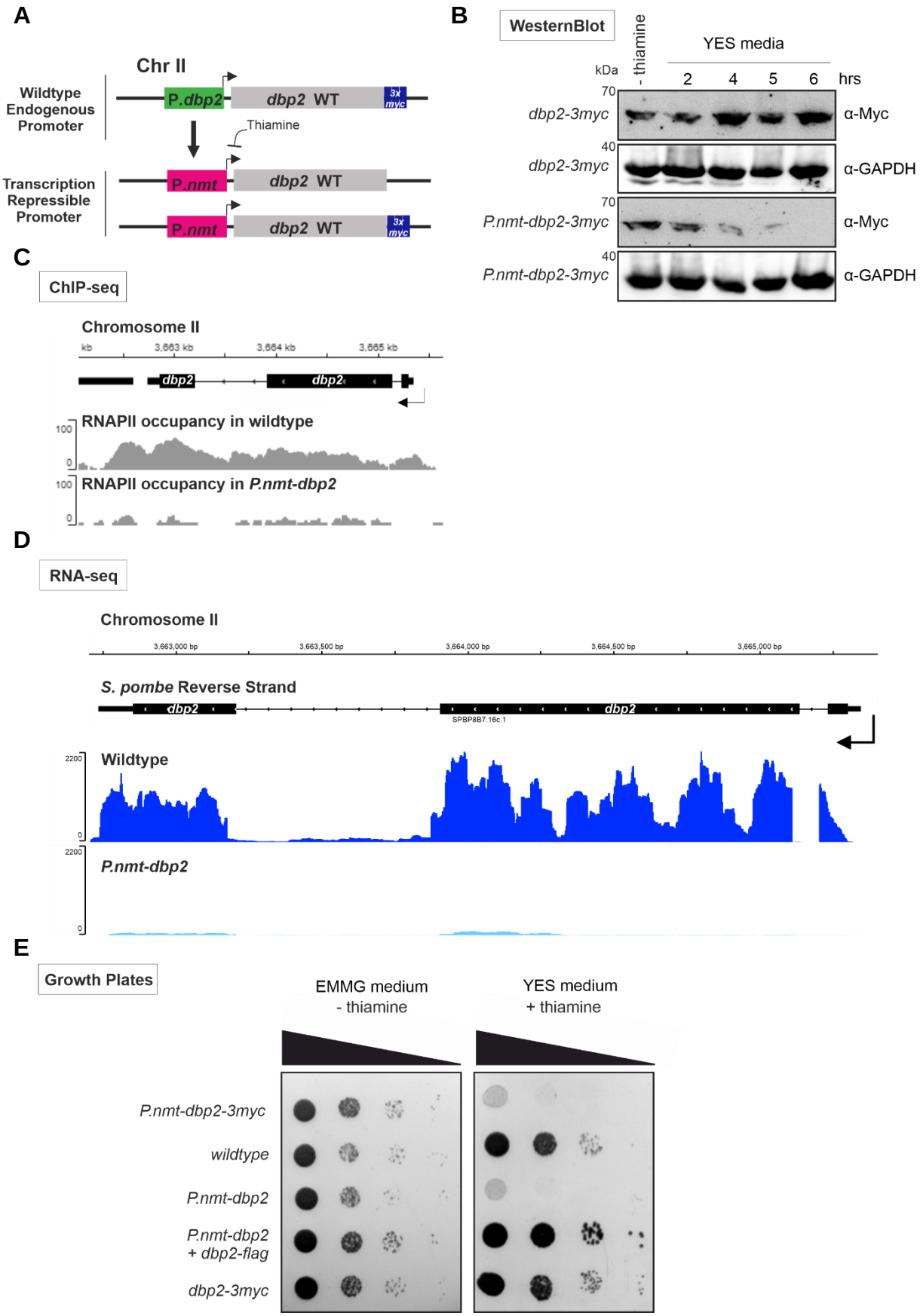
A
Chr II
Wildtype Endogenous Promoter
P.dbp2
dbp2 WT
3x myc
Thiamine
Transcription Repressible Promoter
P.nmt
dbp2 WT
B
WesternBlot
- thiamine
YES media
kDa
2
4
5
6
hrs
70
dbp2-3myc
α-Myc
40
dbp2-3myc
α-GAPDH
70
P.nmt-dbp2-3myc
α-Myc
40
P.nmt-dbp2-3myc
α-GAPDH
C
ChIP-seq
Chromosome II
kb
3,663 kb
3,664 kb
3,665 kb
dbp2
RNAPII occupancy in wildtype
RNAPII occupancy in P.nmt-dbp2
D
RNA-seq
Chromosome II
3,663,000 bp
3,663,500 bp
3,664,000 bp
3,664,500 bp
3,665,000 bp
S. pombe Reverse Strand
SPBP8B7.16c.1
Wildtype
P.nmt-dbp2
E
Growth Plates
EMMG medium
- thiamine
YES medium
+ thiamine
P.nmt-dbp2-3myc
wildtype
P.nmt-dbp2
P.nmt-dbp2
+ dbp2-flag
dbp2-3myc

3.2 Challenges in elucidating Dbp2's ATPase function *in vivo*: due to mutant expression failure

ATP binding and phosphate release dictate the conformational bending of the helicase core, a movement essential for coordinating RNA binding and ATPase activity, and thus central to the function of DEAD-box helicases (Andreou & Klostermeier, 2012). Mutations in the highly conserved motif I (xxxGxG**K**T), highlighted in an orange box in Figure 2.2.1, are known to disrupt ATP binding in DEAD-box ATPases and impair their enzymatic activity (Pause & Sonenberg, 1992). To investigate the functional significance of ATP binding in Dbp2 and gain mechanistic insights, a targeted mutation was introduced, replacing the conserved lysine 172 (K172) residue in motif I with arginine (K172R). This mutation aimed to assess its impact on the enzyme's activity and elucidate how inhibiting ATPase activity might influence Dbp2's roles *in vivo*.

To express both wild type and mutant Dbp2 proteins, a system was used in which ectopic expression of FLAG-tagged Dbp2 variants (*dbp2^{WT} and dbp2^{K172R}*) was integrated at an ectopic *leu1* locus in the genome under the endogenous *dbp2* promoter, in cells where the genomic *dbp2* was under the repressible *nmt1* promoter at its own locus (which only shuts down the gene in the presence of thiamine). Cells were always viable in minimal media lacking thiamine (EMMG), and ectopic expression was induced when shifted to EMMG-LEU (leucine-deficient) medium (Figure 3.2A).

Before proceeding to downstream analyses, initial experiments focused on assessing the expression of wild type and mutant Dbp2. Western blot analysis confirmed successful ectopic expression of the wild type Dbp2 protein (Figure 3.2B). However, the Dbp2^{K172R} mutant did not show a detectable signal by western blot, suggesting a potential issue with the stability or expression of the mutant form. Furthermore, immunofluorescence microscopy was performed using an anti-FLAG antibody to

detect both Dbp2^{WT} and Dbp2^{K172R} mutant. While the wild type Dbp2 showed a clear fluorescent signal within nucleus, indicating successful expression, however yet again no signal was observed for the Dbp2^{K172R} mutant. Overall, these results support the hypothesis that the mutant form of Dbp2 is either not expressed or present at levels below the detection threshold (Figure 3.2B & C), and rule out the possibility of incorporating a mechanistic understanding of Dbp2's enzymatic role in cellular pathways.

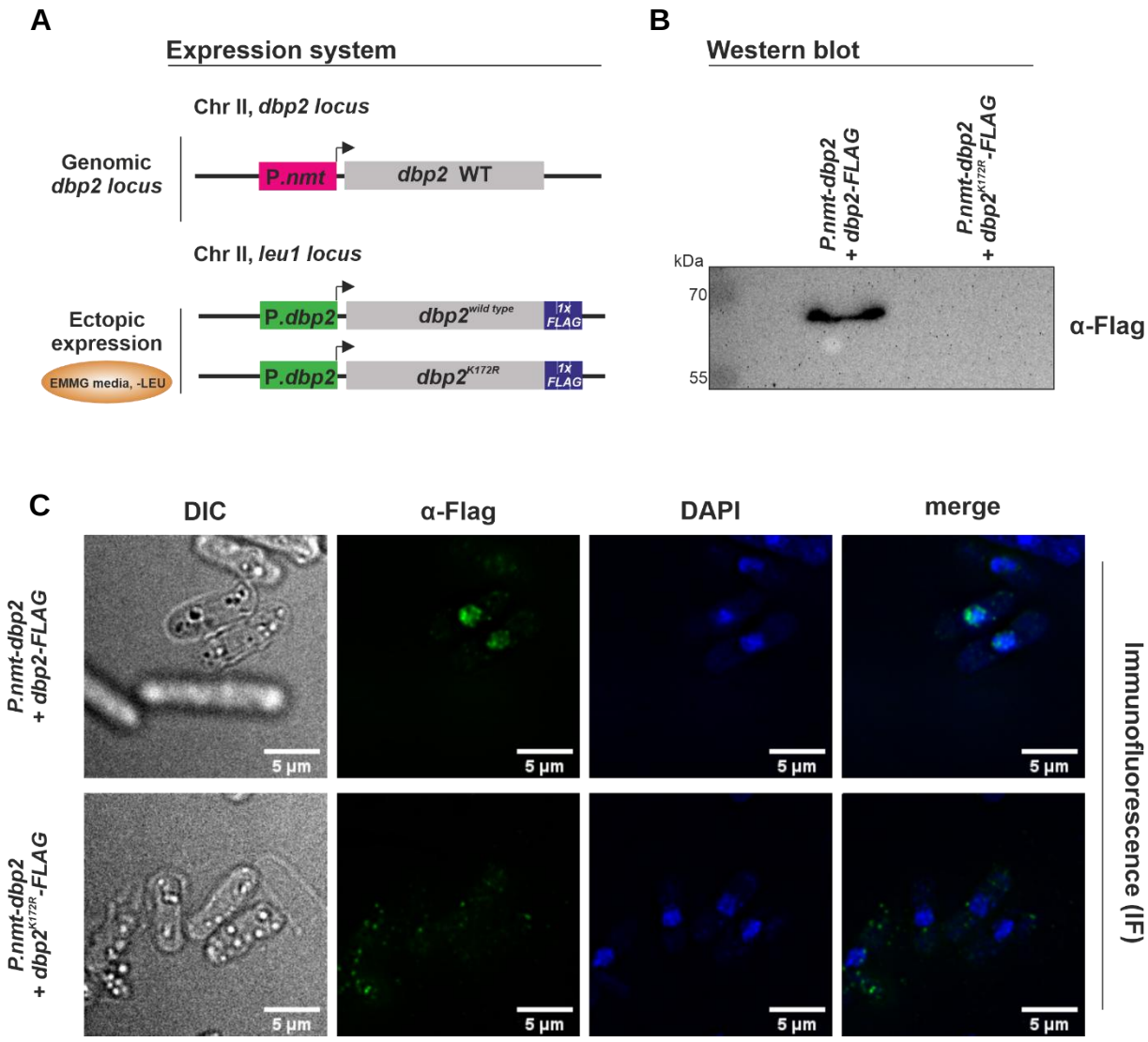

Figure 3.2 | Dbp2-K172R mutant expression fails *in vivo*

A. Schematic representation of the expression system used to assess effects of Dbp2 deletions on cell viability. Cells carry an additional copy of either *dbp2-FLAG* (wild type) or *dbp2^{K172R}-FLAG* (mutant) under its endogenous promoter inserted at an ectopic locus (*leu1*) and endogenous dbp2 is under the nmt1 promoter. **B.** Western blot analysis for Dbp2 protein expression using α-FLAG antibody on cells expressing either wild type Dbp2^{WT} or mutant Dbp2^{K172R}, grown in EMMG-LEU media (n=2). **C.** Immunofluorescence analysis: the image is representative of two independent experiments. Anti-Flag antibody was used in 1:500 dilution, and secondary goat anti-mouse (AF488) antibody in 1:200, grown in EMMG -LEU and DNA compartment counterstained with DAPI.

3.3 Discussion

Dbp2 was confirmed to be essential for cell viability in *S. pombe*. Using the conditional *P.nmt-dbp2* strain, transcriptional repression of *dbp2* effectively depleted Dbp2 protein levels within five hours of thiamine addition. This system enabled the investigation of Dbp2's role in transcription-related cellular functions. The reduction in RNAPII occupancy on the *dbp2* gene locus and *dbp2* transcript levels upon repression demonstrated the functionality of the *P.nmt* promoter and its suitability for studying essential genes. The essentiality of Dbp2 was further validated by the severe growth defects observed under thiamine-repressible conditions, which were rescued by ectopic expression of *dbp2-flag*. These findings highlight Dbp2's critical role, likely in RNA metabolism or other essential processes, and establish the robustness of the *P.nmt* system for the downstream experiments of Dbp2's molecular functions.

One of the aims of this study was to provide mechanistic insights by employing a Dbp2 mutant with a point mutation (K172R) in its conserved motif to inhibit ATP binding and disrupt ATPase activity. This mutant was intended for *in vivo* experiments to examine how the loss of ATPase activity affects mRNP structure and composition. However, despite successful incorporation into the genome, attempts to express the K172R mutant were unsuccessful, as the protein could not be detected by Western blot or

immunofluorescence microscopy. This suggests that the K172R mutation compromises Dbp2's stability through an unknown mechanism. The findings also suggest that ATP binding is critical not only for Dbp2's catalytic activity but also for maintaining its structural integrity, emphasising its dual role in activity and stability. These findings highlight the challenges of studying essential proteins through mutagenesis, as disrupting key catalytic residues often leads to protein instability (Shoichet et al., 1995; Tokuriki et al., 2008). The inability to express the mutant underscores the need for alternative approaches, such as temperature-sensitive alleles, chemical inhibitors, or rescue constructs, to probe Dbp2's ATPase function. Despite this limitation, the study successfully demonstrated Dbp2's essentiality and established a functional depletion system, which was used in this study to assess cellular consequences in Chapter 7.

Chapter4 Genome-wide analysis of Dbp2 in *S. pombe*

4.1 Dbp2 is globally recruited to RNAPII transcribed loci

To characterise a potential function of Dbp2 in early RNA biogenesis in fission yeast, chromatin immunoprecipitation of endogenously C-terminal HTP-tagged Dbp2 followed by sequencing (ChIP-seq) was performed. This analysis included RNAPII (Rpb1 subunit) to identify active transcription sites within the fission yeast genome. This approach allows to evaluate if Dbp2 associates with chromatin and whether these sites correspond to active RNAPII transcription. Additionally, in order to set a stage that would allow in differentiating preferences across transcriptional units, another transcriptional-player— an RNAPII-associated RNA processing factor, serine and arginine-like (SR-like) protein Srp2 (*S. c.* Npl3, *H. s.* SRSF4/5/6), endogenously C-terminal HTP-tagged, which has known roles in splicing and export of mRNAs from nucleus, was also included in the genomic analyses (Klama et al., 2022; Lipp et al., 2015).

Chromatin immunoprecipitation of C-terminally HTP-tagged Dbp2 had confirmed that Dbp2 is recruited to RNAPII-dependent transcription units genome-wide (Figure 4.1A), with a pattern that closely resembles Srp2, and RNAPII itself (Figure 2.4.1, A). For both Dbp2 and Srp2, the extent of recruitment, as determined by linear regression, correlated with the levels of RNAPII at protein-coding genes. This suggests that Dbp2 is recruited to transcribing RNAPII and/or nascent RNA (Figure 4.1B).

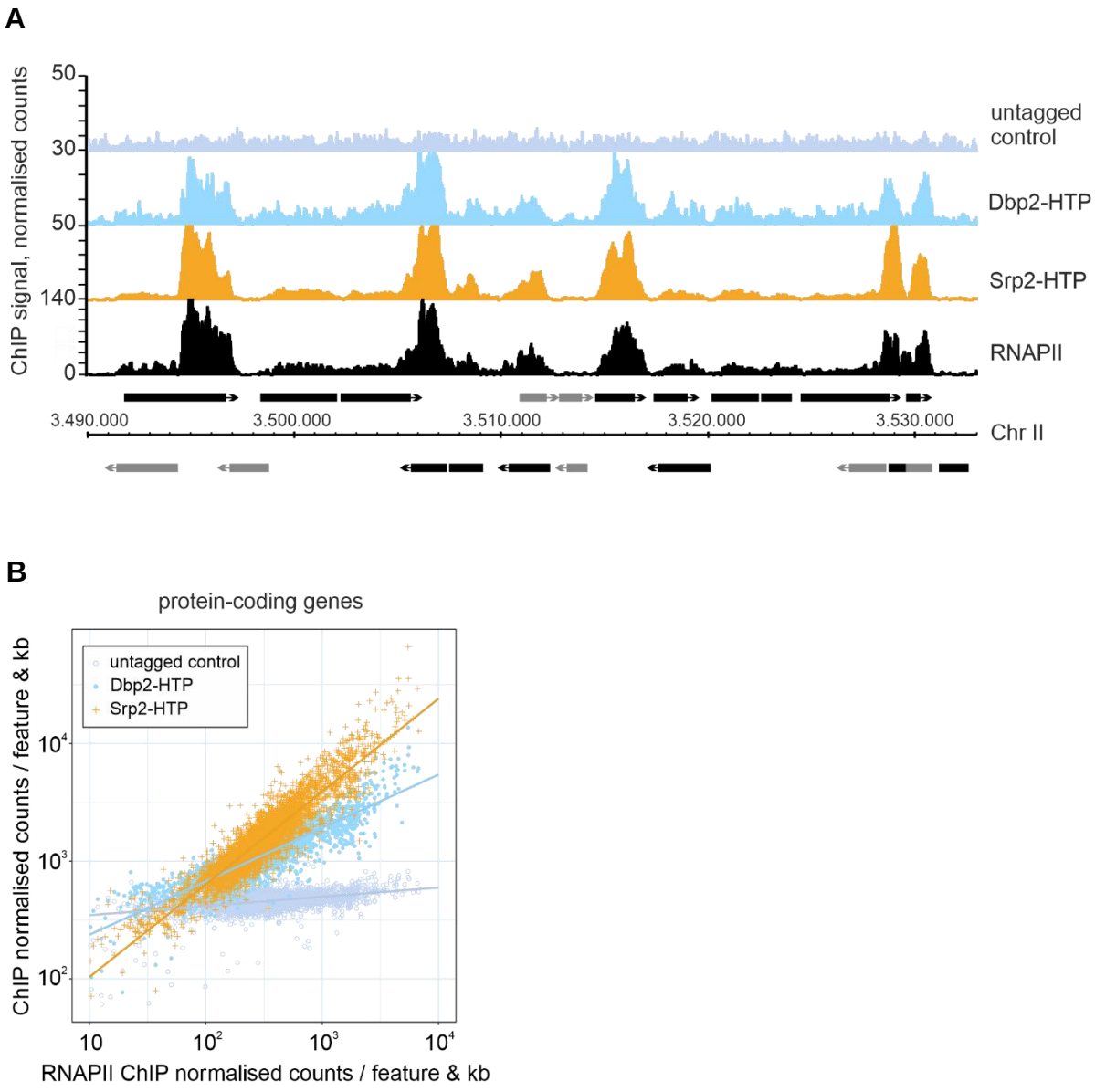

Figure 4.1 | Dbp2 is globally recruited to RNAPII transcribed loci

A. Representative ChIP-seq reads of Dbp2-HTP and Srp2-HTP association with chromatin across a region of *S. pombe* chromosome II. An untagged wild type was included as control. RNAPII-ChIP signal for an isogenic wild type is shown for reference (α-Rpb1, 8WG16) (Kecman et al., 2018; GEO: GSE111326). Positions of protein-coding genes and noncoding genes are indicated in black and grey at the bottom, respectively. **B.** Integrated counts of Dbp2-HTP and Srp2-HTP ChIP-seq signal across protein-coding genes relative to RNAPII, given as average counts per feature and kb * 1,000,000 (n = 3). Only genes with an RNAPII occupancy above a set threshold of 10 normalised counts per feature and kb per million were included. Trendlines were fitted using linear regression. RNAPII ChIP data from Kecman et al., 2018; GEO: GSE111326 (n = 2). ChIP-seq experiments were carried out by Birte Keil for Dbp2-HTP and Srp2-HTP and Cornelia Kilchert for RNAPII.

4.2 Comparative genomic profiling reveals that the recruitment pattern of Dbp2 exhibits a preference of the 3'-ends of genes

Due to the global genomic scale and resolution of the analysis in the previous section, it is not immediately clear whether Dbp2 exhibits a preference in its mapping across transcriptional units. To gain a more detailed understanding of Dbp2's recruitment, a metagene plot was generated to compare the distribution of Dbp2-HTP, Srp2-HTP, and RNAPII across transcriptional units of ribosomal protein genes (RPGs) (Figure 4.2A, upper panel). The metagene analysis were performed against ribosomal protein-coding genes as they are highly expressed, providing strong signal values relative to background noise.

In relation to the mean ChIP-seq coverage of RNAPII, which was found on-site right from the start of transcription until termination, both Dbp2 and Srp2 showed recruitment at similar time during transcription which corresponded to within gene bodies and that their coverage showed gradual increase along gene bodies. However, while the Srp2-HTP coverage exhibited a peak within the gene body and decreased towards the end of the genes, Dbp2's coverage continued to rise until it reached its peak after the cleavage and polyadenylation site (CPA). The metagene analysis had revealed that Dbp2 maps primarily to the 3'-end of genes in the termination window, compared to Srp2 that mapped to gene bodies (Figure 4.2A, upper panel). Furthermore, the peak of Dbp2 at the termination window coincides with the terminating RNAPII (RNAPII^{Ser2P}), as shown by publicly available ChIP-seq data. This data, derived from an isogenic wild type strain, includes analysis of RNAPII and its different post-translationally modified versions of the CTD, which were analysed in the same manner (Kecman, Heo, et al., 2018) (Figure 4.2A, lower panel). This result suggests a function for Dbp2 during RNAPII transcription, particularly at the 3'-end of genes.

When publicly available data on factors involved in 3'-end maturation and termination of RNAPII transcription—such as CFIA cleavage factors Pcf11 and Rna14, CPAC-interacting termination factor Seb1, Ysh1/CPSF73 endonuclease, and Dhp1/Rat1/XRN2 torpedo exoribonuclease—are analysed the same way in relation to RPG transcriptional units, they show a significant peak at the termination zone (Figure 4.2B). Notably, the binding profiles of these factors are nearly identical, suggesting their simultaneous recruitment in this zone, except for Ysh1, which shows an additional slight peak early in transcription. In comparison, Dbp2 recruitment begins within gene bodies and peaks at the termination window, overlapping with the peaks of these factors. This result suggests Dbp2 and these factors may interact in this window, which may influence Dbp2's activity.

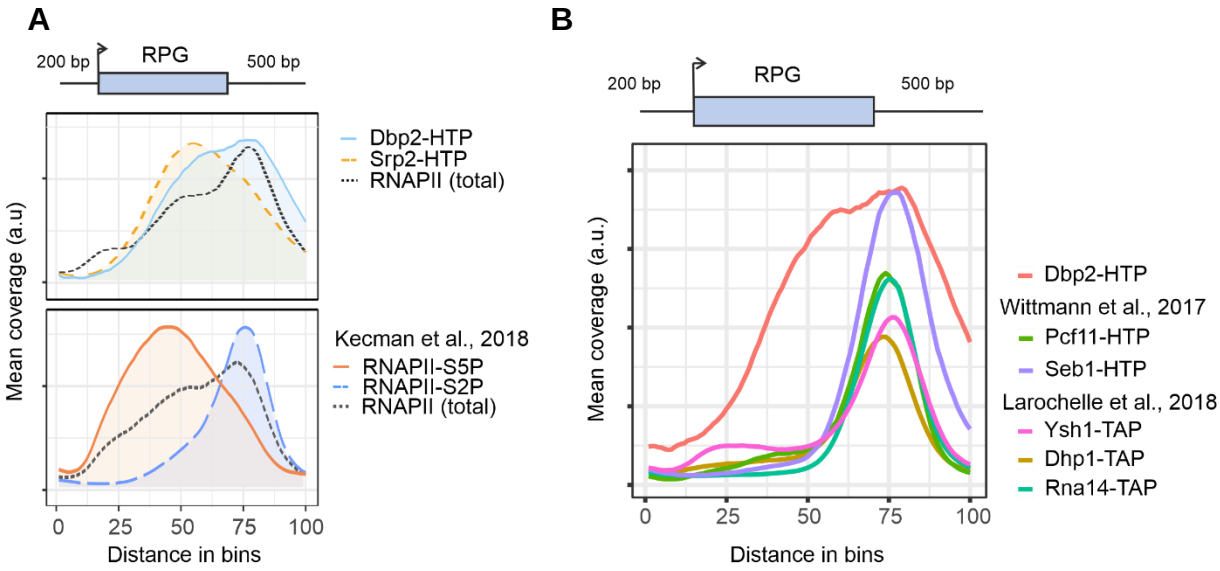

Figure 4.2 | Comparative genomic profiling: Dbp2 is associated with terminating RNAPII

A. Metagene analysis of mean ChIP-seq coverage of Dbp2-HTP and Srp2-HTP (n = 3), and total RNAPII (α-rpb1 (8WG16) in Dbp2-3myc; n = 2) (upper panel) across ribosomal protein genes (RPGs) including 200 bp upstream and 500 bp downstream of the annotated transcription units. Mean coverage given in arbitrary units; to compensate for differences in ChIP capability, mean coverage was adjusted by a constant scaling factor. ChIP-seq experiments were carried out by Birte Keil for Dbp2-HTP and Srp2-HTP and Cornelia Kilchert for RNAPII. Total Rpb1, Rpb1-S5P, and Rpb1-S2P ChIP for an isogenic wild type (n = 2) are included as reference (lower panel; data from Kecman et al., 2018; GEO: GSE111326). Schematic of the gene above the plot corresponds to an RPG of median length. **B.** Metagene analysis of mean ChIP-seq coverage of Dbp2-HTP, Pcf11-HTP, Seb1-HTP, Ysh1-TAP, Dhp1-TAP and Rna14-TAP across ribosomal protein genes (RPGs) (Pcf11-HTP and Seb1-HTP data from Wittmann et al., 2017), n = 2 and (Ysh1-TAP, Dhp1-TAP and Rna14-TAP data from (Larochelle et al., 2018 n=1), n=1.

4.3 Discussion

The genome-wide analysis of Dbp2 in *S. pombe* reveals a dynamic recruitment pattern that links its activity to RNAPII transcriptional processes. The ChIP-seq data presented in this chapter provide compelling evidence that Dbp2 is globally recruited to RNAPII-transcribed loci, indicating its association with active transcription units across the genome. Importantly, the recruitment pattern of Dbp2 aligns closely with RNAPII and the SR-like protein Srp2, reinforcing the idea that Dbp2 is functionally integrated into RNA biogenesis pathways.

The comparative analysis of Dbp2 and Srp2 recruitment provides insights into the distinct roles these factors may play during transcription. Both proteins exhibit increasing association along gene bodies; however, the divergence in their recruitment patterns becomes apparent at the 3'-ends of genes. Srp2 peaks within gene bodies and declines toward gene termination, consistent with its known roles in splicing and mRNA export. In contrast, Dbp2's association continues to rise, peaking in the termination window after the cleavage and polyadenylation site (CPA). This finding suggests that Dbp2 may function during or after termination window, aligning its activity with RNAPII post-transcriptional events.

The metagene analysis of ribosomal protein genes (RPGs), chosen for their robust transcriptional activity and high signal-to-noise ratio, reinforces this conclusion that Dbp2 shows preferential recruitment at the 3'-end of genes, coinciding with terminating RNAPII marked by RNAPII^{Ser2P}. This observation aligns Dbp2 with termination-specific factors such as Pcf11, Rna14, and Seb1, known to facilitate 3'-end processing and RNAPII release. Interestingly, while Dbp2 recruitment initiates within gene bodies, its peak at the termination zone suggests a dual role: it may associate with RNAPII during

elongation but is primarily activated or required during termination. This hypothesis is supported by the temporal overlap between Dbp2 recruitment and the activities of 3'-end processing factors.

Dbp2's functional association with the transcription termination machinery raises intriguing possibilities regarding its molecular role. DEAD-box ATPases are known to facilitate RNA remodelling, which is essential for the dynamic rearrangement of mRNP complexes. The peak of Dbp2 at the termination zone suggests that it could be involved in remodelling nascent RNA or RNA-protein complexes to ensure efficient 3'-end processing. For instance, Dbp2 might assist in the release of terminated RNAPII, stabilise cleaved RNA, or prepare the transcript for export by contributing to mRNP maturation. Additionally, the resemblance between Dbp2's recruitment profile and those of termination-specific factors such as Seb1 and Dhp1/Rat1/Ysh1 suggests that Dbp2 may interact with or function alongside these proteins. It is possible that Dbp2's helicase activity facilitates transcript release or degradation of improperly processed RNA, contributing to RNA quality control mechanisms at the 3'-end of genes.

The results presented in this chapter suggest a model in which Dbp2 plays a significant role in transcription termination and RNA processing at the 3'-end of genes. By associating with transcribing RNAPII and peaking in the termination window, Dbp2 emerges as a potential regulator of RNA biogenesis, with its activity likely coupling transcription termination to downstream RNA processing events. These findings contribute to a broader understanding of the molecular mechanisms coordinating transcription and RNA maturation in eukaryotic cells. The following chapters will provide an in-depth dissection of the precise molecular function of Dbp2 during the transcription termination window.

Chapter5 Proteomics analysis of Dbp2 in *S. pombe*

5.1 Comparative interactome profiling correlates with genome-wide analysis: RNAPII holoenzyme complex copurifies with both proteins

To further characterise Dbp2's role in early RNA biogenesis, identifying its protein interactors is crucial. In this analysis, the Srp2 protein was included once more as a reference, offering an additional point of comparison within the same cellular compartment. Such an analysis complements the genomic studies by providing an additional perspective through comparative protein interactome profiling of Dbp2 and Srp2.

To achieve this, a two-step tandem affinity purification (TAP) approach was employed, wherein each protein was C-terminally HTP-tagged (His_6-TEV-ProteinA) and subsequently purified (Figure 5.1A). Since members of the DEAD-box family of ATPases are known for their weak and transient interactions (Montpetit et al., 2011), mild cross-linking conditions were employed to stabilise potential protein-protein interactions involving Dbp2 and its regulators prior to lysate preparation. Specifically, cells were treated with 0.01% formaldehyde for 10 minutes in culture (Figure 5.1B). Following purification, the eluates were analysed by mass spectrometry to identify co-purified proteins, providing insights into Dbp2's interaction network.

To assess the similarity between the interactome data of both protein purifications, a correlation plot was generated using the log2 mean MS intensities. Consistent with the ChIP-seq results, the proteomic analysis correlated with the genome-wide data, showing that Dbp2-HTP and Srp2-HTP co-purified components of the RNAPII holoenzyme complex, and notably, in similar amounts (Figure 5.1C). The co-

purification of RNAPII, including its Ser5- and Ser2-phosphorylated forms, was further validated by Western blot analysis (Figure 5.1D).

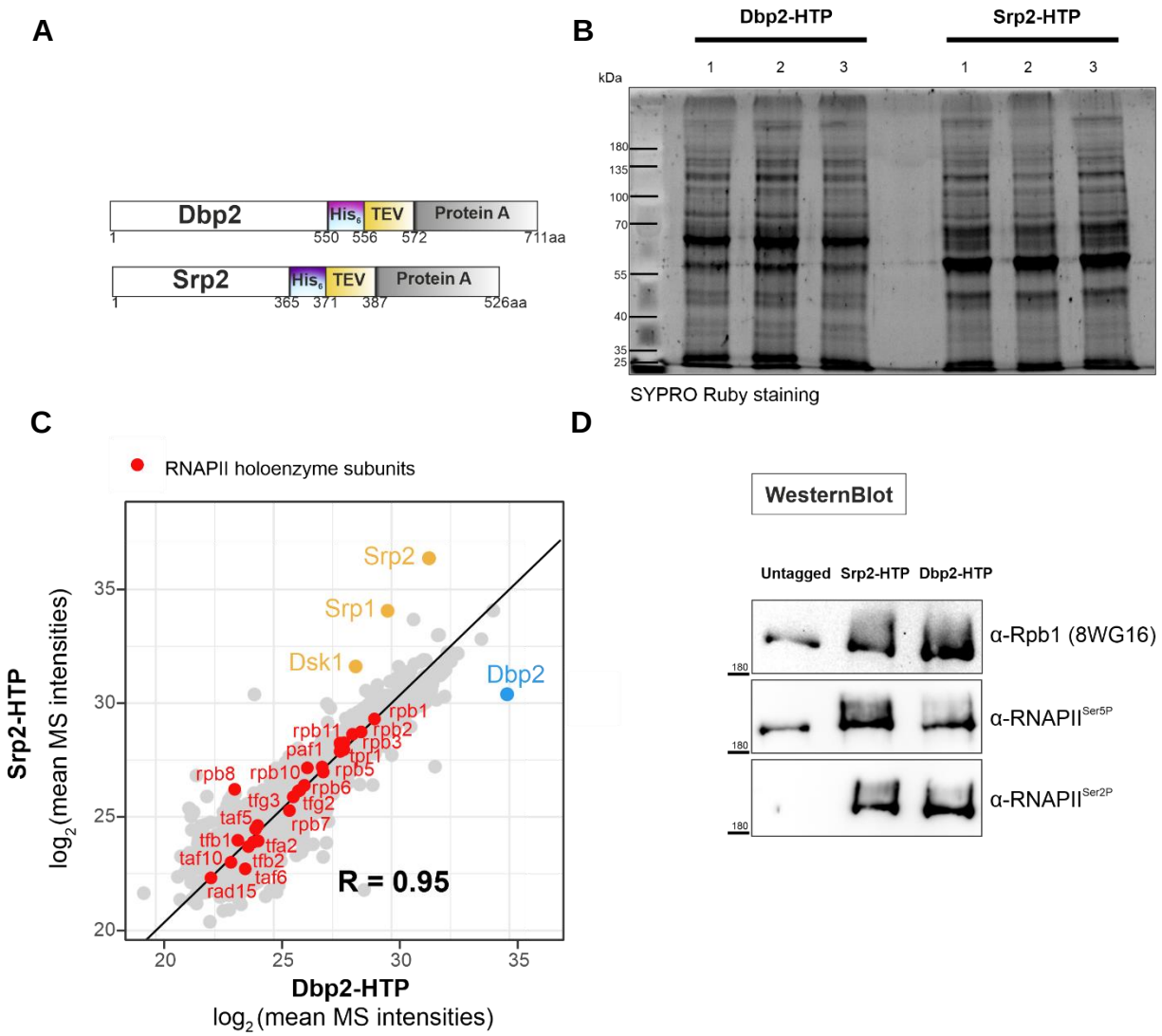

Figure 5.1 | Purification of Dbp2 and Srp2 using HTP as tandem affinity tag: RNAPII holoenzyme complex copurifies with both Dbp2 and Srp2

A. Depiction of constructs for protein purification; endogenous Dbp2 and Srp2 were C-terminally tagged with HTP (His_6-TEV cleavage site-ProteinA). **B.** Eluates of cross-linking HTP purifications of Dbp2-HTP and Srp2-HTP were resolved on 10% SDS-PAGE and stained with SYPRO Ruby. The experiment was carried out with three biological replicates. **C.** Mass spectrometry (MS) analysis of the comparative interaction profiling of Dbp2 and Srp2. Mean protein intensities (log2) recovered in the Dbp2-HTP and Srp2-HTP purifications. Components of the RNAPII holocomplex (GO:0016591) are marked in red, Srp2 and known interactors in orange, and Dbp2 in light blue. Pearson correlation coefficient was calculated as R=0.95 for RNAPII holoenzyme components co-purified with either proteins. Mass spectrometry was carried out in the laboratory of Timo Glatter at the MPI TerMic, (n = 3). **D.** Western blot analysis of Dbp2-HTP and Srp2-HTP eluates using antibodies against hypophosphorylated-RNAPII (8WG16) or Rpb1 with a phosphorylated C-terminal domain, namely Ser5P (α-RNAPII^{Ser5P}) and Ser2P (α-RNAPII^{Ser2P}) in comparison to a control purification from an untagged strain.

5.2 The late RNAPII^{Ser2P} kinase CTDK preferentially co-purifies with Dbp2

Further analysis of the comparative interaction data of Dbp2 and Srp2 purifications revealed a preferential enrichment of the cyclin-dependent kinases (CDKs) that mediate the phosphorylation of RNAPII and Spt5. The phosphorylation of RNAPII CTD and Spt5 occurs in a sequential fashion, which ultimately governs RNA processing (Bowman & Kelly, 2014; Sansó & Fisher, 2013).

P-TEFb (Cdk9/Pch1 in *S. pombe*), an early RNAPII^{Ser2P} kinase complex with strong links to pre-mRNA splicing that has been implicated in the transition from initiation to productive transcription elongation, was significantly enriched in the Srp2-HTP purification. On the contrary, the kinase complex CTDK (Lsk1/Lsc1) responsible for the late RNAPII^{Ser2P} (Bowman & Kelly, 2014), corresponding to the 3'-ends, was preferentially co-purified with Dbp2-HTP (Figure 5.2A & B). In both purifications, only very low levels yet comparable amounts of TFIIH complex were detected. TFIIH is a complex associated with very early phosphorylation marks of transcription, RNAPII^{Ser5P} and RNAPII^{Ser7P} (Akhtar et al., 2009), and having none of the kinase complex components Mcs6/Mcs2 in either purification. This finding provides additional backing for a temporal discrepancy within transcription, and that the recruitment of Srp2 and Dbp2 to transcribing RNAPII occurs after the clearance of the promoter. This aligns with the ChIP-seq profiles, which reveal limited concurrence between chromatin-associated Srp2 and Dbp2 with the promoter-associated RNAPII peak.

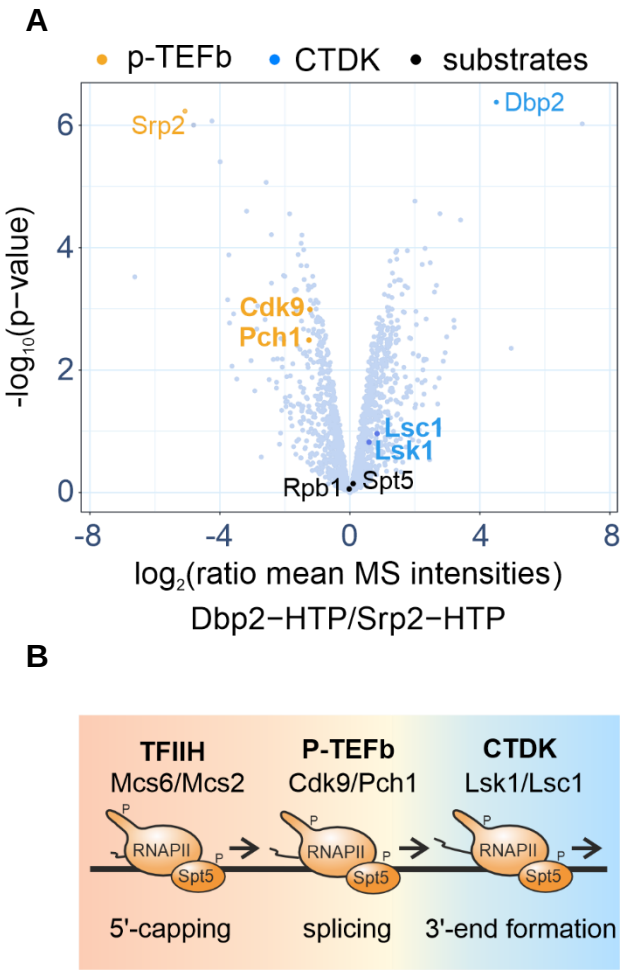

Figure 5.2 | The late RNAPII^{Ser2P} kinase CTDK preferentially co-purifies with Dbp2

A. Relative enrichment of cyclin-dependent kinase (CDK) complexes co-purifying with Dbp2 and Srp2. In the volcano plot, p-values (−log10, moderated Student's t-test) are plotted against the relative enrichment of proteins in the purification of Dbp2-HTP relative to Srp2-HTP based on mean protein intensities (log_2) (n = 3). The P-TEFb- and CTDK-associated CDK/cyclin pairs are marked in yellow and blue, respectively. The CDK substrates Rpb1 and Spt5 are marked in black. **B.** Schematic of the CDK-dependent transcription cycle in fission yeast. In the presence of its cognate cyclin, Mcs2, the TFIIH-associated CDK Mcs6 phosphorylates S5P of the RNAPII CTD and Spt5 at the promoter to recruit capping factors. The activity of PTEFb and its associated CDK/cyclin pair Cdk9/Pch1 is linked to promoter release and splicing. A second S2P-specific CDK complex, CTDK, promotes cleavage and polyadenylation and transcription termination at the 3'-end of genes. Adapted from (Sansó & Fisher, 2013).

5.3 Comparative interaction profiling reveals that Dbp2 is associated with late RNA processing events

The modest 5’ to 3’ shift in the chromatin association patterns of Srp2-HTP and Dbp2-HTP had already suggested a temporal offset in their recruitment to transcribing RNAPII. The comparative interactome data showed a high correlation in the amounts of RNAPII holoenzyme complex components present in both Dbp2 and Srp2 purifications, further suggesting that both proteins are found in the same compartment. Consequently, the co-purification of the transcription machinery along with major co-transcriptional RNA processing complexes, including capping factors, the spliceosome, and the 3’-end processing machinery, was expected in both Dbp2 and Srp2 purifications. To further investigate, the comparative interactome data was analysed to determine whether any known co-transcriptional RNA processing complexes were preferentially enriched in either purification.

In agreement with the proposed function of Srp2 as a splicing regulator, splicing factors and the exon junction complex (EJC), as well as other early transcriptional processing complexes, namely cap-binding complex and mRNA packaging factors, were enriched in the Srp2-HTP purification. Late RNA processing complexes, including 3’-end formation factors and late export factors such as Mlo3, Mlo1, and Mex67, preferentially co-purified with Dbp2-HTP. This finding aligns with Dbp2's involvement during the late stages of the transcription cycle. Additionally, components of the exosome targeting cofactor complex, MTREC, were more enriched in the Dbp2-HTP purification (Figure 5.3A). Overall, the comparative proteomics data correlates with the genomic data suggesting that Dbp2 has a role at the late steps of the transcription cycle.

A

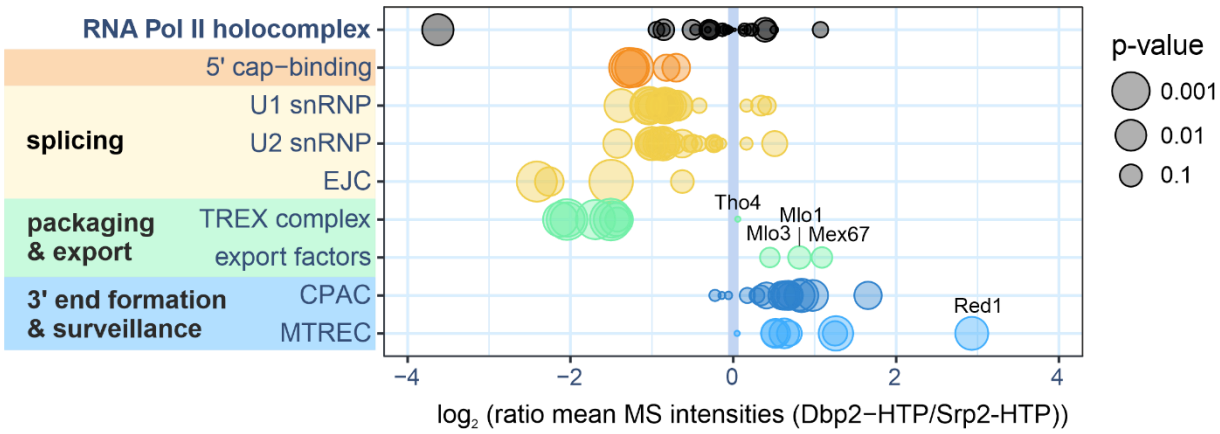

Figure 5.3 | Comparative interaction profiling: Dbp2 preferentially associates with 3'-end formation factors and the nuclear RNA surveillance machinery

A. Relative enrichment of various RNA processing complexes in the comparative interaction profiling of Dbp2 and Srp2 (log2) (n=3). Size of the circles reflects P-values (−log10, moderated Student's t-test). snRNP – small nuclear ribonucleoprotein. EJC – exon junction complex. CPAC – cleavage and polyadenylation complex. MTREC – Mtl1-Red1 core. Annotations were retrieved from Ensemble Fungi using the following GO terms: RNAPII holocomplex - GO:0016591; U1 snRNP - GO:0005685; U2 - GO: snRNP – GO:0005686; mRNA cleavage factor complex - GO:0005849. Export factors: Mex67, Mlo1 and Mlo3.

5.4 Dbp2 associates with export factors

The comparative interactome profiling revealed an intriguing difference in the preferential enrichment of RNA processing factors associated with mRNA export between Srp2 and Dbp2 purifications. In budding yeast, Sub2 (Uap56 in *S. pombe* and humans) and Yra1 (annotated as Mlo3 in *S. pombe*, Aly/REF in humans) together with the THO complex, a nuclear complex required for transcription elongation, form the TREX complex ('TRanscription/EXport'). The TREX complex, an RNA packaging complex suggested to couple mRNA transcription to mRNA export to the cytoplasm (Jimeno et al., 2002; Sträßer et al., 2002), was significantly enriched in the Srp2-HTP purification, with the exception of Tho4, the RNA export adaptor which is homologous to the human TREX component AlyREF/THOC4 (Figure 5.4A).

S. pombe possesses a second AlyREF/THOC4 protein, Mlo3, which was relatively enriched in the Dbp2-HTP purification, along with Mlo1 (homologue of human SARNP/CIP29 and MOS11 in plants) and the mRNA export receptor Mex67/NXF1 (Figure 5.4A).

A

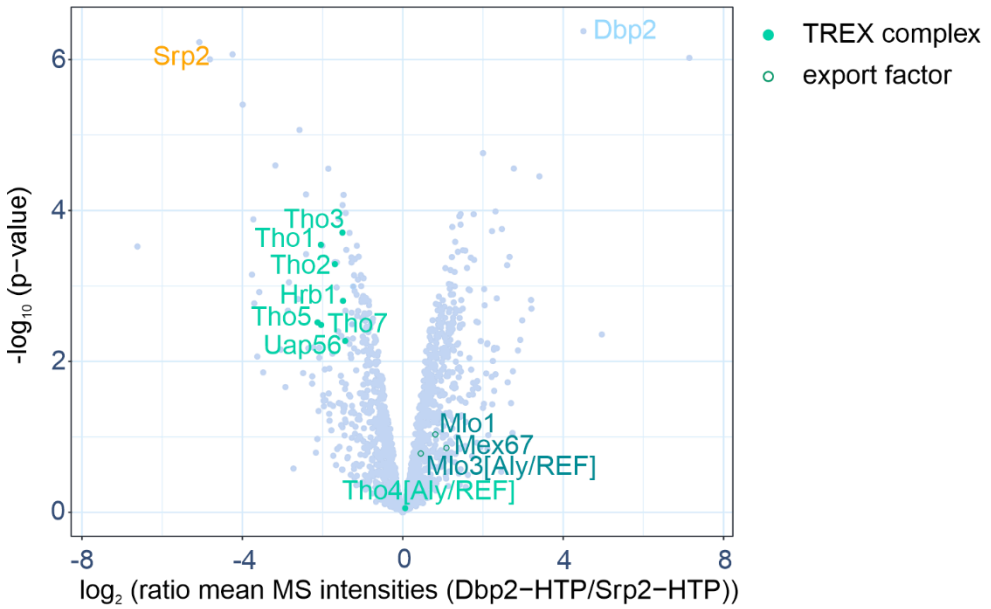

Figure 5.4 | Dbp2 associates with export factors

A. Mass spectrometry (MS) analysis of the comparative interaction profiling of Dbp2 and Srp2 labelled in blue and orange, respectively. In the volcano plot, P-values (−log10, moderated Student's t-test) are plotted against the relative enrichment of proteins in the purification of Dbp2-HTP relative to Srp2-HTP based on mean protein intensities (log2) (n=3). Volcano plots of individual proteins from known TREX complex and selected export factors (export factors: Mex67, Mlo1 and Mlo3) are labelled in green and dark green, respectively.

5.5 Dbp2 co-purifies type I protein arginine N-methyltransferase (PRMT) Rmt1 the most

The protein that was most highly enriched in the purification of Dbp2-HTP was the type I protein arginine N-methyltransferase (PRMT1) Rmt1 (Figure 5.5A). PRMT1 proteins have a strong preference for methylating short motifs such as RGG/RG (Roméo Sébastien Blanc et al., 2017; Thandapani et al., 2013). Furthermore, non-crosslinking

co-immunoprecipitation experiments with Rmt-3HF and Dbp2-HTP further confirmed that Dbp2 and Rmt1 can be pulled as part of a complex that is insensitive to RNase A treatment, supporting an interaction between Dbp2 and Rmt1 that does not require RNA for its formation or stabilisation (Figure 5.5B). The human orthologue DDX5 was reported to be arginine methylated by PRMT5 at its C-terminal RGG motif, which has been linked to R-loop suppression (Mersaoui et al., 2019).

PRMTs catalyse the transfer of a methyl group from S-adenosylmethionine (SAM) to the guanidino nitrogen atoms of arginine. There are three kinds of methylarginines in eukaryotes: mono-methyl arginine (MMA), asymmetric dimethylarginine (aDMA), and symmetric dimethylarginine (sDMA). PRMTs fall into three types based on their catalytic activity: type I (PRMT1, PRMT2, PRMT3, PRMT4, PRMT6, and PRMT8), type II (PRMT5 and PRMT9) and type III (PRMT7). All types can catalyse the initial monomethlyation step; however, type I enzymes process mono-methyl arginine to an asymmetric dimethylarginine (ADMA), whereas type II enzymes produce a symmetric dimethylarginine (sDMA) (Roméo S. Blanc & Richard, 2017; Qualmann & Kessels, 2021).

In *S. pombe,* the poly(A)-binding protein and MTREC/PAXT component Pab2 (PABPN1 in humans) was shown be asymmetrically methylated by Rmt1 on its C-terminal arginine-rich domain, which has been described to regulate its oligomerisation (Perreault et al., 2007). To investigate whether Dbp2 is also asymmetrically methylated by Rmt1, I proceeded to generate an *rmt1* deletion strain; in *S. pombe*, Rmt1 is not essential for cell survival and can be deleted from the genome. At the same time, we sought to reproduce previously published data on Pab2. Early attempts to generate *rmt1Δ* strains revealed variations in Pab2 methylation status in the absence of Rmt1. Only one clone of *rmt1Δ* recapitulated the published result, showing the loss of

asymmetrical dimethylation of Pab2 after co-immunoprecipitation of Pab2 in the presence and absence of Rmt1. Nevertheless, co-immunoprecipitation of Dbp2 showed that the asymmetrical dimethylation status of Dbp2 was maintained in the absence of Rmt1 in all clones tested (Appendix 1). *S. pombe* has more than one PRMT protein, namely Rmt1, Rmt2, Rmt3 and Skb1 (PRMT5 in humans), suggesting that several PRMT may act redundantly to asymmetrically dimethylate Dbp2, comparable to the case of human PABPN1, which is dimethylated at arginines by PRMT1 and PRMT3 *in vitro* (Kölbel et al., 2009).

In the Srp2 purification, its known interactors, the SR family protein Srp1 (SRFS2 in humans) and the SR protein-specific kinase Dsk1 (SRPK1/2/3 in humans and Sky1 in budding yeast) (Lipp et al., 2015; Z. Tang et al., 1998) were significantly enriched. Interestingly, Rpb8 (POLR2H in humans), the eukaryote-specific and shared component among of the holoenzyme complexes of RNAPI, II and III, was moderately enriched in the Srp2 purification, suggesting a direct protein-protein interaction between Srp2 and Rbp8.

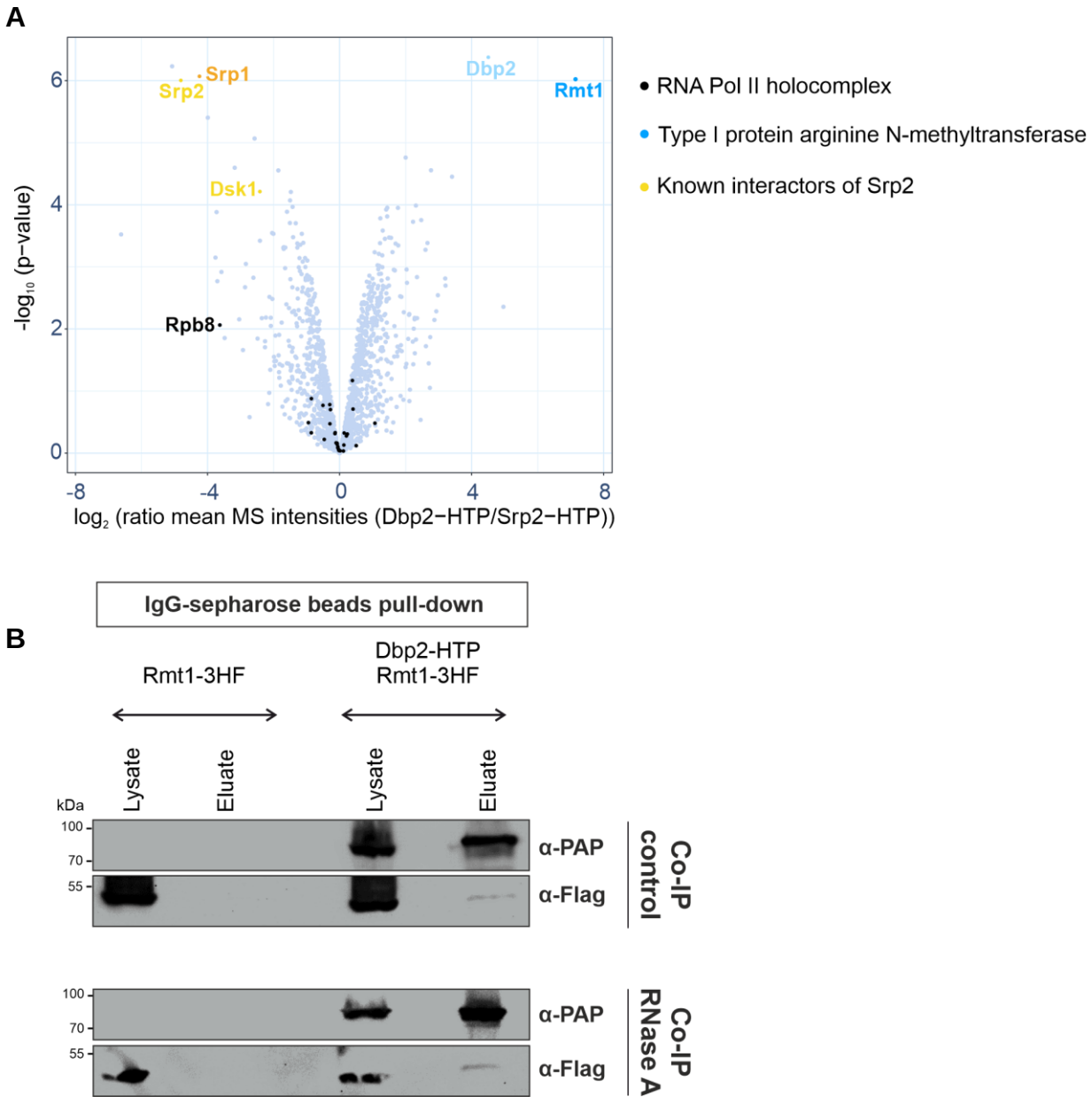

Figure 5.5 | Dbp2 co-purifies type I protein arginine N-methyltransferase (PRMT) Rmt1

A. Mass spectrometry (MS) analysis of the comparative interaction profiling of Dbp2 and Srp2 labelled in blue and orange, respectively. In the volcano plot, p-values (−log10) are plotted against the relative enrichment of proteins in the purification of Dbp2-HTP relative to Srp2-HTP based on mean MS intensities (log2) (n=3). Components of the RNAPII holocomplex (GO:0016591) are marked in black, Srp2 and known interactors in orange, and Dbp2 light blue and its potential direct interactor Rmt1 in darker blue. **B.** Western blot analysis of co-immunoprecipitation (Co-IP) of endogenously HTP-tagged Dbp2 with Rmt1-3HF (3xHA-3xFlag) using IgG sepharose beads. Bound fractions were probed with PAP antibody to detect the Protein A tag on Dbp2 and Flag antibody for Rmt1-specific signal. Control IPs were performed in the absence of the tagged bait protein. For RNase-treated samples, lysates were incubated in the presence of 0.05 mg/ml RNase A at RT for 30 mins prior to IP.

5.6 RSC and FACT complexes showed a strong preference for co-purifying with Dbp2

The RSC (remodels structure of chromatin) complex is a DNA-dependent ATPase complex essential for mitotic growth and the most abundant chromatin remodelling complex in budding yeast, being at least 10-fold more abundant than SWI/SNF (Cairns et al., 1996). RSC and SWI/SNF are related ATP-dependent chromatin remodelling complexes that are both able to slide nucleosomes along DNA, driving conformational rearrangements in nucleosomes, and disengaging histones from DNA (Clapier & Cairns, 2009). RSC is involved in transcription regulation and the removal of nucleosomes to form and maintain nucleosome-depleted regions (NFRs) (Hartley & Madhani, 2009). In the comparative interactome data, RSC showed a strong preference for co-purifying with Dbp2-HTP, with the RSC-specific essential subunits Snf21, Rsc7 and Rsc9 significantly enriched.

The histone chaperone FAcilitates Chromatin Transcription (FACT) complex is associated with transcribed genes *in vivo* and is reported to enhance transcription by destabilising nucleosomes through H2A/H2B dimer displacement, thereby promoting RNAPII progression on chromatin templates (Belotserkovskaya et al., 2003; Pavri et al., 2006; Saunders et al., 2003). Interestingly, the chromatin-reorganising complex FACT was reported to solve R-loop-mediated transcription–replication conflicts both in budding yeast and human (Herrera-Moyano et al., 2014). FACT is composed of two subunits, Spt16/SPT16 and Pob3/SSRP1 (in both yeast models/humans). In addition to the RSC chromatin remodelling complex, both components of the FACT complex, were also modestly enriched in the Dbp2-HTP purification.

A

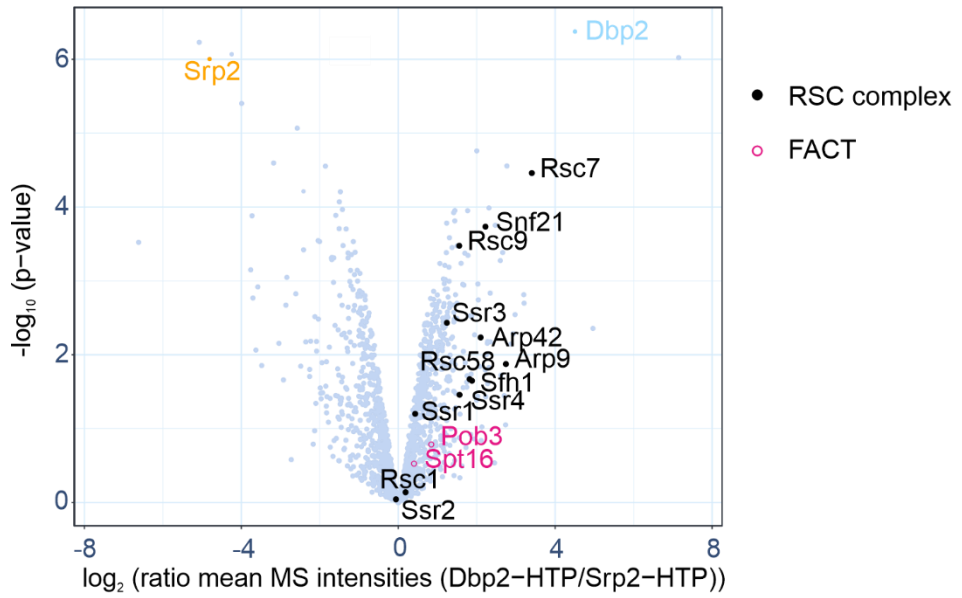

Figure 5.6 | RSC complex shows a strong preference in the Dbp2 purification

A. Mass spectrometry (MS) analysis of the comparative interaction profiling of Dbp2 and Srp2 labelled in blue and orange, respectively. In the volcano plot, p-values (−log10, moderated Student's t-test) are plotted against the relative enrichment of proteins in the purification of Dbp2-HTP relative to Srp2-HTP based on mean protein intensities (log2) (n=3). Components of the RSC complex (GO:0016586) and FACT are labelled in black and magenta, respectively.

| SWI/SNF and RSC components in *S. pombe* based on Monahan et al., 2008

SWI/SNF	RSC
arp42	arp42
arp9	arp9
snf22	rsc1
snf30	rsc4
snf5	rsc58
snf59	rsc7
sol1	rsc9
ssr1	ssr1
ssr2	ssr2
ssr3	ssr3
ssr4	ssr4
tfg3	sfh1
	snf21

5.7 Non-crosslinking validation of protein purification data

Mild crosslinking interactome data revealed interactions between Dbp2 and 3'-end formation factors. To validate these interactions with co-purifying proteins, non-crosslinking co-immunoprecipitation experiments were conducted. The interactions between Dbp2 and the components of the 3'-end formation machinery, namely CFIA components (Rna15 and Pcf11) as well as the CFIB component (Msi2), were confirmed by co-immunoprecipitation using GFP-TRAP magnetic beads as shown in Figure 5.7A, although the interaction with Pcf11 was quite weak. Furthermore, the arginine/serine-rich splicing factor Ydc1 (SPAC25G10.01), a homologue of TRA2B/SFRS10 in humans, was recently shown to possess RNA-binding activity in an RNA-protein interactome capture experiment (Kilchert et al., 2020). Expectedly, Ydc1, a probable factor in splicing compartment, displayed preferential enrichment in Srp2 purification (Figure 5.7B). However, the interaction between Dbp2-HTP and Ydc1 was also validated by co-immunoprecipitation (Figure 5.7C). Notably, Dbp2 and Ydc1 were co-immunoprecipitated reciprocally, though the co-precipitation was reduced by RNase A treatment, indicating that the interaction is RNA-mediated (Figure 5.7D). The interaction of Dbp2 with the splicing factor Ydc1 suggests a functional connection between splicing and later RNA processing steps mediated by Dbp2. The RNA-dependent nature of the Dbp2-Ydc1 interaction highlights the dynamic nature of RNA-protein interactions in these processes.

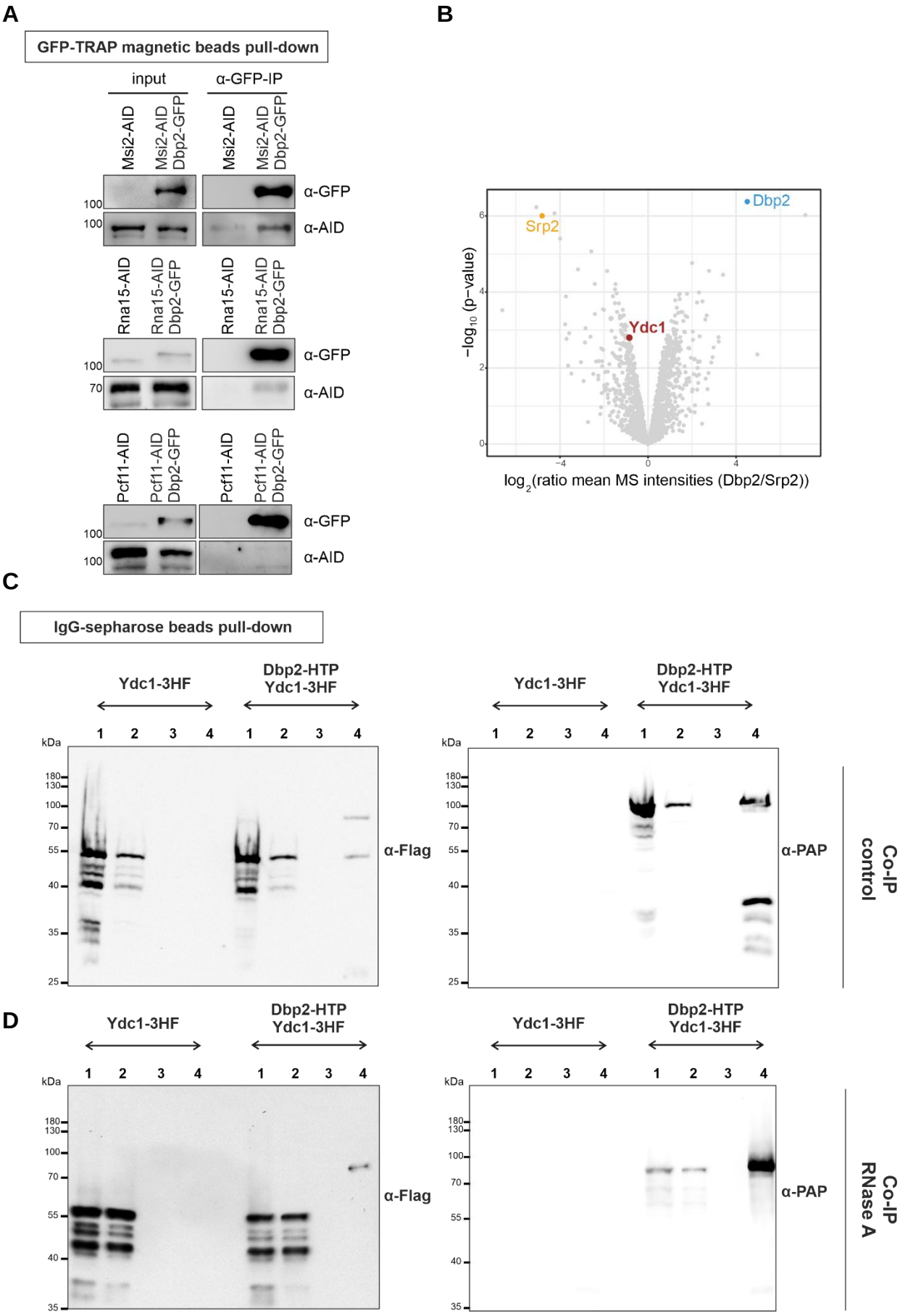
A
GFP-TRAP magnetic beads pull-down
input
α-GFP-IP
Msi2-AID
Msi2-AID Dbp2-GFP
Rna15-AID
Rna15-AID Dbp2-GFP
Pcf11-AID
Pcf11-AID Dbp2-GFP
α-GFP
α-AID
100
70
B
Dbp2
Srp2
Ydc1
−log10 (p−value)
log2(ratio mean MS intensities (Dbp2/Srp2))
C
IgG-sepharose beads pull-down
Ydc1-3HF
Dbp2-HTP Ydc1-3HF
kDa
α-Flag
α-PAP
Co-IP control
D
Co-IP RNase A

Figure 5.7 | Dbp2 interacting partners validated under non-crosslinking conditions using co-immunoprecipitation (Co-IP)

A. Inputs and eluates from Co-IP experiments using GFP-Trap beads were prepared from strains expressing either Msi2-AID, Pcf11-AID, or Rna15-AID, in the presence or absence of GFP-tagged Dbp2. Control strains expressing only the AID-tagged bait proteins without GFP-tagged Dbp2 were included to account for background binding to the beads, resolved on SDS-PAGE and analysed by WB using antibodies against GFP and AID. (n=2). **B.** Volcano plot to signify the preferential enrichment of Ydc1 protein, labelled in dark red. (n=3) from MS analysis of the comparative interaction profiling of Dbp2 and Srp2 labelled in blue and orange, respectively. In the volcano plot, P-values (−log10, moderated Student's t-test) are plotted against the relative enrichment of proteins in the purification of Dbp2-HTP relative to Srp2-HTP based on mean protein intensities (log2). **C.** Co-IP using IgG sepharose beads from strains expressing arginine/serine-rich splicing factor Ydc1-3HF (3xHA-3xFlag) in the presence or absence of HTP-tagged Dbp2 were resolved on SDS-PAGE and analysed by WB against PAP and Flag. Control strains (Ydc1-3HF) expressing only the 3HF bait proteins without HTP-tagged Dbp2 were included to account for background binding to the beads, (n=2). 1. Input 2. Flow-through 3. Wash 4. Eluate **D.** Co-IP experiment on C, was also performed upon RNase A treatment, where lysates were incubated in the presence of 0.05 mg/ml RNase A at RT for 30 mins prior to IP, (n=2).

5.8 Post-translational modifications analyses of the comparative interactome data

In addition to identifying protein-protein interactions, mass spectrometry-based comparative interactome profiling of Dbp2 and Srp2 purifications sought to uncover key post-translational modifications (PTMs), including acetylation (K), phosphorylation (S, T, Y), and dimethylation (K, R). These modifications play pivotal roles in regulating protein function, interactions, and localisation, particularly in dynamic processes such as transcription and RNA biogenesis. PTMs can serve as molecular switches, modulating the interaction of transcriptional regulators with RNAPII, chromatin remodelling complexes, and RNA processing factors. Phosphorylation, for instance, is a key regulatory process in the transcription cycle, influencing RNAPII transition states and the recruitment of processing factors, and has emerged as an critical mechanism for regulating protein phase separation (Nosella & Forman-Kay, 2021). Similarly, acetylation and methylation, often associated with chromatin accessibility and RNA-

binding affinity (Chong et al., 2018; Lorch & Kornberg, 2017), may fine-tune Dbp2 and Srp2 activities during RNA processes.

While the dataset revealed the presence of these modifications within Dbp2 and Srp2 interactomes, the intensities of the modification signals were insufficiently robust to support the accurate quantification and statistical validation of the results. This limitation compromised the resolution of the data, making it difficult to draw definitive conclusions about the relative enrichment or functional implications of specific PTMs in Dbp2 and Srp2-associated proteins.

Despite challenges in the quantitative analysis of the data, the initial analysis successfully identified several potential post-translational modifications (PTMs) within the interactome datasets. Specifically, Dbp2 and Srp2 were found to harbour acetylation and dimethylation sites. Additionally, proteins associated with different RNA processing events, including Paf1, Mmi1, Erh1, Ysh1, and Cft1 exhibited phosphorylation sites, while Xrn1 and Msi2 contained dimethylation sites. The sequences corresponding to these modifications are listed in Table 5.8.

Table 5.8 | PTMs for a number of proteins in the purification data

ID	Acetyl (K)	Phospho (STY)	Dimethyl (KR)
Dbp2	ELVSILSEAKQDIDPKLEEMA, AGAKGTAYTYFTSDNAK	<NA>	DNEYSGNYNGKEDGYNSRGR, GGGRGGFNDGASYGYDQR
Srp2	DIVNDFQGKEFMGSR, ENFRESAASKYPR, ESAASKYPR, ESAASKYPRPR	<NA>	KAGEPTFTDAHRENPGAGVVEFSTEEDMR
Paf1	<NA>	SVEGSLNEELSEEEKPAESR	<NA>
Mmi1	<NA>	ASHSPSLLEPYAHSLPSSVAPVGAYPEK, RPPYTLASEVPSSASAYQAGYSSYPVRSSPQ	<NA>

		LSHEDTR, ASTPPPLNFSR	
Erh1	<NA>	SPPPAESHIILLIQQGSDPK	<NA>
Xrn1	<NA>	<NA>	GNHHSTNGTQSIRGRGGK
Ysh1	<NA>	AINTILPFSEASQNDVSEDDFENEESDDDKIFEQQTK	<NA>
Msi2	<NA>	<NA>	DGRGGNTGGGHSFHPYRR
Cft1	<NA>	LNEITVYKAFLYSNTDKHK	<NA>

5.9 Cellular Dbp2 levels may be regulated through deubiquitination-mediated mechanism

Dbp2 and Srp2 purifications were analysed for acetylation, phosphorylation, and dimethylation but not for ubiquitination. Nonetheless, an exploration of the interactome profiling data revealed differential associations with proteins involved in cysteine-type deubiquitinase activity— the largest family of DUBs, with a significant enrichment of Ubp12 in Dbp2 purification. This activity represents a thiol-dependent isopeptidase mechanism that removes ubiquitin from conjugated target proteins (Clague et al., 2019). Ubiquitination is a conserved and widespread process where ubiquitinated substrates are targeted for proteasomal-mediated degradation. Substrates are also known to be regulated by ubiquitin hydrolases known as deubiquitinating enzymes (DUBs), which may impact protein activity, localisation, or stability (Snyder & Silva, 2021). These findings suggest that cellular Dbp2 protein levels and/or its stability may be regulated through a deubiquitination-dependent mechanism.

A

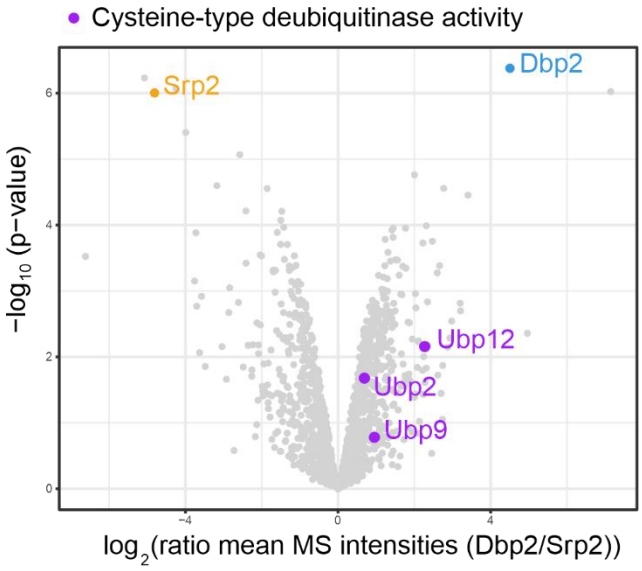

Figure 5.9 | Dbp2 levels may be regulated through deubiquitination-mediated mechanism

A. Volcano plot to signify the preferential enrichment of deubiquitinating enzymes (DUBs), labelled in dark red. (n=3) from MS analysis of the comparative interaction profiling of Dbp2 and Srp2 labelled in blue and orange, respectively. In the volcano plot, P-values (−log10, moderated Student's t-test) are plotted against the relative enrichment of proteins in the purification of Dbp2-HTP relative to Srp2-HTP based on mean protein intensities (log2). Classification of DUBs retrieved from (Kouranti et al., 2010).

5.10 Discussion

In this chapter a comprehensive proteomics analysis of Dbp2, a DEAD-box RNA helicase, in *Schizosaccharomyces pombe* was presented. Through comparative interactome profiling with Srp2, a splicing regulator, the role of Dbp2 in RNA biogenesis and its association with RNA processing machinery were explored. These findings provided valuable insights into the temporal and functional partitioning of Dbp2 and Srp2 within the transcription cycle and RNA processing pathways.

The high correlation between the interactome profiles of Dbp2 and Srp2 confirms their shared association with RNAPII holoenzyme components. This observation supports the hypothesis that both proteins function within the same transcriptional compartment, albeit at different stages of the transcription cycle. The relative abundance of the co-

purification of phosphorylated RNAPII^{Ser2P} forms with Dbp2 further aligns with its role in later transcriptional stages. This distinction, as supported by ChIP-seq data, highlights the complementary utility of proteomics and genomic approaches in delineating temporal events in transcription.

Differential enrichment of transcription-associated kinase complexes was observed between Dbp2 and Srp2. The early RNAPII^{Ser2P} kinase complex P-TEFb was more strongly associated with Srp2, reflecting its role in transcription elongation and splicing. In contrast, the late RNAPII^{Ser2P} kinase complex CTDK was preferentially co-purified with Dbp2, highlighting its involvement in late RNA processing events. This temporal distinction was found to correspond with the observed 5'-to-3' shift in chromatin association between Dbp2 and Srp2, suggesting that both proteins are recruited to transcribing RNAPII after promoter clearance, likely to facilitate earlier RNA processing events, such as splicing for Srp2 and later RNA processing events, such as 3'-end processing for Dbp2. Consistently, the interactome data supported a role for Dbp2 in late RNA processing stages, as evidenced by the preferential co-purification of 3'-end formation factors, export factors, and the MTREC complex. Dbp2's association with these complexes is consistent with its recruitment during the transcriptional elongation-to-termination transition. Furthermore, the enrichment of export factors such as Mex67 suggests that Dbp2 facilitates the coupling of 3'-end formation with mRNA export.

Furthermore, Dbp2's strong enrichment for the arginine N-methyltransferase Rmt1 suggests a potential regulatory mechanism through methylation. While our data did not establish direct methylation of Dbp2 by Rmt1, the interaction between these proteins hints at a broader role for arginine methylation in modulating RNA biogenesis. Dbp2 was shown to contain RGG/RG motifs at both ends, as previously demonstrated in Chapter 2, suggesting that Rmt1-mediated methylation of Dbp2 may be occurring.

Notably, RGG-containing proteins represent the second most abundant class of RNA-binding proteins (RBPs) in the human genome (Ozdilek et al., 2017). Though reports indicate that human orthologues of Dbp2 may be methylated to suppress R-loop formation, which may be a conserved functional mechanism across species (Mersaoui et al., 2019). However, given the strong biochemical affinity of these motifs for RNA (Thandapani et al., 2013), their presence in Dbp2— a highly active RNA helicase— suggests that methylation by Rmt1 may regulate its involvement in RNA-related processes and phase-separated condensates.

Dbp2 preferentially co-purified with the RSC and FACT complexes, both of which are critical for chromatin remodelling and transcription regulation. RSC facilitates nucleosome displacement, while FACT aids in resolving transcription-replication conflicts. The interaction of Dbp2 with these complexes may an indicative of its involvement in maintaining chromatin integrity during transcription elongation, or resolving RNA-DNA hybrids (R-loops), which can hinder transcription progression. Interestingly, RNAPII^{Ser2P} proposed to play a critical role for role in establishing a repressive chromatin state to prevent cryptic antisense transcription in coding regions (Boulanger et al., 2024), a process that also involves factors from the RSC complex, could implicate a role for Dbp2 in the same pathway. Moreover, cellular levels of *dbp2* are regulated at the RNA level, where an (auto-)regulated splicing event in the highly conserved intron 2 of the *dbp2* gene controls Dbp2 expression (I.Barta and R.Iggo, 1995; Kilchert et al., 2015). The fact that deubiquitinases show preferential enrichment in Dbp2 purification suggests that the levels and stability of the Dbp2 protein are also subject to regulation.

The comparative interactome analysis highlighted Srp2's preferential enrichment for splicing factors and components of the TREX complex, reinforcing its role in splicing

and early RNA biogenesis. In contrast, Dbp2's interactions with late export factors such as Mlo3 and Mex67 underline its role in late-stage RNA processing. The proteomics analysis of Dbp2 in *S. pombe* unveils its critical involvement in late transcriptional and RNA processing events. By contrasting its interactome with that of Srp2, our study provides a nuanced understanding of their functional divergence and highlights Dbp2's role in linking 3'-end processing with RNA export, which will be examined in the following chapters.

Chapter6 Cleavage bodies (CBs) – dynamic subnuclear structures in *S. pombe* and their association with Dbp2

6.1 Dbp2 localises to cleavage bodies

It was previously reported that MTREC, the nuclear exosome 3'-5' exoribonuclease subunit Rrp6, and components of the 3'-end processing machinery, co-localise in nuclear bodies in mitotically growing fission yeast, referred to as "nuclear exosome foci" (Egan et al., 2014; Shichino et al., 2020; Sugiyama et al., 2012, 2013; Sugiyama & Sugioka-Sugiyama, 2011; Yamanaka et al., 2010). These nuclear exosome foci have a compositional overlap with the cleavage bodies in human cells and it has been suggested that they could be functionally equivalent (Lei Li et al., 2006; Schul et al., 1996; Sugiyama & Sugioka-Sugiyama, 2011). For conciseness, MTREC-containing foci within the nucleus of *S. pombe* will be referred to as "cleavage bodies" in the rest of this thesis.

The comparative interactome profiling analysis had revealed that multiple components of cleavage bodies were enriched in the Dbp2-HTP purification. To reconstruct the co-localisation of components in cleavage bodies, and assess the subcellular localisation of Dbp2 in relation to them, live microscopy experiments were conducted. C-terminally GFP-tagged component from MTREC Mtl1, the nuclear exosome 3'-5' exoribonuclease subunit Rrp6, the poly(A)-binding protein Pab2, and 3'-end formation factors, including CFIA components Rna15 and Pcf11, CFIB component Msi2, as well as Dbp2, were examined using high-resolution fluorescence microscopy, in relative to the localisation of Red1-tdTomato signal, which exclusively localises to foci and serves as a marker for cleavage bodies (Figure 6.1).

The subcellular distribution of Dbp2-GFP closely resembled that of the nuclear exosome component Rrp6, but differed from the CPAC components Rna15-GFP and Msi2-GFP, as well as the nuclear poly(A)-binding protein Pab2. While Rna15-GFP, Msi2-GFP, and Pab2-GFP were excluded from the nucleolus and dispersed throughout the nucleoplasm, Dbp2-GFP was primarily localised in the nucleus with pronounced enrichment in the nucleolar compartment, and was concentrated in foci often found adjacent to the nucleolus or the nuclear rim. A key feature of all these factors was their co-localisation with Red1-tdTomato in foci, indicating that they are present in the same subnuclear structure. Dbp2-GFP signal within these foci almost universally overlapped with the Red1-tdTomato signal (Figure 6.1). This data confirms that Dbp2 is also a component of cleavage bodies.

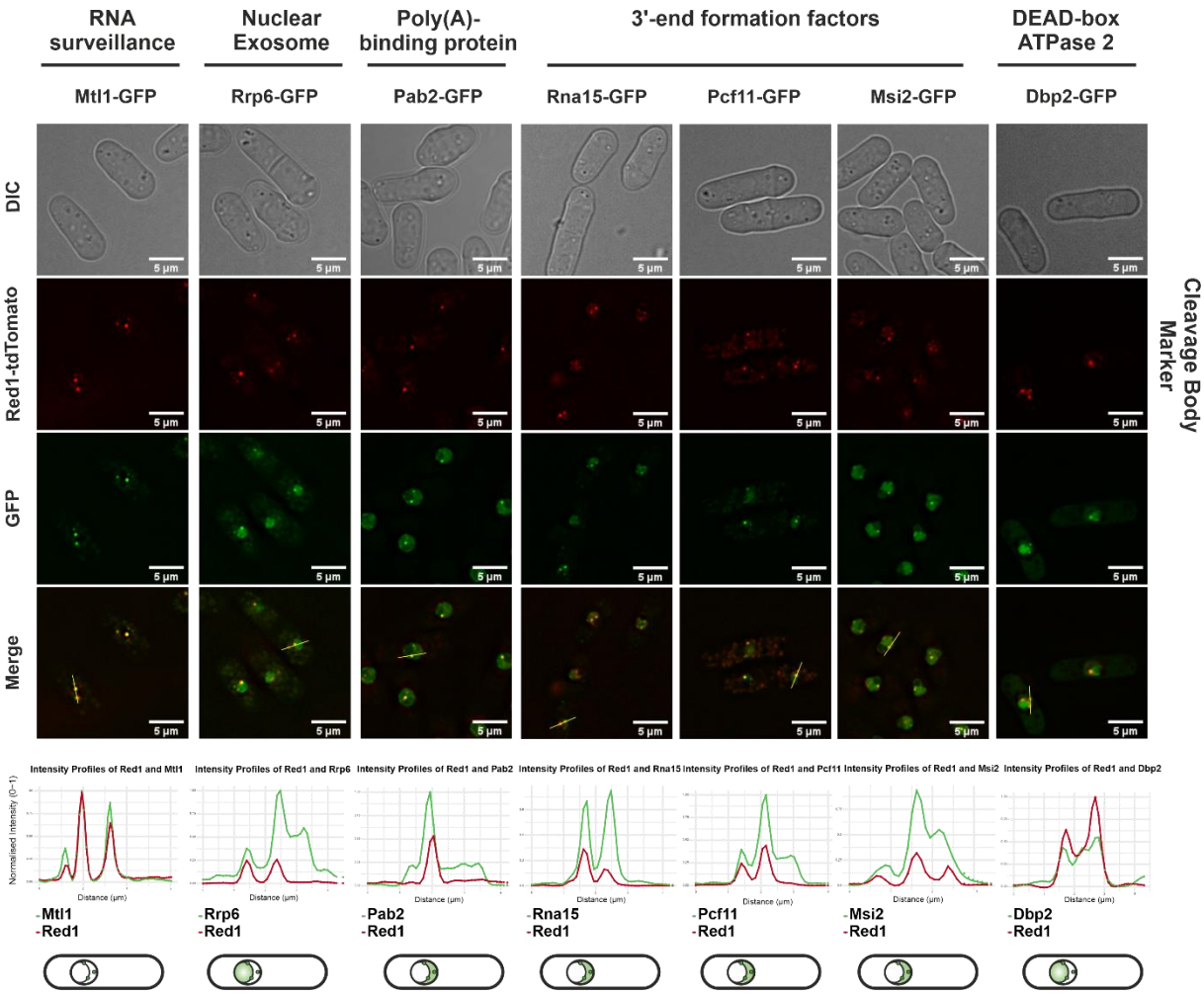

Figure 6.1 | Dbp2 localises to cleavage bodies

Live cell imaging of, upper panel: endogenously tagged Mtl1-GFP (MTREC component), Rrp6-GFP (Exosome component), Pab2-GFP (the nuclear poly(A)-binding protein), Rna15-GFP, Pcf11-GFP and Msi2-GFP (CPAC cleavage factor complex components), and Dbp2-GFP, and the MTREC component Red1-tdTomato used as a marker for cleavage bodies. Cells were grown in YES at 30°C, pelleted and resuspended in EMMG for imaging on poly-lysine-coated coverslips. The merged channel shows Dbp2-GFP in green and Red1-tdTomato in red. Fluorescence intensity profiles were generated along the yellow lines and are shown in the lower panel: fluorescence intensities were measured with Fiji and normalised to a 0-1 range. Images are representative of three independent experiments. Scale bars are 5 µm, (n = 3).

6.2 Dbp2 is not required for the efficient turnover of MTREC-dependent targets of the nuclear exosome

The components of the nuclear exosome MTREC/PAXT were more enriched with Dbp2-HTP purification in the comparative interactome data and its factors co-localised

with Dbp2 in cleavage bodies. MTREC/PAXT does not constitute as a ubiquitous component of the transcription machinery; instead, it is selectively recruited to genes targeted by the nuclear exosome through the discernment of TNAAAC motifs (where N can be any nucleotide) on nascent RNA by the YTH-domain (YT521-B homology) protein Mmi1. Mmi1 orchestrates the tethering of transcripts for decay via the nuclear exosome. Such targets are meiotic transcripts in mitotically growing *S. pombe* as the transcription of meiotic genes is not fully suppressed (Harigaya et al., 2006; Kilchert et al., 2015; Yamashita et al., 2012). Additionally, the nuclear membrane protein, Lem2, though not directly binding to RNA itself, engages with the MTREC/PAXT complex to target RNA precursors and meiotic transcripts for exosome targeting (Martín Caballero et al., 2022). Next, it was sensible to assess whether Dbp2 plays a role in the degradation of exosome targets.

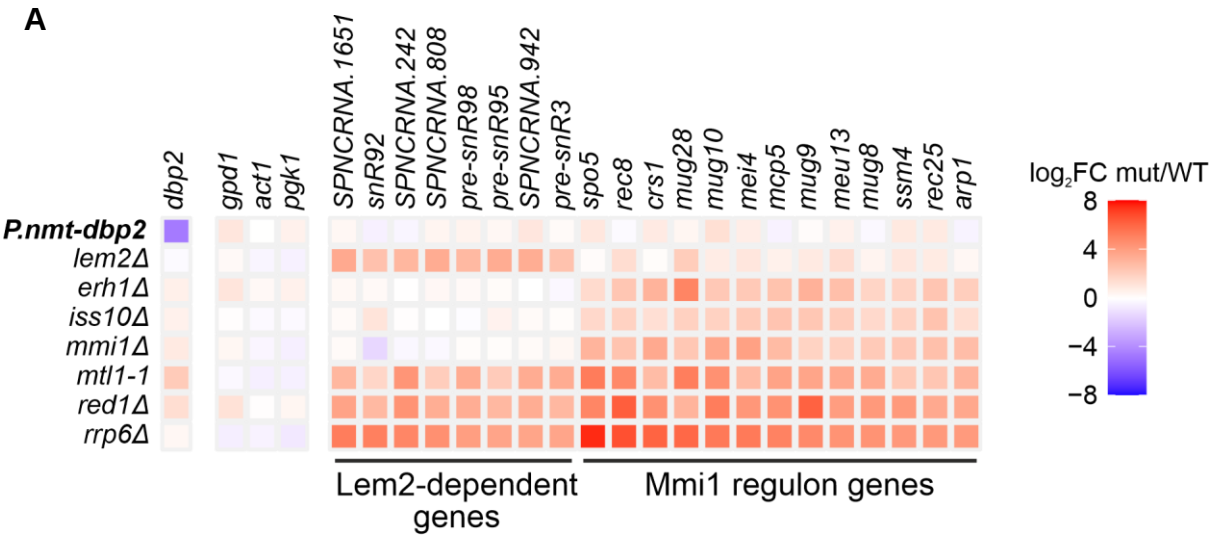

Figure 6.2 | Dbp2 is not required for the efficient turnover of MTREC-dependent targets of the nuclear exosome

A. DESeq2 differential expression analysis of nuclear exosome target genes that are either Lem2-dependent or part of the Mmi1 regulon (Chen et al., 2011; Martín Caballero et al., 2022); *adh1*, *pgk1* and *act1* are housekeeping mRNAs and included as controls. Colour indicates log2 fold change of normalised RNA-seq counts of mutant over wild type. *P.nmt-dbp2* signifies the depletion of Dbp2 for 5 h upon thiamine treatment. MTREC mutant data from (Atkinson et al., 2018) (*rrp6Δ*), (Kilchert et al., 2015) (*mmi1Δ*), (Birot et al., 2021) (*mtl1-1*), and (Martín Caballero et al., 2022) (*red1Δ, iss10Δ, erh1Δ, lem2Δ*); Accessions PRJEB7403, GSE73144, GSE148799, and GSE174347. Analysis was performed by Cornelia Kilchert.

Differential gene expression analysis of the poly(A)-enriched RNA-seq after 5 h of Dbp2 depletion compared to publicly available RNA-seq data of MTREC mutants revealed that depletion of Dbp2 did not lead to a stabilisation of known MTREC-dependent RNA targets of the nuclear exosome. These include meiotic mRNAs governed by the Mmi1 regulon and snoRNA precursors reliant on the nuclear membrane protein Lem2 (H. M. Chen et al., 2011; Kilchert et al., 2015; Martín Caballero et al., 2022), suggesting that Dbp2 is not required for MTREC-dependent RNA turnover.

6.3 Dbp2's recruitment to cleavage bodies is independent of the MTREC complex and exosome

Having established that Dbp2 is a component of cleavage bodies, where it co-localises with MTREC, the nuclear exosome 3'-5' exoribonuclease subunit Rrp6, and components of the 3'-end processing machinery, it was revealed through comparison with publicly available RNA-seq data of MTREC mutants that Dbp2 depletion did not lead to the stabilisation of known MTREC-dependent RNA targets of the nuclear exosome, indicating that the interaction between Dbp2 and MTREC does not play a role in RNA surveillance. Based on these findings, it was considered important to assess whether Dbp2's localisation to cleavage bodies is impaired in cells deficient in key components, such as Red1, Pab2, Iss10, and the nuclear exosome exoribonuclease Rrp6. To monitor the localisation of Dbp2, live microscopy was performed in cells with endogenously GFP-tagged Dbp2, in both wild type, and various genomic deletion mutants, including *rrp6Δ*, *red1Δ*, *iss10Δ*, and *pab2Δ*. Dbp2-GFP was still present in cleavage bodies when either Rrp6, Red1, Iss10, or Pab2 were deleted (Figure 6.3). Overall, the localisation of Dbp2 to cleavage bodies was found to be independent of these factors, further characterising the nature of cleavage bodies and

suggesting that Dbp2's association with them does not rely on components such as Red1, Pab2, Iss10, or Rrp6.

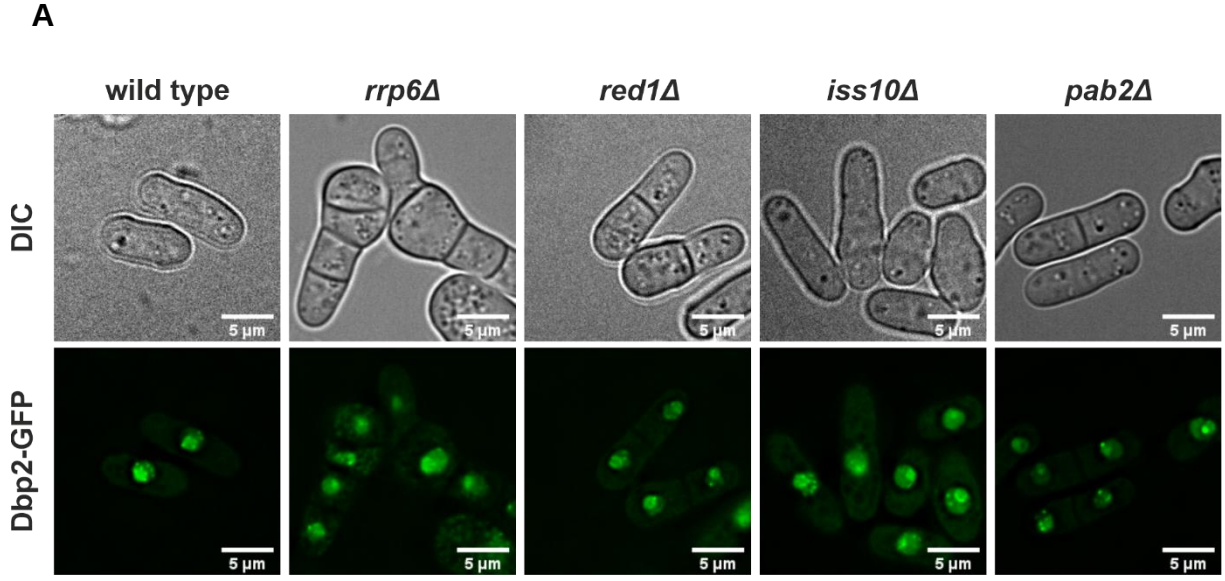

Figure 6.3 | Dbp2's recruitment to cleavage bodies is independent of the MTREC complex and exosome

A. Live cell imaging of genomicaly C-terminal fusion of Dbp2 to GFP in wild type, *rrp6Δ, red1Δ*, *iss10Δ*, and *pab2Δ*, cells grown in YES media for 2.5 h at 30 °C after diluting precultures in OD_{600} 0.2/ml and imaged. Images are representative of three independent experiments. DIC is differential interference contrast used for the detection and segmentation of unstained living adherent cells. Scale bars are 5 µm, (n = 3).

6.4 Cleavage bodies are unlikely to represent sites of co-transcriptional RNA cleavage

At steady-state levels, Dbp2 was observed to localise within cleavage bodies, subnuclear structures that also contain factors involved in RNA surveillance and co-transcriptional 3'-end RNA processing. Having established that Dbp2 does not contribute to the stabilisation of RNA targets for decay via the nuclear exosome, the next step in characterising these cleavage bodies was to investigate whether they serve as sites for bulky 3'-end RNA cleavage. This investigation aims to provide

insights into the timing of these sites within RNA biogenesis, particularly in relation to highly active transcription sites. For this purpose, immunofluorescence (IF) microscopy was performed with an antibody against S2P-modified Rpb1 to detect transcriptionally active RNAPII in a strain where the MTREC component Mtl1 was C-terminally tagged with GFP, which is used as a marker for the cleavage bodies.

Staining for Rpb1-S2P revealed a granular pattern that corresponded to a DNA-rich, crescent-shaped nucleoplasmic region as indicated by DAPI counterstaining (Figure 6.4A & C). Cleavage bodies were often found adjacent to regions with higher Rpb1-S2P density, but this was predominantly limited to the surface of the RNAPII transcriptionally active compartment. This spatial relationship was particularly pronounced along the inner arc of the crescent shape, aligning with the interface of the nucleolus. Overall, most RNAPII transcriptional active sites did not co-localise with cleavage bodies, as Mtl1-GFP foci generally did not coincide with peaks in the Rpb1-S2P signal (Figure 6.4B).

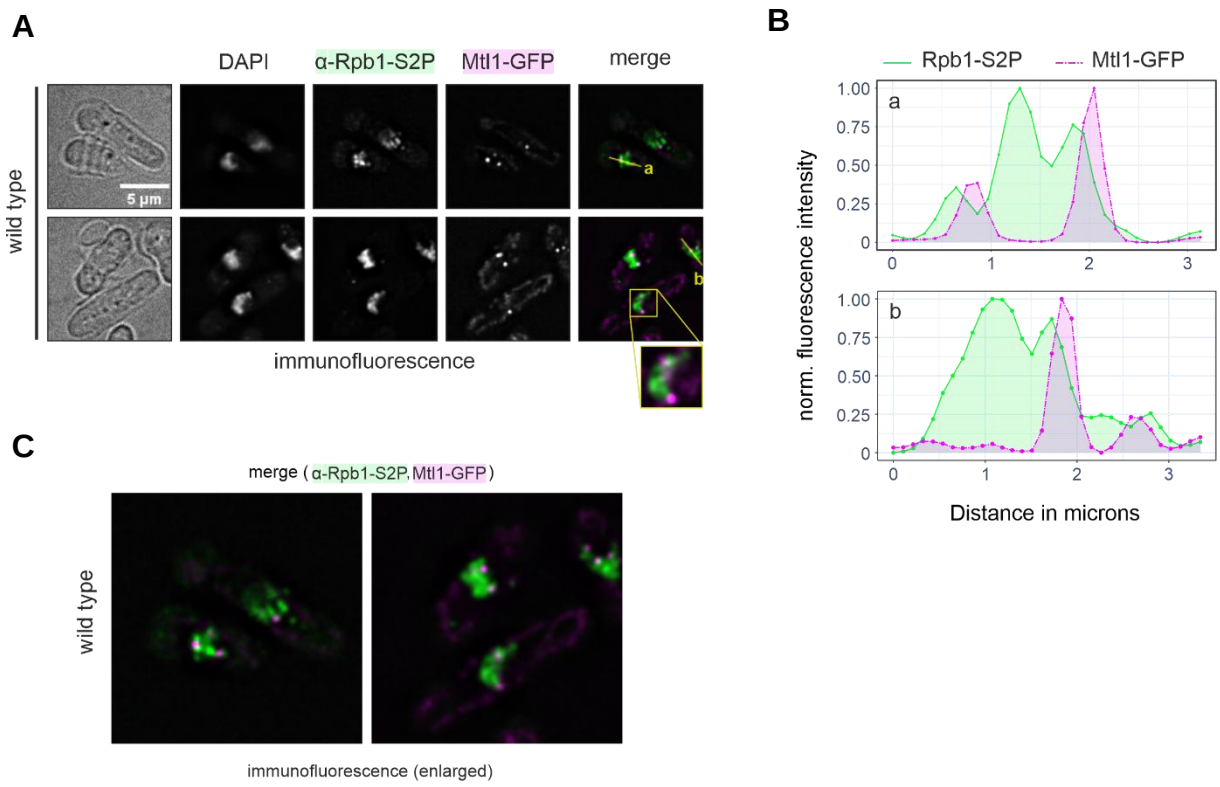

Figure 6.4 | Cleavage bodies are unlikely to represent sites of co-transcriptional RNA cleavage

A. Immunofluorescence against Rbp1-S2P in a strain where MTREC component Mtl1 was endogenously tagged with GFP. Cells were grown in YES at 30 °C and fixed with formaldehyde directly in the growth medium. The merged channel shows Rpb1-S2P in green and Mtl1-GFP in magenta. Fluorescence intensity profiles were generated along the yellow lines and are shown in (B). Images are representative of two independent experiments. **B.** Fluorescence intensity profiles across cleavage bodies and sites of active transcription as indicated in (A). Green line corresponds to the Rpb1-S2P signal, dashed magenta line to the residual Mtl1-GFP signal. Fluorescence intensities were normalised to a 0-1 range. Images are representative of two independent experiments. **C.** Enlarged versions of the merged images of the immunofluorescence shown in (A), with Rpb1-S2P in green and Mtl1-GFP in magenta, without yellow markings. Scale bar 5 µm, (n = 2). Analysis was performed by Cornelia Kilchert.

6.5 Cleavage bodies serve as storage compartments for 3'-end processing factors

It was deduced that cleavage bodies, although containing components of the 3'-end processing machinery, are unlikely to function as the bulky sites of RNA cleavage and polyadenylation. This prompted an investigation into whether cleavage bodies might serve as storage compartments for 3'-end processing factors. To evaluate this

hypothesis, cells expressing C-terminally GFP-tagged Msi2, Pcf11, and Rna15 were analysed following treatment with thiolutin, a compound known to inhibit RNAPII activity and transcription (Qiu et al., 2024). These cells were compared to untreated control cells. In thiolutin-treated cells, the fluorescent signals of Msi2-GFP, Pcf11-GFP, and Rna15-GFP within foci were significantly increased compared to untreated controls. These findings support the notion that cleavage bodies function as storage sites, potentially buffering the levels of CPAC components.

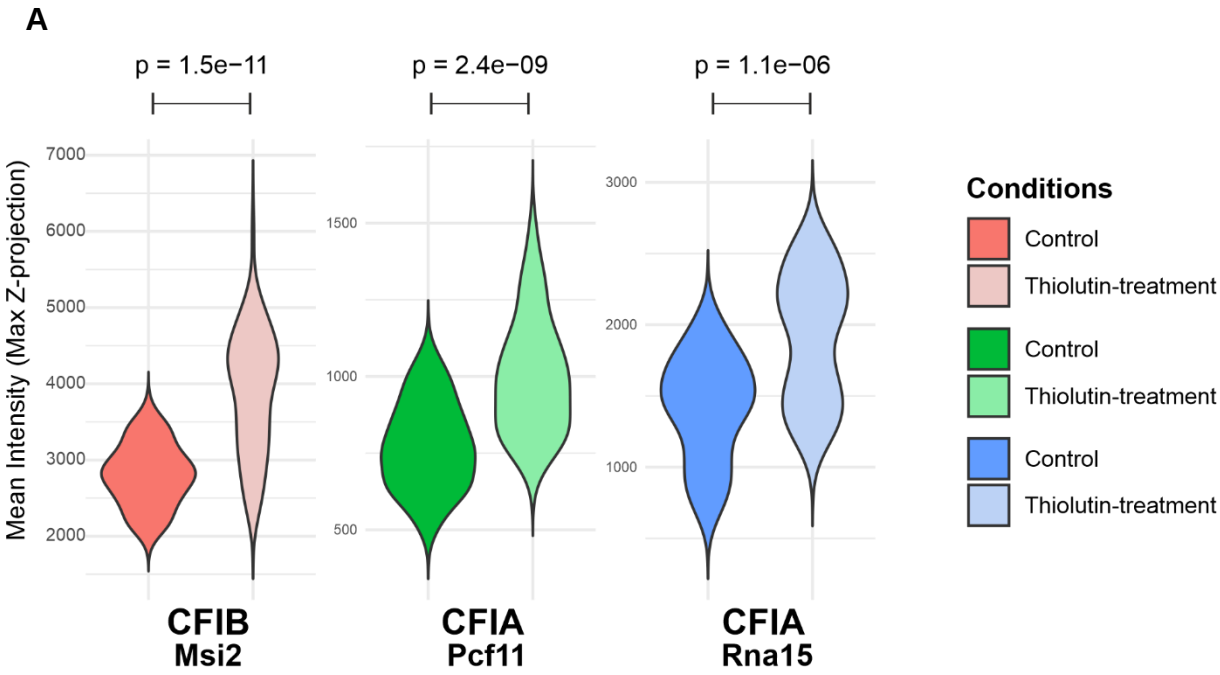

Figure 6.5 | Cleavage bodies may help to buffer CPAC levels

A. Quantification of the transcription inhibitor experiment of cells carrying endogenously Msi2-GFP, Pcf11-GFP and Rna15-GFP, treated with 20 µg thiolutin and incubated in YES for a duration of 60 min at 30 °C, pelleted and resuspended in EMMG for imaging on poly-lysine coated coverslips. For live cell imaging in EMMG-media contained 20µg of thiolutin to ensure the stability of transcription inhibition. Measurements were performed on maximal intensity Z-projections and the mean fluorescence intensity scored for each cell against background. Non-treated mixed cultures were included as controls against background. The displayed p-values for the pair-wise comparisons were calculated using a two-sided Wilcoxon rank sum test (∗p < 0.05; ∗∗p < 0.01; ∗∗∗p < 0.005), (n = 2).

6.6 Discussion

This chapter of the thesis focuses on a more in-depth characterisation of cleavage bodies. The comparative interactome profiling analysis identified several components of cleavage bodies as enriched in the Dbp2-HTP purification. To further investigate the relationship between Dbp2 and these components, live microscopy experiments were conducted. The localisation of GFP-tagged components from the MTREC complex, the nuclear exosome subunit Rrp6, the poly(A)-binding protein Pab2, and 3'-end formation factors such as Rna15, Pcf11, and Msi2, were compared to Dbp2-GFP using high-resolution fluorescence microscopy. The results showed that Dbp2-GFP co-localises with Red1-tdTomato, a marker for cleavage bodies, indicating that Dbp2 is indeed a part of this subnuclear structure. Moreover, Dbp2 was primarily localised to the nucleoplasm with strong enrichment in the nucleolar compartment, where it formed foci, often adjacent to the nucleolus or nuclear rim. This localisation pattern was consistent with the nuclear exosome component Rrp6, implying that Dbp2 may play a role in RNA processing within cleavage bodies. The step was to determine whether Dbp2 plays a role in the degradation of RNA targets via the nuclear exosome, particularly in relation to the MTREC complex, which is known to be involved in the decay of specific RNA targets. The MTREC/PAXT complex is selectively recruited to genes for exosome-mediated degradation through the recognition of specific motifs on nascent RNA by the Mmi1 protein (Harigaya et al., 2006; Kilchert et al., 2015). This recruitment is particularly important for the decay of meiotic transcripts and snoRNA precursors in *S. pombe*, which are governed by the Mmi1 regulon and the nuclear membrane protein Lem2 (Atkinson et al., 2018; Birot et al., 2022; Kilchert et al., 2015; Martín Caballero et al., 2022).

Depletion of Dbp2 was found to have no significant effect on the stability of known MTREC-dependent RNA targets (Figure 6.2). Comparative analysis of RNA-seq data from Dbp2-depleted cells and MTREC mutant strains showed no accumulation of Mmi1-regulated meiotic mRNAs or snoRNA precursors, suggesting that Dbp2 is not essential for the turnover of these RNA targets by the nuclear exosome. This observation supports the idea that Dbp2 may not be directly involved in RNA decay but instead plays a different role within the context of cleavage bodies. Further investigation into the recruitment of Dbp2 to cleavage bodies revealed that its presence in these structures does not depend on the MTREC complex or the nuclear exosome. Live cell imaging of Dbp2-GFP localisation in strains where components of the nuclear exosome or Red1 were deleted showed that Dbp2 was still present in cleavage bodies, even in the absence of Rrp6, Red1, Iss10, or Pab2 (Figure 6.3). This suggests that Dbp2's recruitment to cleavage bodies is independent of these complexes, further supporting the notion that Dbp2 may have a role distinct from RNA degradation within these subnuclear structures.

Cleavage bodies are known to contain factors involved in RNA surveillance and 3'-end RNA processing, leading to the hypothesis that they might serve as sites of co-transcriptional RNA cleavage and polyadenylation (CPA). Given Dbp2's localisation to these foci, it was important to determine whether these bodies are indeed involved in RNA cleavage. To address this, the subcellular localisation of RNAPII in actively transcribed regions was assessed by immunofluorescence using an antibody against phosphorylated Rpb1 (S2P), which marks transcriptionally active RNAPII. While cleavage bodies were often found adjacent to regions with high Rpb1-S2P density, the majority of RNAPII active sites did not co-localise with cleavage bodies. This spatial relationship was most pronounced along the inner arc of the nucleolus, suggesting that

cleavage bodies are more likely to reside in regions adjacent to transcriptionally active sites but not directly within them. The lack of significant overlap between Mtl1-GFP foci (which mark cleavage bodies) and Rpb1-S2P signal indicates that these subnuclear structures are unlikely to represent the sites of co-transcriptional RNA cleavage. This finding is consistent with previous studies that suggest CPA primarily occurs during transcription by RNAPII, with 3'-end processing being tightly coupled to transcription (Mitschka & Mayr, 2022). Instead, cleavage bodies may serve as storage or assembly sites for RNA processing factors that are recruited to active transcription sites as needed. The localisation of cleavage bodies adjacent to transcriptionally active regions may reflect their role in processing RNA precursors post-transcriptionally or during transcriptional pause sites, as it has been suggested that some distal polyadenylation sites are processed post-transcriptionally (P. Tang et al., 2022).

In summary, this chapter has demonstrated that Dbp2 is a component of cleavage bodies in *S. pombe*, co-localising with factors involved in RNA surveillance and 3'-end processing. Dbp2 is recruited to cleavage bodies independently of the MTREC complex and the nuclear exosome, and it does not appear to play a significant role in the degradation of MTREC-dependent RNA targets. Additionally, cleavage bodies, although containing components of the 3'-end processing machinery, are unlikely to serve as the sites of bulky RNA cleavage. Rather, they are likely to represent storage or assembly compartments for RNA processing factors, awaiting their recruitment to active transcription sites for processing. In this chapter, valuable insights into the subnuclear organisation of *S. pombe*, along with its composition and association with RNA processing, were provided. The analyses conducted to understand the functional role of Dbp2 within these structures, along with its involvement in 3'-end maturation,

will be addressed and discussed in the next chapter, focusing on the cellular consequences of Dbp2 loss.

Chapter7 Cellular Consequences of Dbp2 Depletion

7.1 poly(A) + RNA is retained in the nucleus upon loss of Dbp2

In Chapters 4 and 5, Dbp2 was primarily found to map to the termination window and also to interact with the canonical 3'-end processing machinery and RNA export factors. These include the export adaptor Mlo3 (homologous to *S. cerevisiae* Yra1 and *H. sapiens* ALY/REF) and the export receptor Mex67 (*H. sapiens* NXF1/TAP), respectively. Notably, Qu et al., 2009 had previously demonstrated that the presence of Yra1 and Mex67 is critical for the release of CPAC from RNAs. Collectively, these observations raise the possibility that Dbp2 may link the release of CPAC components to RNA export, that its loss might impair RNA export. To examine this possibility, fluorescence *in situ* hybridisation (FISH) approach was employed to investigate the localisation of RNAs with fully processed 3'-ends, using a 50-mer 5′-end Cy3-labelled oligo-d$(T)_{50}$-Cy3 probe on formaldehyde-crosslinked cells.

In wild type cells, the distribution of poly(A)+ RNA was uniform across the cytoplasm, with a moderately higher abundance in the nucleus and a mean ratio of average fluorescence intensities of nucleus over cytoplasm (Figure 7.1A). Following the depletion of Dbp2, poly(A)+ RNA could still be detected in the cytoplasm; however, a relative increase in the nuclear to cytoplasmic signal was observed, and this change was highly significant (Figure 7.1B). Notably, a fraction of the nuclear signal was concentrated in foci. A heat shock treatment, which is known to efficiently block bulk mRNA export in both yeast models, was included as a positive control for export block (Saavedra et al., 1996). Under heat shock conditions, a nearly complete nuclear retention of poly(A)+ RNAs was observed, forming a distinct ring-shaped pattern that excludes chromatin as judged by the DAPI stain. These poly(A)+ RNAs-rich structures are likely to correspond to nucleolar rings, in which essential factors of nuclear RNA

metabolism have been shown to reversibly aggregate during heat stress (Gallardo et al., 2020).

Overall, in the absence of Dbp2, 3'-processed, polyadenylated RNAs are inefficiently exported to the cytoplasm and are retained on DNA-rich region, as evidenced by the overlap of poly(A)+ RNA signal with the DNA-rich nucleoplasmic compartment counterstained with DAPI.

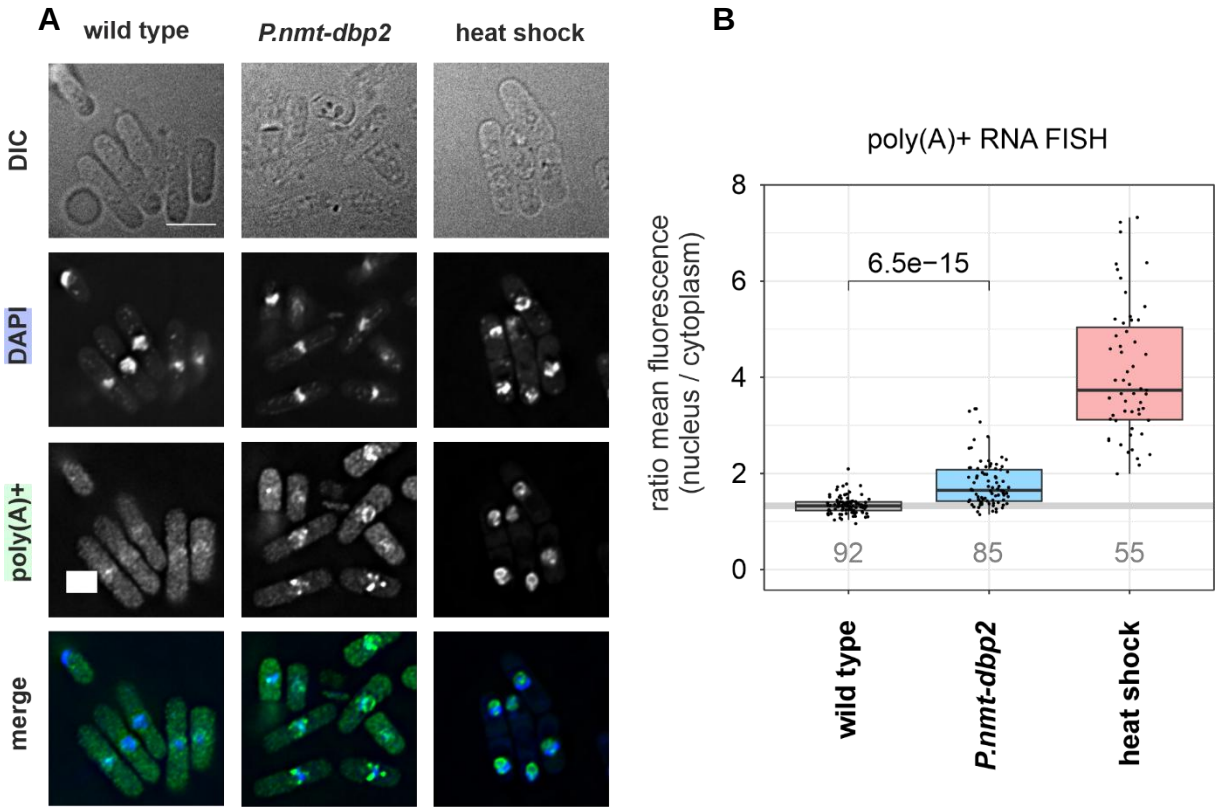

Figure 7.1 | mRNA export: poly(A)+ RNA is retained in the nucleus upon loss of Dbp2

A. Fluorescence *in-situ* hybridisation (FISH) against poly(A)+ RNA using a Cy3-labelled oligo-d(T) probe and DAPI to stain the DNA within the nucleus. Cells were grown overnight in EMMG, then shifted to YES for 5h to shut off the P.*nmt* promoter before formaldehyde fixation. For the heat shock control, wild type cells were shifted to 42 °C for 1h. Images are representative of two independent experiments. The merged channel shows poly(A)+ RNA in green and DAPI in blue. A quantitation of the nuclear/cytoplasmic signal distribution is given in B. **B.** Quantitation of the oligo-d(T) FISH experiment shown in 4C (n = 2). Semi-automated cellular segmentation was carried out by thresholding on the transmitted light channel (cell outlines) and DAPI stain (nuclei). Measurements were performed on average intensity Z-projections for nucleus and cytoplasm (= total cell without nucleus) and the ratio of mean nuclear fluorescence intensity over mean cytoplasmic fluorescence intensity calculated for each cell. The displayed p-values for the pair-wise comparisons were calculated using the Wilcoxon test ($*p < 0.05$; $**p < 0.01$; $***p < 0.005$). Note that the calculated ratios underestimate nuclear RNA retention, particularly in the heat shock sample, because segmentation on the DAPI channel is biased towards the DNA-rich nuclear compartment and can exclude parts of the nucleolus. Scale bar 5 µm. heat shock n= 2, others n =3

7.1.1 A domain of nuclear retained poly(A)+ RNAs upon loss of Dbp2 corresponds to cleavage bodies

In the oligo-d(T) FISH experiment, there was a notable nuclear sequestration of the poly(A)+ RNAs in foci within the nucleoplasm or at the periphery of the nucleolus when Dbp2 was depleted. Given the previous observation that Dbp2 localises to cleavage bodies in wild type cells, the next question to be addressed was whether these sites could be sites where poly(A)+ RNAs accumulate in its absence.

The oligo-d(T) FISH experiment was repeated in wild type and *P.nmt-dbp2* strains, with the cleavage body component Mtl1 C-terminally tagged with GFP. The oligo-d(T)-Cy3 staining in wild type cells exhibited minimal overlap with Mtl1-GFP foci, consistent with findings in human cleavage bodies, where approximately 20% were reported to contain newly transcribed RNA (Schul et al., 1996). Although a significant portion of the poly(A)+ RNA retained in the nucleus of the *P.nmt-dbp2* mutant was dispersed throughout the nucleoplasm, a subset of the poly(A)+ RNA signal partially aggregated in foci that overlapped with the GFP signal of Mtl1. This overlap confirmed that poly(A)+ RNA accumulates in cleavage bodies upon loss of Dbp2 (Figure 7.1.1A & B), suggesting that Dbp2 is essential for the release of poly(A)+ RNA from this compartment.

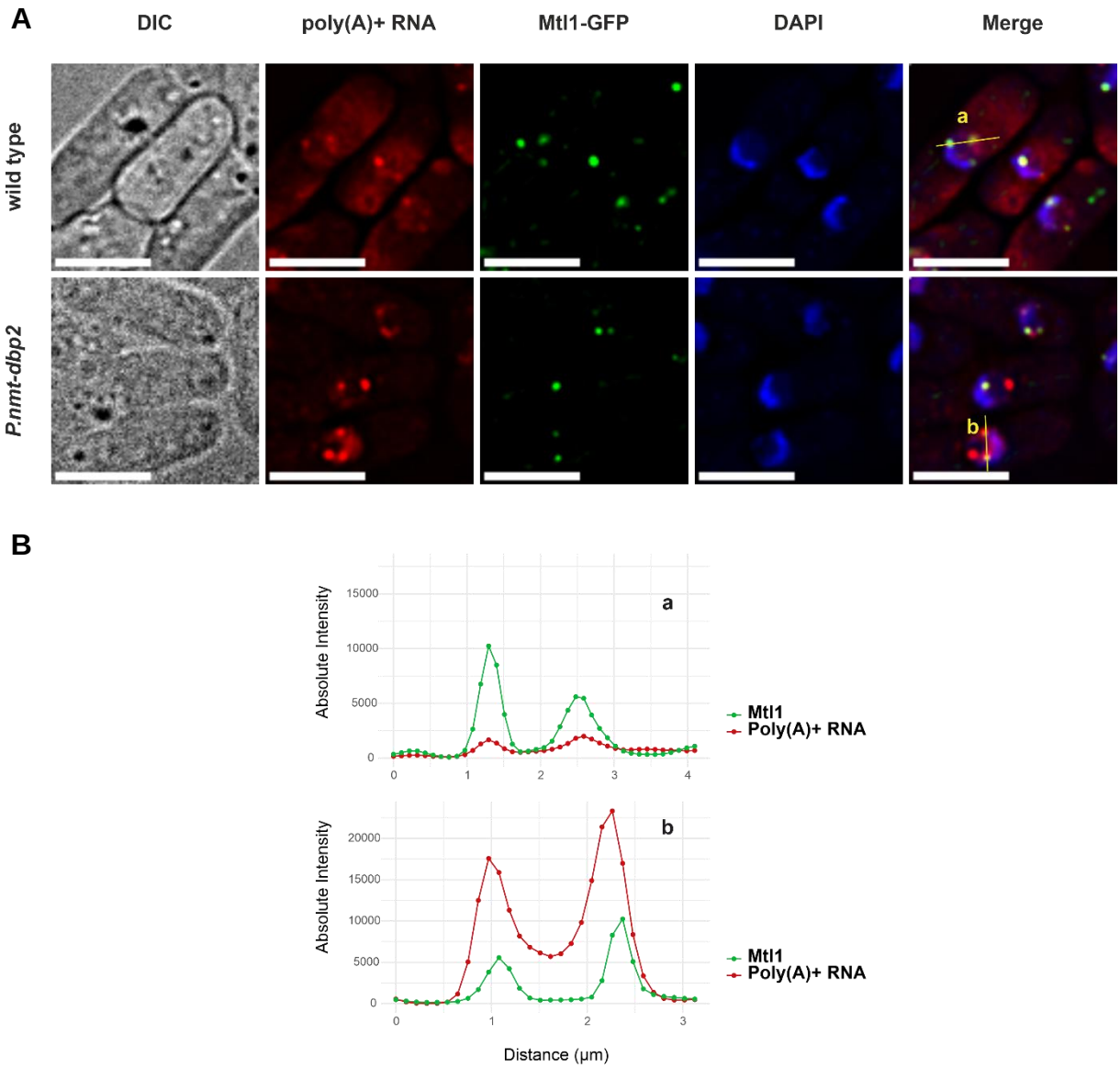

Figure 7.1.1 | A domain of nuclear retained poly(A)+ RNA upon loss of Dbp2 corresponds to cleavage bodies

A. FISH-IF against poly(A)+ RNA using oligo-d(T)-Cy3 in wild type and *P.nmt-dbp2* with the cleavage body marker Mtl1 endogenously tagged with GFP. Cells were grown overnight in EMMG, then shifted to YES for 5 h to shut off the *P.nmt* promoter before formaldehyde fixation. The merged channel shows poly(A)+ RNA in green, Mtl1-GFP in red and DAPI in blue. Fluorescence intensity profiles were generated along the yellow lines and are shown in (B). Images are representative of three independent experiments. **B.** Absolute fluorescence intensity profiles of FISH-IF signal across sites of poly(A)+ RNA accumulation and the adjacent nuclear area from a, and b yellow lines. In fluorescence intensity plots, green line corresponds to the poly(A)+ RNA signal, red line to the Mtl1-GFP signal. Scale bar 5 µm, (n = 3).

7.1.2 MTREC/PAXT components Red1 and Pab2 are not required for the nuclear retention of poly(A)+ RNA in the absence of Dbp2

A fraction of poly(A)+ RNAs accumulates in cleavage bodies upon the loss of Dbp2, indicating the need for Dbp2 in their release from cleavage bodies. Recent studies in human cells have identified ZFC3H1, the homologue of Red1, as a nuclear retention factor for exosome-targeted RNAs. ZFC3H1 can sequester RNA in nuclear condensates in a manner dependent on the nuclear poly(A)-binding protein PABPN1, the homologue of Pab2 (Fan et al., 2018; E. S. Lee et al., 2022; Meola et al., 2016; Silla et al., 2018; Y. Wang et al., 2021). To investigate the involvement of MTREC components in poly(A)+ RNA retention in cleavage bodies upon loss of Dbp2, strains combining *red1Δ*, *pab2Δ* or *iss10Δ* with the *P.nmt-dbp2* construct were used to conduct a set of oligo-d(T) FISH experiments.

Iss10 is a fission yeast-specific component of MTREC (Figure 7.1.2C), which shows high homology to the N-terminal region of ZFC3H1 and is required for the localisation of MTREC to cleavage bodies (Egan et al., 2014; Yamashita et al., 2013; Zhou et al., 2015). The single deletion of *red1Δ* or *pab2Δ* also resulted in the retention of poly(A)+ RNA in nuclear foci; combining either mutant with *P.nmt-dbp2* had an additive effect on retention (Figure 7.1.2A). On the other hand, the single *iss10Δ* deletion showed no export block, with a localisation of poly(A)+ RNA very similar to the wild type; the combination of *iss10Δ* with *P.nmt-dbp2* reduced nuclear poly(A)+ RNA retention compared to the phenotype of the *P.nmt-dbp2* alone, to some extent rescuing the *P.nmt-dbp2* phenotype. In the double mutant strain, the statistical difference in the ratio of average fluorescence intensities of poly(A)+ RNA between the nucleus and cytoplasm was no longer significant when compared to the wild type. However, *P.nmt-dbp2* exhibits a notably larger cell-to-cell variability in observed nuclear over

cytoplasmic signal ratios in any genetic context, including in combination with *iss10Δ*, meaning that granular poly(A)+ RNA signals in the nucleus are still frequently observed in the *iss10Δ P.nmt-dbp2* double mutant (Figure 7.1.2B). These findings indicate that the nuclear poly(A)-binding protein PABPN1-dependent RNA sequestration in nuclear condensates, observed in its human counterpart, is conserved in *S. pombe*. However, given the additive effect on poly(A)+ RNA retention with *red1Δ P.nmt-dbp2* or *pab2Δ P.nmt-dbp2* double mutants, it is likely that two separate pathways are involved. Overall, these results indicate that the poly(A)+RNA retention in the absence of Dbp2 can be only partially rescued by the loss of Iss10, a protein with high homology to the N-terminal region of ZFC3H1 (Red1 in *S. pombe*) but that yet unidentified factors contribute to RNA retention in the *P.nmt-dbp2* background.

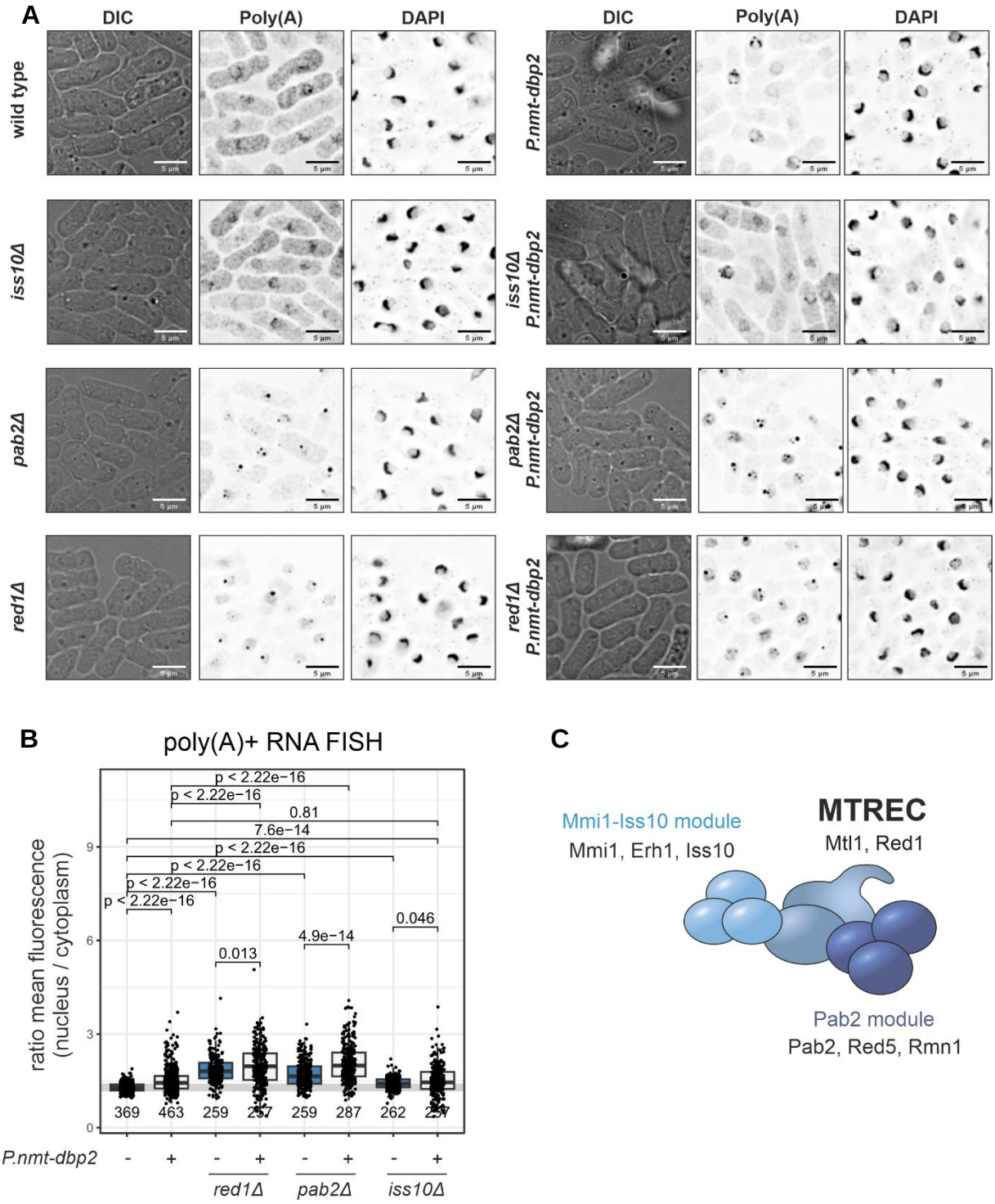

Figure 7.1.2 | MTREC/PAXT components Red1 and Pab2 are not required for the nuclear retention of poly(A)+ RNA in the absence of Dbp2

A. Fluorescence *in-situ* hybridisation (FISH) against poly(A)+ RNA using a Cy3-labelled oligo-d(T) probe and DAPI to stain the DNA within the nucleus. Cells were grown over night in EMMG, then shifted to YES for 5 h to shut off the *P.nmt* promoter before formaldehyde fixation. Fluorescence images were inverted for easier visibility. Images are representative of three independent experiments. **B.** A quantification of the nuclear/cytoplasmic signal distribution of the poly(A)+ RNA FISH experiment of MTREC mutants in (A) combined with *P.nmt-dbp2.* The displayed p-values for pair-wise comparisons were calculated using a two-sided Wilcoxon rank sum test, (∗p < 0.05; ∗∗p < 0.01; ∗∗∗p < 0.005). Scale bar 5 µm, (n = 3). **C.** Schematic of the *S. pombe* nuclear exosome targeting factor MTREC (Mtl1/Red1 core) with its associated modules. Adapted from (Kilchert et al., 2020)**.**

7.1.3 Dbp2 depletion alters subcellular localisation of export factors

In *S. cerevisiae*, mRNA export requires the export receptor Mex67/TAP/NXF1, which marks mature mRNAs by binding to adaptor proteins like Yra1 or Nab2 (Xie & Ren, 2019). Notably, RNA export factors, including the export adaptor Mlo3 (homologous to *S. cerevisiae* Yra1 and *H. sapiens* ALY/REF) and the export receptor Mex67 (*H. sapiens* NXF1/TAP), were preferentially co-purified with Dbp2 in comparative interactome approach. Furthermore, the export of poly(A)+ RNAs was impaired in the absence of Dbp2. To determine whether depletion of Dbp2 affects the subcellular localisation of these export factors, live-cell microscopy was performed in both the presence and absence of Dbp2.

At steady-state, Mex67 has been reported to predominantly localise to the nuclear pore complex (NPC), which was confirmed here using a genomic C-terminal fusion of Mex67 to GFP. Interestingly, the subcellular localisation of Mex67-GFP was altered upon Dbp2 depletion, with Mex67 signal appearing at the nucleolus while maintaining its primary localisation at the NPC (Figure 7.1.3A). This behaviour resembles changes observed under stress conditions, such as heat shock, where poly(A)+ RNA (Figure 7.1, heat shock FISH) and Mex67 is known to reversibly sequester at the nucleolus (Ideue et al., 2004; Yoshida & Tani, 2005). The mechanism underlying the change in Mex67 subcellular localisation into nucleolus upon Dbp2 loss could be interpreted as a similar response mechanism that requires the blockage of RNA export upon stress.

Furthermore, the subcellular localisation of the export adaptor Mlo3/ALYREF/Yra1 was also examined using a genomic C-terminal fusion to GFP in the presence and absence of Dbp2. In wild type cells, Mlo3-GFP predominantly localised to the nucleus in a crescent-like pattern, likely corresponding to the nucleoplasm, and was also observed as multiple punctate structures (Figure 7.1.3B). However, upon Dbp2 depletion, Mlo3-

GFP localisation became diffuse across the nucleus, indicating that its intactness is compromised. This difference is readily visualised when comparing max intensity Z-projections plotted against each other (Figure 7.1.3C).

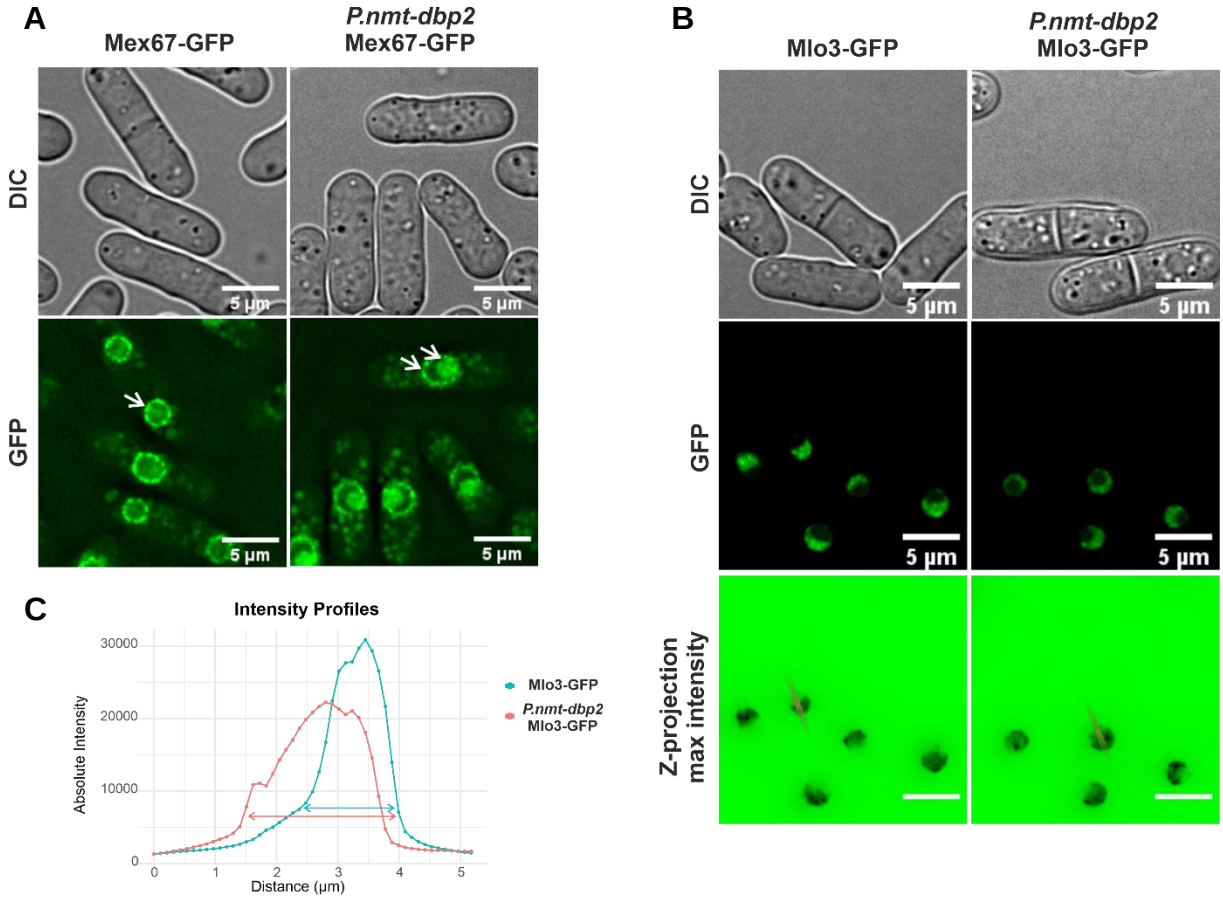

Figure 7.1.3 | Dbp2 depletion alters subcellular localisation of export factors

A. Cells carrying endogenously Mex67-GFP, and **B.** Mlo3-GFP in the presence and absence of Dbp2. Cells were shifted to YES for 5 h at 30 °C. For live cell imaging, cells were pelleted and resuspended in EMMG containing 15 µg of thiamine to maintain the stability of the *nmt* promoter - dependent repression of *dbp2* during the imaging. The brown lines are shown for intensity plot measurement in (C). Images are representative of three independent experiments. **C.** Absolute fluorescence intensity profiles along the brown lines are shown over z-projection max intensity of Mlo3-GFP signal across the nucleus. Scale bar 5 µm, (n = 2).

In budding yeast, Dbp2 has been proposed to be essential for the efficient assembly of Yra1 and Mex67 onto mRNAs (Ma et al., 2013). In turn, Yra1 was suggested to inhibit the helicase activity of Dbp2 (Ma et al., 2016). To examine whether association

of Mlo3 with mRNAs is affected upon loss of Dbp2, RNA-protein immunoprecipitation (RIP) assay was carried out. In Dbp2-depleted cells, co-precipitation of a representative mRNA, *ssa2*, with Mlo3 was markedly reduced, suggesting impaired recruitment of Mlo3. This implies that the nuclear retention of poly(A)+ RNA observed upon Dbp2 loss could result from insufficient recruitment of export adaptors (Appendix 3) and may also account for the compromised localisation of Mlo3 within the nucleus in Dbp2-depleted cells.

7.1.4 Poly(A)-tail length remains unchanged upon Dbp2 depletion

Defects in mRNP assembly manifest in various phenotypes, including read-through transcription, reduced RNA cleavage, slow poly(A) synthesis, hyperadenylation of transcripts, and inhibition of export. Poly(A)+ RNA retention in the nucleus due to defective mRNP assembly can be caused by a variety of factors that affect different stages of RNA processing and export, namely defective mRNA export machinery, mutations in factors involved in 3′-end processing, delayed or defective splicing, defects in RNA surveillance pathways, hyperadenylation, or issues with RNA packaging. Studies have identified factors that specifically link the regulation of polyadenylation with export, which are typically involved in the later stages of mRNP assembly (Bresson et al., 2015; Patricia Hilleren et al., 2001; Jensen et al., 2001). Accordingly, defects in the mRNA export receptor Mex67 in *S. cerevisiae* and its human homologue, NXF1/TAP, an actor in the later stages of mRNP assembly, result in conserved hyperadenylation as well as retention of transcripts at the site of transcription (Patricia Hilleren et al., 2001; Qu et al., 2009). Since Dbp2 interacts with *S. pombe* Mex67, and exhibits nuclear poly(A)+ RNA retention phenotype when depleted, it was next investigated whether Dbp2 depletion also leads to hyperadenylation by poly(A)-tail length assay for bulk mRNAs in wild type and *P.nmt-*

dbp2 mutant cells. This would allow for the distinction between the manifested phenotypes, helping to define the spatiotemporal scale of Dbp2-induced effects in mRNP assembly lifecycle. When the poly(A) lengths of bulk RNAs from Dbp2-depleted cells were compared to those from wild type cells, no observable difference was detected (Figure 7.1.4). Overall, these findings suggest that poly(A)+ RNA retention in the absence of Dbp2 is not due to hyperadenylation, implying a defect at an earlier stage of RNA processing.

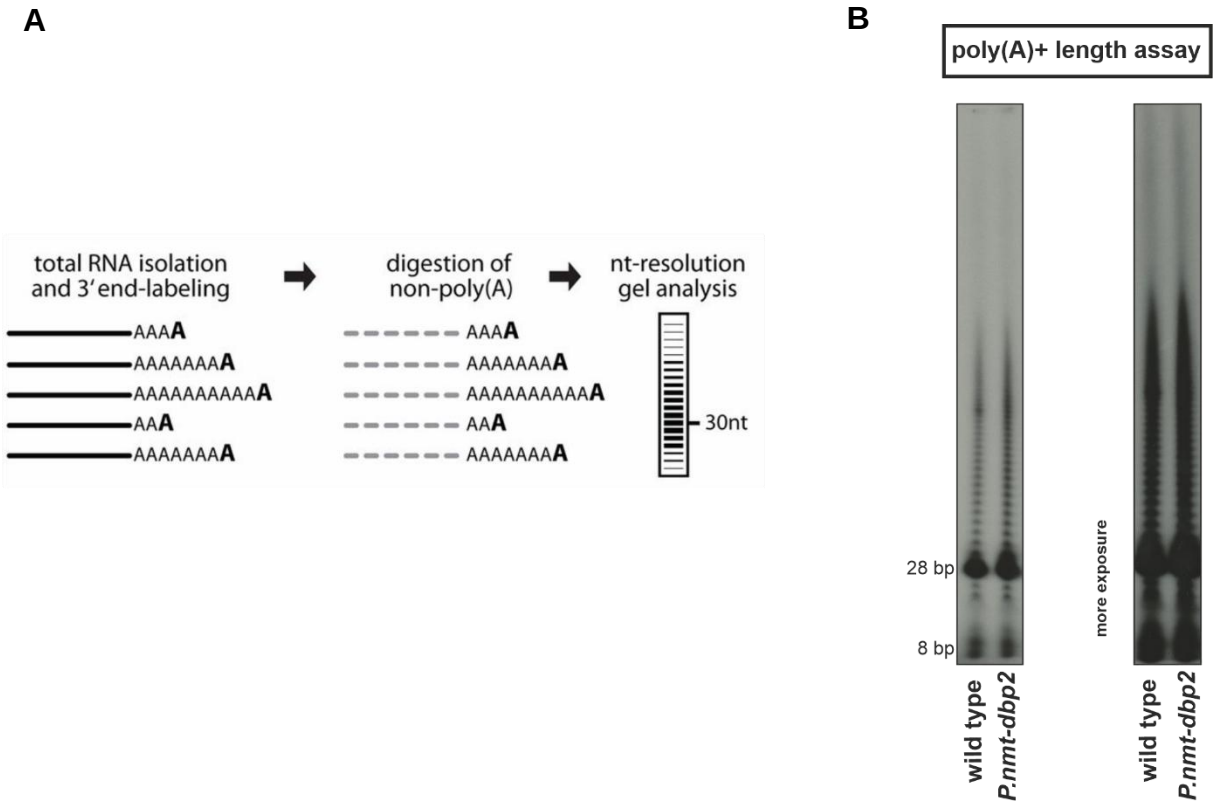

Figure 7.1.4 | Poly(A)-tail length remains unchanged upon Dbp2 depletion

A. Scheme of the experimental procedure for poly(A)+ length assay. Adopted from (Nousch et al., 2013). **B.** Total RNA was isolated from wild type and *P.nmt-dbp2* as described in 9.3.12, labelled with [32P]pCp, digested with RNases A and T1, and size-separated on 20% PAA Urea gel. Size markers were determined by xylene cyanol and bromophenol blue dyes run lengths in 20% gel, followed by exposure to Autoradiography with Amersham Hyperfilm, (n = 1).

7.2 Impact of Dbp2 loss on CPAC component subcellular localisation and distribution

Dbp2 has been proposed to play a key role in early mRNP remodelling (Stewart, 2019), which constitutes the fundamental aim of this study: to investigate Dbp2's role at early checkpoints of mRNA biogenesis. One such checkpoint in mRNP assembly has been identified as the release of CPAC components from mRNAs, a process that depends on the recruitment of export factors (Qu et al., 2009). However, the factors responsible for mediating CPAC release upon the completion of the checkpoint remain unclear. The data presented in this study suggest that Dbp2 interacts with both the 3'-end processing machinery and RNA export factors, indicating that Dbp2 may link these two processes. As a DEAD-box ATPase, Dbp2 could facilitate the release of CPAC components and fulfill the proposed checkpoint. Supporting this, the inefficient export of 3'-processed, polyadenylated RNAs into the cytoplasm in the absence of Dbp2, likely due to impaired recruitment of export factors, was previously discussed in sub-section 7.1. This raises the next question to be addressed: does the retention of already processed RNA result from impaired recruitment of export factors, or from a disruption in a more upstream RNA processing event, specifically during the 3'-end processing step?

7.2.1 CPAC components redistribute to the RNAPII compartment upon loss of Dbp2

If Dbp2 played an active role in the release of CPAC components from processed transcripts within the context of an mRNP assembly checkpoint, its depletion would be expected to result in increased CPAC retention. To investigate whether Dbp2 is involved in CPAC recycling, the subcellular distribution of CFIA component Pcf11 was first examined in the presence and absence of Dbp2 (Figure 7.2.1.1).

To quantitatively assess the differences in the signal intensities of Pcf11 in the presence and absence of Dbp2, cell populations were co-mixed on a microscopy slide (Figure 7.2.1.1A). Wild type cells expressing C-terminally GFP-tagged Pcf11 and NLS-BFP (used to specify the nuclear compartment) were mixed with *P.nmt-dbp2* mutant cells expressing only GFP-tagged C-terminally Pcf11. In wild type cells, Pcf11-GFP compactly localised in nuclear foci, with minimal fluorescence detectable outside of these foci. In contrast, in Dbp2-depleted cells, a substantial portion of the Pcf11-GFP fluorescent signal was dispersed throughout the associated compartment. In the absence of Dbp2, maximal intensity Z-projections were measured, and the maximal green fluorescence intensity was markedly reduced, indicating that the foci localisation of Pcf11-GFP is impaired in Dbp2-depleted cells (Figure 7.2.1.1B). Since the foci localisation of CPAC components represents cleavage bodies, as discussed in Chapter 6, their localisation to cleavage bodies is therefore thought to be impaired in Dbp2-depleted cells. To identify the compartment where Pcf11 disperses upon Dbp2 depletion, cells co-expressing C-terminally GFP-tagged Pcf11 with iRFP-tagged Rpb9, an RNAPII marker, were examined by live microscopy (Figure 7.2.1.1C). In the absence of Dbp2, the Pcf11-GFP fluorescent signal redistributed to the RNAPII-positive compartment (Figure 7.2.1.1D).

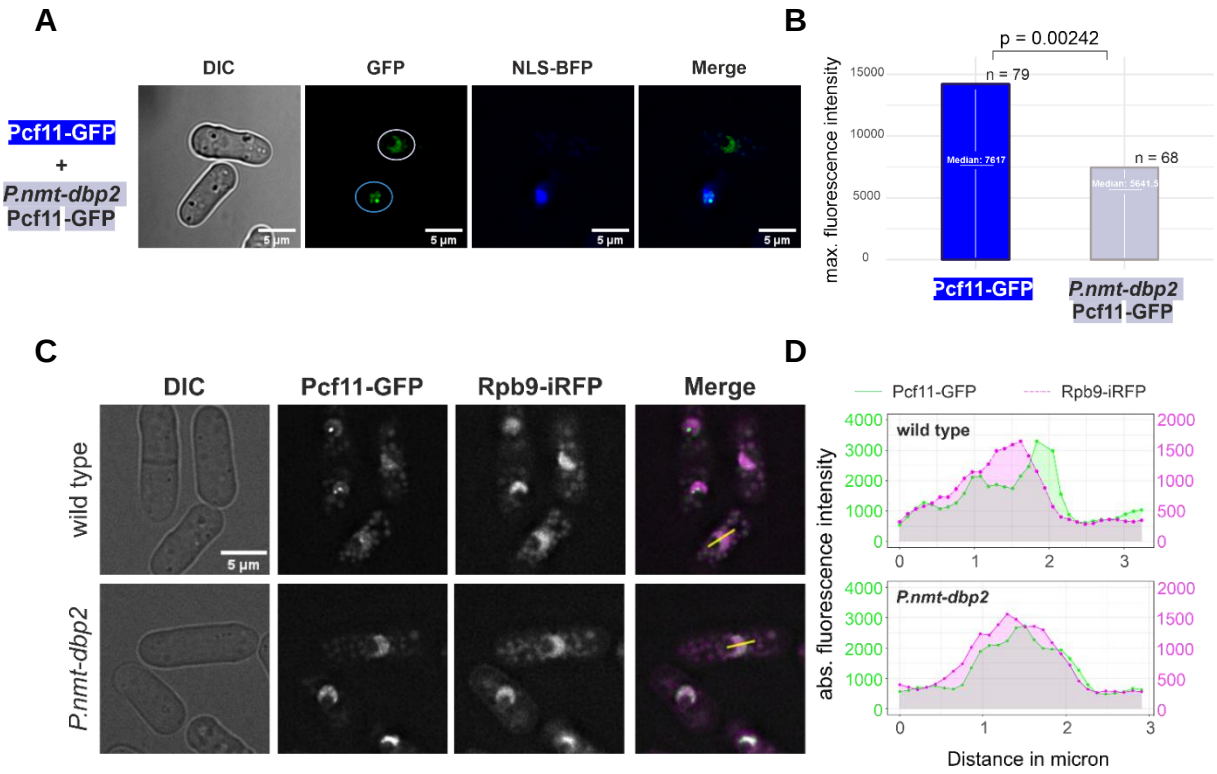

Figure 7.2.1.1 | CPAC components redistribute to the RNAPII compartment upon loss of Dbp2

A. Live cell imaging for Pcf11-GFP in wild type (marked by NLS-BFP) mixed with *P.nmt-dbp2*. Cells were shifted to YES for 5 h. Mixed wild type (+/- BFP) was included as control. Scale bar 5 µm, (n = 2). **B.** Quantification of the experiment shown in (A). Measurements were performed on maximal intensity Z-projections and the maximal green fluorescence intensity scored for each cell, depicted as mean values, including the median values. The displayed p-values for pair-wise comparisons were calculated using a two-sided Wilcoxon rank sum test, (∗p < 0.05; ∗∗p < 0.01; ∗∗∗p < 0.005). **C.** Live cell imaging of genomically tagged Pcf11-GFP and the RNAPII component Rpb9-iRFP. Cells were shifted to YES for 6 h. The merged channel shows Pcf11-GFP in green and Rpb9-iRFP in magenta. Images are representative of two independent experiments. Fluorescence intensity profiles along the yellow lines are shown in (D). **D.** Fluorescence intensity profiles as indicated in (C). Green line corresponds to the Pcf11-GFP signal, dashed magenta line to the Rpb9-iRFP signal. Analysis in C & D was performed by Cornelia Kilchert.

The impact of Dbp2 loss on the subcellular localisation for various other CPAC components, namely cleavage factor component CFIA Rna15, CFIB Msi2 as well as CPAC-interacting protein Seb1, was also monitored by live microscopy.

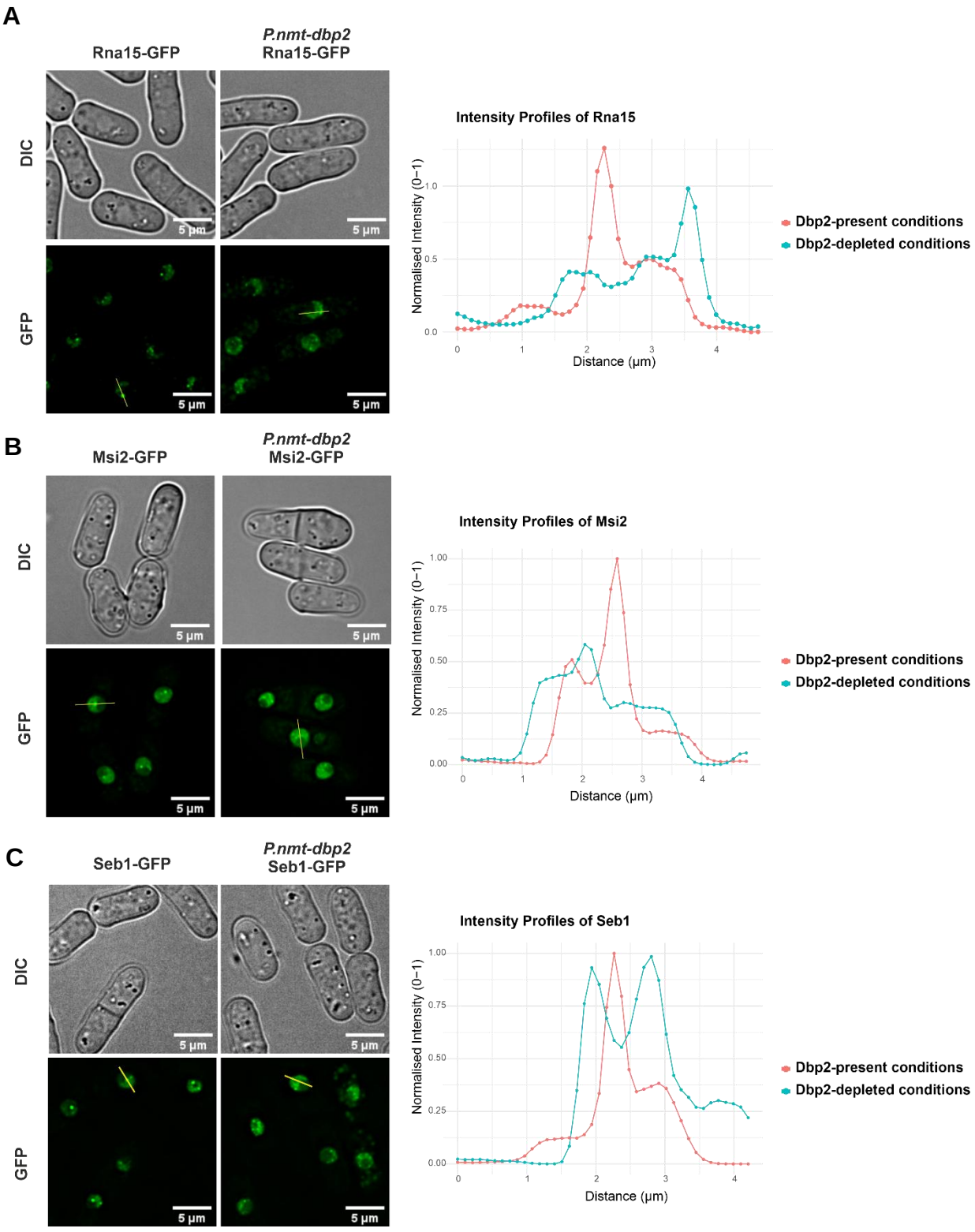

Figure 7.2.1.2 | Loss of Dbp2 impacts the subcellular localisation of the CPAC components

A. Live microscopy of cells carrying endogenously C-terminal GFP-tagged Rna15, **B.** Msi2, and **C.** Seb1 in the presence and absence of Dbp2. Cells were shifted to YES for 5 h at 30 °C, pelleted and resuspended in EMMG for imaging on poly-lysine coated coverslips. For live cell imaging in EMMG-media contained15 µg of thiamine to maintain the stability of the *nmt* promoter repression. Fluorescence intensity profiles across yellow lines in left panel, were measured with Fiji and normalised to a 0-1 range and depicted on the right panel. Scale bar 5 µm. (Images are representative for Rna15-GFP and Msi2-GFP n = 3, and for Seb1-GFP n = 2).

In wild type cells, C-terminally GFP-tagged Rna15, Msi2 and Seb1 showed distinct localisation in nuclear foci (Figure 7.2.1.2), for Rna15 and Msi2 this corresponds to cleavage bodies, as shown in Figure 6.1. Given that Seb1's localisation pattern resembles that of cleavage body components, it is possible that Seb1 may also be a part of it. Specifically, Rna15 exhibited minimal fluorescence detectable in the nucleoplasm outside of foci similar to Pcf11, however for Msi2 and Seb1 nucleoplasmic appearance is rather more discrete in wild type conditions. The common similarity in the localisation patterns of Rna15, Msi2, and Seb1 is that their intact localisation in nuclear foci is considerably impaired upon Dbp2 depletion (Figure 7.2.1.1A, B & C). Given the dispersion of CFIA factor Pcf11 to the RNAPII-positive compartment (Figure 7.2.1.1C, & D) and the resemblance in impaired localisation of Rna15, Msi2 and Seb1 in the absence of Dbp2, it is anticipated that all these factors are redistributed to the RNAPII-positive compartment.

7.2.2 Depletion of CPAC components from cleavage bodies upon Dbp2 loss is restored by transcriptional inhibition

The subcellular localisation of CPAC components and their spatial relationship to cleavage bodies in the presence and absence of Dbp2 were examined in greater detail through live-cell microscopy, with Pcf11 used as a representative example. In wild type cells, C-terminally GFP-tagged Pcf11 compactly co-localised with Red1-tdTomato in cleavage bodies, with minimal fluorescence detectable in the nucleoplasm outside of foci (Figure 7.2.2A, upper panel). Absolute co-localisation of Pcf11 and the cleavage body marker Red1 was demonstrated by the intensity plots (Figure 7.2.2B, upper panel). In contrast, in Dbp2-depleted cells, a substantial portion of Pcf11-GFP fluorescent signal was dispersed throughout the associated-compartment (Figure 7.2.2A, lower panel), revealing an impairment in the co-localisation of Pcf11 and the

cleavage body marker Red1 upon loss of Dbp2, as shown by the intensity plots (Figure 7.2.2B, lower panel). This compartment was previously identified as RNAPII-associated nucleoplasm.

To evaluate whether the dispersion of Pcf11 following the loss of Dbp2 is transcription-dependent, transcription was disrupted using a natural product transcription inhibitor. For this, cultured cells were treated with thiolutin in the presence and absence of Dbp2 for 60 minutes at 30 °C, followed by live cell imaging of Pcf11-GFP in the continued presence of the inhibitor. Thiolutin is a general inhibitor of bacterial and eukaryotic transcription and has been widely used to inhibit transcription initiation in various species (Jimenez et al., 1973; Qiu et al., 2024). Notably, the mislocalisation of Pcf11-GFP completely reversed in Dbp2-depleted cells when transcription was blocked, restoring the cleavage body localisation. This suggests that the transcriptional activity exacerbates the mislocalisation effects of Dbp2 loss, further supporting the storage compartment proposal for cleavage bodies.

Overall, the results presented in this section, combined with earlier findings in Chapter 6 on the characterisation of cleavage bodies, suggest a redistribution of CPAC factors, particularly cleavage factors, from the storage compartment— referred to as cleavage bodies— to the sites of RNA biogenesis in the absence of Dbp2. Furthermore, transcriptional inhibition mitigates this effect, suggesting that ongoing transcriptional activity as the reason for impaired localisation of Pcf11-GFP in Dbp2-deficient cells and that Dbp2's role in RNA biogenesis occurs downstream.

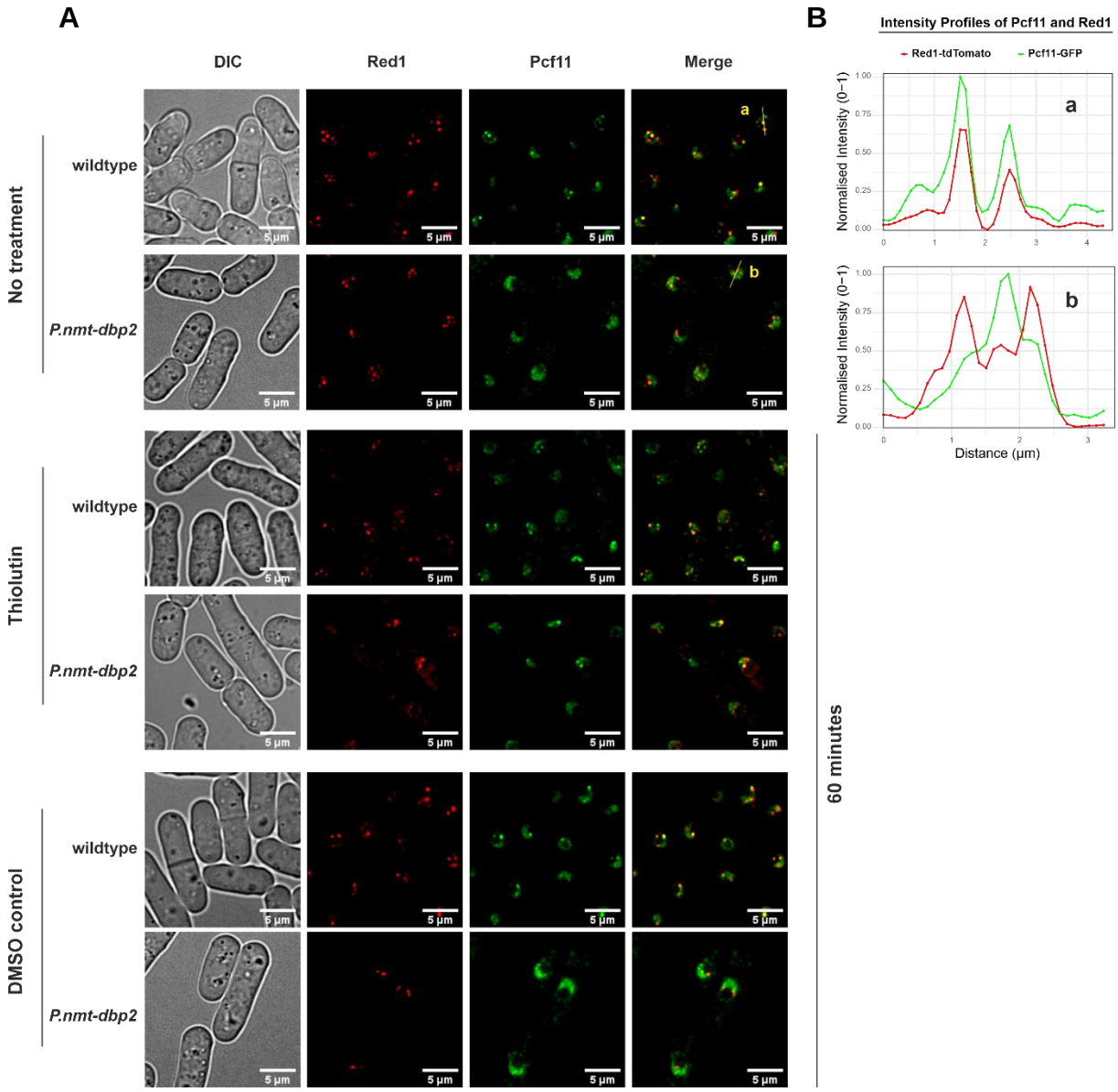

Figure 7.2.2 | Pcf11 is depleted from cleavage bodies upon loss of Dbp2 but is restored when transcription is inhibited

A. Live microscopy of cells carrying endogenously Pcf11-GFP and Red-tdTomato in the presence and absence of Dbp2 were treated with 20 µg thiolutin in DMSO and incubated in YES for a time course of 60 min at 30 °C, pelleted and resuspended in EMMG for imaging on poly-lysine coated coverslips. For live cell imaging in EMMG-media contained15 µg of thiamine to maintain the stability of the *nmt* promoter repression and 20µg of thiolutin to ensure the stability of transcription inhibition. The merged channel shows Pcf11-GFP in green and Red1-tdTomato in red. DMSO was used as a thiolutin-solvent control. DIC is differential interference contrast used for the detection and segmentation of unstained living adherent cells. Scale bar 5 µm, (n = 2). **B.** Fluorescence intensity profiles across yellow lines in upper panel in (A), were measured with Fiji and normalised to a 0-1 range.

7.2.3 CPAC components are depleted from the soluble pool and retained on chromatin upon loss of Dbp2

Furthermore, lysates prepared from the *P.nmt-dbp2* strain contained much lower levels of different CPAC components than the wild type. However, these results were not consistent with the fluorescence microscopy data, where no comparable reduction in the total fluorescent signal of GFP-tagged CPAC components in the mutant was observed (section 7.2). It has been previously reported that the stalling of RNP complexes on chromatin can impede their effective extraction using conventional protocols for chromatin preparation (Rougemaille et al., 2008). It was hypothesised that a similar effect might be responsible for the loss of CPAC components from lysates in the *P.nmt-dbp2* mutant.

To test this hypothesis, protein amounts in standard NP-40 lysates were compared to extracts prepared with the TCA method, which is known to more efficiently extract insoluble material, including the chromatin fraction (Demin et al., 2021; Mehta et al., 2010). While in standard NP-40 lysates, accountable fraction of CPAC components Pcf11 (part of CFIA) and Msi2 (CFIB) were lost when Dbp2 was absent, however in contrast, the yield of these CPAC components in lysates from Dbp2-depleted cells was undistinguishable from wild type levels when TCA lysis was employed (Figure 7.2.3A).

These results indicate that CPAC components are depleted from the soluble pool in the absence of Dbp2, potentially due to their sequestration on poly(A)+ RNAs retained in the nucleus and/or on chromatin. To differentiate between these possibilities, crude NP-40 lysates were treated with RNases or DNase before clearing the lysate by centrifugation (Figure 7.2.3B). Treatment with DNase but not RNase was able to release Msi2-GFP into the soluble fraction in the *P.nmt-dbp2* mutant (Figure 7.2.3C), suggesting that the protein is retained on chromatin.

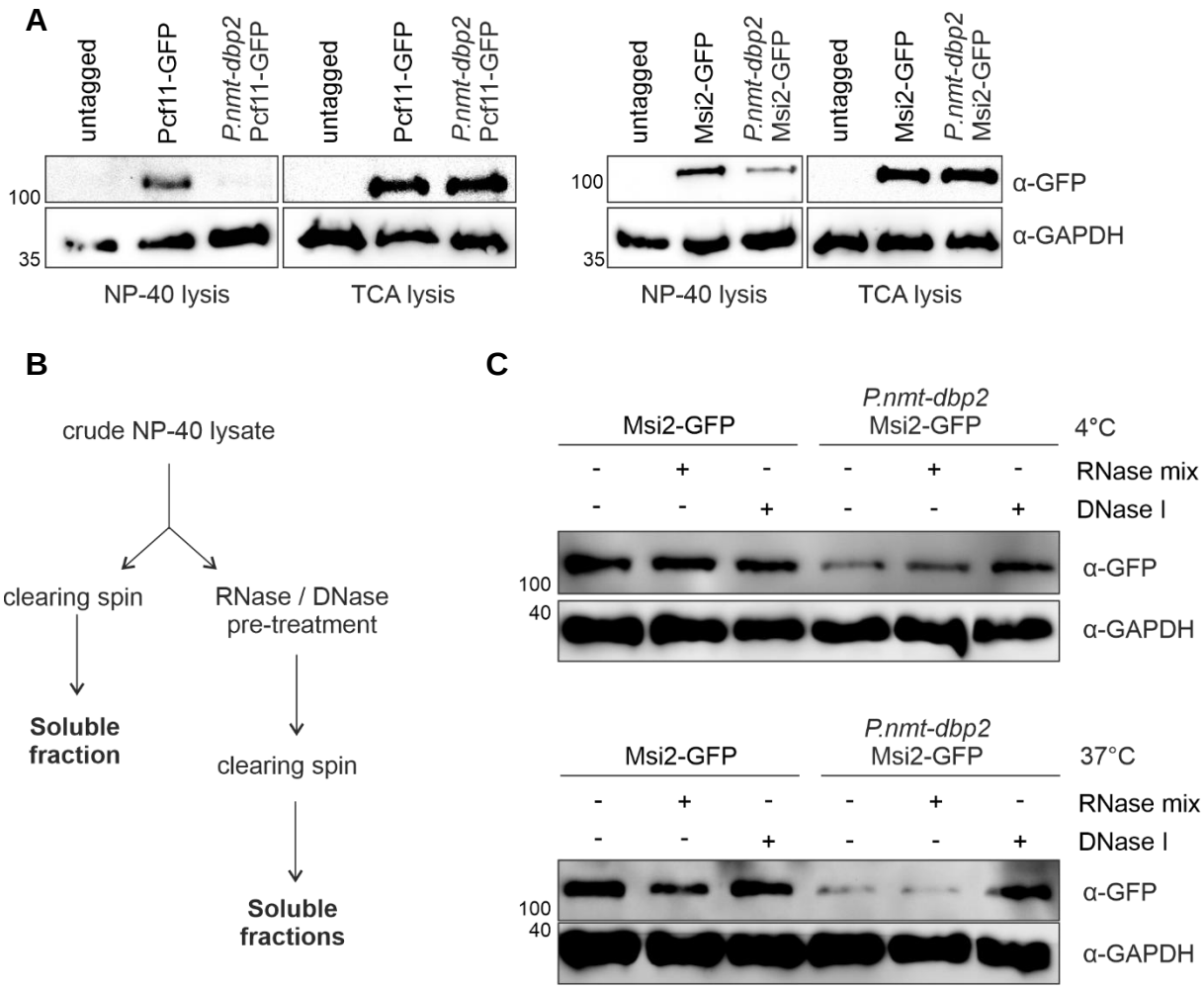

Figure 7.2.3 | CPAC components are depleted from the soluble pool and retained on chromatin upon loss of Dbp2

A. Western blot analysis of cell extracts generated by NP-40 lysis (soluble cell extracts) or TCA lysis (total cell extracts) for CFIA component Pcf11-GFP (left panels) and CFIB component Msi2-GFP (right panels). Cells were grown in EMMG overnight at 30 °C and shifted to YES for 5 h before lysis. GAPDH was detected on the same blot and is included as a loading control. The numbers on the left indicate the molecular weight marker in kDa. Images are representative of two independent experiments. **B**. Schematic to depict the NP-40 lysate generation in A, and treatments in C. **C.** Western blot analysis of NP-40 lysates incubated with RNases or DNase for either 30 min at 4 °C (top panel) or 15 min at 37 °C (bottom panel) prior to the clearing spin to release RNA- or DNA-associated proteins into the soluble pool. Lysates incubated without enzymes added were included as control. Images are representative of two independent experiments.

Overall, these results suggest that, in the absence of Dbp2, CPAC components are depleted from cleavage bodies, which represent the soluble pool, likely due to their retention on chromatin within the nucleus. This is evidenced by the recovery of CPAC components, such as Msi2, in lysates from Dbp2-depleted cells only after DNase

treatment, indicating their sequestration on chromatin. This sequestration is likely responsible for the reduced levels of CPAC components observed in lysates from Dbp2-depleted cells.

7.2.4 A subpopulation of poly(A)+ RNA localises with the chromatin-retained CPAC pool upon loss of Dbp2

While a domain of poly(A)+ RNAs retained in the nucleus accumulate in cleavage bodies upon loss of Dbp2, CPAC components are depleted from these bodies and instead become sequestered on chromatin. However, poly(A)+ RNA retention in the nucleus extends beyond cleavage bodies in the absence of Dbp2. The sequestration of CPAC components on chromatin was confirmed by DNase treatment, which released CPAC components, while RNase treatment had no effect. To gain a better understanding of the impact of Dbp2 loss on the distribution of poly(A)+ RNA in relation to CPAC components, combined oligo-d(T) FISH and immunofluorescence analyses were performed in wild type cells and *P.nmt-dbp2* cells with endogenously GFP-tagged Pcf11. Consistent with previous findings, poly(A)+ RNA under steady-state conditions was distributed throughout the cell, with moderate nuclear abundance overlapping the cleavage body localisation of Pcf11-GFP. Notably, the poly(A)+ RNA content in cleavage bodies was limited under wild type conditions, which aligns with previous findings in human cleavage bodies, where only about 20% of the bodies contain newly transcribed RNA (Schul et al., 1996). However, upon Dbp2 depletion, Pcf11 becomes sequestered on chromatin, accompanied by the sudden accumulation of poly(A)+ RNA, corresponding to a subpopulation distinct from cleavage bodies, within this chromatin-associated pool. This implies that fully processed RNAs could also be

retained at the site of transcription, suggesting a potential role for Dbp2 in facilitating the ultimate release of these poly(A)+ RNAs from the chromatin-associated fraction.

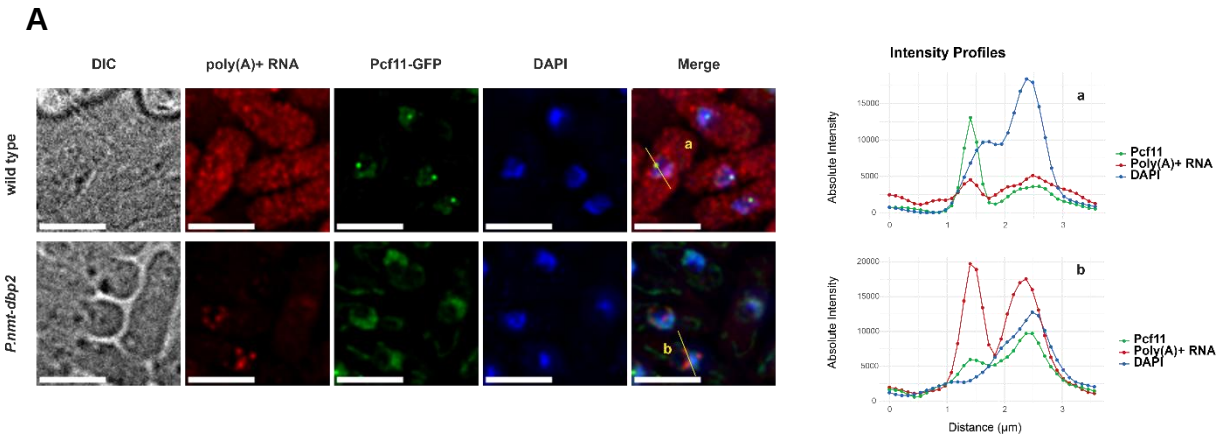

Figure 7.2.4 | A subpopulation of poly(A)+ RNA localises with the chromatin-retained CPAC pool upon loss of Dbp2

A. Left panel, FISH-IF against poly(A)+ RNA using oligo-d(T)-Cy3 in wild type and *P.nmt-dbp2* with Pcf11 endogenously tagged with GFP. Cells were grown overnight in EMMG, then shifted to YES for 5 h to shut off the *P.nmt* promoter before formaldehyde fixation. The merged channel shows poly(A)+ RNA in green, Pcf11-GFP in red and DAPI in blue. Images are representative of three independent experiments. Right panel, absolute fluorescence intensity profiles of FISH-IF signal across sites of poly(A)+ RNA accumulation and the adjacent nuclear area from a, and b yellow lines. In fluorescence intensity plots, green line corresponds to the poly(A)+ RNA signal, red line to the Pcf11-GFP signal. Scale bar 5 µm, (n = 3).

7.3 Loss of Dbp2 results in the widespread occurrence of 3′-extended transcripts

Reduced levels of soluble CPAC components in Dbp2-depleted cells, with the postulation that this fraction corresponds to those available to execute the 3'-end processing of nascent transcripts, led to the hypothesis that RNA cleavage efficiency would be reduced as a result. In eukaryotes, protein-coding genes may contain multiple polyadenylation signal (PAS) sites within the 3' untranslated region (3'-UTR).

The usage of either a proximally or distally located PAS site relative to the stop codon results in the generation of isoforms with varying 3'-UTR lengths (Mata, 2013; Mitschka & Mayr, 2022). Inefficient RNA cleavage is known to be manifested by readthrough

transcription far downstream of canonical cleavage site, leading to 3'-UTR lengthening. To monitor the impact of Dbp2 depletion on PAS usage, poly(A)-enriched transcriptome analysis was performed in the presence and absence of Dbp2. *S. cerevisiae* cells served as a spike-in for normalisation, enabling the assessment of the global effects on mRNA expression levels. Principal component analysis (PCA) showed a clear separation of RNA-seq profiles between wild type and *P.nmt-dbp2* mutant cells (Figure 7.3A). Following Dbp2 depletion, a widespread reduction in RNA levels was observed, reinforcing the crucial role of Dbp2 as a global regulator of RNAPII-dependent RNA biogenesis (Figure 7.3B). For many mRNAs, a relative increase in sequencing reads over extended 3'-UTR isoforms or beyond the canonical cleavage site of annotated features was observed following Dbp2 depletion, suggesting a general tendency of the mutant to bypass cleavage sites and continue transcription to downstream regions (Figure 7.3C). Many mRNAs possess multiple PAS, which may have evolved as a fail-safe mechanism to prevent transcription into downstream genes (Turtola et al., 2021). Several instances from the RNA-seq data show that read-through is correlated with decreased expression of downstream convergent genes (Figure 7.3D). Notably, an increased read-through signal was detected for almost any transcript with a sufficiently high expression level in the RNA-seq data. However, the severity of the phenotype was transcript-dependent and is possibly related to the strength of the corresponding PAS. Northern blotting with DIG-labelled RNA probes directed against the gene bodies confirmed the presence of extended transcript isoforms for several mRNAs (Figure 7.3E). For *rpl2501* mRNA, a probe targeting the extended 3'-UTR was included to confirm the increased presence of 3'-extended transcripts in the mutant (Figure 7.3F, left panel). The analysis of cleavage site usage on this transcript was then confirmed through RT-PCR amplification using an anchored $(T)_{12}VN$ primer, which further validated the alternative

PAS usage and 3'-UTR lengthening in the absence of Dbp2. This phenotype, typically observed following the depletion of core poly(A) factors, suggests that one or more CPAC components may become limiting in the *P.nmt-dbp2* mutant.

Overall, the reduced cleavage efficiency at RNAPII-transcribed genes observed upon Dbp2 depletion is consistent with the increased occurrence of PAS skipping at the RNA level. This is taken as evidence that the depletion of CPAC components from the soluble pool in the absence of Dbp2 limits their availability, rendering them insufficient to maintain optimal 3'-end processing.

Figure 7.3 | Loss of Dbp2 results in the widespread occurrence of 3′-extended transcripts

A. Principal component analysis (PCA) of RNA-seq peaks for wild type and *P.nmt-dbp2* shown after normalising counts to the number of total *S. cerevisiae* reads for each sample before calculating the mean. Cells were grown in EMMG overnight at 30°C, harvested, and cultured in YES + 15 µM thiamine for 5 h, then mixed with *S. cerevisiae* in a 5:1 OD_{600} ratio prior to RNA isolation. **B.** Mean integrated counts of RNA-seq reads over annotated features in wild type and *P.nmt-dbp2* after a 5 h depletion period. Contours of a 2d density estimate are shown in grey. **C.** Representative RNA-seq traces across the region of chromosome I encompassing the *atp19* gene (negative strand) and downstream convergent *pcf3* gene (positive strand) with reads for wild type in grey, for *P.nmt-dbp2* in light blue. Read counts were normalised to a 0–1 range. RNA-seq traces analysis was performed by Cornelia Kilchert. RNA-seq datasets, n = 3 biological replicates. **D.** Plot displaying the gene expression differences of the downstream convergent *pcf3* gene in wild type and *P.nmt-dbp2* strains, with normalised mean expression for wild type shown in grey and for *P.nmt-dbp2* in light blue. **E.** Northern blots for *tma19*, *asl1*, and *rpl1001* mRNA using a strand-specific DIG-labelled RNA probe against the gene body. 18S band stained with methylene blue is shown as a loading control. Arrows indicate positions of extended transcripts. The marker is a double-stranded DNA size marker (Roche, Molecular Weight Marker VIII, DIG-labelled). **F.** Left panel, Northern blot for *rpl2501* mRNA using strand-specific DIG-labelled RNA probes against the gene body or the 3'-extension. Right panel, analysis of poly(A) site usage by RT-PCR amplification using an anchored $(T)_{12}VN$ primer. Upper panel, depicting the positions of primers used for the gene body or the 3'-extension, polyadenylation signals (AAUAAA) is highlighted as red bars, the Northern probes shown as dotted lines and the forward primer used for PCR amplification as green arrowhead. Usage of the AAUAAAA sites marked is expected to lead to amplicons of ~140 bp and ~350 bp, respectively. Amplicons that reflect usage of distal poly(A) sites are marked with arrows. Experiments in (F) were performed by Silke Schreiner. Images are representative of three independent experiments.

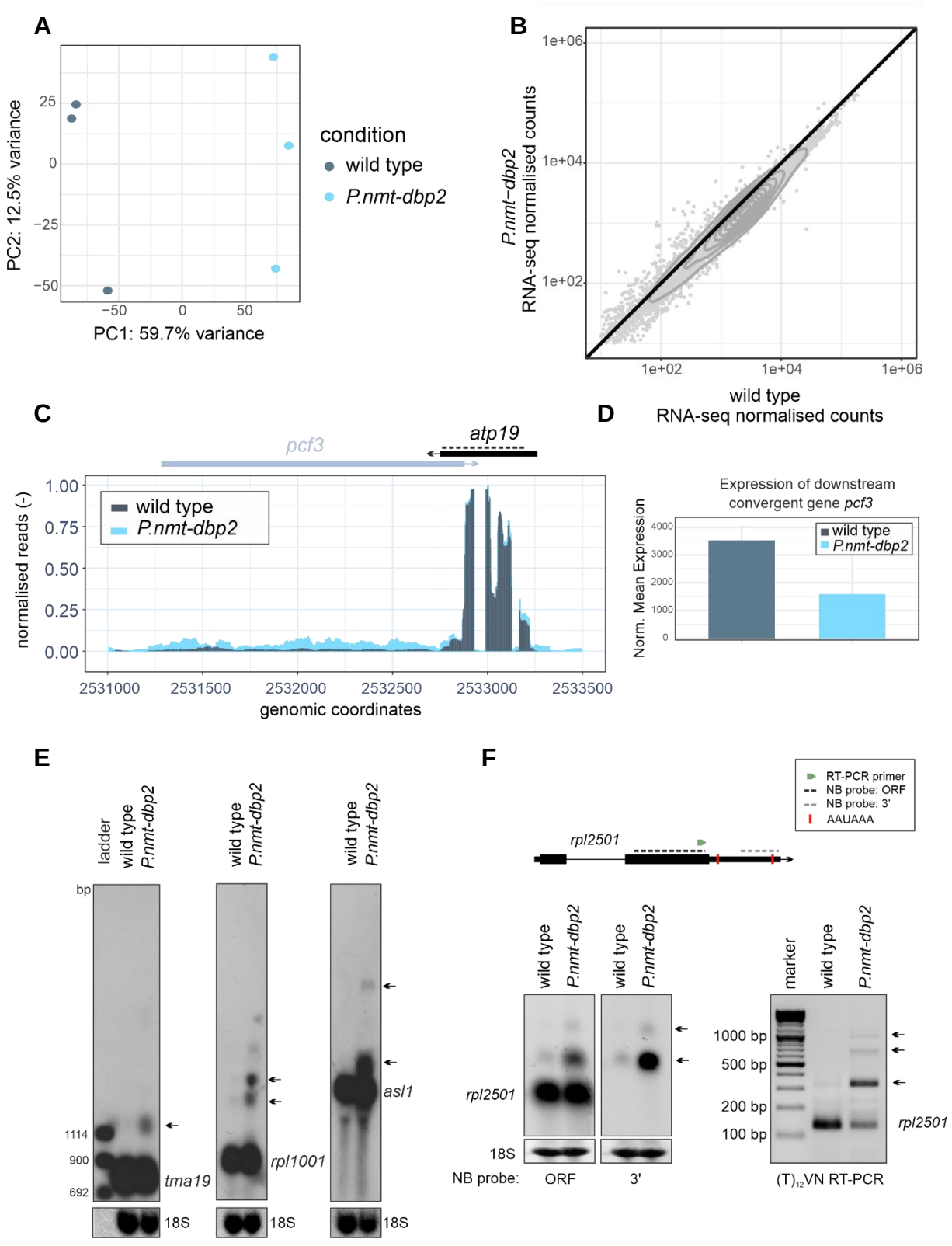
A
PC2: 12.5% variance
PC1: 59.7% variance
condition
wild type
P.nmt-dbp2
B
P.nmt−dbp2 RNA-seq normalised counts
wild type RNA-seq normalised counts
C
pcf3
atp19
normalised reads (-)
wild type
P.nmt-dbp2
genomic coordinates
D
Expression of downstream convergent gene pcf3
Norm. Mean Expression
E
ladder
wild type
P.nmt-dbp2
bp
tma19
rpl1001
asl1
18S
F
RT-PCR primer
NB probe: ORF
NB probe: 3'
AAUAAA
rpl2501
NB probe:
ORF
3'
marker
1000 bp
500 bp
200 bp
100 bp
(T)12VN RT-PCR

7.3.1 MTREC/PAXT mutants do not improve RNA cleavage efficiency in Dbp2-depleted cells

In Section 7.1, it was shown that a significant portion of poly(A)+ RNA is retained in the nucleus upon loss of Dbp2, with a fraction of these RNAs corresponding to cleavage bodies, a storage compartment where Dbp2 colocalises with components of the MTREC/PAXT complex. This suggested that Dbp2 is needed to release fully processed RNAs from these structures. However, further investigations revealed that MTREC/PAXT components Red1 and Pab2 are not required for the nuclear retention of poly(A)+ RNA in the absence of Dbp2. Additionally, the retention of poly(A)+ RNA in the absence of Dbp2 was only partially rescued by the loss of Iss10, suggesting that MTREC is not involved in the retention mechanism triggered by the loss of Dbp2. Initially, it was hypothesised that retention resulted from inefficient recruitment of export factors, but subsequent analyses showed that CPAC components had reduced levels in soluble fraction and remained on-site in the absence of Dbp2, which reduced RNA cleavage efficiency, leading to increased usage of distal PAS sites and the widespread occurrence of 3'-UTR extended isoforms. Nevertheless, it remains worth investigating whether MTREC mutants rescue the increased skipping of canonical cleavage and polyadenylation sites upon Dbp2 depletion.

The impact of MTREC complex components on RNA cleavage efficiency upon loss of Dbp2 was assessed using strains combining *red1Δ*, *pab2Δ*, or *iss10Δ* with *P.nmt-dbp2,* along with a wild type control by Northern blotting. A DIG-labelled RNA probe directed against the gene body was used to check for the presence of the extended isoform of the *asl1* transcript. Notably, the single deletion of *red1Δ*, *pab2Δ, or iss10Δ* showed no prevalence of the extended *asl1* isoform, similar to wild type control. However, all *red1Δ* P.nmt-dbp2, *pab2Δ P.nmt-dbp2, and iss10Δ P.nmt-dbp2* double

mutants exhibited persistent failure in RNA cleavage. While the *red1Δ* P.nmt-dbp2 *and iss10Δ P.nmt-dbp2* double mutant strains showed moderately similar levels of the extended *asl1* isoform, the double *pab2Δ P.nmt-dbp2* mutant strain showed an additive effect supported by the increased levels of the extended *asl1* isoform. It is difficult to assess the relative amounts of the *asl1* wild type transcripts between samples due to the strength of the signal. However, considering the corresponding 18S rRNA levels, the increased levels in the *pab2Δ P.nmt-dbp2* double mutant strain are affirmed. This result may indicate a Pab2-driven impairment in RNA surveillance and suggest that

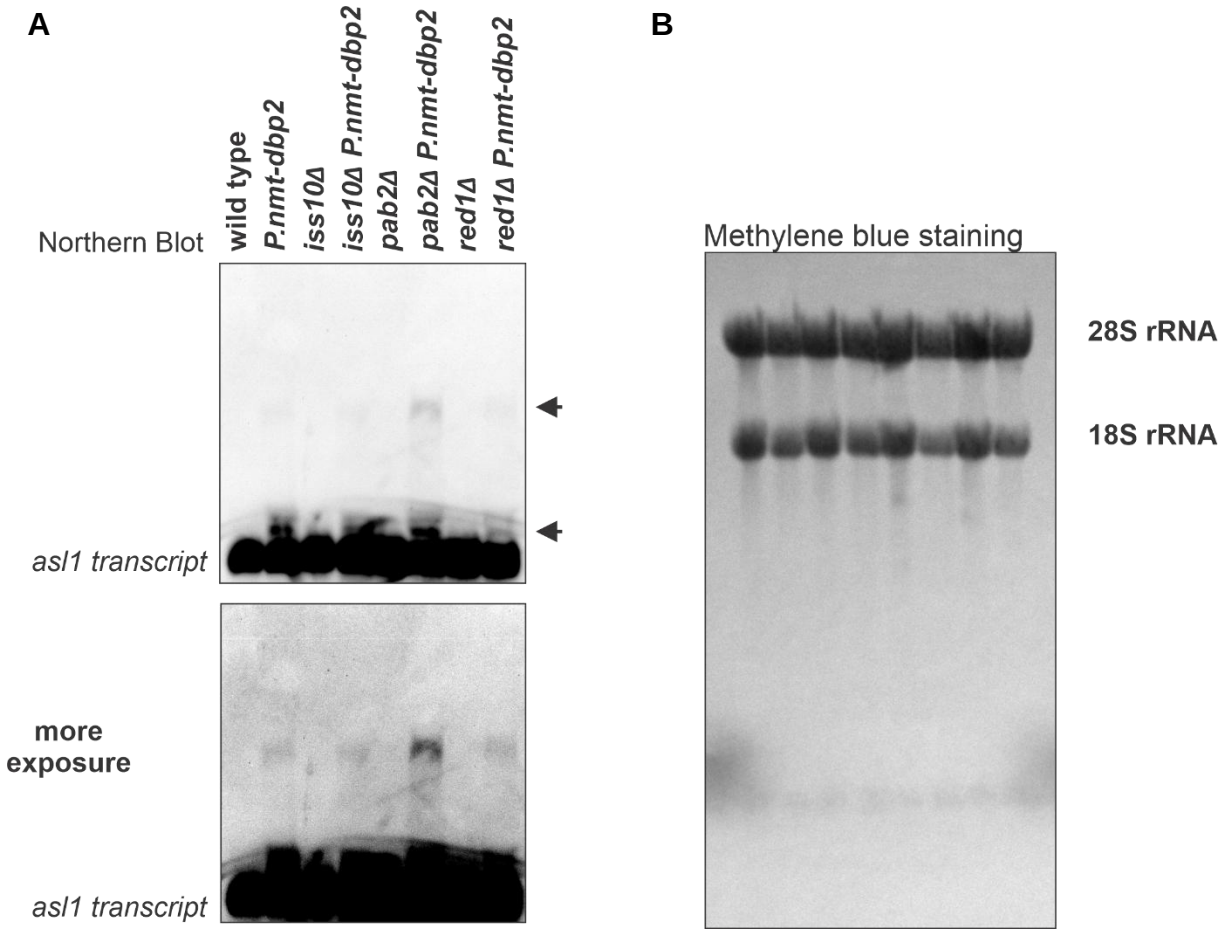

Figure 7.3.1 | MTREC/PAXT mutants do not improve RNA cleavage efficiency in the absence of Dbp2

A. Northern blot analysis against *asl1* transcript using a strand-specific DIG-labelled RNA probe against the gene body, lower panel is upon more exposure. Cells were grown in EMMG overnight at 30 °C, harvested, and cultured in YES medium + 15 µM thiamine for 5 h prior to RNA isolation. Arrows indicate positions of extended transcripts. **B**. Methylene blue staining of the blot showing 18S and 28S rRNA bands, used as a loading control. Images are representative of two independent experiments.

Pab2 plays a specific role in the decay of extended transcripts. In its absence, defective transcripts produced in the *P.nmt-dbp2* mutant strain may no longer be effectively targeted.

7.4 Transcription termination is delayed in the absence of Dbp2

The reduced levels of CPAC components in the soluble pool, unable to sustain normal 3'-end processing, lead to decreased RNA cleavage efficiency in Dbp2-depleted cells. Although RNA cleavage and transcription termination are distinct events, transcription termination is linked to co-transcriptional RNA cleavage (Rodríguez-Molina et al., 2023), this raises the question of whether Dbp2 depletion also affects transcription termination. In order to assess the impact of Dbp2 loss on RNAPII transcription termination, chromatin-immunoprecipitation of RNAPII followed by sequencing had been carried out with wild type (*dbp2-3myc*) and *P.nmt-dbp2* (*P.nmt-dbp2-3myc*) cells. Using *S. cerevisiae* spike-in for normalisation of levels, a global reduction of RNAPII levels at transcribed genes was observed upon depletion of Dbp2 (Figure 7.4A). To assess whether transcription termination was impacted upon loss of Dbp2, metagene analysis of RNAPII coverage across the transcription units of RPGs was performed. The peak in RNAPII coverage at the 3'-end of genes was shifted downstream in Dbp2-depleted cells when compared to wild type cells, suggesting a delay in transcription termination (Figure 7.4B).

As discussed in section 1.2.2.3 of the introduction, one of the widely accepted models for termination of RNAPII-mediated transcription is cleavage-coupled transcription termination, in which RNAPII kinetically competes with the 5'-3' exonuclease Dhp1/Rat1/Xrn2. Dhp1 degrades the nascent 3'-fragment generated during cleavage and promotes transcription termination upon reaching RNAPII (Kim et al., 2004;

Larochelle et al., 2018; West et al., 2004). Due to this competition, both faster RNAPII elongation rates and delays in RNA cleavage can delay transcription termination. Even though it is not possible to definitively distinguish between these two possibilities, as the rates of RNAPII during transcription have not been measured in mutant and wild type cells. However, when the RNAPII ChIP signal was normalised to the annotated PAS-cleavage site, cumulative levels of RNAPII density across the termination zones appeared in Dbp2-depleted cells in relative to declined RNAPII density at this zone in the wild type cells (Figure 7.4C), indicating a slow transition of RNAPII through the termination zone in the mutant.

Figure 7.4 | RNAPII density across the termination zone increased upon the depletion of Dbp2

A. Mean integrated counts of RNAPII-ChIP-seq reads over annotated features in dbp2-3myc or *P.nmt-dbp2-3myc* (n = 2) after a 9 h depletion period. Cells were grown in EMMG overnight at 30 °C, harvested, and cultured in YES for 9 h, then mixed with *S. cerevisiae* in a 5:1 OD_{600} ratio prior to chromatin isolation and IP against total RNAPII (α-Rpb1 (8WG16), n=2). ChIP-seq was carried out by Cornelia Kilchert. Contours of a 2d density estimate are shown in grey. Integrated counts were normalised to the number of total *S. cerevisiae* reads for each sample before calculating the mean. **B.** Metagene analysis of the mean RNAPII ChIP-seq signal was performed across ribosomal protein genes (RPGs), including 200 bp upstream and 500 bp downstream of the annotated transcription units. Mean coverage was normalised to the maximal peak height by applying a constant scaling factor, indicated by the grey horizontal line. The schematic above the left panel represents an RPG of median length. In the left panel, the positions of the transcription start and end sites within the metagene are distributed around the given coordinate due to varying feature compression depending on gene length. **C.** Metagene analysis of the mean RNAPII ChIP-seq signal was performed across ribosomal protein genes (RPGs), including 200 bp upstream and 500 bp downstream of the annotated transcription units around the polyadenylation and cleavage site (PAS). Mean coverage was normalized to RNAPII levels at the PAS by applying a constant scaling factor, indicated by the grey horizontal line. The schematic above the left panel represents an RPG of median length. In the left panel, the positions of the transcription start and end sites within the metagene are distributed around the given coordinate due to varying feature compression depending on gene length. **D.** Co-immunoprecipitation of the largest subunit of RNAPII, Rpb1-HTP, was performed in the presence and absence of Dbp2 using IgG sepharose beads. The pull-down was probed with α-His_6 antibody to detect Rpb1 levels, α-Ubi to examine the ubiquitination pattern of Rpb1, and α-GAPDH as a loading control for the input samples. 10% SDS-PAGE gels were used, with molecular sizes indicated on the left. Images are representative of three independent experiments, (n = 3).

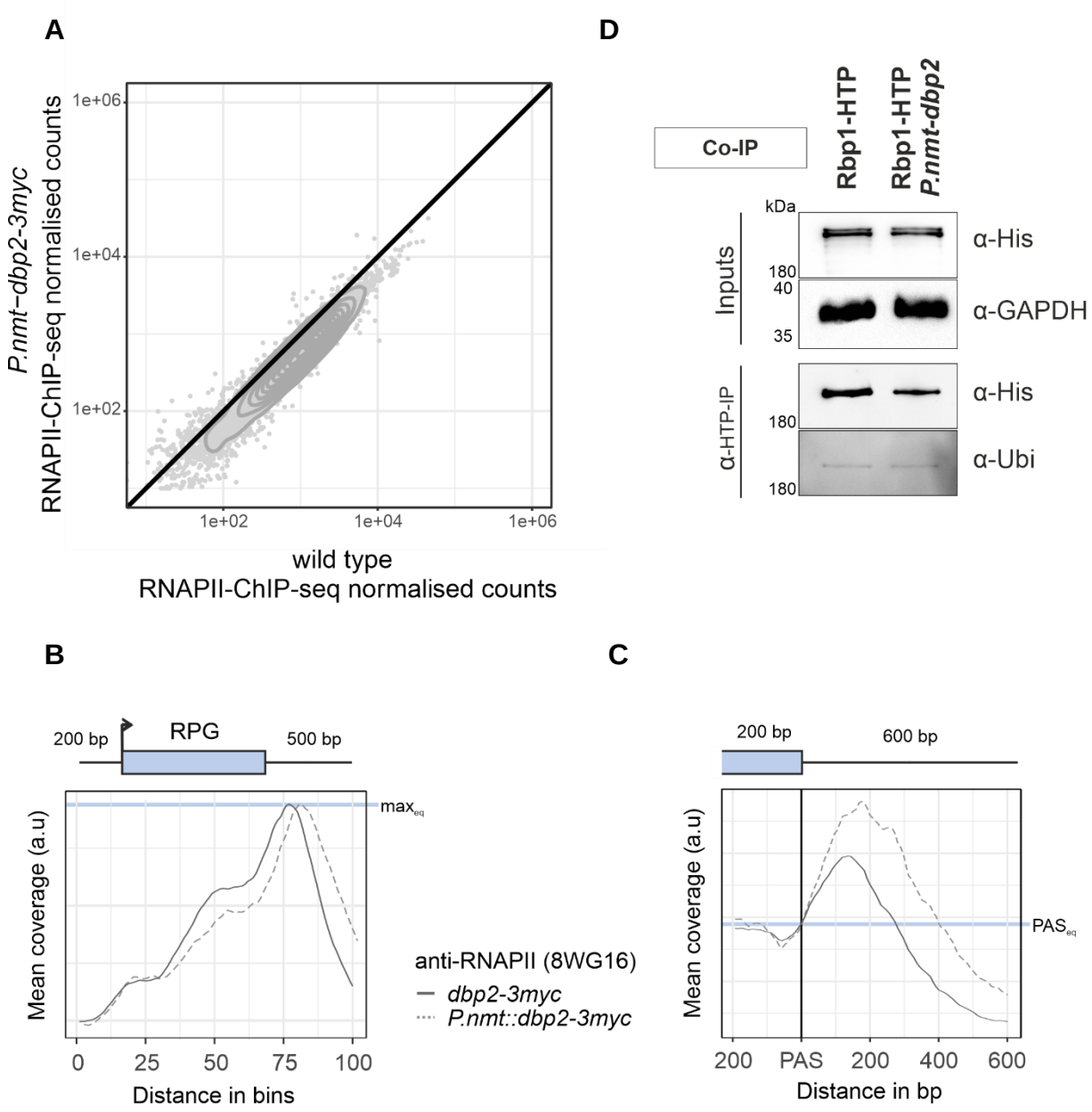

Furthermore, higher RNAPII occupancy observed in the termination window of Dbp2-depleted cells, which may indicate RNAPII stalling. A conserved mechanism for removing stalled RNAPII from DNA involves its ubiquitination followed by degradation via the proteasome complex (Gómez-Herreros et al., 2012). To determine whether ubiquitinated RNAPII levels increase in the absence of Dbp2, affinity purification of C-terminally HTP-tagged Rpb1, the largest subunit of RNAPII, was performed both in the presence and absence of Dbp2. The ubiquitination status was then analysed using an anti-ubiquitin antibody (Figure 7.4D). No significant difference in Rpb1 ubiquitination

levels was detected between wild type and Dbp2-depleted cells, suggesting that the accumulated RNAPII density at the termination zone upon Dbp2 loss does not involve stalling-dependent ubiquitination of RNAPII. This may be attributed to the abundance of RNAPII-CTD serine 5 phosphorylation in Dbp2-depleted cells (Figure 5.1D), a modification known to inhibit RNAPII ubiquitination (Somesh et al., 2005).

7.5 Discussion

Chapter 7 examines the cellular consequences of Dbp2 depletion to define the specific mRNP stage at which Dbp2 functions, with a detailed assessment of the impact of its loss on phenotypes associated with a given RNA processing step, as well as the subcellular localisation and distribution of poly(A)+ RNA and CPAC components. Detailed analysis is particularly critical, as pleiotropic effects complicate the study of RBPs, with mutations often resulting in broad and overlapping phenotypes that cannot be easily linked to a singular RNA processing event (Albulescu et al., 2012; Herzel et al., 2018; M. J. Moore & Proudfoot, 2009).

A central finding in the first section of this chapter is that Dbp2 is essential for the release of poly(A)+ RNAs from nuclear compartments and the regulation of their subsequent export to the cytoplasm. In addition to the general nuclear retention of poly(A)+ RNA, a fraction of this RNA accumulates in structures known as cleavage bodies. Further assessments addressing the retention in cleavage bodies using double mutants with the MTREC complex have revealed distinct retention pathways, implying that different factors contribute to RNA retention in the *P.nmt-dbp2* background. As poly(A)+ RNA retention could be due to impaired RNA export, the observed changes in the subcellular localisation of these export factors and the impaired recruitment of Mlo3 to poly(A)+ RNA in the absence of Dbp2 further support the importance of Dbp2

in the proper recruitment of RNA export factors. Finally, the retention of poly(A)+ RNA in the absence of Dbp2 is not due to hyperadenylation. This finding helps clarify the distinction between early and later mRNP assembly-associated phenotypes within the broader mRNA maturation pathway with respect to the stage at which Dbp2 acts. These results suggest that Dbp2 may be involved in processes preceding polyadenylation, such as mRNP assembly or the recruitment of export factors, rather than in the regulation of poly(A)-tail length itself.

A critical finding is the depletion of CPAC components from the soluble fraction upon Dbp2 depletion, coupled with their retention on chromatin. The CPAC factors, which should be released into the soluble pool after mRNA processing, remain trapped on chromatin in Dbp2-depleted cells. This phenomenon, the reduced solubility of CPAC components in Dbp2-depleted cells, is where CPAC components becomes sequestered in the chromatin-associated fraction, likely as part of a larger mRNP complex still associated with nascent RNA. The use of DNase treatment, which releases chromatin-associated CPAC components, further supports this hypothesis, highlighting the physical interaction of CPAC factors with chromatin in Dbp2-depleted cells. This, in turn, could contribute to the observed defects in RNA cleavage and the accumulation of 3’-extended transcripts (section 7.3). This reduction in the soluble CPAC pool may limit the number of processing factors available to complete cleavage, leading to readthrough transcription and the generation of longer 3'-UTRs. This indicates that Dbp2 plays an essential role in the release and recycling of CPAC components from mRNAs after they have undergone 3'-end processing. These results highlight Dbp2 as a key regulator in the spatial and temporal coordination of mRNA assembly by regulating a checkpoint in mRNP assembly, which was previously established (Qu et al., 2009). The sequestration on chromatin is likely the contributing

factor for the observed nuclear retention of poly(A)+ RNAs, preventing them from being efficiently exported to the cytoplasm. This suggests that Dbp2 functions as a dynamic regulator of mRNA flux, controlling the release of mRNA processing factors and ensuring the timely maturation and export of mRNAs. It also explains Dbp2's role as a global regulator of RNAPII-dependent RNA biogenesis. Upon checkpoint failure in Dbp2-depleted cells, RNA processing intermediates stall or accumulate on chromatin, disrupting the flow of RNA maturation. This possibly in turn results in a global reduction in both RNAPII recruitment to chromatin and subsequently lowered transcript levels, occurring as a secondary effect in cellular gene regulation.

The initial set of experiments demonstrated that the depletion of Dbp2 leads to a redistribution of CPAC components, such as Pcf11, Rna15, Msi2, and CPAC-interacting protein Seb1, from their typical localised nuclear foci to the RNAPII compartment. Moreover, the fact that transcriptional inhibition can rescue the mislocalisation of CPAC components in Dbp2-depleted cells is particularly insightful. This suggests that Dbp2's action is dependent on ongoing transcription and the nascent RNA's interaction with chromatin. The restoration of Pcf11 localisation in the absence of Dbp2 under these conditions reinforces the idea that Dbp2's role in RNA processing occurs downstream of transcription. It indicates that the proper localisation and release of CPAC components are likely tightly coupled to transcriptional events, and Dbp2 functions in the context of mRNA biogenesis as the transcript is being synthesised and processed.

Dbp2 might act to facilitate a transition from the "chromatin" phase of mRNA processing to the "export" phase by coordinating the release of processing factors at the appropriate time in response to transcriptional cues. The observation that CPAC components become sequestered on chromatin in the absence of Dbp2 reveals a

potentially overlooked aspect of chromatin's involvement in RNA maturation. The improper retention of mRNA processing factors on chromatin, instead of in the soluble mRNP pool, points to an important regulatory mechanism: the sequestration of processing machinery can stall mRNA maturation and prevent the correct assembly of export-competent mRNPs. This highlights a mechanism through which chromatin-associated factors could potentially regulate the fate of mRNA transcripts by influencing their transition from processing to export.

Finally, the analysis of transcription termination in Dbp2-depleted cells revealed a delay in the proper termination of RNAPII-mediated transcription. The shift of RNAPII coverage downstream of the canonical termination site suggests that transcription termination is delayed in the absence of Dbp2. This delay may be a consequence of impaired RNA cleavage, as cleavage-coupled termination is thought to rely on the proper processing of nascent transcripts. Furthermore, the increased RNAPII density in the termination region in Dbp2-depleted cells suggests that RNAPII elongation may be prolonged, possibly due to the accumulation of unprocessed or improperly processed RNA. Increased RNAPII density is often associated with stalling of the polymerase, which may explain the reduction in the expression of downstream convergent genes (Figure 7.3D) (Hobson et al., 2012; Lemay & Bachand, 2015). The lack of increased ubiquitination of RNAPII in these cells however suggests that the delay in termination is not due to RNAPII stalling but rather to a defect in transcription termination that is indirectly linked to Dbp2’s role in RNA processing.

Challenging the hypothesis that MTREC/PAXT components compensate for RNA cleavage inefficiency upon Dbp2 loss, mutants like Red1, Pab2, and Iss10 deletions do not improve RNA cleavage in Dbp2-depleted cells. This indicates that Dbp2's role in 3′-end processing is not compensated by MTREC/PAXT. Therefore, Dbp2’s function

in releasing CPAC components and ensuring efficient RNA cleavage is independent of the MTREC/PAXT pathway in this context. Pab2, however, appears to be involved in the decay of defective extended transcripts, as its absence in Dbp2-depleted cells leads to higher accumulation of these isoforms. This suggests that Pab2, as part of the MTREC complex, plays a role in RNA surveillance and degradation of defective extended transcripts, consistent with the additive effect on poly(A)+ RNA retention in double mutant cells (sub-section 7.1.2). Increasing evidence points to a complex interplay between 3′-end processing and nuclear surveillance, where RNA transcripts directed to decay are cleaved by the CPAC complex and handed over to the MTREC complex (Bresson et al., 2015; Chen et al., 2011; Lee et al., 2020; Vo et al., 2019; Yamanaka et al., 2010; Zhou et al., 2015). Msi2's direct interaction with Pab2 and/or Mmi1 may suggest a new pathway for the decay of defective extended transcripts (Soni et al., 2023).

The results of this study paint a coherent picture of how Dbp2, a DEAD-box ATPase, orchestrates key steps in the early stages of mRNA biogenesis, licensing for RNA export and is coupled to the release and recycling of the cleavage and polyadenylation complex (CPAC).

Chapter8 GENERAL DISCUSSION AND CONCLUSION

In this thesis, a novel function of the DEAD-box ATPase Dbp2 was identified, revealing its critical role in coordinating mRNA export by facilitating the release of CPAC components, supporting the mRNP assembly checkpoint at 3′-ends proposed by Qu et al., 2009.

The study starts with a biochemical characterisation of *S. pombe* Dbp2 and *in vitro* analyses to assess its enzymatic activity, revealing that its highly conserved helicase core supports active RNA helicase functions, facilitating efficient RNA duplex unwinding (Chapter 2). These findings supported the hypothesis of this thesis, proposing a potential role for Dbp2 as an RNPase in mRNP assembly within the cellular environment through the regulation of RNA-protein complexes. The genome-wide mapping of Dbp2 revealed its mapping primarily to the 3'-end of genes in the termination window (Chapter 4). Further analysis of its interactome demonstrated its association with factors involved in RNA processing, particularly CPAC and several RNA export factors, including Mex67 and the Yra1 the homologue Mlo3.

Notably, the interactome data also identified an interaction between Dbp2 and the MTREC (Mtl1-Red1 core) complex, which plays a role in RNA surveillance by targeting transcripts for degradation by the nuclear exosome (Chapter 5). Before proceeding with mutant analyses to assess the functional consequences of Dbp2 loss in cells, the interactome data prompted a revisit of previously reported subnuclear structures in *S. pombe*, referred to in this study as cleavage bodies due to their similarity in composition to human cleavage bodies (Li, et al., 2006; Schul et al., 1996; Sugiyama & Sugioka-Sugiyama, 2011) (Chapter 6). The 3’-end formation factors and MTREC were known to co-localise in cleavage bodies in *S. pombe* (Sugiyama et al., 2012, 2013; Sugiyama & Sugioka-Sugiyama, 2011; Yamanaka et al., 2010), Dbp2 was

also found to co-localise with these RNA processing and surveillance factors within these bodies, supporting the interactome data. Further analyses suggested that cleavage bodies potentially function as storage compartments for CPAC factors, buffering their levels until recruitment to active transcription sites for processing, rather than being sites of bulk RNA cleavage. This raises an interesting question of whether the recruitment of these factors from cleavage bodies to their functional sites is also subjected to a regulation.

When the cellular consequences of Dbp2 depletion were assessed (Chapter 7), a disruption in the balance of mRNP assembly was observed, primarily triggered by the unavailability of the CPAC components in the unbound fraction, due to their sequestration on chromatin, leading to a detrimental chain of events in the downstream steps of mRNP assembly, including inefficient RNA cleavage and increased usage of distal PAS sites, leading to 3'-UTR extensions and delayed transcription termination, subsequent poly(A)+ RNA retention within the nucleus.

Among the core 3'-end processing factors, only Hrp1 (the Msi2 *S. cerevisiae* orthologue) shuttles between the nucleus and cytoplasm, suggesting that most CPAC components must be released and recycled within the nucleus (Hammell et al., 2002). These findings position Dbp2 at the intersection of 3′-end RNA processing and RNA export, marking it as a key enzyme at this intersecting mRNP assembly checkpoint. This checkpoint likely represents a critical step in RNA biogenesis, where the ATP-driven action of Dbp2 may facilitate the transition of RNA from a chromatin-bound to an export-competent form. This process is regulated by the release and recycling of CPAC components, potentially in an energetically controlled manner, and prepares the processed transcripts for export to the cytoplasm.

8.1 What is the mechanism of retention on chromatin in the absence of Dbp2?

Defects in mRNA processing have long been shown to result in the retention of transcripts at the transcription site (Custódio et al., 1999; Eberle et al., 2010; P. Hilleren & Parker, 2001; Palazzo et al., 2024; Rougemaille et al., 2007), suggesting the existence of quality control checkpoints during early mRNP assembly that ensure proper mRNA processing. The checkpoint (Qu et al., 2009) that is mediated by Dbp2 corresponds to the release and recycling of CPAC components into the soluble pool for subsequent rounds of pre-mRNA processing. In the absence of Dbp2, CPAC retention on chromatin is observed as a result of incomplete mRNP checkpoint completion, and RNA retention is likely due to a failure to release RNA from chromatin after transcription. Although the precise mechanism by which Dbp2 mediates the release of CPAC and/or RNA from chromatin—likely as part of a coupled process—is not yet fully understood, a hypothetical model can be proposed based on the findings of this work and several other studies.

One possibility aligns with such a retention mechanism revolves around Msi2-Mex67 axis (the *S. pombe* homologues of Hpr1-Mex67). In *S. cerevisiae*, auxiliary sequences at the PAS are recognised through direct interactions with the RRM domains of cleavage factors Rna15 (CFIA) and Hpr1 (CFIB), with Rna14 (CFIA) serving as a bridging factor (Barnwal et al., 2012; Chen & Moore, 1992; Pancevac et al., 2010; Pérez-Cãadillas, 2006). If Hrp1 is the only component of CFI which is exported, CFIA (Rna14-Rna15-Clp1-Pcf11) must be dissociated from Hrp1 and the processed mRNA in order for both efficient export of the transcript and intranuclear recycling of CFIA to proceed. Supportingly, the RNA-interactome capture (RIC) in *S. pombe* has revealed significant enrichment of Rna14, Rna15, and Msi2 in wild type cells, while other CFIA subunits, including Pcf11, Clp1, and Ctf1, were not detected by crosslinking (Kilchert

et al., 2020). These findings suggest that the release of Rna14, Rna15, and Msi2 may represent a rate-limiting step, with Dbp2-driven mRNP remodelling potentially occurring along the Msi2-CFIA axis. This remodelling, possibly through direct interaction with the export receptor Mex67, could facilitate the dissociation of CFIA from Msi2, which is bridged by Rna14, while Msi2 remains bound to RNA, a mark for export competency. In support of this, the budding yeast Hrp1 has been shown to recruit the export receptor Mex67 following proper 3'-end cleavage, thereby directing the mRNP to the export pathway (Li et al., 2023). The Dbp2-Msi2-Mex67 axis appears to be critical for export competency. Consistent with this, in budding yeast, Dbp2 has been proposed to facilitate the formation of the Yra1-Mex67-Nab2 complex (Ma et al., 2013), which is essential for proper mRNA export. Therefore, hypothetically, Dbp2-mediated mRNP remodelling occur at the 3'-end of the genes, mediating the release of CFIA components (Rna14-Rna15-Pcf11) upon the recruitment of the export receptor, Mex67.

The mRNP remodelling by Dbp2 corresponds to an early RNA biogenesis step during the life cycles of mRNAs, possibly leads to the destabilisation of CFIA both from Msi2/Hrp1 and mRNAs. Given the importance of Msi2/Hrp1 in the formation of Dbp2-mediated, export-competent mRNPs, this raises the question of conservation. In higher eukaryotes, no orthologues of Msi2/Hrp1 are annotated, which leads to concerns whether the Dbp2/DDX5-mediated remodelling process is conserved across species. In mammalians, CFI(m)68/CPSF6 is the only known component of CPAC complex that shuttles between nucleus and cytoplasm and also to interact with the export receptor, NXF1 (Mex67) and stimulate mRNA export (Ruepp et al., 2009), which increases the likelihood that Msi2/Hrp1 and CFI(m)68 could be functionally redundant. A complementation assay will help to identify if that is the case.

A similar RNA retention phenotype of 3'-processed transcripts at the transcription site was also observed in RNAPII-CTD truncation, indicating that the RNAPII-CTD is also essential for mRNA release from chromatin (Custódio et al., 2007). This could be due to its impaired phosphorylation status in the truncated version, since its differential phosphorylation facilitates the recruitment of necessary factors during transcription cycle (Corden, 2016). This raises an intriguing possibility for an alternative retention mechanism, where the release from chromatin could be an independent step in gene expression, requiring an active component typically recruited by the full-length RNAPII-CTD, possibly via its serine 2 phosphorylation. For the RNAPII-CTD & 3'-end processing axis, the interactions of RNAPII^{Ser2P} with the CFIA components, Rna14 and Pcf11, as well as with the CPAC-interacting Seb1, have been reported (Barillà et al., 2001; Mayer, Schreieck, et al., 2012; Sadowski et al., 2003; Wittmann et al., 2017). Interestingly, Dbp2 was identified as one of the most highly enriched protein in Seb1 purification (Lemay et al., 2016). Notably, the RIC analysis in *S. pombe* using wild type cells revealed strong enrichment of the CPAC-interacting protein Seb1 on poly(A)+ RNA, alongside Rna14, Rna15, and Msi2 (Kilchert et al., 2020), classifying Seb1 into the rate-limiting factor category for the release and recycling of CPAC, & - associated factors.

Since the resemblance of phenotypes from both RNAPII-CTD and Dbp2 mutant studies, have led to the possibility of the RNA release from chromatin as an independent step, a possible mechanism might be via formation of transient condensates at the termination window. If that were the case, RNAPII-^{Ser2P} would play the critical part, as this phosphorylation marks the termination window and allows the recruitment of these 3'-end RNA processing and associated factors. This possible scenario is in line with the published reports for each protein, Dbp2, RNAPII-CTD, and

Seb1, as all have the ability to induce phase separation (Ding et al., 2023; Flores-Solis et al., 2023; Hondele et al., 2019).

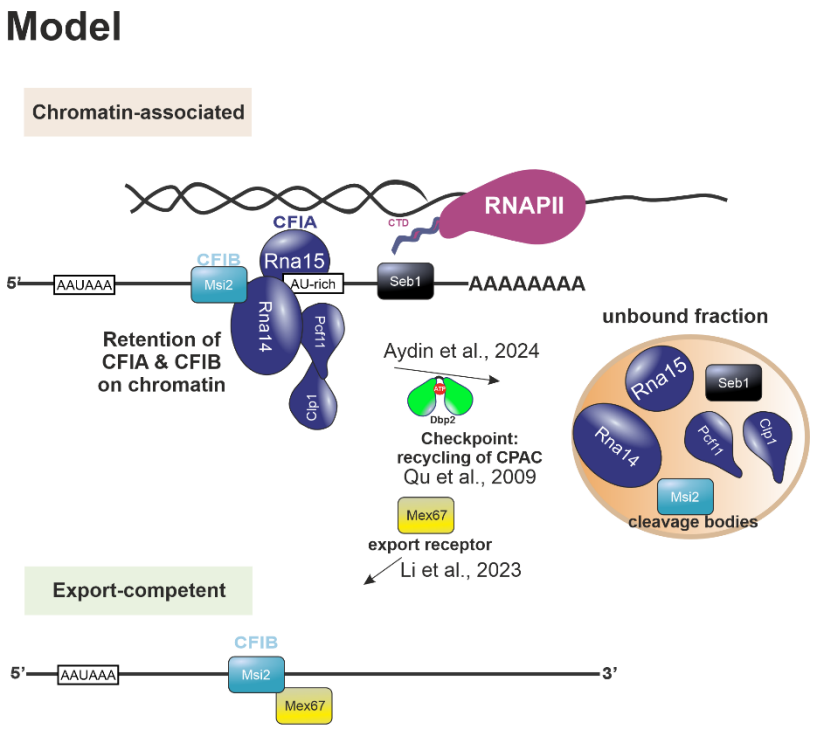

Figure 8.1 | A hypothetical model depicting Dbp2-mediated checkpoint completion for the assembly of export-competent mRNP

Qu et al., 2009, proposed the presence of a checkpoint during mRNP assembly, where the recycling of 3'-end processing factors enables their reuse on new precursor transcripts and is coupled with the recruitment of export factors. Li et al., 2023, proposed that budding yeast Hrp1 (the homologue of Msi2 in *S. pombe*) recruits the export receptor Mex67 upon 3'-end cleavage, directing the mRNP to the export pathway. This current study shows strong evidence that Dbp2-driven RNPase activity occurs at the 3'-ends, mediates the release of the cleavage body complex (CFIA) components. The retention of RNA is possibly as a result of a failure in the recruitment of export receptor.

Furthermore, in this study, no evidence has been found linking Dbp2 directly to MTREC function. Interestingly, recent studies suggest that 3’-end processing and the nuclear surveillance machinery work in a coordinated manner, where RNA transcripts destined for degradation are cleaved by the CPAC complex and then transferred to the MTREC complex (Bresson et al., 2015; H. M. Chen et al., 2011; S. Y. Lee et al., 2020; Vo et al., 2019; Yamanaka et al., 2010; Zhou et al., 2015). Notably, Msi2 has been shown to directly interact with Pab2 and/or Mmi1 components of the MTREC complex (Soni et

al., 2023). In light of the Dbp2-MTREC-CPAC axis findings from this study, the interaction between Dbp2 and Msi2 may further be the critical link in this network, suggesting the potential existence of a novel link on RNA surveillance mechanism.

8.2 Is Dbp2-dependent mechanism conserved in higher eukaryotes?

Choi et al., 2024 conducted pulse-chase mRNA interactome-capture experiments in humans to track mRNA-protein interactions across the mRNA life cycle. Their study, which led to a publicly accessible database of over 800 human RBPs, calculated the peak binding times (in minutes) for poly(A)-RNA-binding proteins. Depending on their peak binding times, these proteins were categorised into seven clusters, with Cluster I representing the earliest binding times and Cluster VII the latest. Notably, the human Dbp2 orthologue, DDX5 and its paralogue DDX17 were classified in Cluster II, which also includes most 3'-end maturation as well as some splicing factors, indicating that their temporal recruitment patterns match. This clustering overlap suggests a possible conserved role for Dbp2/DDX5 in higher eukaryotes at the 3′-end of genes, where the DEAD-box may help release and recycle CPAC factors after they have executed their function. Furthermore, this overlap may also reflect the greater complexity of mRNA processing in mammals, where 3'-end maturation is intricately linked to splicing. In mammals, the crosstalk between RNA 3'-end formation and splicing is well established, and splicing efficiency is considered as a determinant of 3′-end cleavage (Reimer et al., 2021). For example, the sequences within the final intron of the human triosephosphate isomerase (TPI) gene are essential for proper 3'-end formation (Nesic et al., 1993). U1 small nuclear ribonucleoprotein (snRNP) binding to introns is known to repress premature 3′-end cleavage (Berg et al., 2012; So et al., 2019; Vagner et al., 2000), whereas interactions of U2 snRNP with CPAC factors promote cleavage ensuring proper 3'-end processing (Kyburz et al., 2006).

8.3 Graphical summary

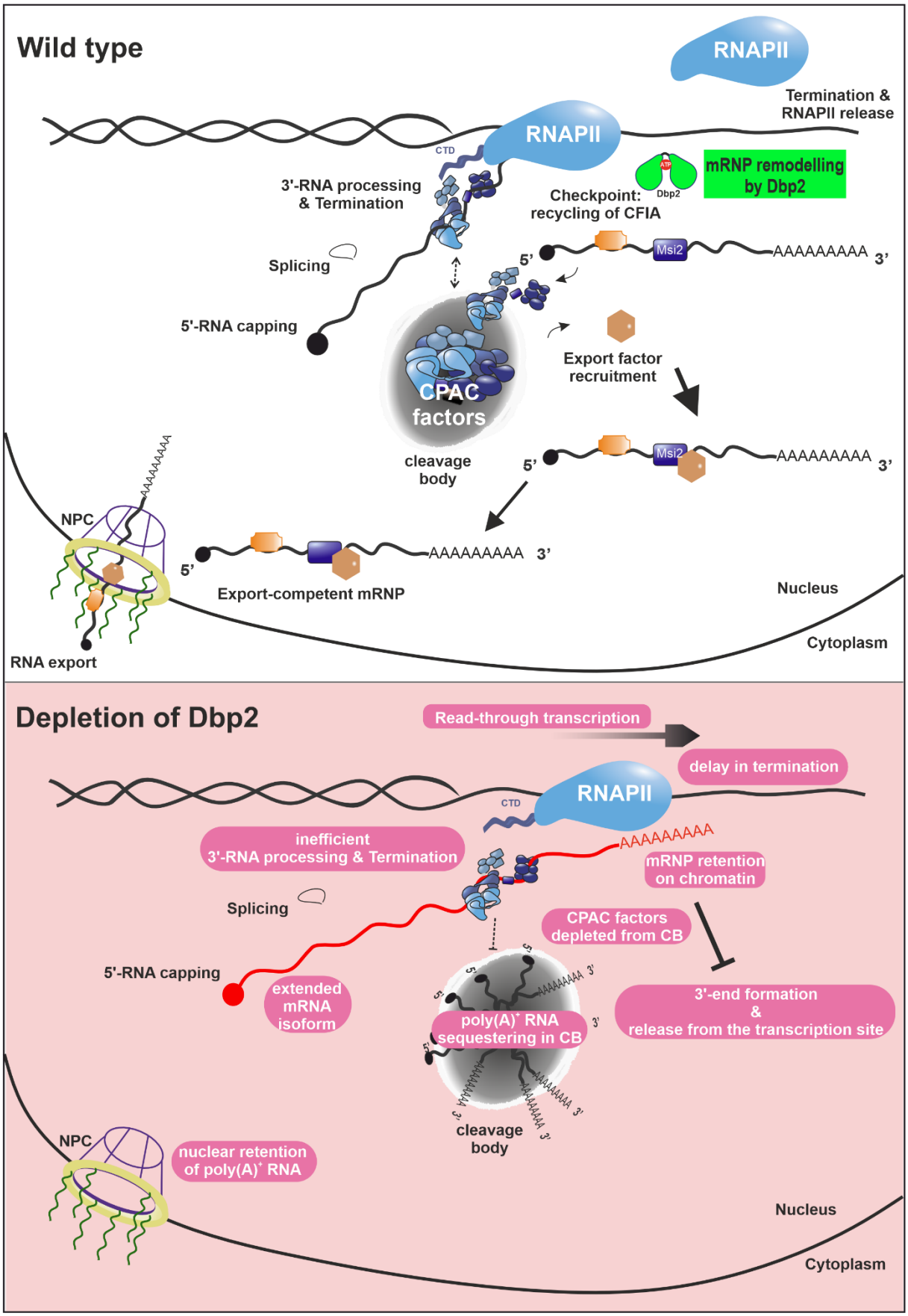

In this study, the interaction of Dbp2 with the cleavage and polyadenylation complex (CPAC) is demonstrated, and its localisation to cleavage bodies, enriched for 3’-end processing factors and proteins associated with nuclear RNA surveillance, is observed. Upon loss of Dbp2, 3’-processed & polyadenylated RNAs accumulate on chromatin and within cleavage bodies, coinciding with a depletion of CPAC components from the soluble pool (unbound fraction). Under such circumstances, cells exhibit an increased propensity to bypass polyadenylation sites, coupled with a delay in transcription termination, indicating inadequate availability of CPAC components to uphold normal levels of 3’-end processing. These findings align with a proposed model wherein Dbp2 is implicated in formerly proposed an mRNP remodelling checkpoint (Qu et al., 2009) that licenses RNA export, intricately linked to the release of CPAC.

8.4 Future directions and outlook

In this study, an RNP-remodelling helicase Dbp2 shown to play a key role in facilitating the release of CPAC factors into the soluble pool. In its absence, both CPAC factors and 3'-processed transcripts are retained on chromatin. This highlights the need for more refined subcellular fractionation techniques in yeast models, particularly for differentiating between nuclear compartments such as chromatin and nucleoplasm, a challenge that persists in this system. In contrast, the resolution and effectiveness of subcellular fractionation methods in mammalian cells are well-established. A recent study by Ietswaart et al. (2024) demonstrates the utility of this approach, revealing that chromatin release is a rate-limiting step for subsequent nuclear export, as measured by RNA residence times in different compartments. Notably, transcripts with extended residence on chromatin were shown to have longer poly(A)-tails (Ietswaart et al., 2024), a key factor as poly(A)-tail length is linked to mRNA metabolism (Passmore & Coller, 2022). Identifying transcripts in the chromatin or nucleoplasm fractions upon

subnuclear fractionation in mutant cells will help characterise compartment-specific features of mRNAs, which is a goal for future studies. A fraction of poly(A)+ RNA retained in the absence of Dbp2 is sequestered in cleavage bodies (Figure 7.1.1). To explore whether these 3’-processed, polyadenylated RNAs share common features, biotin-dependent proximity labelling (e.g., APEX) (Fazal et al., 2019) can be used. A scenario for the sequestration of poly(A)+ RNA in cleavage bodies upon Dbp2 depletion could involve slower splicing kinetics, potentially leading to a higher prevalence of intron-containing transcripts in these structures. This method biotinylates RNAs within 10-20 nm, allowing the detection of specific RNA populations in close proximity, which could help address the question.

Building on the findings of this study, which provide strong evidence for Dbp2’s novel role as an mRNP remodeller during RNAPII-mediated transcription, it would be highly interesting to investigate the compositional differences of mRNPs at different stages of remodelling. This could involve examining the roles of other transcriptionally-potent DEAD-box ATPases, such as Uap56 (Sub2) and Dbp5, alongside Dbp2. A promising method to achieve this could be poly(A)-interactome capture (RIC) of UV-crosslinked RNA-protein complexes, enabling the identification and comparison of mRNP compositions. Based on the indications in this study, 3'-end formation factors, particularly CFIA components, are expected to be enriched on poly(A)+ RNA in the absence of Dbp2, and this could be further validated using this method and help uncover potentially a novel layer in regulation of gene expression.

Furthermore, RNAPII density at the termination zone was found to be increased in Dbp2-depleted cells using RNAPII-ChIP-seq. However, standard ChIP analysis lacks strand specificity, limiting its resolution in identifying the exact cause of RNAPII accumulation. To address this, the crosslinking and cDNA analysis (CRAC) approach, which targets RNA–protein complexes by pulling down the largest subunit of RNAPII,

followed by RNA isolation, reverse transcription, library preparation, and sequencing, could be employed. When applied to both wild type and Dbp2-depleted cells, this method would pinpoint specific RNA sites of RNAPII binding and help determine whether RNAPII crosslinking downstream of the 3'-UTRs is obstructed by bound proteins or terminator structures. This would provide deeper insights into the regulation of gene expression in the absence of Dbp2.

Previous studies have demonstrated that slow elongation, induced by the Rpb1-R749H mutant, leads to more proximal termination, while fast elongation, caused by the Rpb1-E1126G mutant, results in more distal termination (Fong et al., 2015). To explicitly differentiate whether the transcription termination delay observed in Dbp2-depleted cells is exclusively due to inefficient cleavage rather than alterations in RNAPII elongation speed, it would be valuable to investigate whether termination defects in Dbp2-depleted cells can be suppressed by introducing the slow RNAPII mutant.

A key question in the field of DEAD-box ATPases is how family members with similar helicase core and no RNA sequence specificity perform diverse functions. Some DEAD-box helicases are tightly regulated and activated by specific co-factors. Therefore, understanding whether Dbp2's mRNP remodelling activity at gene 3′-ends is influenced by interactions with other factors is crucial. In this context, Rmt1, an arginine methyltransferase, was found to be highly enriched in Dbp2 purification data (sub-chapter 5.5), and Dbp2 exhibits very efficient helicase activity *in vitro* (sub-chapter 2.3). This suggests that Dbp2's activity may be regulated by a protein-protein interaction, possibly involving Rmt1-mediated arginine methylation. Rmt1-mediated arginine methylation of proteins however seems to show different effects when it comes to their biochemical and cellular activities (Hung et al., 2010; Perreault et al., 2007). Therefore, investigating the Dbp2-Rmt1 interaction in future studies would be particularly interesting.

Chapter9 Materials and Methods

9.1 Materials

9.1.1 List of chemicals and consumables

Chemicals and Consumables	Supplier
2-mercaptoethanol	Merck
2-Propanol	Carl Roth
Acetic acid	VWR Chemicals
Acrylamide 4K solution (30 %) – Mix 37:5	AppliChem Gmbh
Adenine hemisulfate salt	Sigma-Aldrich
Agar bacteriology grade	Applichem Gmbh
Agarose	Applichem Gmbh
Ambion Maxiscript-T7 *In Vitro* Transcription Kit	Thermo Scientific
Amersham Hybond nylon membranes	GE Healthcare
Ammonium persulfate (APS)	VWR Chemicals
Ampicillin	Applichem Gmbh
Anti-Digoxigenin AP Fab fragments	Roche Diagnostics
ATP	Jena Bioscience
BCA Protein Assay Kit	Novagen
Benzamidine HCl	MP Biomedicals
BLX-254, UV-crosslinker	Vilber Lourmat
Bacto™ Yeast extract	BD Biosciences
Boric acid (BH3O3)	Applichem Gmbh
Bovine serum albumin (BSA)	Sigma-Aldrich
Bromophenol blue	Applichem Gmbh
CDP-Star AP substrate	EMD Millipore
Chloroform	Merck
Clarity Max ECL solution	Bio-Rad
Coomassie Brilliant Blue G-250	Applichem Gmbh
Coomassie Brilliant Blue R-250	Applichem Gmbh
D-Glucose Monohydrate	Sigma-Aldrich
Dialysis membrane Membra-Cel™	Carl Roth
DIG-Easy-Hyb solution	Roche diagnostics
Dimethyl sulfoxide (DMSO)	Grüssing GmbH
Disodium hydrogen phosphate	Sigma-Aldrich
Dipotassium phosphate (K_2HPO_4)	Grüssing GmbH
Disodium phosphate (Na_2HPO_4)	Carl Roth
Dithiothreitol (DTT)	Sigma-Aldrich
dNTPs (dATP, dTTP, dCTP, dGTP)	New England BioLabs
D-Sorbitol	Carl Roth
Dynabeads™ Protein G	Invitrogen
Ethanol	Fisher Chemical
Ethylenediaminetetraacetic acid (EDTA)	Sigma-Aldrich
Ethyleneglycol-bis(aminoethylether)tetraacetic acid (EGTA)	Merck
Ficoll 400®	Carl Roth
Formaldehyde	ORG Laborchemie

Formamide	Merck
Gel loading dye, purple (6x)	NEB
Gene ruler 1kb	Thermo Scientific
Gel loading dye, purple (6x) w/o SDS	NEB
GFP-TRAP magnetic beads	Chromotek
Glass beads Acid-washed, 425-600 µm	Sigma-Aldrich
Genetecin (G418)	ThermoFisher (Gibco)
Glycerol	Carl Roth
Glycine	Labochem international
Glycogen	Sigma (Merck)
Glycogen Blue	Invitrogen Thermo Fischer
HDGreen™ DNA stain	Intas
HEPES	Carl Roth
Herring Sperm DNA	ThermoFisher (Invitrogen)
HiFi DNA Assembly NEBuilder	New England Biolabs
Hydrochloric acid (HCl)	Carl Roth
Hydroxyethyl Urea	Applichem Gmbh
Hygromycin	MP Biomedicals
IGEPAL CA-630	Sigma-Aldrich
IgG-coupled Dynabeads (tosylactivated M28)	Thermo Scientific
IgG Sepharose 6 Fast Flow	GE Healthcare
Imidazole	Merck
Isopropyl β-D-1-thiogalactopyranoside (IPTG)	Carl Roth
L-Glutamic acid monosodium salt	Sigma Aldrich
L-Histidine	Sigma-Aldrich
L-Leucine	Sigma-Aldrich
L-Lysine Monohydrochloride	Sigma-Aldrich
Liquid Nitrogen	Linde
Lithium acetate	Carl Roth
Lithium chloride	Merck
Magnesium chloride	Merck
Methanol	Merck-Millipore
Monopotassium phosphate (KH_2PO_4)	Carl Roth
Monosodium phosphate (NaH_2PO_4)	Merck
Nitrocellulose membrane	Bio-Rad
Nuclease free H_2O	NEB
Nucleospin Gel and PCR Clean-Up	Macherey & Nagel
NucleoSpin® Plasmid (NoLid)	Macherey & Nagel
NP-40	Sigma-Aldrich
Parafilm® "M" Laboratory Film	BEMIS®
Phenylmethane sulfonyl fluoride (PMSF)	Carl Roth
Phosphoric acid	Carl Roth
Plate reader Tecan Infinite F200 pro	Tecan Group
Polyethylene glycol (PEG) 3800/4000	Carl Roth
Polylysine	Sigma-Aldrich
Polysorbate 20 (Tween 20)	Merck
Polyvinylpyrrolidone (PVP)	Sigma-Aldrich
Ponceau S	Serva
Potassium chloride	ORG Laborchemie
Potassium phthalate monobasic	Sigma-Aldrich
Potassium hydroxide	Merck

Powdered milk, fat free, blotting grade	Carl Roth
PageRuler™ Prestained Protein Ladder, 10 to 180 kDa	Thermo Scientific
Protease inhibitor cocktail	Sigma Merck
Protino® Ni-NTA Agarose	Macherey-Nagel
Protino Ni-IDA 150 columns	Macherey-Nagel
Rothi®-Mount FluorCare DAPI	Carl Roth
Roti®-Aqua-Phenol	Carl Roth
Salmon sperm DNA	Applichem GmbH
Sodium acetate	Merck
Sodium chloride	Merck
Sodium citrate	Carl Roth
Sodium deoxycholate	Sigma-Aldrich
Sodium dodecyl sulfate	Serva
Sodium hydroxide	Merck
Sodium phosphate dibasic dihydrate	Sigma Aldrich
Sulfosalicylic acid	Merck
Tetramethylethylenediamine (TEMED)	VWR
Thiamine hydrochloride	Sigma Aldrich
Thiolutin	Cayman Chemical Company
Trichloroacetic acid (TCA)	Merck
TRIS	Carl Roth
Triton X-100	AppliChem Gmbh
TRIzol™ Reagent	Invitrogen
tRNA from *E. coli* MRE600	Roche diagnostics
Uracil	Sigma-Aldrich
Zero Blunt™ TOPO™ PCR Cloning Kit	Invitrogen

9.1.2 List of equipment and devices

Equipment and devices	**Company**
70 Ti	Beckman Coulter
AM100, micro scale	Mettler-Toledo
Avanti JXN-26 Centrifuge	Beckman Coulter
Bioruptor UCD-200, Sonication System	Diagenode
ChemoCam Imager ECL HR 16-3200	Intas
Deltavision Ultra High-Resolution Microscope	GE Healthcare
EPS 301, electrophoresis power supply	GE Healthcare
FastPrep-24TM 5G	MP Biomedicals
Freezer/Mill® 6870D	Spex®SamplePrep
Gel iX20, Transilluminator/gel docu	Intas
Hera safe, laminar flow cabinet	Thermo Fisher Scientific
HeraFreeze HFU T Series	Thermo Scientific
HT Multitron Pro shaking incubator	Infors
HXP 120 V, light source	Kübler Codix
IKA® KS 4000 ic control, shaking incubator	IKA Labortechnik
IKAMAG® RCT, magnetic stirrer	IKA Labortechnik
Incubator with HT Labotron, shaker	Aqua Lytic / Infors
Incubator KS 400	IKA Labortechnik
JLA-8.1, JA-25.50, JA-10	Beckman Coulter

Lab phenomenal pH 1000L, pH meter	VWR
LED bluelight transilluminator	Nippon genetics
Megafuge 40R	Thermo Scientific, Heraeus
Micromanipulator the lens of 20X LWD/0.30	Singer Instruments MSM
Milli-Q® integral water purification system	Merck
Mini-Protean® Tetra Electrophoresis Cell	Bio-Rad
Multi-functional Orbital Shaker PSU-20i	Grant-bio
ND-1000, Spectrophotometer	NanoDrop
Optima XPN-80 Ultracentrifuge	Beckman Coulter
PCR Thermocycler	Biometra Tadvanced
Pipetboy	IBS Integra Biosciences
PM2000, scale	Mettler-Toledo
Roller mixer Srt6	Stuart BioCote
RCT basic, magnetic stirrer	IKA Labortechnik
Research Pipettes 2.5, 10, 20, 100, 200, 1000, 5000 µl	Eppendorf
Rotator	neoLab
SBH130D, block heater	Stuart®
Sonifier 250	Branson UltrasonicsTM
Sunrise Microplate Absorbance Reader	Tecan Group
SW22, shaking waterbath	Julabo
Tabletop Centrifuge 5425, 5424R	Eppendorf
Thermomixer	Eppendorf
Trans-Blot® Turbo Transfer System	Bio-Rad
Unichromat 1500	Uniequip
Vakulan CVC 3000	Vacuubrand
Vortex-Genie 2	Scientific Industries
VX-150, autoclave	Systec
WT 12, tumbling shaker	Biometra

9.1.3 List of enzymes

Enzyme	**Supplier**
Q5® High-Fidelity DNA Polymerase	NEB
Phire Hot Start II DNA Polymerase	Thermo Fisher Scientific
SuperScript III RT	Invitrogen
Biozym cDNA Synthesis Kit	Biozym
Tobacco etch virus (TEV)-protease	in-house
Zymolyase 100T	Carl Roth
Benzonase	in-house
Restriction Enzymes	NEB
Proteinase K	Sigma Aldrich
Pronase	Merck
Pierce™ HRV 3C Protease	Thermo Fisher Scientific
DNase I	Thermo Fisher Scientific
RNase A	Applichem GmbH
RNase T1	Thermo Fisher Scientific
RNase III	Invitrogen
RNase H	NEB
KpnI	NEB

HindIII	NEB
RNase I	Jena Bioscience
Protease Inhibitor Cocktail	Sigma Aldrich

9.1.4 List of enzyme inhibitors

Enzyme Inhibitors	Supplier
RNasin	Promega
RNaseOUT	Invitrogen

9.1.5 List of Antibodies

Primary Antibody	Supplier
Anti-GAPDH (GA1R) mouse mAb	Medimabs
Anti-Flag M2 mouse mAb	Sigma Aldrich
Anti-dimethyl-Arginine (ASYM24) rabbit pAb	EMD Millipore
Anti-Rpb1 mouse mAb (8WG16)	EMD Millipore
Anti-mini-AID	Biozol MBL
Peroxidase-Anti-Peroxidase (PAP)	Sigma Aldrich
Anti-CTDSer2P rat mAb	Abcam
Anti-CTDSer5P mouse mAb (H14)	Hiss
Anti-c-Myc-HRP (clone 9E10) mouse mAb	Biomol
Anti-Ubiquitin mouse mAb	Sigma Aldrich
Anti-GFP mouse mAb lgG1κ	Roche
Secondary Antibody	**Supplier**
Goat Anti-rat HRP	Abcam
Goat Anti-rabbit HRP	Sigma Aldrich
Goat Anti-mouse HRP	Sigma Aldrich
Goat Anti-mouse (AF488)	Elabscience
Goat Anti-rat (AF594)	Jackson ImmunoResearch Laboratories

Note: for Western blot analyses all primary antibodies were diluted in 1:1000 dilution, except peroxidase anti-peroxidase (PAP), which was in 1:5000. All secondary antibodies used for western blotting and subsequent protein detection diluted in 1:3000.

9.1.6 Antibiotics

A 1000x stock solution of each antibiotic was prepared in MQ H_2O (see table below) and used at a final concentration of 1:1000 dilution.

	Antibiotics	Concentration	Source
1	G418 (Geneticin)	100 mg/ml	ThermoFisher (Gibco)
2	Hygromycin	100 mg/ml	MP Biomedicals
3	Nourseothricin	100 mg/ml	Jena Biosciences
4	Kanamycin	50 mg/ml	Applichem GmbH
5	Ampicillin	100 mg/ml	Applichem GmbH
6	Chloramphenicol	100 mg/ml	Applichem GmbH

9.1.7 Media and Solutions

YES (Yeast Extract with Supplements) – "Rich media"	**EMMG (Edinburgh Minimal Media Glutamate) – "Minimal media"**	**ME (Malt Extract) – "mating media"**	**EMMG -URA**
Yeast extract: 5 g	Potassium hydrogen Phthalate: 3 g	Malt extract: 30 g	Potassium hydrogen Phthalate: 3 g
Glucose: 30 g	Sodium phosphate dibasic dihydrate: 2.2 g	Agar: 20 g	Sodium phosphate dibasic dihydrate: 2.2 g
Adenine hemisulfate: 0.225 g	L-Glutamic acid, monosodium salt monohydrate: 3.7 g	Uracil: 0.225 g	L-Glutamic acid, monosodium salt monohydrate: 3.7 g
Leucine: 0.225 g	10 x amino acid stock 100 ml	Histidine: 0.225 g	Adenine hemisulfate: 0.225 g
Lysine hydrochloride: 0.225 g	50 x salt stock: 20 ml	Leucine: 0.225 g	Leucine: 0.225 g
Histidine: 0.225 g	1,000 x vitamin stock: 1 ml	Lysine: hydrochloride 0.225 g	Lysine hydrochloride: 0.225 g
Uracil: 0.225 g	10,000 x mineral stock: 0.1 ml	Adjust pH to 5.5	Histidine: 0.225 g
	20% Glucose stock: 150 ml		50 x salt stock: 20 ml 1000 x vitamin stock: 1 ml
			10000 x mineral stock: 0.1 ml
			20% Glucose stock: 150 ml
Ingredients/ 1 litre			
For solid media, add 20 g agar			

50 x salt	1,000 x vitamin	10,000 x mineral	10 x Amino Acid-Stock
$MgCl_2$: 52.5 g KCl: 50 g $NaSO_4$: 2 g $CaCl_2$: 0.735 g	Nicotinic CID: 10 g Inositol: 10 g Pantothenic acid: 1 g Biotin: 0.010 g	Citric acid: 10 g Boric acid: 5 g $MnSO_4$: 4 g $ZnSO_4$: 4 g $FeCl_2$: 2 g Potassium iodide: 1 g $CuSO_4$: 0.4 g	Adenine: 2.25 mg Leucine: 2.25 mg Histidine: 2.25 mg Lysine: 2.25 mg Uracil: 2.25 mg
Supplements in 1 litre			

Stock solutions

10 x TE (pH 7.5):	100 mM Tris-HCl (pH 7.5), 10 mM EDTA
1 M LiAc (pH 7.5):	102.02 g LiAc to 800 ml MQ H_2O
1 M Tris/HCl (pH 7.5):	121.1 g Tris to 800 ml MQ H_2O
0.5 mM EDTA:	192.04 g dissolved in 1 l MQ H_2O
50% PEG3350:	Dissolve 250 g of PEG3350 (or PEG4000) in 350 ml of MQ H_2O (heat to >50 °C with stirring).
10 x PBS (pH 7.3):	1.4 M NaCl, 27 mM KCl, 43 mM Na_2HPO_4,14 mM KH_2PO_4, in 2 litres
Ponceau staining:	0.2% w/v Ponceau s, 3% TCA in 250 ml MQ H_2O
5 x SDS running buffer:	60.4 g TRIS, 288 g Glycine, 14.88 g EDTA, 20 g SDS in 4 litre MQ H_2O
10 x transfer buffer:	30.28 g TRIS, 144.14 g Glycine, in 1 litre MQ H_2O
1 x transfer buffer:	100 ml methanol, 100 ml 10 x transfer buffer, 800 ml MQ H_2O
4 x separating buffer:	181.7 g TRIS, 3 g EDTA, 4 g SDS pH 8.8 in 1 litre MQ H_2O
4 x stacking buffer:	60.6 g TRIS, 3 g EDTA, 4 g SDS pH 6.8 in 1 litre MQ H_2O

10% separating gel: 1.67 ml acrylamide (30 % – mix 37:5), 1.995 ml MQ H_2O, 1.25 ml 4 x separating buffer, 25 µl 10% APS, 50 µl 10% SDS, 10 µl TEMED, in 5 ml total volume

4% stacking gel: 0.67 ml acrylamide (30% – mix 37:5), 2.995 ml MQ H_2O, 1.25 ml 4 x stacking buffer, 25 µl 10% APS, 50 µl 10% SDS, 10 µl TEMED, in 5 ml total volume

20 x TBS: 60 g TRIS, 160 g NaCl, 4 g KCl pH 7.4 in 1 litre MQ H_2O

1 x TBST: 1 x TBS, 0.5 % Tween 20

10x TBE: 1 M Tris, 1 M boric acid, 25 mM EDTA in 1 litre MQ H_2O

100% w/v TCA solution: 500 g TCA in 227 ml MQ H2O

9.1.8 Organisms

9.1.8.1 List of *S. pombe* strains

List of Strains used in this study				
Strain	**Name**	**Genotype**	**Construction / Source**	**Reference**
YP144	wild type	*h+ leu1-32 ura4D18 ade6-M216*		Lemieux et al., 2011
YPCK426	wild type	*h+ leu1-32 ura4D18 ade6-M216*	cross YP144	Aydin et al., 2024
YPCK100	Dbp2-HTP	*h+ leu1-32 ura4D1 ade6-M2 dbp2::dbp2-(his6-TEV-protein A):kanMX6*	YP144 transformed with *dbp2-HTP:kanMX*6 generated by two-step PCR using oligos #41/44/45/43 on pBS1479-HTP-KanMX6	Aydin et al., 2024
YPCK172	Srp2-HTP	*h+ leu1-32 ura4D1 ade6-M2 srp2::srp2-(his6-TEV-protein A):kanMX6*	YP144 transformed with *srp2-HTP:kanMX6* generated by two-step PCR using oligos #363-366 on	Aydin et al., 2024

			pBS1479-HTP-KanMX6	
YP510	*P.nmt-seb1*	*h+ ura4-294 leu1-32 ade6-M210 seb1::ura4:P.nmt1-seb1-FLAG:NatMX*		Wittmann et al., 2017
FY14996	Dbp2-GFP	*h90 ade6-216 leu1-32 lys1-131 ura4-D18 dbp2::dbp2-GFP-HA:KanR*	via NBRP Japan	Hayashi et al., 2009
YPCK111	Dbp2-GFP	*h+ ade6-216 leu1-32 ura4-D18 dbp2::dbp2-GFP-HA:KanR*	cross FY14996 x YP144	Aydin et al., 2024
YPCK424	Dbp2-GFP	*h- ade6-216 leu1-32 ura4-D18 dbp2::dbp2-GFP-HA:KanR*	cross YPCK111	Aydin et al., 2024
YPCK625	Msi2-AID	*h+ leu1-32 ura4-D18 ade6-M216 msi2::msi2-3xsAID:kanMX6*	YPCK426 transformed with msi2-3xsAID:kanMX6 generated by two-step-PCR using oligos #1039-1042 on pFA6a-kanMX6-3xsAID	Aydin et al., 2024
YPCK645	Msi2-AID Dbp2-GFP	*h? leu1-32 ura4-D18 ade6-M216 msi2::msi2-3xsAID:kanMX6 dbp2::dbp2-GFP-HA:KanR*	cross YPCK625 x YPCK424	Aydin et al., 2024
FY23618	Red1-tdTomato	*h- leu1-32 uraD18 ade6-M210 red1::red1-tdTomato:kanR*	via NBRP Japan	Sugiyama & Sugioka-Sugiyama, 2011
YPCK340	Red1-tdTomato Dbp2-GFP	*h? leu1-32 uraD18 ade6-M210 red1::red1-tdTomato:kanR dbp2::dbp2-GFP-HA:KanR*	cross FY23618 x YPCK111	Aydin et al., 2024
FY23603	Red1-tdTomato Mtl1-GFP	*h90 leu1-32 ura4-D18 ade6-M216 red1::red1-tdTomato:hphMX4 mtl1::mtl1-GFP:kanR*	via NBRP Japan	Sugiyama & Sugioka-Sugiyama, 2011

YPCK476	Pab2-tdTomato Dbp2-GFP	*h+ ade6-216 leu1-32 ura4-D18 dbp2::dbp2-GFP-HA:KanR pab2::pab2-tdTomato:hphMX4*	YPCK111 transformed with *pab2-tdTomato:hygMX* generated by two-step PCR using oligos #333/814/815/336 on FY23603	Aydin et al., 2024
YPCK554	Mtl1-GFP	*h+ leu1-32 ura4-D18 ade6-M216 mtl1::mtl1-GFP:kanMX6*	cross FY23603	Aydin et al., 2024
YP748	*P.nmt-dbp2*	*h+ leu1-32 ura4D18 ade6-M216 his3-D1 dbp2::ura4:P.nmt1-dbp2*	YP144 transformed with *ura4:P.nmt1-dbp2* generated with oligos #5381/5087//5088/3516 on YP510	Aydin et al., 2024
YP428	*dbp2-i2Δ*	*h+ leu1-32 ura4D18 ade6-M216 his3-D1 dbp2::dbp2-i2Δ*	strain generated by pop-in/pop-out: cassette containing deletion generated with oligos ex2-F/Di-R//Di-F/RTclose-R subcloned into pCRII blunt TOPO, NotI/BamHI fragment ligated into NotI/BamHI-restricted pKS-URA4; resulting vector sequenced, linearized with BseRI and transformed into YP144	Kilchert lab
YP787	*P.nmt-dbp2* + dbp2-FLAG	*h+ ura4D18 ade6-M216 dbp2::ura4:P.nmt1-dbp2 leu1-32::P.dbp2-dbp2-FLAG:leu1*	YP748 transformed with pDUAL-dbp2-FLAG linearized with NotI-HF	Aydin et al., 2024
YP791	*P.nmt-dbp2* + dbp2^{K172R}-FLAG	*h+ ura4D18 ade6-M216 dbp2::ura4:P.nmt1-dbp2 leu1-32::P.dbp2-dbp2^{K172R}-FLAG:leu1*	YP748 transformed with pDUAL-dbp2^{K172R}-FLAG linearized with NotI-HF	Kilchert lab
YP805	Dbp2-myc	*h+ leu1-32 ura4D18 ade6-M216 dbp2::dbp2-3myc:kanMX6*	YP144 transformed with *dbp2-3myc:KanMX* generated by 2-step-PCR using oligos	Aydin et al., 2024

			#41/5315/45/43 on pYM4	
YP818	*P.nmt-dbp2-myc*	*h+ leu1-32 ura4D18 ade6-M216 his3-D1 dbp2::ura4:P.nmt1-dbp2-3myc:kanMX6*	YP805 transformed with *ura4:P.nmt1-dbp2* generated with oligos #5381/5087//5088/3516	Aydin et al., 2024
SP253	*red1Δ*	*h90 ade6-210 leu1-32 ura4D::18 red1Δ::KAN MX*		Sugiyama & Sugioka-Sugiyama, 2011
YPCK606	*P.nmt-dbp2 red1Δ*	*h+ leu1-32 ura4-D18 ade6-M216/210? his3Δ::1? dbp2::ura4:P.nmt1-dbp2 red1Δ::kanMX6*	cross LV748 x SP253	Aydin et al., 2024
FBY107	*pab2Δ*	*h- leu1-32 ura4D18 ade6-M216 his3Δ::1 pab2Δ::kanMX6*		Lemieux et al., 2011
YPCK609	*P.nmt-dbp2 pab2Δ*	*h? leu1-32 ura4-D18 ade6-M216/210? his3Δ::1? dbp2::ura4:P.nmt1-dbp2 pab2Δ::kanMX6*	cross LV748 x FBY107	Aydin et al., 2024
FY23936	*iss10Δ*	*h+ SPAC7D4.14c::kanR ade6-M21? leu1-32 ura4-D18*	via NBRP Japan	Chen et al., 2014
YPCK607	*P.nmt-dbp2 iss10Δ*	*h? leu1-32 ura4-D18 ade6-M216/210? his3Δ::1? dbp2::ura4:P.nmt1-dbp2 iss10Δ::kanMX6*	cross LV748 x FY23936 (via h-)	Aydin et al., 2024
YPCK447	Red1-tdTomato	*h+ leu1-32 uraD18 ade6-M210 red1::red1-tdTomato:kanR*	cross FY23618	Aydin et al., 2024
FY23522	Rhn1-tdTomato Pcf11-GFP	*h90 leu1-32 ura4-D18 ade6-M210 rhn1-tdTomato::hph pcf11-GFP::kan*	via NBRP Japan	Sugiyama et al., 2012
YPCK602	*P.nmt-dbp2*	*h- leu1-32 ura4D18 ade6-M216 his3-D1 dbp2::ura4:P.nmt1-dbp2*	cross LV748YPCK138	Aydin et al., 2024

YPCK138	Cbc2-HTP	*h+ leu1-32 ura4-D18 ade6-M216/210? his3Δ::1 cbc2::cbc2-HTP:kanR*	YP144 transformed with Cbc2-his6-TEV-Prot A::KANMX generated by two-step PCR (#337-#340) on pBS1479 His-TEV-Prot. A KanMX (BLV #3879).	Kilchert lab
YPCK604	*P.nmt-dbp2 Pcf11-GFP*	*h- leu1-32 ura4-D18 ade6-M216/210? his3Δ::1 dbp2::ura4:P.nmt1-dbp2 pcf11::pcf11-GFP:kanR*	cross CK602 x FY23522	Aydin et al., 2024
YPCK610	Pcf11-GFP	*h- leu1-32 ura4-D18 ade6-M216/210? his3Δ::1 pcf11::pcf11-GFP:kanR*	cross CK602 x FY23522	Aydin et al., 2024
YPCK649	Pcf11-GFP Red1-tdTomato	*h? leu1-32 ura4-D18 ade6-M216/210? his3Δ::1 pcf11::pcf11-GFP:kanR red1::red1-tdTomato:kanR*	cross YPCK604 x 447	Aydin et al., 2024
YPCK648	*P.nmt-dbp2 Pcf11-GFP Red1-tdTomato*	*h? leu1-32 ura4-D18 ade6-M216/210? his3Δ::1 dbp2::ura4:P.nmt1-dbp2 pcf11::pcf11-GFP:kanR red1::red1-tdTomato:kanR*	cross YPCK604 x 447	Aydin et al., 2024
YPCK621	Msi2-GFP	*h+ leu1-32 ura4-D18 ade6-M216 msi2::msi2-GFP:kanMX6*	YPCK426 transformed with msi2-GFP:kanMX generated by two-step-PCR using oligos #1039/1040//1041/1042	Aydin et al., 2024
YPCK632	*P.nmt-dbp2 Msi2-GFP*	*h? leu1-32 ura4-D18 ade6-M216 msi2::msi2-GFP:kanMX6 dbp2::ura4:P.nmt1-dbp2*	cross YPCK621 x YPCK602	Aydin et al., 2024
YPCK361	Rmt1-3HF	*h+ leu1-32 ura4D1 ade6-M2 rmt1::rmt1-(3xHA-3xflag):NatMX*	YPLV144 transformed with rmt1-3HF-NAT	This study

			generated by two-step PCR using oligos #560/561/562/563	
YPCK366	Rmt1-3HF Dbp2-HTP	*h+ leu1-32 ura4D1 ade6-M2 rmt1::rmt1-(3xHA-3xflag):NatMX dbp2::dbp2-(his6-TEV-protein A):kanMX6*	YPCK100 transformed with rmt1-3HF-NAT generated by two-step PCR using oligos #560/561/562/563	This study
YPCK189	Ydc1-3HF	*h+ leu1-32 ura4D1 ade6-M2 ydc1::ydc1-(3xHA-3xflag):NatMX*	YPLV144 transformed with rmt1-3HF-NAT generated by two-step PCR using oligos #267/268/269/273	This study
YPCK190	Ydc1-3HF Dbp2-HTP	*h+ leu1-32 ura4D1 ade6-M2 ydc1::ydc1-(3xHA-3xflag):NatMX dbp2::dbp2-(his6-TEV-protein A):kanMX6*	YPCK100 transformed with rmt1-3HF-NAT generated by two-step PCR using oligos #267/268/269/273	This study
YPCK690	Rpb1-HTP	*h+ leu1-32 rpb1::rpb1-HTP::natMX6*		Domenico Libri
YPCK700	Rpb1-HTP *P.nmt-dbp2*	*leu1-32 ura4D::18 ade6-M2? dbp2::ura4-P.nmt1-dbp2 rpb1::rpb1-his6-TEV-ProtA::::natMX*	cross YPCK602xYPCK690	This study
YPCK620	Mlo3-GFP	*leu1-32 ura4-D18 ade6-M216 mlo3-GFP::kanMX*	YPCK426 transformed with mlo3-GFP::kanMX made by two-step-PCR (L3/L4-pFA//L5-pFA/L6 = #325/500//501/328) on TOPO-L3/L6-rrp6-GFP(BCK9) (KanMX-C2-rc/KanMX-L5-rc-long = #20/114)	This study
YPCK635	Mlo3-GFP	*leu1-32 ura4-D18 ade6-M216 mlo3::mlo3-GFP::kanMX*	cross YPCK620xYPCK602	This study
YPCK631	Mlo3-GFP *P.nmt-dbp2*	*leu1-32 ura4-D18 ade6-M216 mlo3::mlo3-GFP::kanMX dbp2::ura4:P.nmt1-dbp2*	cross YPCK620xYPCK602	This study

YPCK649	Pcf11-GFP Red1-tdTomato	*leu1-32 ura4-D18 ade6-M216/210? his3D::1 pcf11-GFP::kan red1-tdTomato::kanR*	cross YPCK604xYPCK447	Aydin et al., 2024
YPCK664	Msi2-GFP Red1-tdTomato	*leu1-32 ura4-D18 ade6-M216 msi2-GFP::kanMX red1-tdTomato::hphMX*	cross YPCK621xYPCK555	Aydin et al., 2024
YPCK662	Rna15-GFP Red1-tdTomato	*leu1-32 ura4-D18 ade6-M216 rna15-GFP::kanMX red1-tdTomato::hphMX*	cross YPCK518xYPCK55	Aydin et al., 2024
YPCK759	Seb1-GFP	*leu1-32 ura4-D18 ade6-M216 seb1::seb1-GFP:kanMX*	YPCK426 transformed with seb1-GFP:kanMX generated by two-step PCR on BCK9 using oligos #20/114 and 13/1173//1174/16.	Kilchert lab
YPCK779	Seb1-GFP *P.nmt-dbp2*	*leu1-32 ura4-D18 ade6-M216 seb1::seb1-GFP:kanMX dbp2::ura4:P.nmt-dbp2*	Cross YPCK759xYPCK602	Kilchert lab
YPCK555	Mtl1-GFP	h- *leu1-32 ura4-D18 ade6-M216 mtl1::mtl1-GFP::kanMX*	cross YPCK6xYPCK506	Kilchert lab
YPCK570	Mtl1-GFP *P.nmt-dbp2*	*leu1-32 ura4-D18 ade6-M216 seb1::seb1-GFP:kanMX dbp2::ura4:P.nmt-dbp2*	cross YPCK748xYPCK554	Kilchert lab
YPCK506	Cut11-iRFP	*h- 1L::Padh1-SynPCB2.1<<bsd cut11-iRFP<<kan*	via NBRP Japan	
YPCK633	Rna15-GFP	*leu1-32 ura4-D18 ade6-M216 rna15::rna15-GFP::kanMX*	cross YPCK618xYPCK602	Kilchert lab
YPCK629	Rna15-GFP *P.nmt-dbp2*	*leu1-32 ura4-D18 ade6-M216 rna15::rna15-GFP::kanMX dbp2::ura4:P.nmt1-dbp2*	cross YPCK618xYPCK602	Kilchert lab

YPCK630	Mex67-GFP *P.nmt-dbp2*	*leu1-32 ura4-D18 ade6-M216 mex67::mex67-GFP::kanMX dbp2::ura4:P.nmt1-dbp2*	cross YPCK619xYPCK602	Kilchert lab
YPCK634	Mex67-GFP	*leu1-32 ura4-D18 ade6-M216 mex67::mex67-GFP::kanMX*	cross YPCK619xYPCK602;	Kilchert lab
YPCK619	Mex67-GFP	*h+ leu1-32 ura4-D18 ade6-M216 mex67-GFP::kanMX*	YPCK426 transformed with mex67-GFP::kanMX made by two-step-PCR (L3/L4-pFA//L5-pFA/L6 = #687/1025//1026/690) on TOPO-L3/L6-rrp6-GFP(BCK9) (KanMX-C2-rc/KanMX-L5-rc-long = #20/114)	Kilchert lab
YPCK618	Rna15-GFP	*h+ leu1-32 ura4-D18 ade6-M216 rna15-GFP::kanMX*	YPCK426 transformed with rna15-GFP::kanMX made by two-step-PCR (L3/L4-pFA//L5-pFA/L6 = #1050/1051//1052/1053) on TOPO-L3/L6-rrp6-GFP(BCK9) (KanMX-C2-rc/KanMX-L5-rc-long = #20/114	Kilchert lab
YPCK873	Dbp2-GFP *rrp6Δ*	*ade6-216 leu1-32 lys1-131 ura4-D18 dbp2::dbp2-GFP-HA-KanR rrp6Δ::kanMX*	Cross YPCK762 x CK424	This study
YPCK519	Dbp2-GFP *pab2Δ*	*ade6-216 leu1-32 lys1-131 ura4-D18 dbp2::dbp2-GFP-HA-KanR pab2Δ::kanMX*	Cross YPCK111xYPLV145	This study
YPCK514	Dbp2-GFP *red1Δ*	*ade6-216 leu1-32 lys1-131 ura4-D18 dbp2::dbp2-GFP-HA-KanR red1Δ::kanMX*	Cross YPCK424xYPLV70	This study
YPCK439	Dbp2-GFP *iss10Δ*	*ade6-216 leu1-32 lys1-131 ura4-D18 dbp2::dbp2-GFP-HA-KanR iss10Δ::kanMX*	Cross YPCK403xYPCK424	Kilchert lab

9.1.8.2 *Escherichia coli* strains

For any kind of cloning chemically competent DH5α cells were used. BL21(DE3)pLysS cells were used for protein expression.

***E. coli* strain**	**Genotype**	**Reference**
DH5α	*F– endA1 glnV44 thi-1 recA1 relA1 gyrA96 deoR nupG purB20 φ80dlacZΔM15 Δ(lacZYA-argF)U169, hsdR17(rK–mK+), λ–*	Taylor et al., 1993
BL21(DE3)pLysS	*F- ompT hsdSB(rB- mB-) gal dcm (DE3) pLysS (CamR)*	Weiner et al., 1994

9.1.9 Constructs

9.1.9.1 List of plasmids used in *S. pombe* strains

Plasmid No	**Name**	**Description**	**Construction**	**Reference**
3879	pBS1479-HTP-KanMX6	for C-terminal tagging with His6-TEV-Protein A in *S. pombe* using KanMX marker, Amp resistance, pUC ori		Kilchert et al., 2015
2700	pYM4	for C-terminal tagging with 3xMyc tag, kanMX6, f1+ ori, AmpR		Knop et al., 1999
3842	pDUAL	plasmid for episomal maintenance or chromosomal integration; ura4+, leu1 (5' and 3', flanking ura4), AmpR		Matsuyama et al., 2004
4117	pDUAL-Dbp2-FLAG	pDUAL with Dbp2-FLAG insert for ectopic expression of Dbp2 in *S. pombe* under control of endogenous promoter; AmpR, 5' leu1/3'leu1 marker; ura4 marker; integrate into leu1 locus after digestion with Not1	*P.dbp2-dbp2-FLAG* was amplified using oligos #5086/5125 on genomic DNA, digested with SphI/BamHI and ligated into SphI/BamHI-restricted pDUAL (Matsuyama et al., 2004)	Aydin et al., 2024

80	pFA6a-kanMX6-3xsAID	C-terminal tagging with three tandem copies of 36-amino-acid sequence of the Arabidopsis IAA17 protein as auxin-inducible degron; kanMX, AmpR		Zhang et al., 2022
81	pEASY-ura4	integration vector for ura4-D18 strains		Zhang et al., 2022
91	pSKI-BSD-1L-A1-M-SynPCB2.1	linearize with ApaI(?) to integrate upstream of mug165 locus (ChrI:: 1508642 to 1509391 - 1507772 to 1508521); bsd, AmpR; carries a phycocyanobilin (PCB) biosynthesis system that produces PCB as a cofactor for iRFP		Sakai et al., 2021
96	pHBCA11-NLS-mTagBFP2-NLS	linearize with ApaI for integration into C locus (ChrI:5,516,347-5,256,460); hphMX, AmpR; blue fluorescent nuclear marker; 405nm / 420-450nm		Sakai et al., 2021
9	pCRII-TOPO-L3/L6-rrp6-GFP-KanMX	tagging vector for C-terminal GFP::kanMX cassette, compatible with standard L4-pFA/L5-pFA primers	rrp6-GFP-kanMX amplified from YP85 with oligos #32/35 integrated in to pCRII blunt TOPO	Aydin et al., 2024
4027	pAG25-HA-Flag	for C-terminal tagging with 3xHA, 3xFlag with 6xGly linker,terminator, natMX4, AmpR		Kecman, Kuś, et al., 2018

9.1.9.2 List of plasmids used in *Escherichia coli* strains

Plasmid No	Name	Description	Construction	Reference
BCK70	pOPINS3C-mod Dbp2-ORF	HiFi assembly: KpnI/HindIII-restricted BLV4017 with Dbp2-WT	Recombinant expression	This study

		(#244/245 on pOPINS3C-Dbp2-WT) digestion of PCR reaction with transformation; sequence was checked by sequencing		
BCK71	pOPINS3C-mod Dbp2-K172R-ORF	HiFI assembly: KpnI/HindIII-restricted BLV4017 with Dbp2-K172R (#244/247 and #246/245 on pOPINS3C-Dbp2-K172R) digestion of PCR reaction with transformation; sequence was checked by sequencing	Recombinant expression	This study
BLV4017	pOPINS3C_modified	T7 promoter and terminator, SUMO-tag followed by 3C cleavage site (for N-terminal tagging), AmpR, pUC	Recombinant expression	Wittmann et al., 2017

9.1.10 List of oligonucleotides

No	Name	Sequence	Use
18	HTP-L4-rc	caccatcaccatcaccatgatt	strain construction
19	HTP-L5-rc	cctgtttagcttgcctcgtc	strain construction
20	KanMX-C2-rc	CGGATCCCCGGGTTAATTAA	strain construction
21	KanMX-L2-rc	CGTACGCTGCAGGTCGAC	strain construction
22	KanMX-L5-rc	ATCGATGAATTCGAGCTCG	strain construction
41	dbp2-ex3F	AAGCCAAGCAGGACATTGAT	strain construction
44	dbp2-L4-pFA	ttaattaacccggggatccg CCAACGTGAACGCGCAAGGG GGGCAGAATTACT	strain construction

5315	dbp2-pYM4-L4	ccaacgtgaacgcgcaaggggggcagaattact	strain construction
45	dbp2-L5-pFA	cgagctcgaattcatcgatGTTCAGTAAC CGCTTTCGTAGA	strain construction
43	dbp2-RT-R	TTTCAAGCCTCTTCGCTCTT	strain construction
363	srp2-L3	CTTATCGTCCCGGCAGAGAT	strain construction
364	srp2-L4-pFA	ttaattaacccggggatccgCCATTCAGC AGCGACCTGTCCTTCAGCGCTACCGTT ACCTACATCAG	strain construction
365	srp2-L5-pFa	cgagctcgaattcatcgatTCCTGTCATA TGTCTGTGGTCT	strain construction
366	srp2-L6	CCGCTTGCGCTCATTATGAA	strain construction
1039	msi2-L3	CGAAAATGAGTCCGCCGTAG	strain construction
1040	msi2-L4-pFA	ttaattaacccggggatccgTCGACGAT ATGGATGGAAGCTGTGCCC	strain construction
1041	msi2-L5-pFA	cgagctcgaattcatcgatAAATATGTTT TAAATTATGAAAATGGACAGTC	strain construction
1042	msi2-L6	CTTGCCCTTTACCTCGTGTG	strain construction
38	dbp2-promF	CCATAGAATTGATTGTTTTTAGC TCTTTAG	strain construction
5087	dbp2-nmt4	gtcatagctgtttcctgtgtgaaCTGCCCGG CTAACTGTTAAG	strain construction
5088	dbp2-nmt5	acttatagtcgctttgttaactcgaCGCCTTAC CGCCTGTTAATT	strain construction
40	dbp2-ex2R	ACCAGAACCCGTAGCTGAAA	strain construction
333	pab2-L3	AATGGATCGATGTTGCATGA	strain construction
814	pab2-L4-pFA	TTAATTAACCCGGGGATCCGATAC GGAGCGAAACCACG	strain construction
815	pab2-L5-pFA	CGAGCTCGAATTCATCGATTCGC TTTGATGACTTGAAAAA	strain construction
336	pab2-L6	GAATTGAAGGGTCGGTGAAT	strain construction
5086	SphI-dbp2-promF	AGGgcatgcCCATAGAATTGATTGT TTTTAGCTCTTTAG	plasmid construction
5125	dbp2-flag-BamHI-R	TACggatccTCACTTATCATCGTC GTCCTTGTAGTCagaaccaccaccacc CCAACGTGAACGCGCAAGGGGGG CAGAATTACT	plasmid construction
1039	msi2-L3	CGAAAATGAGTCCGCCGTAG	strain construction
1040	msi2-L4-pFA	ttaattaacccggggatccgTCGACGATAT GGATGGAAGCTGTGCCC	strain construction

1041	msi2-L5-pFA	cgagctcgaattcatcgatAAATATGTTTTA AATTATGAAAATGGACAGTC	strain construction
1042	mis2-L6	CTTGCCCTTTACCTCGTGTG	strain construction
5856	rpl2501-ORF-F	GCCCAAGTATGCTCGCAAG	Northern probes, ivT
5857	rpl2501-ORF-R-T7	TAATACGACTCACTATAGGGA GGTGCCACCAACAATAGCCTT	Northern probes, ivT
5854	tma19-ORF-F	AACCCTGCCCTAAACTGTGA	Northern probes, ivT
5855	tma19-ORF-R-T7	TAATACGACTCACTATAGGGA GACGAGCCTTGATAGCCTTCA	Northern probes, ivT
5840	rpl1001-ORF-F	TTGCCTCATCCTGTGTGACT	Northern probes, ivT
5841	rpl1001-ORF-R-T7	TAATACGACTCACTATAGGGA GCGGTTTGCAATCTATCGGCA	Northern probes, ivT
5846	asl1-ORF-F	TGGTGCTTCAACGGCTTTAC	Northern probes, ivT
5847	asl1-ORF-R-T7	TAATACGACTCACTATAGGGA GACAGAGGAAACGACAGCTGA	Northern probes, ivT
1151	rpl2501-3prF	TGCTCTTGATGTTGCTAACCG	Poly(A) site usage assay
687	mex6-L6	TTCATTTGCTGGATCGCTCG	strain construction
688	mex6-L4-PFA	aatcatggtgatggtgatggtgTGAAAATGCTTC GGCTGGTATAACATTTCGCGA	strain construction
689	mex6-L5-pFA	gacgaggcaagctaaacaggAGTGACGTGTAT AGATAGATATGGTT	strain construction
690	mex6-L6	CGTCTCTCAATACCCGTCGA	strain construction
13	seb1-L3	AAGATTTTGCTATGCGTCGT	strain construction
16	seb1-L6	TCGCAGATTTGATCTTTTTG	strain construction
1173	seb1-L4-pFA	ttaattaacccggggatccgTTGGGGTTGCCAA GGAGGTTGTGAGACATACCCAGAAG	strain construction
1174	seb1-L5-pFA	cgagctcgaattcatcgatATGTGTTAAAAGAC GCTTACAAGT	strain construction
244	Dbp2ORF_into_pOPINSmod_F	Ctgtttcagggccccggtacctcttacagag ataacgaatatagtggaaattacaatg	Recombinant expression
245	Dbp2ORF_into_pOPINSmod_R	Aatcacaaactggtctagaatcaccaacgt gaacgcgc	Recombinant expression
246	DBP2-K172R-F	TTTCAGCTACGGGTTCTGGTcgg ACACTTTCTTATTGTCTTCCTGC	Recombinant expression
247	DBP2-K172R-R	GCAGGAAGACAATAAGAAAGTGT ccgACCAGAACCCGTAGCTGAAA	Recombinant expression
214	Dbp2_HiFi-F1:	TCAGGGTCCTATGTCTTACAGAG ATAACGAATATAGTGGAAATTAC	Recombinant expression

215	Dbp2_HiFi-R1:	GGTCGACGGTTCACCAACGTGAACGCGC	Recombinant expression
216	pOPINS3C_HiFi_F1	ACGTTGGTGAACCGTCGACCCGACTGGA	Recombinant expression
217	pOPINS3C_HiFi_R1:	TGTAAGACATAGGACCCTGAAACAGAACTTCC	Recombinant expression
244	Dbp2ORF_into_pOPINSmod_F	Ctgtttcagggccccggtacctcttacagagataacgaatatagtggaaattacaatg	Recombinant expression
245	Dbp2ORF_into_pOPINSmod_R	Aatcacaaactggtctagaatcaccaacgtgaacgcgc	Recombinant expression
987	ssa2-F	TCCATGGGTATCGAGACTGC	RT-PCR
988	ssa2-R	CACGCTCACCTTCAAACACT	RT-PCR
267	ydc1 – L3	CAGAATGCAAGAGGACGAGC	strain construction
268	ydc1 – L4 – pFA	ttaattaacccggggatccgTTGATCTTCGTTTGGAGGCAC	strain construction
269	ydc1 – L5 – pFA	cgagctcgaattcatcgatCCTTTTTATCATATATCGCTACTCTTTTTG	strain construction
273	ydc1 – L6	AAGCACCAATAACAGCACCG	strain construction
681	rmt1-L1	TTCCTCAACAACGGTGGTCT	strain construction
682	rmt1-L2	gtcgacctgcagcgtacgAACCAGTCCTACCCTACCCT	strain construction
560	rmt1-L3	GCCCAGATTCAACTAGCAGC	strain construction
561	rmt1-L4-pFA	ttaattaacccggggatccgACACCTGCCAAAGTTAGTAATTTAA	strain construction
562	rmt1-L5-pFA	cgagctcgaattcatcgatAATCACACATTTATCATTGCAAGTG	strain construction
563	rmt1-L6	CCCGATACTGCCACGAAAAG	strain construction
325	mlo3-L3	TAGATCAGTCCTTGGACGCC	strain construction
618	mlo3-L4-pFA	ttaattaacccggggatccgCTCCTTCTCATTTGATCCAAAATAATCATCCATCTCCTTGTCGAGCTC	strain construction
619	mlo3-L5-pFA mlo3-R	cgagctcgaattcatcgatACGACCTATACAACATACTCCCT	strain construction
328	mlo3-L6	CAAAACCTCCAACCCAACGT	strain construction

9.1.10.1 Special primers

Name	Sequence	Use	Supplier/Resource
Oligo $d(T)_{50}$-Cy3	50x T coupled with Cy3 fluorescent dye	FISH	Microsynth
PAT-$(T)_{12}$VN-2	GCGAGCTCCGCGGCCGCGTTTTTTTTTTTTVN	Poly(A) site usage assay	anchored TVN primer for reverse transcription Jänicke et al., 2012
Universal_pr_2	GCGAGCTCCGCGGCCGCG	Poly(A) site usage assay	universal PCR primer, reverse Jänicke et al., 2012

9.1.10.2 List of *in vitro* substrates

Name	Sequence (5'-3')	Modification
RNA_Putnam13_BHQ2	AGC-ACC-GUA-AAG-A	BHQ2 3'
RNA_Putnam_13_25_Cy5	UCU-UUA-CGG-UGC-UUA-AAA-CAA-AAC-AAA-ACA-AAA-CAA-AA	Cy5 5'
RNA_Ma_16_BHQ2	AGC-ACC-GUA-AAG-ACG-C	BHQ2 3'
RNA_Ma_16_21_Cy5	GCG-UCU-UUA-CGG-UGC-UUA-AAA-CAA-AAC-AAA-ACA-AAA-C	Cy5 5'

Putnam substrates are from (Putnam and Jankowsky, 2013), Ma substrates are derived from (Ma et al., 2013).

9.1.11 Software, Algorithms and Webservers

Name	Source	Version	Use
AlphaFold Server	Abramson et al., 2024	AlphaFold 3	Protein structure analysis
APE	M. Wayne Davis and Jorgensen 2022	v3.1.4	A plasmid editor
R Studio	R Core Team (2021)	version 4.2.3	Complex data analysis and visualisation
Primer3	Whitehead Institute for Biomedical Research, Steve Rozen, Andreas Untergasser, Maido Remm, Triinu Koressaar and Helen Skaletsky.	4.1.0	Primer design
EnsemblFungi	Martin et al., 2023	Ensembl 2023	Genomic resources
FIJI	Schindelin et al. 2012	2.15.0	Image editing and quantification
Integrative Genomics Viewer (IGV)	James T. Robinson Nature Biotechnology 29, 24–26 (2011) MIT open-source license.	2.17.2	Sequencing data visualisation
Pombase.org	Val Wood, Kim Rutherford (Harris et al., 2022)	Last updated: 2024-03-03	Fission yeast iterature curation, analysis tools, genome annotation and access to large-scale data sets
CLUSTAL omega	EBI web server	EMBL 2023	Multiple sequence aligner
Jalview	Waterhouse AM, Procter JB, Martin DMA, Clamp M, Barton GJ (2009) Jalview Version 2 -	2.11.3.2	A multiple sequence alignment editor and analysis workbench
usegalaxy.eu	Web open source	version 23.2.2.dev	Genomic analysis
OriginLab Pro 2023	OriginLab Corporation, Northampton, MA, USA.	Origin 2023b (10.05)	Numerical data analysis
Bowtie2	Langmead and Salzberg, 2012	2.5.3+galaxy1	Genomic alignment
Samtools	Li et al., 2009	1.20+galaxy3	Seq-read filtering
DESeq2	Love et al., 2014	2.11.40.8+galaxy0	Differential gene expression
Trimmomatic	Bolger et al., 2014	0.39+galaxy2	Seq-read trimming
RNA STAR	Dobin et al., 2013	2.7.11a+galaxy1	RNA-seq read mapper

9.2 Methods

9.2.1 *S. pombe* Techniques

9.2.1.1 *S. pombe* cell culture

Yeast strains used in this study are derived from FBY106. Rich and minimal media was prepared as in (Forsburg & Rhind, 2006). If otherwise stated, all strains were grown on YES rich-media. However, depletion of Dbp2 was performed by inoculating pre-cultures from all set of strains including controls in EMMG minimal media using colonies from cryo-stocks in 25% glycerol that were prepared by collecting cells from freshly streaked plates, and grown at 30 °C overnight with constant shaking at 180 rpm. Next day, cells were pelleted down at 1,962 g for 3 min to get rid of remnant EMMG minimal media and were then transferred to an appropriate volume of YES rich media with 15µM thiamine addition to induce depletion of Dbp2, by collecting OD_{600} of 0.2/ml from pre-cultures among all control and test strains. Usually, this 5-hours period allows cells to reach OD_{600} of about 0.5–0.6/ml. Cells were then harvested and treated accordingly based on the nature of ultimate genomic, proteomic and imaging analyses.

9.2.1.2 Transformation in *S. pombe* with LiOAc

Transformation of *S. pombe* cells was performed using the lithium acetate (LiOAc) as described by Hyun Soo Kim, Keogh lab, AECOM. *S. pombe* cells were grown in corresponding liquid media to OD_{600} 0.3 -0.7 (~ 0.5 x 10^7 cells/ml). 10-15 ml cells per transformation are pelleted down at 845 rcf for 2 min, then resuspended in 1 ml MQ H_2O and transferred into 1.5 ml microfuge tube and pelleted again. Pellets were then washed with 1 ml LiTE (0.1 M Lithium acetate, 1x TE) solution. Cell pellets were finally gently resuspended in 100 µl LiTE solution. 20 µg denatured carrier ssDNA, plus 100-1000 ng of transformant DNA (e.g PCR product), with not exceeding ≤10 µl in total volume, to be integrated were added into the mix and gently pipetted up and down and

incubated at RT for 10 min. After adding 260 µl PLATE (40% PEG/ 0.1 M LiAc/ 1x TE) into the mix and again gently pipetting up and down, cells were incubated for 1 h at 30 °C. 43 µl of dimethyl sulfoxide (DMSO) was added and a heat shock step for 5 min at 42 °C followed. Upon shortly cooling down samples at RT for 2 min, cell pellets were then briefly centrifuged for about 10 sec and supernatant was discarded. Cell pellets were then resuspended in 1 ml YES for antibiotic selection and allowed to recover 3-6 h at 30 °C with agitation before plating on antibiotic-containing YES agar plates. After the completion of recovery in YES, cells were pelleted one last time and resuspend in 500 µl MQ H_2O and then total of 2 plates used with each 250 µl of volume to spread on appropriate selection plates and incubated at 30 °C until colonies were formed. Positive colonies were confirmed both by colony screening PCR and protein signal using western blots.

For introduction of the C-terminally *flag* fused wild type *dbp2* gene into an ectopic location in the strain where endogenous *dbp2* gene's promoter replaced with *nmt* for depletion, the pDUAL plasmid was stably integrated into the *leu1* locus as described (Matsuyama et al., 2004).

9.2.1.3 Genomic manipulations in *S. pombe*

For endogenous epitope tagging or gene replacement, a standard two-step PCR method was used, as described by Bähler et al., 1998. Q5 polymerase was used to generate PCR fragments for transformation, with the following cycling conditions:

		PCR Cycler Settings	
5x Q5 Reaction Buffer	5 µl		
2mM dNTP mix	2.5 µl	98 °C 3 min	
Forward primer	1.25 µl	98 °C 15 sec	
Reverse primer	1.25 µl	64 °C 15 sec	32x
H_2O	14.5 µl	72 °C 1min 15sec	
Q5 Polymerase	0.5 µl	72 °C 5 min	
Volume:	25 µl	10 °C	

Genetic manipulations in *S. pombe* for this study

§ Gene deletion by replacing the target gene with a resistance marker gene

§ For endogenous epitope tagging

L1: Upstream 5'UTR, forward
L2: Upstream 5'UTR, reverse
L3: CDS, forward
L4: Just before the stop codon, reverse
L5: 3'UTR forward,
L6: 3'UTR/downstream, reverse

S. pombe GOI locus

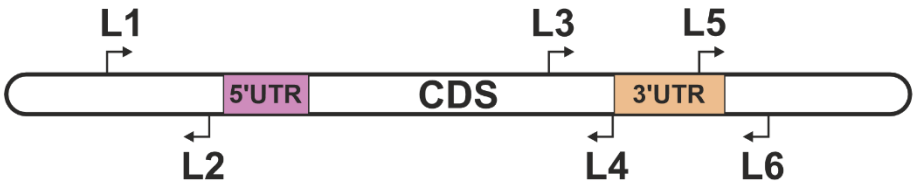

1st - step PCR

- PCR amplification of flanking regions with complementary parts to the GOI

Reaction 1: L3 – L4 **Reaction 2:** L5 – L6 C-terminal tagging

Reaction 1: L1 – L2 **Reaction 2:** L5 – L6 Deletion

- PCR amplification of flanking regions with resistance marker and/or tag

Reaction 3: PCR with F+R plasmid specific primer pair

2nd - step PCR

- PCR amplification to fuse genomic flanking regions with the cassette

Reaction 4: Reaction 1 + Reaction 3

Reaction 5: Reaction 2 + Reaction 3

Lithium Acetate Transformation

Selective media growth

C-terminal tagging

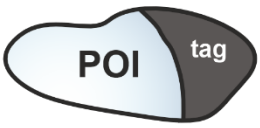

Deletion

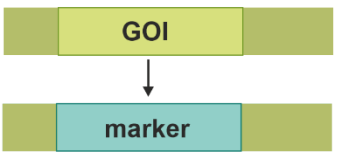

9.2.1.4 Colony PCR

For verification of gene tagging and/or disruptions from endogenous loci, colony PCR with 25 µl each total volume PCR reactions were performed in a thermocycler (Biometra/TADVANCED) on colonies formed. Same PCR settings were used for bacterial colony check. At first, a tiny portion of yeast cells were added to the PCR mix without inclusion of the Phire polymerase and boiled for 11 min at 98 °C to lyse the cells. PCR reaction tubes were then switched onto ice and Phire Polymerase was then added to each PCR reaction tube, gently mixed and briefly spun down and the PCR program resumed. 10 µl/PCR products were then analysed by 1.5% agarose gel electrophoresis.

		PCR Cycler Settings	
		98 °C 11 min	
5x Phire Reaction Buffer	5 µl	+ Phire Polymerase	
2mM dNTP mix	2.5 µl	98 °C 3 min	
Forward primer	1.25 µl	98 °C 15 sec	
Reverse primer	1.25 µl	64 °C 15 sec	30x
H_2O	14.5 µl	72 °C 1min 15sec	
Phire Polymerase	0.5 µl	72 °C 5 min	
Volume:	25µl	10 °C	

9.2.1.5 Genetic crossing of *S. pombe* strains and tetrad-dissection for genomic selection

In order to generate a strain carrying a desired genotype, genetic crosses with two opposite mating types of heterothallic strains was conducted essentially as mentioned in the publication with minor alterations (Moreno et al., 1991). Mating and sporulation can be induced in *S. pombe* under the conditions of nutrient starvation, that is upon nitrogen deprivation. ME medium was used for genetic crosses. Homothallic and heterothallic strains were distinguished in an ME plate by exposing the cells to iodine vapour. While spore-containing colonies from haploid meiosis are stained darker

shades, those not spore-containing colonies are stained yellow. ME plate was pre-warmed at RT prior to crossing. To cross two strains, using the tip of sterile wooden sticks a bit of h^- strain and a bit of h^+ strain was collected from cryo-glycerol stocks, and gently mixed together on a 9 cm ME plate in an area of about 1cm and incubated at RT until four-spore-asci containing cells formed, usually after 3-5 days. Before streaking four-spore-asci containing colonies into a fresh appropriate medium plate, sporulation was first confirmed simply by the morphology under the light microscope. For tetrad analysis, four-spore-asci containing crosses was streaked out vertically on a 1-2 cm width corner of an appropriate pre-warmed to RT agar-medium plate, then asci were placed in a horizontal row in a line about 2 mm apart using a micromanipulator (Singer Instruments MSM the lens of 20X LWD/0.30). The asci walls were then left to break down at 16 °C overnight. Next day, four-spores were free of their asci, and dissected horizontally using the needle of the micromanipulator and left for growth at 30 °C incubator for 5-7 days. Haploid cells containing desired genotypes were then selected by transferring cells using tip of sterile toothpicks to selective plates containing either selection markers and /or auxotrophic markers.

9.2.1.6 Dot-Spots Assay (Spot dilution assay)

Dot-spot assay was used to monitor cell viability upon manipulations on gene and/or protein. Pre-cultures were prepared in EMMG complete media a day before and 0.1 OD_{600}/ml per cell strain was transferred into main cultures on the next day morning. Cells were allowed to grow for 2-3 h and pelleted when they reached at ~ 0.2 OD_{600}/ml. Plates were pre-warmed to RT temperature and labelled accordingly. A 10-fold serial dilution was made as 1:1, 1:10, 1:100, and 1:1000 for each strain and 3 µl of each dilution were spotted on respective media plate, air dried and incubated at 30 °C for 2-3 days.

9.2.1.7 Long-term storage of *S. pombe* strains

Freshly growing cells that were kept on respective media-plate no longer than 3 days were collected carefully by sterile wooden-sticks, resuspended in 800 µl of 25% sterile glycerol in screw-capped cryo-stock tubes, briefly vortexed and switched to –80 °C for long-term storage.

9.3 *S. pombe in vivo* methods

9.3.1 Protein extract preparation (whole cell lysate) using glass beads and vortexing

100 ml cultures were grown to 1.0 OD_{600}/ml and harvested by centrifugation for 2 min 3,000 g at 4 ˚C and washed with ice cold 1 ml MQ H_2O and transferred into 2 ml safety lock microcentrifuge tubes and spun full-speed for 15 seconds at 4 ˚C. Pellets were lysed by adding 400 µl glass beads and 150 µl of lysis buffer and vortexed for 20 min with 30 seconds on/off time intervals on ice. The lysis buffer contained 10 mM Tris-HCl pH 8.0, 200 mM KCl, 2.5 mM $MgCl_2$, 0.5 mM EDTA pH 8.0, 0.5% NP-40, freshly added 1:10,000 dilution of protease inhibitor cocktail (Sigma Merck, P8215), and 1mM PMSF (Carl Roth). Lysates were transferred into new 1.5 ml microcentrifuge tubes after puncturing bottoms with 22-gauge ½ inch needle by centrifugation at 376 rcf, 5 min at 4 °C and further cleared by spinning at full-speed for 5 min at 4 °C. Protein concentration was determined by BCA assay (Novagen BCA Protein Assay Kit) using Nanodrop. 10 µg/cell lysate in 15 µl total volume of HU loading buffer (8 M urea, 5% SDS, 200 mM Tris-HCl pH 6.5, 20 mM dithiothreitol (DTT), 1.5 mM bromophenol blue) cooked at 95 °C for 5 min and cooled down at RT for 5 min. Finally, 15 µl lysate per sample was run on 10% SDS-PAGE gel.

9.3.2 TCA whole cell extract preparation

50 ml of cells were grown to 0.5-0.6OD_{600}/ml in respective media. Exactly total 25 OD_{600}/sample was harvested by centrifugation for 2 min 3,000 g at 4°C and washed with ice cold 1 ml MQ H_2O and transferred into 2 ml safety lock microcentrifuge tubes and spun full-speed for 15 seconds at 4 °C. First pellets washed once with ice cold 20% TCA and spun full-speed for 15 seconds at 4 °C. Excess 20% TCA was discarded. Then, 500 µl glass beads and 500 µl 20% TCA were added into each pellet. Each sample was then vortexed at max. speed 3x1 min with 1-min incubation break on ice. Upon the completion of lysis, the bottom of 2 ml safety lock microcentrifuge tubes were punctured with a hot 22-gauge ½ inch needle and lysates were transferred into new 1.5 ml microcentrifuge tubes by spinning at 376 rcf, 2 min, 4˚C. Beads on the 2 ml safety lock microcentrifuge tubes were washed once with 600µl ice cold 5% TCA just before discarding and collected into the corresponding sample's 1.5 ml microcentrifuge tube by spinning at 376 rcf, 2 min, 4 °C. Samples were then further spun at 18,407 rcf, 10 min, 4 °C. Excess liquid was discarded and pellets were washed with 1 ml of 100% EtOH (from -20˚C) at max speed, 5 min, 4 °C. Excess liquid was discarded again and pellets were finally added 84 µl 1 M Tris pH 10.0 and plus 167 µl HU loading buffer (8 M urea, 5% SDS, 200 mM Tris-HCl pH 6.5, 20 mM dithiothreitol (DTT), 1.5 mM bromophenol blue) and fully dissolved by gently pipetting up and down. Samples were then boiled for 5 min at 95 °C and briefly let cool-down at RT and a final spun at 18,407 rcf, 5 min, RT. While the supernatants from each sample were transferred into new corresponding 1.5 ml microcentrifuge tube, the bottom debris was discarded. 15 µl lysate was used per sample to run on an 10% SDS-PAGE gel.

9.3.3 RNase/DNase Treatment Assay for Monitoring Retained Fractions

Cells were grown in 100 ml YES from EMMG-grown pre-cultures to an OD_{600} of 0.8/ml. Cells were washed with 1 ml ice-cold MQ H_2O and transferred into 2 ml microcentrifuge tubes pelleted via brief centrifugation at full-speed and snap frozen in liquid nitrogen until use. Cell pellets were added 500 µl glass beads (425-600 µm Ø) and 500 µl lysis buffer (10 mM Tris-HCl pH 8.0, 200 mM KCl, 2.5 mM $MgCl_2$, 0.5 mM EDTA pH 8.0, 0.5% NP-40, freshly added 1:10,000 dilution of protease inhibitor cocktail and 1mM PMSF) and lysed by vortexing for a total of 20 min (30 s vortexing and 30 s on ice). Respective crude NP-40 cell lysates were then divided into two separate 1.5 ml microcentrifuge tubes. One of the pairs was spun at full-speed for 5 min at 4 °C for clearance, the supernatant was transferred into a new tube and used as a pool of soluble fractions, and total of 1 mg in 50 ml total volume from the other pair crude NP-40 cell lysate was first treated with 5 µl of RNase mix (100 µl RNase A (100 µg/ml), 100 µl RNase T1 (1000 U/µl), 2 µl RNase III (1 U/µl), 1 µl RNase H (5000 U/µl), 50 µl RNase I (100 U/µl) or 5 µl of DNase I (Invitrogen™) equivalent to total of 1800U upon measuring protein concentration using a BCA assay (Novagen BCA Protein Assay Kit) on a NanoDrop Microvolume Spectrophotometer (Fisher Scientific). The crude NP-40 lysates from pre-treated samples were then cleared by centrifugation at full-speed for 5 min at 4 °C and supernatant was transferred into new tubes. 30 µg total protein in 15 µl was used per sample and resolved per lane on a 10% SDS-PAGE gel. The antibodies, anti-GFP from mouse monoclonal IgG1κ (clones 7.1 and 13.1) (Sigma, 11814460001), and mouse monoclonal anti-GAPDH, clone GA1R (biomol, MM-0163-P) were used to detect proteins.

9.3.4 SDS-PAGE

Sodium dodecyl sulphate polyacrylamide gel electrophoresis (SDS-PAGE) was done based on (Laemmli, 1970) with the use of HU loading dye buffer (8 M urea, 5% SDS, 200 mM Tris-HCl pH 6.5, 20 mM dithiothreitol (DTT), 1.5 mM bromophenol blue) and after denaturing proteins at 95 °C for 5 min. The Mini-PROTEAN II system (Bio-Rad) gel pouring and electrophoresis system was used to cast all gels. Depending on protein size, between 10% and 15% polyacrylamide resolving gel was prepared containing a 4% stacking gel. Gels were run at 100 V for 10 min, followed by 200 V for 50 min using gel electrophoresis and then either transferred to nitrocellulose membranes for subsequent Western blotting or stained with 0.25% Coomassie Brilliant Blue R-250 in 30% (v/v) ethanol and 10% (v/v) acetic acid for 1 h at RT followed by several rounds of de-staining with 10% (v/v) acetic acid until the background was clear. For comparative protein interactome profiling experiment, gels were stained with SYPRO Ruby according to the manufacturer's instructions. Destaining for SYPRO Ruby stain was performed according to the manufacturer's instructions.

9.3.5 Western blotting

To detect proteins from a given sample, SDS-PAGE gel electrophoresis was followed by Western blotting. Directly after electrophoresis, the proteins were transferred onto a nitrocellulose membrane (Bio-Rad) as the binding matrix, via a semi dry blotting device (Trans-Blot Turbo Transfer System; Bio-Rad) and in 25 mM Tris, 192 mM glycine, and 20% (v/v) methanol as the transfer buffer. The transfer was performed at 2.5A, 20V, 60 min. Next, the membrane was blocked with 1 x TBST (50 mM Tris-HCl pH 7.5, 150 mM NaCl, 0.1% Tween-20) + 5% (w/v) skim milk powder for 1 h at RT (for anti-ASYM24 antibody, the blocking was done in 5% bovine serum albumin in 1 x TBST), followed by incubation with primary antibody overnight at 4 °C. The membrane

was then washed once for ~ 30 sec and three times for 5 min with 1 x TBST. The membrane was further incubated with a secondary antibody for 1 h at RT with the corresponding secondary antibody and washed 3 x for 5 min with 1 x TBST. Proteins were eventually visualised by addition of Clarity Max ECL Western (Bio-Rad) to the membrane according to the manufacturer's instructions, and the chemiluminescence signal was detected with a ChemoCam Imager (Intas).

9.3.6 Crosslinking two-step affinity protein purification coupled with mass spectrometry

Strains Dbp2-HTP and Srp2-HTP were generated by integration of the HTP (His_6-TEV-ProtA) tag into the genome C-terminal of the *dbp2* and *srp2* endogenous genes, respectively, by homologous recombination as described in Bähler *et al.* (1998). 2 litre culture/sample were grown to OD_{600} 3.9 and 0.01% formaldehyde was used to crosslink for 10 min at 30 °C just before harvesting. Harvested cell pellets were washed once with the lysis buffer containing freshly added 1mM DTT and snap frozen in liquid nitrogen and pellets were kept at -80 °C until lysed. Lysis buffer: 20 mM HEPES pH 8.0, 100 mM KAc, 2 mM $MgCl_2$, 3 mM EDTA, 0.1% NP-40, 10% glycerol + freshly supplemented with 1 mM DTT, and 1 x protease inhibitor (from 100 x PI in 50 ml EtOH: 6.85 mg Pepstatin A, 1.42 mg Leupeptin, 0.85 g PMSF, 1.65 g Benzamidine HCl). Each cell pellet lysed by hand cryo-milling for 30 min, and lysates were pre-cleared at 3,488 g for 12 min at 4 °C. Cleared lysates were then centrifuged for 1 h at 45,000 rpm (Optima XPN-80 Ultracentrifuge with 70 Ti, Beckman Coulter) at 4 °C. Supernatant/lysates were further incubated with 600 µl IgG sepharose beads slurry (pre-washed in lysis buffer without inhibitors, 2 x washing at 872 g, 2 min) for 2 h at 4 °C in a rotating wheel (Ti70 rotor, Beckman Coulter Ultracentrifuge). Bound-beads were then washed 5 times with lysis buffer containing protease inhibitors and collected

in fresh 200 µl lysis buffer, incubated for 1 h 15 min at 16 °C with 20 µgr home-made TEV enzyme. Cleaved eluates were then incubated with 200 µl of Ni-NTA agarose beads (prior to use, Ni-NTA agarose beads were also washed twice with the wash buffer for Ni-NTA agarose beads: 20 mM HEPES pH 8.0, 250 mM NaCl, 10 mM imidazole) for 1 h at 4 °C in a rotating wheel for the second-step purification. Ni-NTA beads bound were then eluted for 30 min at 4 °C in a rotating wheel with the elution buffer (Elution buffer for Ni-NTA agarose beads: 20 mM HEPES pH 8.0, 150 mM NaCl, 300 mM imidazole).

9.3.7 Detection of protein interactor by liquid chromatography-mass spectrometry

Liquid chromatography-coupled mass spectrometry analysis from mild crosslinking protein purifications of Dbp2-HTP and Srp2-HTP were performed by Dr. Timo Glatter, Mass Spectrometry and Proteomics facility at the Max Planck Institute for Terrestrial Microbiology, Marburg, Germany. Experimental details are available in Aydin et al., 2024.

9.3.8 Co-immunoprecipitation (Co-IP)

Cell lysates were prepared by resuspending the pellets from total 240 OD_{600} units in 400 µl lysis buffer. The lysis buffer contained 10 mM Tris-HCl pH 8.0, 200 mM KCl, 2.5 mM $MgCl_2$, 0.5 mM EDTA pH 8.0, 0.5% NP-40, freshly added 1:10,000 dilution of protease inhibitor cocktail (Sigma Merck, P8215), and 1 mM PMSF (Carl Roth). Cells were lysed by adding 400 µl glass beads to cell suspension and vortexed for 20 min with 30 seconds on/off time intervals on ice. Lysates were transferred into new microcentrifuge tubes after puncturing bottoms with 22-gauge ½ inch needle by centrifugation at 376 g, 5 min at 4 °C and further cleared by spinning at full-speed for 5 min at 4 °C. Protein concentration was determined by BCA (Novagen BCA Protein

Assay Kit) assay using Nanodrop. Whole cell lysate samples were prepared from cell extracts at this stage in 1:10 dilution mixed with HU loading buffer (8 M urea, 5% SDS, 200 mM Tris-HCl pH 6.5, 20 mM dithiothreitol (DTT), 1.5 mM bromophenol blue) and cooked at 95 °C for 5 min. 15 µl IgG Sepharose 6 Fast Flow (GE Healthcare) slurry was used for strains with protein A-tagged strains and 15 µl magnetic GFP-TRAP (Chromotek) beads was used for GFP-tagged protein immunoprecipitations. For washing and/or spinning steps using sepharose slurry centrifuging was done as 376 rcf; 2 min; 4 °C and for GFP-TRAP magnetic beads magnetic rack was used (DynaMag-2 Thermo Fisher). Either beads were washed three times with 1 ml lysis buffer without protease inhibitors. Clarified cell lysates were incubated with pre-equilibrated beads for 2 h on a rotator at 4 °C. Beads were washed 6x with 1 ml lysis buffer with freshly added protease inhibitors and the last two washes on a rotator at 4 °C for 5 min. After the last washing step, 60 µl HU loading buffer (8 M urea, 5% SDS, 200 mM Tris-HCl pH 6.5, 20 mM dithiothreitol (DTT), 1.5 mM bromophenol blue) was added into each co-immunoprecipitated samples and cooked at 95 °C for 5 min. Samples were cooled down at RT for 5 min and transferred into new microcentrifuge tubes. 20 µl per Co-IP and 10 µl per input (1:10) were loaded onto 10% SDS-PAGE gel. For RNase treatment 0.05 mg/ml RNase A was mixed with lysates and incubated at RT for 30 min.

9.3.9 Fluorescence *in situ* Hybridisation using oligo d(T) probes

OD_{600} of 0.2/ml per sample was used for main cultures and cells were grown for 5 h. 8.75 ml cell culture for non-heat shock samples were fixed with 1.25 ml formaldehyde adding and incubated for 1.5 h on a roller mixer at room temperature. For the heat-shock samples, 5.5 ml of cells were mixed with 3.3 ml pre-warmed corresponding media first shifted to 42 °C for 1 h in agitation. Upon the addition of 1.25 ml

formaldehyde, cells were further placed back at 42 °C for 20 more min before placing them on a roller mixer for another 1.5 h at room temperature. After fixation, cells were spun for 5 min at 845 rcf and cells were washed with 5 ml of 0.1 M KPO_4 pH 6.4. Cells were then transferred into 1.5 ml Eppendorf tubes by collecting them in 1 ml of 0.1 M KPO_4 pH 6.4 and centrifuged again for 5 min at 845 rcf and resuspended in 1 ml of 0.1 M KPO_4/1.2 M sorbitol (wash buffer) and stored overnight at 4 °C. Next day, samples were spun for 3 min at 845 rcf and resuspended in 200 µl wash buffer containing 100 µg of zymolase 100T for 1 h at 37 °C. Cells were then centrifuged for 4 min at 376 rcf and washed once with 1 ml wash buffer. Cells were resuspended in 200 µl 2 x SCC and incubated at room temperature for 10 min and followed by a spin step for 4 min at 376 rcf and the excess volume of 2 x SCC was discarded. Cells were then resuspended in 30 µl pre-hybridisation buffer (PHB) and incubated for 1 h at 37 °C. 1 µl of 1 pmol/µl Cy3-labelled oligo $d(T)_{50}$ probe was added into the sample mix and further incubated at 37 °C overnight under dark conditions. In the following day, cells were first centrifuged for 4 min at 376 rcf and the excess volume of PHB was carefully discarded. Cells were gently resuspended in 600 µl of 0.5 x SCC and incubated on a rotating wheel for 30 min in the dark at room temperature. In parallel, poly-lysine coated coverslips were prepared by adding 50 µl poly-lysine solution onto corresponding coverslip and let sit for 8-10 min, and excess amount was removed and coverslips were let dry. Cells were centrifuged again for 4 min at 376 rcf and washed with 600 µl of 1 x PBS. The pellets were gently resuspended in 40-60 µl of 1 x PBS containing 0.1% NaN_3 and 30 µl of this volume was placed on poly-lysine treated coverslip and let sit for 30 min in room temperature. Non-adherent cells were removed by aspiration and 5 µl DAPI-containing mounting media was added to the complimentary microscope slide which then covered with its complimentary coverslips. Samples were incubated overnight before analysed by microscope and kept at room temperature under dark

conditions. 20 x SSC pH 7.0 solution: 3 M NaCl and 0.3 M sodium citrate. Pre-hybridisation buffer: 50% formamide, 10% dextran sulphate, 125 µg/ml of *E. coli* tRNA, 500 µg/ml herring sperm DNA, 4 x SSC and 1 x Denhardt's solution (0.02% polyvinyl pyrrolidone, 0.02% BSA, 0.02% Ficoll-400). Pre-hybridisation buffer and 50 x Denhardt's solution were stored at –20 °C.

9.3.10 Immunofluorescence (IF)

An immunofluorescence protocol was essentially performed by the modification of the protocol as described in Hagan I. M. 2016. 0.2 OD_{600}/ml cells from pre-cultures were incubated in 10 ml YES rich-media for one life cycle ~2.5 h. 9 ml culture were transferred into 50 ml Falcon tubes and fixed by adding 1 ml from 37% formaldehyde and placed on a rotator and incubated for 60 min at RT. Fixed cells were then pelleted by spinning at 872 g for 3 min and resuspended in 1 ml PEM and transferred to 1.5 ml microcentrifuge tubes. Cells were washed twice with 1 ml PEM. After the second wash, cells were then resuspended in 200 µl PEMS containing 0.5 mg/ml zymolyase 100T and incubated at 37 °C for 1 h for digesting cell walls. After cell wall digestion, cells were pelleted at 376 rcf for 3 min and resuspended in 500 µl PEMS containing 1% Triton X-100 to permeabilise cells where cells were shortly incubated in about 30 seconds and pelleted again at 376 rcf for 3 min. Upon three washing steps with 500 µl PEM, cells were finally resuspended in 200 µl PEMBAL solution and rotated for 30 min at room temperature. Cells were then pelleted again at 376 rcf for 3 min and resuspended in 100 µl PEMBAL solution with respective primary antibody (1/100 dilution for anti-$Rbp1^{Ser2P}$ antibody, and 1/500 dilution for anti-Flag antibody), and placed on a rotating wheel at 4 °C for overnight. On the following day, cells were pelleted down at 376 rcf for 3 min and washed twice with 100 µl PEMBAL. Cells were gently resuspended in 100 µl PEMBAL and incubated for 10 min at room temperature.

After one final round of pelleting at 376 rcf for 3 min, cells were again gently resuspended in fresh 100 µl PEMBAL containing the secondary antibody of interest (1/400 dilution of goat anti-rat (Alexa Fluor 594), and 1/200 dilution of goat anti-mouse (Alexa Fluor 488)) under light limiting conditions. Tubes were then wrapped in aluminium foil and placed on a rotating wheel for overnight at 4 °C. Next day, cells were pelleted and washed twice with 200 µl PEMBAL and one time with 500 µl PBS, and each step of centrifugation at 376 rcf for 3 min. After the last pelleting down, cells were resuspended in 40 µl PBS containing 0.1% NaN_3. Before mounting, 50 µl of poly-lysine solution was applied on each coverslip for coating and incubated for 15 min at room temperature and then each coverslip was rinsed with distilled water and let to dry completely. 20 µl of cell suspension was dropped on respective poly-lysine coated-coverslip and incubated for 10 min in the dark. Unbound cells were washed away by carefully tilting the coverslip and pipetting any excess liquid off and let to dry completely in the dark conditions. Once coverslip dried thoroughly, 5 µl mounting medium containing DAPI (Roth ROTI®Mount) was added onto a clean slide, each respective cell-coated coverslip was anchored to the DAPI containing mounting medium slide upon inverting and coverslips were gently pressed on slides until the mounting medium spread evenly across the entire surface between slide and coverslip. Sample slides were analysed immediately. PEM Fixation Solution (100 mM piperazine-N,N′-bis (2-ethanesulfonic acid) (PIPES), 1 mM EGTA pH 8.0, 1 mM $MgSO_4$ – For adjusting the pH to 6.9 it is important to use the sodium and not potassium salt of PIPES). PEMS (1.2 M Sorbitol in PEM fixation solution). PEMBAL (1% Bovine serum albumin (essentially fatty acid– and globulin-free), 100 mM Lysine hydrochloride, 0.1% NaN_3 in PEM fixation solution).

9.3.11 Chromatin immunoprecipitation

ChIP-seq was carried out as in Wittmann et al., 2017, with minor modifications and performed by Dr. Birte Keil (post-doctoral researcher, Kilchert lab) for Dbp2-HTP and Srp2-HTP, and by Cornelia Kilchert for Rpb1 (8WG16). Exponentially growing cells (200 ml) were crosslinked with 1% formaldehyde for 20 min at room temperature. For calibrated ChIP-seq of RNAPII, *S. cerevisiae* cells were added to the culture in a 1:5 OD_{600} ratio prior to crosslinking. 30 ml of a solution of 3 M glycine, 20 mM Tris were added to quench the reaction. Cells were pelleted and washed once with cold TBS and once with FA lysis buffer / 0.1% SDS (50 mM Hepes-KOH pH 7.5, 150 mM NaCl, 1 mM EDTA, 1% Triton X-100, 0.1% Na Deoxycholate). After resuspension in 1.4 ml FA lysis buffer / 0.5% SDS, cells were distributed to two screw-cap micro tubes containing 300 µl glass beads and lysed in a FastPrep instrument (MP Biomedicals) at 3 x 45 s 6 m/s, with 2 min breaks on ice. Lysed cells were recovered with FA lysis buffer / 0.1% SDS and ultracentrifuged at 24,000 rpm, 20 min, 4 °C in a 70 Ti rotor. The chromatin pellet was resuspended in FA lysis buffer / 0.1% SDS and sheared with a Bioruptor sonicator (Diagenode) at 15 s ON / 45 s OFF for 80 min. HTP-tagged proteins were immunoprecipitated with IgG-coupled dynabeads (tosylactivated M280, Thermo Scientific), RNAPII with antibody against Rpb1 (8WG16, Millipore) coupled to 20 µl of protein-G dynabeads (Life Technologies). After washing and elution of bound material from the beads, proteins were digested by incubation with 0.6 mg pronase for 1 h at 42 °C, followed by decrosslinking at 65 °C overnight and DNA extraction.

9.3.12 RNA extraction

Overnight *S. pombe* cultures in EMMG were switched to 200 ml YES media with 15 µM thiamine on the day and cultured for 5 h to a log phase of OD_{600} ~0.5-0.6/ml. For harvesting, cells were centrifuged for 2 min at 1,962 g and excess media discarded

and cells were washed with 1 ml cold MQ H_2O and transferred to 1.5 ml RNase-free tubes. Cells were then pelleted again with 2 min at 845 rcf and excess MQ H_2O was removed. Pellets were flash frozen in liquid nitrogen first and kept at -80 °C until further use. For RNA isolation, cell pellets were resuspended in 400 µl cold AE buffer (50 mM NaAc pH 5.0, 10 mM EDTA, pH 8.0) and 50 µl 10% SDS and 500 µl (an equal volume) of fresh phenol:chloroform:isoamylalcohol mixture (PCI, 25:24.:1, pH 4.5) added and vortexed 15 seconds at max speed and then transferred to 65 °C heat-block for 5 min. Samples were rapidly cooled down on ice and centrifuged for 15 min; 11,000 g at 4 °C. Top aqueous phase was transferred into a new tube and 500 µl of chloroform was added and vortexed for 15 seconds at max speed and spun for 15 min; 11,000 g at 4 °C. Top aqueous phase was transferred one last time into a new tube with the addition of 40 µl of 3 M NaAc (pH 5.3-6.5) and 1 ml ice-cold 100% EtOH and tubes were gently inverted 6-7 times to mix properly, and precipitated at -20 °C for 1 h. Samples were then centrifuged at full-speed for 30 min at 4 °C and washed with ice-cold 80% EtOH followed by spinning again at max speed for 5 min at 4 °C. Pellets were air-dried on ice and dissolved in ~400 µl ice cold nuclease-free H_2O and total RNA yield was quantified using Nanodrop. Samples were then flash frozen and stored at -80 °C until use.

9.3.13 RT-PCR amplification using an anchored PAT- $(T)_{12}$VN primer

In order to assess poly(A) site usage, a protocol published in Jänicke et al., 2012 was used and performed by Silke Schreiner. Briefly, total RNAs were isolated as described in section 9.3.12. 1 µg of total RNA/sample (11 µl, RNA+H_2O) was incubated with 1 µl of PAT-$(T)_{12}$VN primer in total of 12 µl reaction volume for 5 min at 80 °C. Upon flash-spinning and cooling down to 42 °C, 7 µl of master mix containing: 4 µl 5 x SSIII buffer, 1 µl 0.1 mM DTT, 1 µl 10 mM dNTPs, 1 µl RNaseOUT, first incubated at 42 °C for 1 min, then 1 µl Super Script III Reverse Transcriptase (SSIII) reverse transcriptase was

added, making up a total volume of 20 µl per reaction. Reverse transcription reaction was then performed for 15 min at 42 °C, 15 min at 47 °C, 15 min at 55 °C and SSIII enzyme was deactivated for 10 min at 80 °C. cDNAs were diluted in 1:10 with H_2O in preparation for PCR amplification. 5 µl cDNA/sample was used for PCR amplification using Phire polymerase with gene specific forward and universal reverse primers, in 25 µl total PCR reaction for 10 min at 95 °C, 20 sec at 95 °C, 20 sec at 60 °C for 30 cycles, 30 sec at 72 °C, 1 min at 72 °C, an indefinite pause at 10 °C. Finally, 10 µl volume/PCR sample used to run in 2% agarose gels and stained with ethidium bromide and imaged.

9.3.14 Phenol-chloroform extraction of genomic DNA

The protocol was adapted from (Hoffman & Winston, 1987) for rapid genomic DNA extraction. Yeast cultures were grown to 1 OD_{600} /ml and collected by centrifugation for 3 min at 1,962 g and transferred into 1.5 ml microcentrifuge tubes in 1 ml MQ H_2O, and quickly spun. Supernatant was then discarded and 0.2 ml of Buffer A (2% Triton X-100, 1% SDS, 100 mM NaCl, 10 mM Tris-HCl pH 8.0, 1 mM EDTA pH 8.0), 0.2 ml glass beads, and 0.2 ml phenol:chloroform:isoamyl alcohol (25:24:1; ~pH 7), all were added into each sample. The mixture was vortexed for 3 min at 4 °C full-speed and after a quick spun down, 0.2 ml MQ H_2O was added into each sample and briefly vortexed for mixture. Next, samples were centrifuged for 5 min at 10,000 g and the top aqueous phase was transferred into new tubes. 1 ml 100% EtOH (RT) was added into each sample tube, and inverted to mix, and spun for 2 min at full-speed. After washing the genomic DNA pellet once with 70% EtOH, pellets were then resuspended in 0.4-0.6 ml MQ H_2O. For PCR, 1 µl of a 1:10 dilution was used.

9.3.15 *In vitro* transcription for dig-labelled RNA probes

The probes used in Northern blot assay were designed against the gene body and labelled with DIG using *in vitro* transcription assay. 2 x PCR reactions per probe were performed with gene body specific primer pairs using gDNA template of the wild type strain as template and reaction volumes were then pooled together and precipitated with 1 µl glycogen resuspended 40 µl nuclease-free H_2O. Concentrations were measured by Nanodrop. All buffers were kept at RT before generating RNA probes with Ambion Maxiscript Kit. Per reaction 1–1.5 µg DNA template was used in up to 12 µl; 2 µl of 10 x Buffer; 1 µl of each ATP/CTP/GTP; 0.6 µl of UTP, 0.4 µl of dig-11-UTP, 2 µl of Ambion Maxiscript polymerase were mixed and incubated for 1 h at 37 °C. Later, 1 µl of Turbo DNase I was added into each reaction mix and further incubated for 15 min at 37 °C. RNA probes were then precipitated by addition of 30 µl nuclease-free H_2O; 1 µl glycogen; 5 µl 5 M ammonium acetate; 150 µl 100% EtOH and incubated overnight at -20 °C. Precipitated RNA probes were then pelleted down at full-speed for 30 min, at 4 °C and once washed with 70% EtOH and spun again at full-speed for 5 min at 4 °C and finally resuspended in 50 µl nuclease-free H_2O. Concentrations were measured by Nanodrop, and probes were aliquoted in 35 µg/ml and stored at -80 °C. Oligonucleotides used to generate DNA templates for RNA probes are listed in section 9.1.10.

9.3.16 Northern blotting

Total RNAs were isolated from cells as described in RNA extraction section. 10 µg of RNA per sample in up to 90 µl nuclease-free H_2O was further precipitated with 10 µl 3 M NaAc, 1 µl glycogen, 250 µl 100% EtOH for 1 h at -20 °C and pelleted for 20 min; full-speed; at 4 °C and washed once in 70 % EtOH. Residual liquid was discarded and pellets were air-dried on ice. 2 µl nuclease-free H_2O was used to resuspend per 10 µg

RNA pellet and 15 µl glyoxal mix was added into it. (Glyoxal mix is stored for long-term at -80 °C and at -20 °C for routine use and ingredients per 10 ml are: 6 ml DMSO, 2 ml of 40% glyoxal solution (Sigma), 1.2 ml 10 x BPTE, 0.6 ml 80% glycerol). The RNA sample with glyoxal mix was incubated at 55 °C for 1 h and 1.2% agarose in 1 x BPTE was prepared (10 x BPTE in 1 l: 30 g PIPES free acid, 60 g Bis-Tris free base, 20 ml 0.5 M EDTA pH 8.0) and let polymerised during this incubation period. Glyoxal-treated RNA samples were quickly spun down and 18 µl per sample was loaded directly while still hot onto gel pockets and run 150V for ~ 2.5 h. Upon completion of running, gel was first incubated in 10 mM NaOH for 20 min at RT shaking, then quickly rinsed with nuclease-free H_2O and further incubated in 20 x SSC buffer for 5 min and later in 10 x SSC for 40 min. Transfer from gel on Hybond-N+ nylon membrane (GE Healthcare) was performed overnight by capillary transfer in 10 x SSC buffer (20 x SSC Stock: 175.3 g of NaCl and 88.2 g of sodium citrate dissolved in 800 ml of water pH adjusted to 7). RNAs were then immobilised on the nylon membrane by UV-crosslinking at 254 nm and 120 mJ/cm2. Crosslinked membrane was first washed with 3% acetic acid for 10 min at RT and then stained with 0.04% methylene blue / 0.5 M Na-Acetate pH 5.2-6.5 until ribosomal bands appeared. Briefly rinsed with nuclease-free H_2O until the background is white enough and imaged to be used as a loading control. Blots were transferred to hybridisation tubes and pre-hybridised with 10 ml pre-warmed DIG Easy Hyb solution (Roche, 1796895001) for 3-6 h at 60 °C. An equal volume of formamide was added to the Dig-labelled RNA probe and the mix was first incubated for 15 min at 65 °C then added directly to the pre-hyb solution at a final concentration of 100 ng/ml and incubated overnight at 60 °C on a rotator. Probe hybridised blots were first washed three times with 2 x SSC / 0.1% SDS for 15 min each at 60 °C and then two times with 0.2 x SSC / 0.1% SDS for 10 min each at 60 °C. Following washes, blots were rinsed with 1 x PBS for 2 min at RT and blocked in 1 x Blocking solution (Roche,

11096176001) (10 x blocking solution 10% w/v Blocking Reagent (Roche, 11096176001) in Maleic Acid buffer w/o Tween-20) for 30 min at RT. 1:10,000 of anti-DIG alkaline-phosphatase-conjugated antibody, Fab fragments (Roche) was directly added into the blocking solution and incubate for 1 h at RT. Blots were first washed five times with 1 x PBS for 5 min each at RT and then washed two times with DIG P3 buffer (100 mM Tris-HCl, pH 9.5) for 10 min each agitating at RT. ~25 µl/cm^2 CDP-Star® Chemiluminescent Substrate solution (Millipore) was used for the imaging of signals.

9.3.17 poly(A)+ length assay

To measure the length of poly(A)-tails, total RNA was labelled with [32P]-pCp following the protocol outlined in (Minvielle-Sebastia et al., 1991). Total RNA was extracted as described in section 9.3.12. 1 µg of RNA was incubated with 1 mM ATP, 10% DMSO, 0.25 µM [32P]-pCp, and 10 U of T4 RNA ligase in a 30 µl reaction volume overnight at 4 °C for radioactive labelling. Upon labelling, samples were subjected to additional digestion to digest away all RNAs leaving the poly(A)-tails. This was done by incubating samples for 2 hours at 37 °C in an 80 µl reaction containing 80 U of RNase T1, 4 µg of RNase A, 10 mM Tris-HCl (pH 7.5), and 300 mM NaCl. After digestion, radiolabelled RNA samples were re-extracted and precipitated as described in section 9.3.12, and resuspended in 10 µl of nuclease free H_2O water, and mixed with 10 µl RNA loading dye containing xylene cyanol and bromophenol blue dyes. The samples were then heated at 95 °C for 5 minutes, and 10 µl per sample was loaded in a 20% PAA-8M urea gel that was pre-run for 30 minutes at 180 V until the dye reached the bottom, followed by overnight exposure to Autoradiography with Amersham Hyperfilm, (n = 1).

9.3.18 RNA immunoprecipitation (RIP) assay

Corresponding strains were grown overnight in EMMG media. Next day, 0.2 OD_{600}/ml of cells were cultured in 400 ml YES media together with addition of 15µM thiamine incubated for 5 h at 30 °C, shaking at 180 rpm. Cells were harvested after washing pellets with MQ H_2O and snap frozen in liquid nitrogen, and stored at -80 °C until needed. Cell pellets in 2 ml safety-capped nuclease free tubes were filled with 500 µl glass beads and lysed in 1 ml RIP buffer containing 25 mM Tris HCl pH 7.5, 200 mM NaCl, 2 mM $MgCl_2$, 0.2% Triton-X-100, freshly added 1 mM PMSF, 1:10,000 PIC and 10 U/ml RNasin (Promega) by vortexing with glass beads for a total of 20 min (30 s vortexing and 30 s on ice). After centrifugation at 18,407 rcf at 4 °C for 5 min, the supernatant was transferred into new tubes and centrifuged again at 18,407 rcf 4 °C for 10min. This yields to the total of 1.1-1.3 ml lysate/sample. Before proceeding to downstream steps in the protocol, total protein concentration for each sample was determined using BCA assay (as in manufacturer's protocol, Novagen BCA Protein Assay Kit). Total volume of lysate was subjected to incubation with 1800 U DNase I (Thermo Fisher) for 30 min on ice. After adjusting protein concentrations of each sample proportional to lowest protein concentration containing sample, two sets of nuclease-free microcentrifuge tubes prepared; one set for input and another set for immunoprecipitated (IP) samples derived from lysates and beads, respectively. In the meanwhile, 20 µl GFP-TRAP magnetic beads slurry per sample were washed and equilibrated three times with 1 ml RIP buffer without protease inhibitors. Lysates were then incubated with GFP-trap beads at 4 °C for 2 h on a rotator. Supernatant was discarded and bound beads were washed 8 times with RIP buffer containing 1 mM PMSF, 1:10,000 PIC and 10 U/ml RNasin. The isolation of RNAs as well as proteins was achieved by adding 1 ml TRIzol into lysates for inputs and directly into beads for immunoprecipitated (IP) samples and vortexed at max. speed for 10 sec and incubated

samples for 5 min at RT. 200 µl chloroform was added into each sample and vortexed strongly for 10 seconds and incubated for 5 min at RT. Samples were then centrifuged at 18,407 rcf; 15 min; 4 °C. The upper phase was transferred into new nuclease-free microcentrifuge tubes and the bottom TRIzol containing part is kept for the isolation of proteins. For the isolation of RNAs, 1 ml isopropanol was added into tubes containing the upper phase and incubated at -20 °C for 1 h and after that centrifuged at 18,407 rcf; 20 min; 4 °C. Pellets were washed once with 80% ethanol and centrifuge at 18,407 rcf; 5 min; 4 °C. Excess ethanol was discarded and pellets were let dry completely on ice. 50 µl nuclease free water was used to resolve each pellet and samples can be frozen and stored at this stage for future use at -80 °C. For the precipitation of proteins from each sample, 1 ml acetone was added into the lower phase and incubated at -20 °C overnight and then centrifuged at 18,407 rcf; 1 h; 4 °C. Pellets were washed once with acetone and centrifuged 18,407 rcf; 30 min; 4 °C. After drying pellets for at least 15 min on ice 30 µl HU loading buffer (8 M urea, 5% SDS, 200 mM Tris-HCl pH 6.5, 20 mM dithiothreitol (DTT), 1.5 mM bromophenol blue) was added into each sample and incubated for 10 mins at 95 °C. Samples at this stage can be stored at -20 °C until further use. Transcript analysis was performed using oligo-d(T) primer at the reverse transcription step and transcript specific primers at PCR amplification step.

9.3.19 Reverse transcription PCR (RT-PCR)

Reverse transcription (RT) was performed to synthesise cDNA from RNA templates, as part of RIP assay. Reverse transcription reactions were done with Biozym cDNA synthesis kit according to the manufacturer's instructions. 1 µg of input and 2 µl of IP samples per reverse transcription reaction were used to generate cDNA in total reaction volume of 20 µl. Oligo-d(T) primer was used to obtain cDNA levels. Reverse transcriptions without reverse transcriptase (no RT control) were performed as the

negative controls, to ensure signal was not derived from any contaminant DNA. 2.5 µl per cDNA reaction volume were then amplified with Phire polymerase using gene specific primers for total of 26 cycles. 10 µl from RT-PCR reaction was loaded into 2% agarose gel and stained with HD-green. Primers used for the study are listed in section 9.1.10.

9.4 *In vitro* protein biochemistry methods

9.4.1 Cloning of expression plasmids

The Zero Blunt™ TOPO™ PCR Cloning Kit was used to clone the *S. pombe* Dbp2 ORF, which was retrieved from the YP428 strain. Full-length Dbp2 mRNA was reverse transcribed using a gene-specific primer, as listed in 9.1.10. ATP-binding mutant K172R (deficient in ATPase activity) was introduced by point mutations into this plasmid using site-directed mutagenesis with primers that contain the necessary nucleotide changes. The blunt-end cDNA products of *dbp2* were inserted into the pCR-Blunt-II-TOPO vector, and the resulting constructs were subsequently cloned into pOPINS3C (L. E. Bird, 2011). This plasmid allows the expression of full-length Dbp2 and an ATP-binding K172R mutant with an N-terminal His_6-tag in *E. coli*. The pOPINS3C plasmid was KpnI and HindIII digested and the cDNA PCR fragments assembled using HiFi assembly kit. NEBuilder HiFi assembly master mix was performed according to manufacturer's recommendations (NEB). Assembly reaction contained 50–500 ng of linear vector, an appropriate amount of insert DNA in a 1:2 vector to insert molar ratio and 2 x NEBuilder HiFi. NEBuilder HiFi assembled products were transformed into TOP10 *E. coli* (Invitrogen) by heat shock according to the manufacturer's protocols. Transformed cells were spread on plates containing 50 µg/ml Ampicillin, 25 µg/ml Kanamycin. The assembly reaction was incubated at 50 °C for 1 h. 5 µl of the mixture was used for transformation in *E. coli* p(Lys)S cells.

9.4.2 Transformation of *E. coli* cells and plasmid extraction

All transformations were performed using chemically competent cells. 50 µl iced thawed competent cells were transformed with 5 µl HiFi assembly mix or 50 ng plasmid DNA. Cells were incubated ice for 5 min and then heat shocked at 42 °C for 30 sec followed by an incubation on ice for 5 min. Cells were recovered in 270 µl SOC medium (20 g/l tryptone, 5 g/l yeast extract, 0.59 g/l NaCl, 0.186 g/l KCl, 2.03 g/l $MgCl_2$ x $6H_2O$, 2.46 g/l $MgSO_4$ x 7 H_2O) and incubated for 1 h at 37 °C on a shaker at 200 rpm. 100 µl of cell suspension was spread out on selective Lysogeny broth (LB) plates (10 g/l tryptone, 5 g/l yeast extract, 10 g/l NaCl, 20 g/l agar) containing 50 µg/ml Ampicillin, 25 µg/ml kanamycin and/or 34 µg/ml chloramphenicol antibiotics and incubated overnight at 37 °C. Single colony was picked and checked by colony PCR using Phire-polymerase as described in section 9.2.1.4, validated positive colony was then inoculated in 5 ml liquid LB containing the appropriate antibiotics and incubated at 37 °C and 180 rpm overnight. Cultures were then subjected to plasmid extraction using the NucleoSpin® Plasmid (Macherey & Nagel) according to the manufacturer's instructions.

9.4.3 Recombinant expression and purification of proteins

Recombinant constructs are expressed with an N-terminal His_6-SUMO-3C-tag allowing affinity purification and the tag is cleavable due to the presence of a Rhinovirus 3C protease recognition site (LEVLQFGP). Both wild type full-length Dbp2 and ATP-binding K172R mutant Dbp2 were expressed in BL21(DE3)pLysS cells. 400 ml of cells were grown at 37 °C and 180 rpm in LB supplemented with 50 µg/ml kanamycin and 25 µg/ml chloramphenicol until OD_{600} ~0.8/ml was reached. Protein expression was induced by the addition of 0.2 mM isopropyl β-D-1-thiogalactopyranoside (IPTG) into the cell cultures followed by further growth at 25 °C for 3 h. Cells were harvested by

centrifugation at 4 °C and 6,200 g for 15 min and flash frozen kept until use at -80 °C. For lysing cells re-suspended in 10 ml lysis buffer (150 mM KCl, 50 mM HEPES pH 7.5, 10% glycerol (v/v), 15 mM imidazole, 0.15% NP-40 (v/v) with freshly added 1 mM dithiothreitol (DTT), 1mM PMSF) and sonicated (30 secs on and 30 secs off intervals for 10-15 mins) on ice. The suspension was ultracentrifuged at 4 °C and 40,000rpm (70 Ti rotor) for 40 min and lysates added to the pre-equilibrated 400 µl Ni-NTA agarose slurry beads 2 times with lysis buffer and incubated at 4 °C on a rotator for 2 hrs. Beads were then washed 6 times with lysis buffer, spinning down after each washing step at 1,800 rpm for 2 min. Proteins were eluted from beads after incubating in 200 µl elution buffer (150 mM KCl, 50 mM HEPES pH 7.5, 10% glycerol (v/v), 300 mM imidazole, 0.15% NP-40 (v/v)) for 30 min at 4 °C on a rotator. Full-length wild type and K172R mutant Dbp2 were then dialysed (Dialysis membrane Membra-Cel™, 14000 MWCO), a method to primarily used to remove small molecules and exchange buffer, in a buffer containing 40 mM Tris/HCl pH 8.0, 50 mM NaCl, freshly added 5 mM ß-mer. and at the same time subjected to human Rhinovirus (HRV) 3C Protease (Thermo Scientific Pierce) cut from the cleavage site (LEVLQFGP) used in 1:50 ratio for overnight at 4 °C. At this point, the solution contains traces of uncleaved Dbp2 constructs, His_6-tagged 3C protease, and mostly cleaved Dbp2 constructs. The cleaved Dbp2 constructs were collected in the flow-through after the reverse Ni-NTA approach. This was achieved by incubating the solution with 100 µl Ni-NTA agarose beads slurry for 1 hour at 4°C, following the reverse Ni-NTA strategy. All cleaved Dbp2 constructs were successfully recovered in the flow-through during this step.

All protein concentrations were determined using a NanoDrop. A final concentration of 33% (v/v) glycerol was added to the elution fractions before freezing in liquid nitrogen

and storage at -80 °C for long-term storage. The uncleaved and 3C cleaved products can be detected by Coomassie staining the SDS gels (Figure 2.3.1B&C).

9.4.4 Annealing of RNA substrates

Before using double-stranded substrates for the helicase assay, two single-stranded substrates (listed in section 9.1.10.2) were annealed to each other, as outlined by (Putnam & Jankowsky, 2013a). Putnam 2013 RNA sequence consist of a 13 bp-BHQ2 label at 3'-end and a 25 nt overhang-Cy5 labelled at 5'-end. Ma 2013 RNA sequence consist of a 16 bp-BHQ label at 3'-end and a 21 nt overhang-Cy5 labelled at 5'-end. The ssRNA substrates, labelled with Cy5 (shorter sequence) and BHQ2 (longer sequence), were annealed before use. Annealed dsRNA substrates were used for *in vitro* helicase assay testing the unwinding reactions. The annealing reaction involved mixing equimolar amounts of each ssRNA in 1x annealing buffer (composed of 60 mM KCl, 6 mM HEPES pH 7.5, and 0.2 mM $MgCl_2$). The mixture was subjected to a thermal cycling program:

	PCR Cycler Settings
1 µl 100 µM RNA Cy5, 13 or 16 bp 1 µl 100 µM RNA BHQ2, 21 or 25 nt 10 µl 10xAnnealing buffer 88 µl nuclease-free H2O	95°C for 10 minutes 90°C for 5 minutes 85°C for 5 minutes 80°C for 5 minutes : :
Total volume: 100 µl	Continue decreasing by 5°C steps, each for 5 minutes, until reaching 10°C
	pause at 4°C

The substrates were then aliquoted and kept at -80 °C under dark conditions for long term storage.

9.4.5 *In vitro* helicase assay

The helicase assay used for testing the unwinding activity of Dbp2 recombinant proteins were performed in reaction buffer containing 40 mM Tris-HCl pH 8.0 50 mM NaCl 5mM β-mer. A strand of the dsRNA was labelled at the 5'-end with a Cy5 fluorophore, while the other ssRNA was labelled at the 3'-end with a BHQ2 quencher. BHQ2 quenches the signal emitted by Cy5 when unwound and in closed proximity to the Cy5. However, upon substrate unwinding, unwound Cy5 emit a fluorescent signal, which can be measured in real-time. The helicase assay was performed at room temperature under dark condition using the plate reader Tecan Infinite F200 pro. Total reaction volume used was 100 µl/well. Reaction mixture of helicase buffer contained in total concentrations of the followings: 600 nM of either recombinant Dbp2 proteins, 10 nM of either dsRNA substrate were first mixed and signal was measured, and then 2 mM ATP and 2 mM $MgCl_2$ were programmed to be sprayed into each reaction (Figure 2.3.2B) during real-time and signal emitted was measured every second for a period of 2 mins. Flat-bottomed black 96-well plates were used for reactions. The Cy5 fluorophore was excited at a wavelength of 620 nm and the emitted fluorescence signal measured at a wavelength of 670 nm.

9.5 High-Resolution Microscopy

9.5.1 Image acquisition

The Deltavision Ultra High-Resolution Microscope was used for image acquisition for both live cell and immunofluorescence microscopy and 18mmx18mm, 170±5 µm high precision coverslips were used for sample preparation. Acquired Z-stack images were deconvolved with the softWoRx software using settings as in the following: sample thickness 5.00, Z-section spacing 0.25 µm, number of sections 20, experimental type 3D, exposure time 0.500, percent of transmission for red channel 40% for green

channel 5% for blue channel 5%. Upon acquisition, image samples were deconvolved with method set to enhanced ratio (aggressive), noise filtering to high 300 nm. Line profiles were generated with Fiji (Schindelin et al., 2012) and plotted in R.

9.5.2 Live microscopy

Precultures were inoculated in respective liquid media from cryo-stocks, incubated on a shaker overnight at 30 °C. The next day, for Dbp2 depleting conditions, cells were first pelleted down at 1,962 g for 3 mins to get rid of residual EMMG and only then diluted in rich YES media with 15 µM thiamine to an OD_{600} of 0.2 and grown under agitation at 30 °C for 5 h. Any other cell strains were precultured and grown in YES media. 50 µl of poly-lysine coating solution was applied on each cover slip and incubated for 15 min at room temperature. Cover slips were then briefly rinsed with MQ H_2O to remove leftover poly-lysine as well as dust particles away. 1 ml cell suspension per sample was transferred to 1.5 ml microcentrifuge tubes and spun at 376 rcf, for 1 min at RT. Excess media was discarded and cells were resuspended either in 100 µl of EMMG media + containing 15 µM thiamine for Dbp2 depleting conditions, 100 µl of EMMG media for any other strain of cells, and for ectopic expression of Dbp2 variants, cells were resuspended in 100 µl of EMMG -LEU (lacking leucine) media. 30 µl cell suspension was transferred onto poly-lysine coated coverslip and incubated 8-10 min. Cell suspension on each coverslip was gently pipetted up and down to get excess and non-adherent cells away. Each coverslip then inverted and carefully placed onto its corresponding microscope slide.

9.5.3 Image analysis and quantification

Image quantification was performed using Fiji with a semiautomated ImageJ macro script (detailed in Aydin et al., 2024). Briefly, cellular segmentation was achieved by thresholding the transmitted light channel (to define cell outlines) and the DAPI stain

(to identify nuclei). The oligo-d(T)$_{50}$ signal was quantified on average intensity Z-projections for both the nucleus and the cytoplasm (defined as the total cell excluding the nucleus). For each cell, the nuclear-to-cytoplasmic fluorescence intensity ratio was calculated by dividing the mean nuclear fluorescence intensity by the mean cytoplasmic fluorescence intensity. Statistical analyses for pairwise comparisons were conducted using the Wilcoxon test, with p-values calculated via the ggpubr package in R (Kassambara, A., 2022. Ggpubr: 'Ggplot2' Based Publication Ready Plots. CRAN link). Scale bars in the images were defined using the following parameters in Fiji's "Set Scale" settings: Distance in pixels: 9.2746; Known distance: 1.00; Pixel aspect ratio: 1; Unit of length: micron, corresponding to 9.2746 pixels/micron.

9.6 High-throughput data analysis and bioinformatics methods

9.6.1 Genome-wide transcriptome sequencing (RNA-seq)

For RNA sequencing, pellets from *S. pombe* and *S. cerevisiae* cultures were pooled in a 5:1 OD_{600} ratio immediately before cell lysis. Total RNA was extracted with the hot phenol method. The construction of the sequencing library was performed by Dr. Stefan Guenther at the Max Planck Institute for Heart and Lung Research Bad Nauheim sequencing facility.

The raw RNA-seq FASTA files were processed by Cornelia Kilchert to generate BAM files, which underwent rigorous quality control (QC) checks. Briefly, the processing pipeline included adapter trimming, quality filtering, and removal of low-quality reads to ensure high data integrity. In depth, after read trimming with Trimmomatic, (Bolger et al., 2014) RNA-seq data were aligned to versions ASM294v2 and R64-1-1 of the *S. pomb*e and *S. cerevisiae* genome using the STAR aligner (Dobin et al., 2013) on the Galaxy server (Jalili et al., 2021). All reads aligning to both yeasts were filtered out

using SAMtools (H. Li et al., 2009). For normalisation purposes, the reads were additionally aligned to the *S. cerevisiae* genome (R64-1-1 version). Post-alignment, the resulting BAM files were used for downstream expression analyses. Differential gene expression analysis was carried out with the DESeq2 tool (Love et al., 2014) after read counting with HTSeq-count (Anders et al., 2015) in Union mode on the ASM294v2.57 gene model provided by EnsemblFungi (Martin et al., 2023).

9.6.2 Genome-wide ChIP-sequencing (ChIP-Seq)

Chromatin preparation, protein pull-down and DNA precipitation steps were done by Dr. Birte Keil (post-doctoral researcher, Kilchert lab) for Dbp2-HTP, Srp2-HTP and for total RNAPII (α-rpb1 (8WG16) in Dbp2-3myc by Dr. Cornelia Kilchert as described in section 9.3.11. Samples were in duplicates. The construction of the sequencing library for Dbp2-HTP and Srp2-HTP associated DNA was performed by Dr. Stefan Guenther at the Max Planck Institute for Heart and Lung Research Bad Nauheim sequencing facility.

The raw ChIP-seq data in FASTQ format were processed by Dr. Cornelia Kilchert following standard quality control (QC) procedures. Initial steps included trimming of adapter sequences and filtering out low-quality reads using tools as mentioned in section 9.6.1. ChIP-seq data were aligned with BowTie2 (Langmead & Salzberg, 2012), ensuring optimal mapping of reads to the genome. After alignment, the resulting BAM files were used for downstream analyses. Genomic ranges for metagene plots and heatmaps were selected using the packages rtracklayer and GenomicAlignments in R, and metagenes generated with the metagene2 package without normalisation before geometric scaling (Fournier, E., Joly Beauparlant, C., Lippens, C. & Droit, A., 2022, metagene2: A package to produce metagene plots. R package version 1.14.0, Lawrence et al., 2009, 2013). GO term annotations were retrieved using biomaRt

(Durinck et al., 2009). Plots were generated with the ggplot2 package in R (Wickham, H. Ggplot2: Elegant Graphics for Data Analysis, Springer-Verlag New York, 2016).

9.6.3 Visualisation of aligned reads

The web application version of “Integrative Genomics Viewer” (IGV-Web) was used to visualise aligned reads for any bedgraph dataset (Robinson et al., 2011, 2017, 2023; Thorvaldsdóttir et al., 2013).

9.6.4 Liquid chromatography-mass spectrometry (LC-MS)

Liquid chromatography-coupled mass spectrometry analysis from mild crosslinking protein purifications of Dbp2-HTP and Srp2-HTP were performed by Dr. Timo Glatter, Mass Spectrometry and Proteomics facility at the Max Planck Institute for Terrestrial Microbiology, Marburg, Germany. Experimental details are available in Aydin et al., 2024.

9.6.5 Protein computational analysis

A disorder prediction of the full-length Dbp2 protein was performed using the Disorder Prediction MetaServer (DisMeta) (Y. J. Huang et al., 2014). The Dismeta server defines consensus disorder prediction results of a given protein, and any disorder consensus above 0.5 as an indicator for disorder, which is exhibited by dashed line in the plot. The uniprot primary accession number for *S. pombe* Dbp2 as “P24782” was used for the DisMeta analysis. The boundaries of two helicase core domains with the hinge region in between, being used here is as annotated in uniprot P24782 accession number.

The predicted alignment error (PAE) matrices were generated by AlphaFold 3 to provide estimates of the relative positional errors between aligned amino acids across the sequences of the respective orthologues (Abramson et al., 2024).

9.6.6 Data availability

Raw (fastq) and processed (bedgraph) sequencing data can be downloaded from EBI ArrayExpress with the accession numbers E-MTAB-13712, E-MTAB-13714 and E-MTAB-13717. The mass spectrometry proteomics data have been deposited to the ProteomeXchange Consortium via the PRIDE (Deutsch et al., 2023) partner repository with the dataset identifier PXD048560.

Chapter10 Appendix

APPENDIX 1

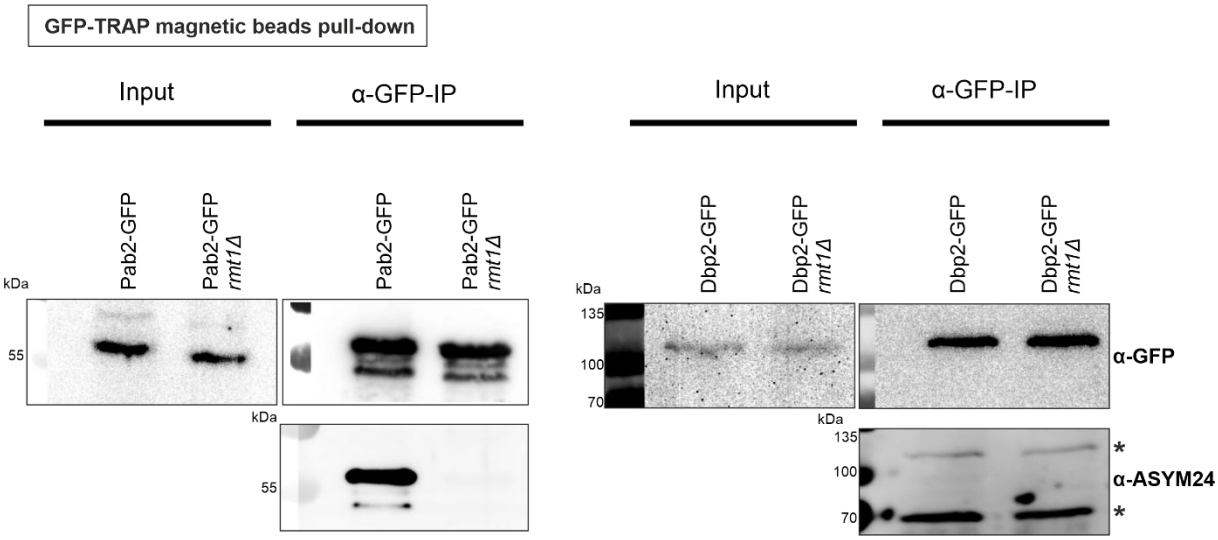

Appendix 1 | Dbp2 is still asymmetrically dimethylated in the absence of Rmt1

Inputs and eluates from Co-IP experiments using GFP-Trap beads were prepared from strains expressing either Pab2-GFP, Pab2-GFP *rmt1Δ*, Dbp2-GFP, or Dbp2-GFP *rmt1Δ*. On left panel Pab2-GFP and Pab2-GFP *rmt1Δ* was used as control, for the reconstitution of already published result of Pab2 being solely asymmetrically dimethylated by Rmt1. On right panel is Dbp2-GFP pull-down in the presence and absence of Rmt1. Samples were resolved on SDS-PAGE and analysed by WB using antibodies against α-GFP and α-ASYM24. Upper and lower asterisks appeared with α-ASYM24 antibody, where the upper band is at the height of pulled down Dbp2-GFP, and the lower band likely corresponds to a form of asymmetrically dimethylated Dbp2. The image is representative of two independent experiments, (n=2).

APPENDIX 2

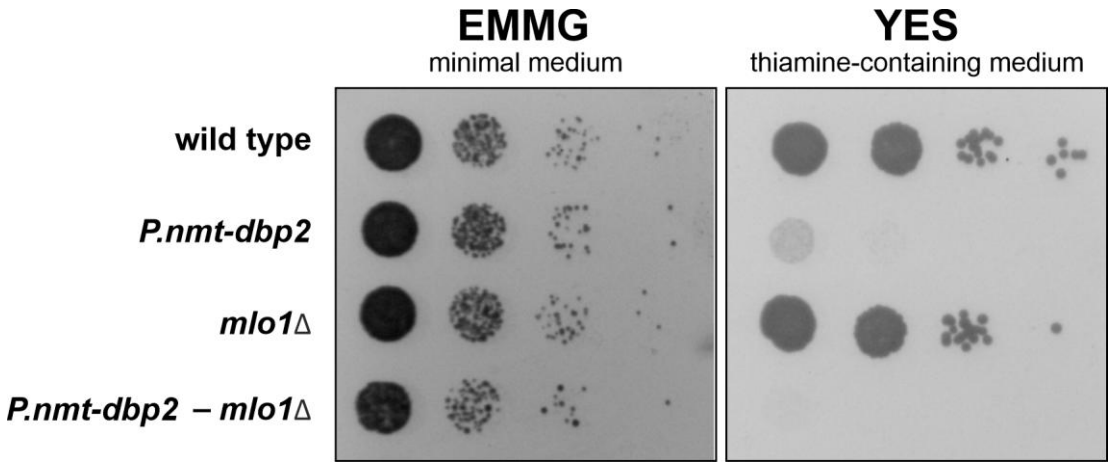

Appendix 2 | Mlo1 becomes synthetical lethal with Dbp2 depletion

Plate-based cell-growth assay of wild type, *P.nmt-dbp2, mlo1*Δ, or *P.nmt-dbp2 mlo1*Δ double mutant. The growth phenotype of *P.nmt-dbp2* mutant cells in thiamine-containing media (YES) is exacerbated upon deletion of the *mlo1* gene in *S. pombe*. The indicated strains were cultured overnight in EMMG, serially diluted (1:10), and spotted onto EMMG or YES plates, followed by incubation at 30 °C for 2-3 days. The image represents data from two independent experiments, (n = 2).

Mlo1 homologues (*S. cerevisiae* Tho1, *H. sapiens* SARNP/CIP29 and MOS11 in *A. thaliana*.) are implicated in poly(A)+ RNA export pathway. Mlo1 is not required for cell viability in *S. pombe,* its genomic deletion alone does not lead to any growth defect on cell-growth assay. *P.nmt-dbp2* is a thiamine-repressible promoter exchange of *dbp2*, in the presence of thiamine *dbp2* transcription is repressed. Combining *mlo1*Δ with *P.nmt-dbp2* results in synthetic lethality for *mlo1*, implicating the essential role of Dbp2 for Mlo1 functions, possibly related to RNA export.

APPENDIX 3

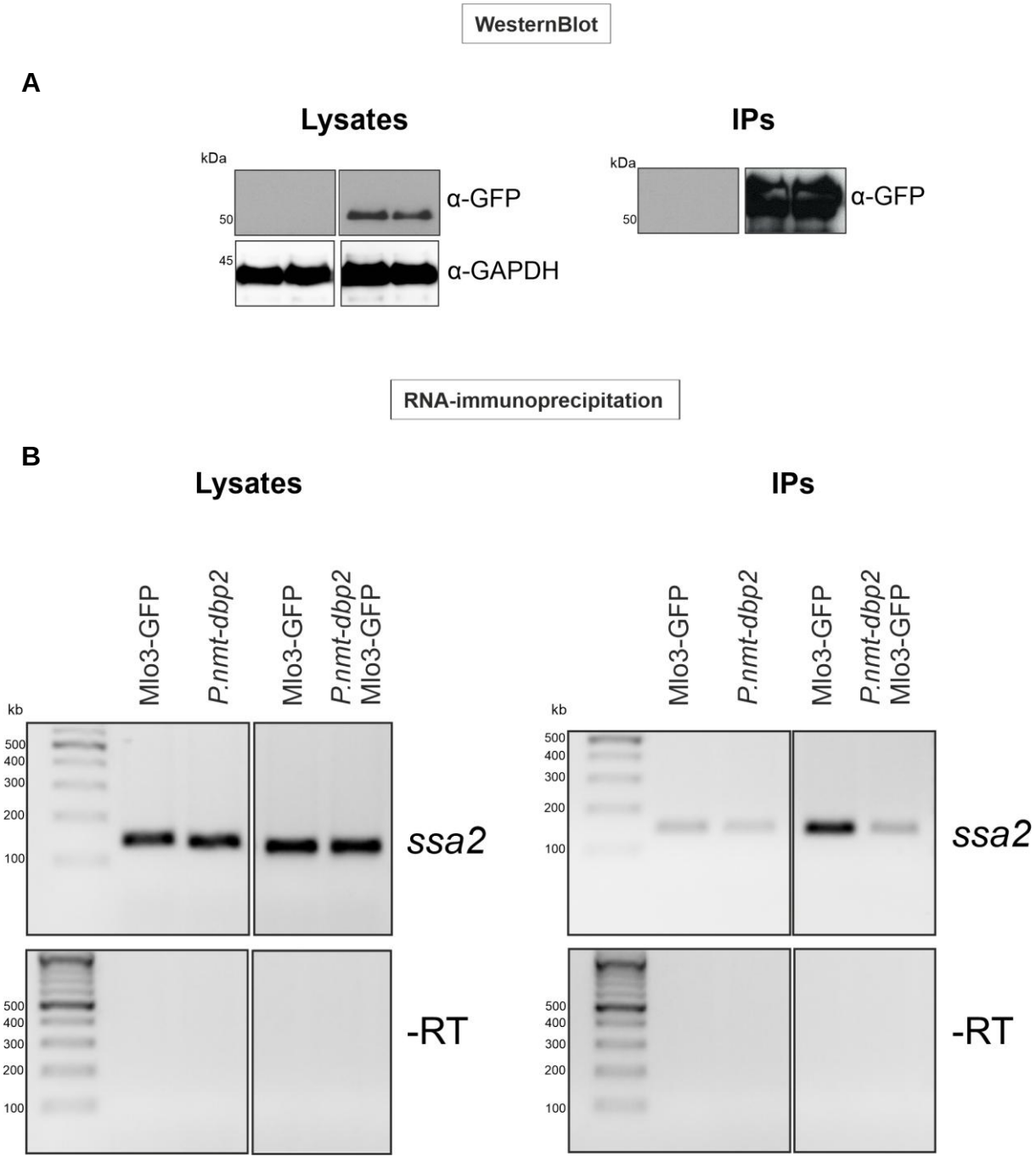

Appendix 3 | Export adaptor Mlo3 is insufficiently recruited on mRNAs upon loss of Dbp2

A. Western blot analysis of lysates and immunoprecipitated (IP) samples from Mlo3-GFP and Mlo3-GFP *P.nmt-dbp2*. Cells were grown in EMMG overnight and shifted to YES medium for 5 h at 30 °C. IP was performed using GFP-TRAP magnetic beads and bound fractions were probed with GFP antibody. GAPDH was used as a loading control. **B.** Analysis of Mlo3 recruitment on poly(A)+ RNAs by RIP. For reverse-transcription (RT) reaction oligo-d(T) primer was used. 1 µg of lysate and 2 µl of IP of RT RNA volumes were used to generate cDNA. cDNA was prepared from gene specific primers, for *ssa2* transcript using RT-PCR. 2 µl of RT was used for RT-PCR reactions. RT-PCR cycles run at 53 °C set as the annealing temperature for total of 26 cycles. 10 µl from cDNA was loaded into 2% agarose gel. For minus reverse transcription (-RT) samples, reactions were run without the use of reverse transcriptase, (n = 1).

Chapter11 References

Abramson, J., Adler, J., Dunger, J., Evans, R., Green, T., Pritzel, A., Ronneberger, O., Willmore, L., Ballard, A. J., Bambrick, J., Bodenstein, S. W., Evans, D. A., Hung, C. C., O'Neill, M., Reiman, D., Tunyasuvunakool, K., Wu, Z., Žemgulytė, A., Arvaniti, E., … Jumper, J. M. (2024). Accurate structure prediction of biomolecular interactions with AlphaFold 3. *Nature*, *630*(8016), 493–500. https://doi.org/10.1038/s41586-024-07487-w

Ahn, S. H., Kim, M., & Buratowski, S. (2004). Phosphorylation of Serine 2 within the RNA Polymerase II C-Terminal Domain Couples Transcription and 3′ End Processing. *Molecular Cell*, *13*(1), 67–76. https://doi.org/10.1016/S1097-2765(03)00492-1

Akhtar, M. S., Heidemann, M., Tietjen, J. R., Zhang, D. W., Chapman, R. D., Eick, D., & Ansari, A. Z. (2009). TFIIH Kinase Places Bivalent Marks on the Carboxy-Terminal Domain of RNA Polymerase II. *Molecular Cell*, *34*(3), 387–393. https://doi.org/10.1016/j.molcel.2009.04.016

Albulescu, L. O., Sabet, N., Gudipati, M., Stepankiw, N., Bergman, Z. J., Huffaker, T. C., & Pleiss, J. A. (2012). A quantitative, high-throughput reverse genetic screen reveals novel connections between pre-mRNA splicing and 5′ and 3′ end transcript determinants. *PLoS Genetics*, *8*(3). https://doi.org/10.1371/journal.pgen.1002530

Alcázar-Román, A. R., Tran, E. J., Guo, S., & Wente, S. R. (2006). Inositol hexakisphosphate and Gle1 activate the DEAD-box protein Dbp5 for nuclear mRNA export. *Nature Cell Biology*, *8*(7), 711–716. https://doi.org/10.1038/ncb1427

Ali, M. A. M. (2021). DEAD-box RNA helicases: The driving forces behind RNA metabolism at the crossroad of viral replication and antiviral innate immunity. *Virus Research*, *296*(February). https://doi.org/10.1016/j.virusres.2021.198352

Allen, B. L., & Taatjes, D. J. (2015). The Mediator complex: A central integrator of transcription. *Nature Reviews Molecular Cell Biology*, *16*(3), 155–166. https://doi.org/10.1038/nrm3951

Allshire, R. C., & Ekwall, K. (2015). Epigenetic regulation of chromatin states in *Schizosaccharomyces pombe*. *Cold Spring Harbor Perspectives in Biology*, *7*(7), 1–25. https://doi.org/10.1101/cshperspect.a018770

Allshire, R. C., Nimmo, E. R., Ekwall, K., Javerzat, J. P., & Cranston, G. (1995). Mutations derepressing silent centromeric domains in fission yeast disrupt chromosome segregation. *Genes and Development*, *9*(2), 218–233. https://doi.org/10.1101/gad.9.2.218

Amberg, D. C., Goldstein, A. L., & Cole, C. N. (1992). Isolation and characterization of RAT1: An essential gene of *Saccharomyces cerevisiae* required for the efficient nucleocytoplasmic trafficking of mRNA. *Genes and Development*, *6*(7), 1173–1189. https://doi.org/10.1101/gad.6.7.1173

Anders, S., Pyl, P. T., & Huber, W. (2015). HTSeq-A Python framework to work with high-throughput sequencing data. *Bioinformatics*, *31*(2), 166–169. https://doi.org/10.1093/bioinformatics/btu638

Andersen, C. B. F., Ballut, L., Johansen, J. S., Chamieh, H., Nielsen, K. H., Oliveira, C. L. P., Pedersen, J. S., Séraphin, B., Hir, H. Le, & Andersen, G. R. (2006). Structure of the exon junction core complex with a trapped DEAD-Box ATPase bound to RNA. *Science*, *313*(5795), 1968–1972. https://doi.org/10.1126/science.1131981

Andreou, A. Z., & Klostermeier, D. (2012). Conformational changes of DEAD-Box helicases monitored by single molecule fluorescence resonance energy transfer. In *Methods in Enzymology* (1st ed., Vol. 511). Elsevier Inc. https://doi.org/10.1016/B978-0-12-396546-2.00004-8

Arigo, J. T., Carroll, K. L., Ames, J. M., & Corden, J. L. (2006). Regulation of yeast NRD1 expression by premature transcription termination. *Molecular Cell*, *21*(5), 641–651. https://doi.org/10.1016/j.molcel.2006.02.005

Arigo, J. T., Eyler, D. E., Carroll, K. L., & Corden, J. L. (2006). Termination of Cryptic Unstable Transcripts Is Directed by Yeast RNA-Binding Proteins Nrd1 and Nab3. *Molecular Cell*, *23*(6), 841–851. https://doi.org/10.1016/j.molcel.2006.07.024

Ast, G. (2004). How did alternative splicing evolve? *Nature Reviews Genetics*, *5*(10), 773–782. https://doi.org/10.1038/nrg1451

Atkinson, S. R., Marguerat, S., Bitton, D. A., Rodríguez-López, M., Rallis, C., Lemay, J. F., Cotobal, C., Malecki, M., Smialowski, P., Mata, J., Korber, P., Bachand, F., & Bähler, J. (2018). Long noncoding RNA repertoire and targeting by nuclear exosome, cytoplasmic exonuclease, and RNAi in fission yeast. *Rna*, *24*(9), 1195–1213. https://doi.org/10.1261/rna.065524.118

Bähler, J., Wu, J., Longtine, M. S., Shah, N. G., Mckenzie III, A., Steever, A. B., Wach, A., Philippsen, P., & Pringle, J. R. (1998). Heterologous modules for efficient and versatile PCR-based gene targeting in *Schizosaccharomyces pombe*. *Yeast*, *14*(10), 943–951. https://doi.org/10.1002/(sici)1097-0061(199807)14:10<943::aid-yea292>3.3.co;2-p

Baillat, D., Hakimi, M. A., Näär, A. M., Shilatifard, A., Cooch, N., & Shiekhattar, R. (2005). Integrator, a multiprotein mediator of small nuclear RNA processing, associates with the C-terminal repeat of RNA polymerase II. *Cell*, *123*(2), 265–276. https://doi.org/10.1016/j.cell.2005.08.019

Ballut, L., Marchadier, B., Baguet, A., Tomasetto, C., Séraphin, B., & Le Hir, H. (2005). The exon junction core complex is locked onto RNA by inhibition of eIF4AIII ATPase activity. *Nature Structural and Molecular Biology*, *12*(10), 861–869. https://doi.org/10.1038/nsmb990

Banani, S. F., Lee, H. O., Hyman, A. A., & Rosen, M. K. (2017). Biomolecular condensates: Organizers of cellular biochemistry. *Nature Reviews Molecular Cell Biology*, *18*(5), 285–298. https://doi.org/10.1038/nrm.2017.7

Bannerman, B. P., Kramer, S., Dorrell, R. G., & Carrington, M. (2018). Multispecies reconstructions uncover widespread conservation, and lineage-specific elaborations in eukaryotic mRNA metabolism. *PLoS ONE*, *13*(3), 1–23. https://doi.org/10.1371/journal.pone.0192633

Banroques, J., Cordin, O., Doère, M., Linder, P., & Tanner, N. K. (2008). A Conserved Phenylalanine of Motif IV in Superfamily 2 Helicases Is Required for Cooperative,

ATP-Dependent Binding of RNA Substrates in DEAD-Box Proteins. *Molecular and Cellular Biology*, *28*(10), 3359–3371. https://doi.org/10.1128/mcb.01555-07

Banroques, J., Cordin, O., Doère, M., Linder, P., & Tanner, N. K. (2011). Analyses of the functional regions of DEAD-box RNA "helicases" with deletion and chimera constructs tested in vivo and in vitro. *Journal of Molecular Biology*, *413*(2), 451–472. https://doi.org/10.1016/j.jmb.2011.08.032

Barillà, D., Lee, B. A., & Proudfoot, N. J. (2001). Cleavage/polyadenylation factor IA associates with the carboxyl-terminal domain of RNA polymerase II in *Saccharomyces cerevisiae*. *Proceedings of the National Academy of Sciences*, *98*(2), 445–450. https://doi.org/10.1073/pnas.98.2.445

Barnwal, R. P., Lee, S. D., Moore, C., & Varani, G. (2012). Structural and biochemical analysis of the assembly and function of the yeast pre-mRNA 3′ end processing complex CF I. *Proceedings of the National Academy of Sciences of the United States of America*, *109*(52), 21342–21347. https://doi.org/10.1073/pnas.1214102110

Barrales, R. R., Forn, M., Georgescu, P. R., Sarkadi, Z., & Braun, S. (2016). Control of heterochromatin localization and silencing by the nuclear membrane protein Lem2. *Genes and Development*, *30*(2), 133–148. https://doi.org/10.1101/gad.271288.115

Belotserkovskaya, R., Oh, S., Bondarenko, V. A., Orphanides, G., Studitsky, V. M., & Reinberg, D. (2003). FACT facilitates transcription-dependent nucleosome alteration. *Science*, *301*(5636), 1090–1093. https://doi.org/10.1126/science.1085703

Ben-Yishay, R., Mor, A., Shraga, A., Ashkenazy-Titelman, A., Kinor, N., Schwed-Gross, A., Jacob, A., Kozer, N., Kumar, P., Garini, Y., & Shav-Tal, Y. (2019). Imaging within single NPCs reveals NXF1's role in mRNA export on the cytoplasmic side of the pore. *Journal of Cell Biology*, *218*(9), 2962–2981. https://doi.org/10.1083/JCB.201901127

Bentley, D. L. (2014). Coupling mRNA processing with transcription in time and space. *Nature Reviews Genetics*, *15*(3), 163–175. https://doi.org/10.1038/nrg3662

Berg, M. G., Singh, L. N., Younis, I., Liu, Q., Pinto, A. M., Kaida, D., Zhang, Z., Cho, S., Sherrill-Mix, S., Wan, L., & Dreyfuss, G. (2012). U1 snRNP determines mRNA length and regulates isoform expression. *Cell*, *150*(1), 53–64. https://doi.org/10.1016/j.cell.2012.05.029

Bhattacharjee, S., Roche, B., & Martienssen, R. A. (2019). RNA-induced initiation of transcriptional silencing (RITS) complex structure and function. *RNA Biology*, *16*(9), 1133–1146. https://doi.org/10.1080/15476286.2019.1621624

Bienroth, S., Wahle, E., Suter-Crazzolara, C., & Keller, W. (1991). Purification of the cleavage and polyadenylation factor involved in the 3′-processing of messenger RNA precursors. *Journal of Biological Chemistry*, *266*(29), 19768–19776. https://doi.org/10.1016/s0021-9258(18)55058-4

Bird, G., Zorio, D. A. R., & Bentley, D. L. (2004). RNA Polymerase II Carboxy-Terminal Domain Phosphorylation Is Required for Cotranscriptional Pre-mRNA Splicing and 3'-End Formation. *Molecular and Cellular Biology*, *24*(20), 8963–8969.

https://doi.org/10.1128/mcb.24.20.8963-8969.2004

Bird, Gregory, Zorio, D. A. R., & Bentley, D. L. (2004). RNA Polymerase II Carboxy-Terminal Domain Phosphorylation Is Required for Cotranscriptional Pre-mRNA Splicing and 3′-End Formation. *Molecular and Cellular Biology*, *24*(20), 8963–8969. https://doi.org/10.1128/mcb.24.20.8963-8969.2004

Bird, L. E. (2011). High throughput construction and small scale expression screening of multi-tag vectors in *Escherichia coli. Methods*, *55*(1), 29–37. https://doi.org/10.1016/j.ymeth.2011.08.002

Birot, A., Kus, K., Priest, E., Al Alwash, A., Castello, A., Mohammed, S., Vasiljeva, L., & Kilchert, C. (2022). RNA-binding protein Mub1 and the nuclear RNA exosome act to fine-tune environmental stress response. *Life Science Alliance*, *5*(2), 1–15. https://doi.org/10.26508/lsa.202101111

Birse, C. E., Minvielle-Sebastia, L., Lee, B. A., Keller, W., & Proudfoot, N. J. (1998). Coupling termination of transcription to messenger RNA maturation in yeast. *Science*, *280*(5361), 298–301. https://doi.org/10.1126/science.280.5361.298

Blanc, Roméo S., & Richard, S. (2017). Arginine Methylation: The Coming of Age. *Molecular Cell*, *65*(1), 8–24. https://doi.org/10.1016/j.molcel.2016.11.003

Blanc, Roméo Sébastien, Vogel, G., Li, X., Yu, Z., Li, S., & Richard, S. (2017). Arginine Methylation by PRMT1 Regulates Muscle Stem Cell Fate. *Molecular and Cellular Biology*, *37*(3). https://doi.org/10.1128/mcb.00457-16

Blum, S., Schmid, S. R., Pause, A., Buser, P., Linder, P., Sonenberg, N., & Trachsel, H. (1992). ATP hydrolysis by initiation factor 4A is required for translation initiation in *Saccharomyces cerevisiae*. *Proceedings of the National Academy of Sciences of the United States of America*, *89*(16), 7664–7668. https://doi.org/10.1073/pnas.89.16.7664

Bohnsack, K. E., Yi, S., Venus, S., Jankowsky, E., & Bohnsack, M. T. (2023). Cellular functions of eukaryotic RNA helicases and their links to human diseases. *Nature Reviews Molecular Cell Biology*, *24*(October), 749–769. https://doi.org/10.1038/s41580-023-00628-5

Boireau, S., Maiuri, P., Basyuk, E., De La Mata, M., Knezevich, A., Pradet-Balade, B., Bäcker, V., Kornblihtt, A., Marcello, A., & Bertrand, E. (2007). The transcriptional cycle of HIV-1 in real-time and live cells. *Journal of Cell Biology*, *179*(2), 291–304. https://doi.org/10.1083/jcb.200706018

Boisramé, A., Devillers, H., Onésime, D., Brunel, F., Pouch, J., Piot, M., & Neuvéglise, C. (2019). Exon junction complex components Y14 and Mago still play a role in budding yeast. *Scientific Reports*, *9*(1), 1–18. https://doi.org/10.1038/s41598-018-36785-3

Bolger, A. M., Lohse, M., & Usadel, B. (2014). Trimmomatic: A flexible trimmer for Illumina sequence data. *Bioinformatics*, *30*(15), 2114–2120. https://doi.org/10.1093/bioinformatics/btu170

Bonaventure, B., & Goujon, C. (2022). DExH/D-box helicases at the frontline of intrinsic and innate immunity against viral infections. *Journal of General Virology*, *103*(8), 1–19. https://doi.org/10.1099/jgv.0.001766

Bono, F., Ebert, J., Lorentzen, E., & Conti, E. (2006). The Crystal Structure of the Exon Junction Complex Reveals How It Maintains a Stable Grip on mRNA. *Cell*, *126*(4), 713–725. https://doi.org/10.1016/j.cell.2006.08.006

Boreikaitė, V., & Passmore, L. A. (2023). 3′-End Processing of Eukaryotic mRNA: Machinery, Regulation, and Impact on Gene Expression. *Annual Review of Biochemistry*, *92*, 199–225. https://doi.org/10.1146/annurev-biochem-052521-012445

Boulanger, C., Haidara, N., Yague-Sanz, C., Larochelle, M., Jacques, P. É., Hermand, D., & Bachand, F. (2024). Repression of pervasive antisense transcription is the primary role of fission yeast RNA polymerase II CTD serine 2 phosphorylation. *Nucleic Acids Research*, *52*(13), 7572–7589. https://doi.org/10.1093/nar/gkae436

Bourgeois, C. F., Mortreux, F., & Auboeuf, D. (2016). The multiple functions of RNA helicases as drivers and regulators of gene expression. *Nature Reviews Molecular Cell Biology*, *17*(7), 426–438. https://doi.org/10.1038/nrm.2016.50

Bowers, H. A., Maroney, P. A., Fairman, M. E., Kastner, B., Lührmann, R., Nilsen, T. W., & Jankowsky, E. (2006). Discriminatory RNP remodeling by the DEAD-box protein DED1. *Rna*, *12*(5), 903–912. https://doi.org/10.1261/rna.2323406

Bowman, E. A., & Kelly, W. G. (2014). *Nucl-5-224*. *5*(3), 224–236.

Bresson, S. M., & Conrad, N. K. (2013). The Human Nuclear Poly(A)-Binding Protein Promotes RNA Hyperadenylation and Decay. *PLoS Genetics*, *9*(10). https://doi.org/10.1371/journal.pgen.1003893

Bresson, S. M., Hunter, O. V., Hunter, A. C., & Conrad, N. K. (2015). Canonical Poly(A) Polymerase Activity Promotes the Decay of a Wide Variety of Mammalian Nuclear RNAs. *PLoS Genetics*, *11*(10), 1–25. https://doi.org/10.1371/journal.pgen.1005610

Brian K. Kay, Michael P. Williamson, and M. S. (2000). *The importance of being proline: the interaction of proline-rich motifs in signaling proteins with their cognate domains* (pp. 231–241). The FASEB Journal. https://doi.org/10.1096/fasebj.14.2.231

Briggs, S. D., Bryk, M., Strahl, B. D., Cheung, W. L., Davie, J. K., Dent, S. Y. R., Winston, F., & David Allis, C. (2001). Histone H3 lysine 4 methylation is mediated by Set1 and required for cell growth and rDNA silencing in *Saccharomyces cerevisiae*. *Genes and Development*, *15*(24), 3286–3295. https://doi.org/10.1101/gad.940201

Buratowski, S. (2009). Progression through the RNA Polymerase II CTD Cycle. *Molecular Cell*, *36*(4), 541–546. https://doi.org/10.1016/j.molcel.2009.10.019

Cáceres, J. F., & Kornblihtt, A. R. (2002). Alternative splicing: Multiple control mechanisms and involvement in human disease. *Trends in Genetics*, *18*(4), 186–193. https://doi.org/10.1016/S0168-9525(01)02626-9

Cairns, B. R., Lorch, Y., Li, Y., Zhang, M., Lacomis, L., Erdjument-Bromage, H., Tempst, P., Du, J., Laurent, B., & Kornberg, R. D. (1996). RSC, an essential, abundant chromatin-remodeling complex. *Cell*, *87*(7), 1249–1260. https://doi.org/10.1016/S0092-8674(00)81820-6

Caretti, G., Lei, E. P., & Sartorelli, V. (2007). The DEAD-box p68/p72 proteins and the noncoding RNA steroid receptor activator SRA: Eclectic regulators of disparate biological functions. *Cell Cycle*, *6*(10), 1172–1176. https://doi.org/10.4161/cc.6.10.4228

Chen, H. M., Futcher, B., & Leatherwood, J. (2011). The fission yeast rna binding protein mmi1 regulates meiotic genes by controlling intron specific splicing and polyadenylation coupled rna turnover. *PLoS ONE*, *6*(10). https://doi.org/10.1371/journal.pone.0026804

Chen, J., & Moore, C. (1992). Separation of Factors Required for Cleavage and Polyadenylation of Yeast Pre-mRNA. *Molecular and Cellular Biology*, *12*(8), 3470–3481. https://doi.org/10.1128/mcb.12.8.3470-3481.1992

Chen, J. Y. F., Stands, L., Staley, J. P., Jackups, R. R., Latus, L. J., & Chang, T. H. (2001). Specific alterations of U1-C protein or U1 Small nuclear RNA can eliminate the requirement of Prp28p, an essential DEAD Box splicing factor. *Molecular Cell*, *7*(1), 227–232. https://doi.org/10.1016/S1097-2765(01)00170-8

Chen, Y., Potratz, J. P., Tijerina, P., Del Campo, M., Lambowitz, A. M., & Russell, R. (2008). DEAD-box proteins can completely separate an RNA duplex using a single ATP. *Proceedings of the National Academy of Sciences of the United States of America*, *105*(51), 20203–20208. https://doi.org/10.1073/pnas.0811075106

Cheng, H., Dufu, K., Lee, C. S., Hsu, J. L., Dias, A., & Reed, R. (2006). Human mRNA Export Machinery Recruited to the 5′ End of mRNA. In *Cell* (Vol. 127, Issue 7, pp. 1389–1400). https://doi.org/10.1016/j.cell.2006.10.044

Cheng, Z., Coller, J., Parker, R., & Song, H. (2005). Crystal structure and functional analysis of DEAD-box protein Dhh1p. *Rna*, *11*(8), 1258–1270. https://doi.org/10.1261/rna.2920905

Cho, E. J., Kobor, M. S., Kim, M., Greenblatt, J., & Buratowski, S. (2001). Opposing effects of Ctk1 kinase and Fcp1 phosphatase at Ser 2 of the RNA polymerase II C-terminal domain. *Genes and Development*, *15*(24), 3319–3329. https://doi.org/10.1101/gad.935901

Choi, Y., Um, B., Na, Y., Kim, J., Kim, J. S., & Kim, V. N. (2024). Time-resolved profiling of RNA binding proteins throughout the mRNA life cycle. *Molecular Cell*, *84*(9), 1764-1782.e10. https://doi.org/10.1016/j.molcel.2024.03.012

Chong, P. A., Vernon, R. M., & Forman-Kay, J. D. (2018). RGG/RG Motif Regions in RNA Binding and Phase Separation. *Journal of Molecular Biology*, *430*(23), 4650–4665. https://doi.org/10.1016/j.jmb.2018.06.014

Clague, M. J., Urbé, S., & Komander, D. (2019). Breaking the chains: deubiquitylating enzyme specificity begets function. *Nature Reviews Molecular Cell Biology*, *20*(6), 338–352. https://doi.org/10.1038/s41580-019-0099-1

Clapier, C. R., & Cairns, B. R. (2009). The biology of chromatin remodeling complexes. *Annual Review of Biochemistry*, *78*, 273–304. https://doi.org/10.1146/annurev.biochem.77.062706.153223

Clark, E. L., Coulson, A., Dalgliesh, C., Rajan, P., Nicol, S. M., Fleming, S., Heer, R., Gaughan, L., Leung, H. Y., Elliott, D. J., Fuller-Pace, F. V., & Robson, C. N. (2008). The RNA helicase p68 is a novel androgen receptor coactivator involved in

splicing and is overexpressed in prostate cancer. *Cancer Research*, *68*(19), 7938–7946. https://doi.org/10.1158/0008-5472.CAN-08-0932

Cloutier, S. C., Ma, W. K., Nguyen, L. T., & Tran, E. J. (2012). The DEAD-box RNA helicase Dbp2 connects RNA quality control with repression of aberrant transcription. *Journal of Biological Chemistry*, *287*(31), 26155–26166. https://doi.org/10.1074/jbc.M112.383075

Cloutier, S. C., Wang, S., Ma, W. K., Al Husini, N., Dhoondia, Z., Ansari, A., Pascuzzi, P. E., & Tran, E. J. (2016). Regulated Formation of lncRNA-DNA Hybrids Enables Faster Transcriptional Induction and Environmental Adaptation. *Molecular Cell*, *61*(3), 393–404. https://doi.org/10.1016/j.molcel.2015.12.024

Cloutier, S. C., Wang, S., Ma, W. K., Petell, C. J., & Tran, E. J. (2013). Long Noncoding RNAs Promote Transcriptional Poising of Inducible Genes. *PLoS Biology*, *11*(11), 32–34. https://doi.org/10.1371/journal.pbio.1001715

Coban, I., Lamping, J. P., Hirsch, A. G., Wasilewski, S., Shomroni, O., Giesbrecht, O., Salinas, G., & Krebber, H. (2024). dsRNA formation leads to preferential nuclear export and gene expression. *Nature*, *631*(8020), 432–438. https://doi.org/10.1038/s41586-024-07576-w

Connelly, S., & Manley, J. L. (1988). A functional mRNA polyadenylation signal is required for transcription termination by RNA polymerase II. *Genes & Development*, *2*(4), 440–452. https://doi.org/10.1101/gad.2.4.440

Corden, J. L. (1990). Tails of RNA polymerase II. *Trends in Biochemical Sciences*, *15*(10), 383–387. https://doi.org/10.1016/0968-0004(90)90236-5

Corden, J. L. (2016). Pol II CTD Code Light. *Molecular Cell*, *61*(2), 183–184. https://doi.org/10.1016/j.molcel.2016.01.005

Cordin, O., Banroques, J., Tanner, N. K., & Linder, P. (2006). The DEAD-box protein family of RNA helicases. *Gene*, *367*(1–2), 17–37. https://doi.org/10.1016/j.gene.2005.10.019

Cordin, O., Hahn, D., & Beggs, J. D. (2012). Structure, function and regulation of spliceosomal RNA helicases. *Current Opinion in Cell Biology*, *24*(3), 431–438. https://doi.org/10.1016/j.ceb.2012.03.004

Cortazar, M. A., Sheridan, R. M., Erickson, B., Fong, N., Glover-Cutter, K., Brannan, K., & Bentley, D. L. (2019). Control of RNA Pol II Speed by PNUTS-PP1 and Spt5 Dephosphorylation Facilitates Termination by a "Sitting Duck Torpedo" Mechanism. *Molecular Cell*, *76*(6), 896-908.e4. https://doi.org/10.1016/j.molcel.2019.09.031

Creamer, K. M., & Partridge, J. F. (2011). RITS-connecting transcription, RNA interference, and heterochromatin assembly in fission yeast. *Wiley Interdisciplinary Reviews: RNA*, *2*(5), 632–646. https://doi.org/10.1002/wrna.80

Custódio, N., Carmo-Fonseca, M., Geraghty, F., Pereira, H. S., Grosveld, F., & Antoniou, M. (1999). Inefficient processing impairs release of RNA from the site of transcription. *EMBO Journal*, *18*(10), 2855–2866. https://doi.org/10.1093/emboj/18.10.2855

Custódio, N., Vivo, M., Antoniou, M., & Carmo-Fonseca, M. (2007). Splicing- and

cleavage-independent requirement of RNA polymerase II CTD for mRNA release from the transcription site. *Journal of Cell Biology*, *179*(2), 199–207. https://doi.org/10.1083/jcb.200612109

Dardenne, E., PolayEspinoza, M., Fattet, L., Germann, S., Lambert, M. P., Neil, H., Zonta, E., Mortada, H., Gratadou, L., Deygas, M., Chakrama, F. Z., Samaan, S., Desmet, F. O., Tranchevent, L. C., Dutertre, M., Rimokh, R., Bourgeois, C. F., & Auboeuf, D. (2014). RNA Helicases DDX5 and DDX17 Dynamically Orchestrate Transcription, miRNA, and Splicing Programs in Cell Differentiation. *Cell Reports*, *7*(6), 1900–1913. https://doi.org/10.1016/j.celrep.2014.05.010

Darnell, J. E. (1982). Variety in the level of gene control in eukaryotic cells. *Nature*, *297*(5865), 365–371. https://doi.org/10.1038/297365a0

Dattilo, D., Di Timoteo, G., Setti, A., Giuliani, A., Peruzzi, G., Beltran Nebot, M., Centrón-Broco, A., Mariani, D., Mozzetta, C., & Bozzoni, I. (2023). The m6A reader YTHDC1 and the RNA helicase DDX5 control the production of rhabdomyosarcoma-enriched circRNAs. *Nature Communications*, *14*(1). https://doi.org/10.1038/s41467-023-37578-7

Daugeron, M. C., & Linder, P. (1998). Dbp7p, a putative ATP-dependent RNA helicase from *Saccharomyces cerevisiae*, is required for 60S ribosomal subunit assembly. *Rna*, *4*(5), 566–581. https://doi.org/10.1017/S1355838298980190

Davidson, L., Muniz, L., & West, S. (2014). 3' end formation of pre-mRNA and phosphorylation of Ser2 on the RNA polymerase II CTD are reciprocally coupled in human cells. *Genes and Development*, *28*(4), 342–356. https://doi.org/10.1101/gad.231274.113

De Bortoli, F., Espinosa, S., & Zhao, R. (2021). DEAH-Box RNA Helicases in Pre-mRNA Splicing. *Trends in Biochemical Sciences*, *46*(3), 225–238. https://doi.org/10.1016/j.tibs.2020.10.006

Demin, A. A., Hirota, K., Tsuda, M., Adamowicz, M., Hailstone, R., Brazina, J., Gittens, W., Kalasova, I., Shao, Z., Zha, S., Sasanuma, H., Hanzlikova, H., Takeda, S., & Caldecott, K. W. (2021). XRCC1 prevents toxic PARP1 trapping during DNA base excision repair. *Molecular Cell*, *81*(14), 3018-3030.e5. https://doi.org/10.1016/j.molcel.2021.05.009

Derrer, C. P., Mancini, R., Vallotton, P., Huet, S., Weis, K., & Dultz, E. (2019). The RNA export factor Mex67 functions as a mobile nucleoporin. *Journal of Cell Biology*, *218*(12), 3967–3976. https://doi.org/10.1083/JCB.201909028

Deutsch, E. W., Bandeira, N., Perez-Riverol, Y., Sharma, V., Carver, J. J., Mendoza, L., Kundu, D. J., Wang, S., Bandla, C., Kamatchinathan, S., Hewapathirana, S., Pullman, B. S., Wertz, J., Sun, Z., Kawano, S., Okuda, S., Watanabe, Y., Maclean, B., Maccoss, M. J., … Vizcaíno, J. A. (2023). The ProteomeXchange consortium at 10 years: 2023 update. *Nucleic Acids Research*, *51*(D1), D1539–D1548. https://doi.org/10.1093/nar/gkac1040

Dichtl, B., & Keller, W. (2001). Recognition of polyadenylation sites in yeast pre-mRNAs by cleavage and polyadenylation factor. *EMBO Journal*, *20*(12), 3197–3209. https://doi.org/10.1093/emboj/20.12.3197

Ding, D.-Q., Okamasa, K., Yoshimura, Y., Matsuda, A., Yamamoto, T. G., Hiraoka, Y.,

Nakayama, J., & Da-Qiao Ding, C. (2023). The mechanism of homologous chromosome recognition and pairing facilitated by chromosome-tethered protein-RNA condensates. *BioRxiv*, 2023.12.24.573283. https://www.biorxiv.org/content/10.1101/2023.12.24.573283v1%0Ahttps://www.biorxiv.org/content/10.1101/2023.12.24.573283v1.abstract

Dobin, A., Davis, C. A., Schlesinger, F., Drenkow, J., Zaleski, C., Jha, S., Batut, P., Chaisson, M., & Gingeras, T. R. (2013). STAR: Ultrafast universal RNA-seq aligner. *Bioinformatics*, *29*(1), 15–21. https://doi.org/10.1093/bioinformatics/bts635

Donny D. Licatalosi, Gabrielle Geiger, M. M., Stephanie Schroeder, K. C., J. Bryan McNeil, & Bentley, and D. L. (2002). Functional Interaction of Yeast Pre-mRNA 3' End Processing Factors with RNA Polymerase II. *Molecular Cell*, *9*, 1101–1111. https://doi.org/10.1016/s1097-2765(02)00518-x

Dreyfuss, G., Matunis, M. J., Piñol-Roma, S., & Burd, C. G. (1993). hnRNP proteins and the biogenesis of mRNA. *Annual Review of Biochemistry*, *62*, 289–321. https://doi.org/10.1146/annurev.bi.62.070193.001445

Dufu, K., Livingstone, M. J., Seebacher, J., Gygi, S. P., Wilson, S. A., & Reed, R. (2010). ATP is required for interactions between UAP56 and two conserved mRNA export proteins, Aly and CIP29, to assemble the TREX complex. *Genes and Development*, *24*(18), 2043–2053. https://doi.org/10.1101/gad.1898610

Durinck, S., Spellman, P. T., Birney, E., & Huber, W. (2009). Mapping identifiers for the integration of genomic datasets with the R/ Bioconductor package biomaRt. *Nature Protocols*, *4*(8), 1184–1191. https://doi.org/10.1038/nprot.2009.97

Eberle, A. B., Hessle, V., Helbig, R., Dantoft, W., Gimber, N., & Visa, N. (2010). Splice-site mutations cause Rrp6-mediated nuclear retention of the unspliced RNAs and transcriptional down-regulation of the splicing-defective genes. *PLoS ONE*, *5*(7). https://doi.org/10.1371/journal.pone.0011540

Edgcomb, S. P., Carmel, A. B., Naji, S., Ambrus-Aikelin, G., Reyes, J. R., Saphire, A. C. S., Gerace, L., & Williamson, J. R. (2012). DDX1 is an RNA-dependent ATPase involved in HIV-1 Rev function and virus replication. *Journal of Molecular Biology*, *415*(1), 61–74. https://doi.org/10.1016/j.jmb.2011.10.032

Egan, E. D., Braun, C. R., Gygi, S. P., & Moazed, D. (2014). Post-transcriptional regulation of meiotic genes by a nuclear RNA silencing complex. *Rna*, *20*(6), 867–881. https://doi.org/10.1261/rna.044479.114

Egel, R., Beach, D. H., & Klar, A. J. S. (1984). Genes required for initiation and resolution steps of mating-type switching in fission yeast. *Proceedings of the National Academy of Sciences of the United States of America*, *81*(11 I), 3481–3485. https://doi.org/10.1073/pnas.81.11.3481

Egloff, S., Szczepaniak, S. A., Dienstbier, M., Taylor, A., Knight, S., & Murphy, S. (2010). The integrator complex recognizes a new double mark on the RNA polymerase II carboxyl-terminal domain. *Journal of Biological Chemistry*, *285*(27), 20564–20569. https://doi.org/10.1074/jbc.M110.132530

Ehara, H., Kujirai, T., Shirouzu, M., Kurumizaka, H., & Sekine, S. I. (2022). Structural basis of nucleosome disassembly and reassembly by RNAPII elongation complex

with FACT. *Science*, *377*(6611). https://doi.org/10.1126/science.abp9466

Eick, D., & Geyer, M. (2013). *The RNA Polymerase II Carboxy-Terminal Domain (CTD) Code*.

Emilia Herrera-Moyano, Xenia Mergui, Maria L. Garcia-Rubio, Sonia Barroso, and A. A. (2014). The yeast and human FACT chromatin- reorganizing complexes solve R-loop- mediated transcription – replication conflicts. *Cold Spring Harbor Laboratory Press*, 735–748. https://doi.org/10.1101/gad.234070.113.1

Ezzeddine, N., Chen, J., Waltenspiel, B., Burch, B., Albrecht, T., Zhuo, M., Warren, W. D., Marzluff, W. F., & Wagner, E. J. (2011). A Subset of Drosophila Integrator Proteins Is Essential for Efficient U7 snRNA and Spliceosomal snRNA 3′-End Formation . *Molecular and Cellular Biology*, *31*(2), 328–341. https://doi.org/10.1128/mcb.00943-10

Fabrizio, P., Dannenberg, J., Dube, P., Kastner, B., Stark, H., Urlaub, H., & Lührmann, R. (2009). The Evolutionarily Conserved Core Design of the Catalytic Activation Step of the Yeast Spliceosome. *Molecular Cell*, *36*(4), 593–608. https://doi.org/10.1016/j.molcel.2009.09.040

Fairman-Williams, M. E., Guenther, U.-P., & Jankowsky, E. (2010). SF1 and SF2 : family matters. *Current Opinion in Structural Biology*, *20*(3), 313–324. https://doi.org/10.1016/j.sbi.2010.03.011.SF1

Fan, J., Kuai, B., Wang, K., Wang, L., Wang, Y., Wu, X., Chi, B., Li, G., & Cheng, H. (2018). MRNAs are sorted for export or degradation before passing through nuclear speckles. *Nucleic Acids Research*, *46*(16), 8404–8416. https://doi.org/10.1093/nar/gky650

Fazal, F. M., Han, S., Parker, K. R., Kaewsapsak, P., Xu, J., Boettiger, A. N., Chang, H. Y., & Ting, A. Y. (2019). Atlas of Subcellular RNA Localization Revealed by APEX-Seq. *Cell*, *178*(2), 473-490.e26. https://doi.org/10.1016/j.cell.2019.05.027

Fleckner, J., Zhang, M., Valcárcel, J., & Green, M. R. (1997). U2AF65 recruits a novel human DEAD box protein required for the U2 snRNP-branchpoint interaction. *Genes and Development*, *11*(14), 1864–1872. https://doi.org/10.1101/gad.11.14.1864

Flores-Solis, D., Lushpinskaia, I. P., Polyansky, A. A., Changiarath, A., Boehning, M., Mirkovic, M., Walshe, J., Pietrek, L. M., Cramer, P., Stelzl, L. S., Zagrovic, B., & Zweckstetter, M. (2023). Driving forces behind phase separation of the carboxy-terminal domain of RNA polymerase II. *Nature Communications*, *14*(1). https://doi.org/10.1038/s41467-023-41633-8

Fong, N., Brannan, K., Erickson, B., Kim, H., Cortazar, M. A., Sheridan, R. M., Nguyen, T., Karp, S., & Bentley, D. L. (2015). Effects of Transcription Elongation Rate and Xrn2 Exonuclease Activity on RNA Polymerase II Termination Suggest Widespread Kinetic Competition. *Molecular Cell*, *60*(2), 256–267. https://doi.org/10.1016/j.molcel.2015.09.026

Forsburg, S. L., & Rhind, N. (2006). Basic methods for fission yeast. *Yeast*, *23*(3), 173–183. https://doi.org/10.1002/yea.1347

Foucher, A. E., Touat-Todeschini, L., Juarez-Martinez, A. B., Rakitch, A., Laroussi, H., Karczewski, C., Acajjaoui, S., Soler-López, M., Cusack, S., Mackereth, C. D.,

Verdel, A., & Kadlec, J. (2022). Structural analysis of Red1 as a conserved scaffold of the RNA-targeting MTREC/PAXT complex. *Nature Communications*, *13*(1). https://doi.org/10.1038/s41467-022-32542-3

Fujita, K. ichi, Ito, M., Irie, M., Harada, K., Fujiwara, N., Ikeda, Y., Yoshioka, H., Yamazaki, T., Kojima, M., Mikami, B., Mayeda, A., & Masuda, S. (2024). Structural differences between the closely related RNA helicases, UAP56 and URH49, fashion distinct functional apo-complexes. *Nature Communications*, *15*(1), 1–16. https://doi.org/10.1038/s41467-023-44217-8

Fuller-Pace, F. V. (2006). DExD/H box RNA helicases: Multifunctional proteins with important roles in transcriptional regulation. *Nucleic Acids Research*, *34*(15), 4206–4215. https://doi.org/10.1093/nar/gkl460

Fuller-Pace, F. V. (2013). The DEAD box proteins DDX5 (p68) and DDX17 (p72): Multi-tasking transcriptional regulators. *Biochimica et Biophysica Acta - Gene Regulatory Mechanisms*, *1829*(8), 756–763. https://doi.org/10.1016/j.bbagrm.2013.03.004

Gallardo, P., Real-Calderón, P., Flor-Parra, I., Salas-Pino, S., & Daga, R. R. (2020). Acute Heat Stress Leads to Reversible Aggregation of Nuclear Proteins into Nucleolar Rings in Fission Yeast. *Cell Reports*, *33*(6). https://doi.org/10.1016/j.celrep.2020.108377

Giacometti, S., Benbahouche, N. E. H., Domanski, M., Robert, M. C., Meola, N., Lubas, M., Bukenborg, J., Andersen, J. S., Schulze, W. M., Verheggen, C., Kudla, G., Jensen, T. H., & Bertrand, E. (2017). Mutually Exclusive CBC-Containing Complexes Contribute to RNA Fate. *Cell Reports*, *18*(11), 2635–2650. https://doi.org/10.1016/j.celrep.2017.02.046

Gilbert, W., & Guthrie, C. (2004). The Glc7p Nuclear Phosphatase Promotes mRNA Export by Facilitating Association of Mex67p with mRNA export in *S. cerevisiae* and for viral RNA export in HIV-infected cells, indicated that a similar mechanism could direct messenger RNA export (for review see. *Molecular Cell*, *13*(1), 201–212.

Gilbert, W., Siebel, C. W., & Guthrie, C. (2001). Phosphorylation by Sky1p promotes Npl3p shuttling and mRNA dissociation. *Rna*, *7*(2), 302–313. https://doi.org/10.1017/S1355838201002369

Gilman, B., Tijerina, P., & Russell, R. (2017). Distinct RNA-unwinding mechanisms of DEAD-box and DEAH-box RNA helicase proteins in remodeling structured RNAs and RNPs. In *Biochemical Society Transactions* (Vol. 45, Issue 6, pp. 1313–1321). Portland Press Ltd. https://doi.org/10.1042/BST20170095

Goffeau, A., Barrell, B. G., Bussey, H., Davis, R. W., Dujon, B., Feldmann, H., Galibert, F., Hoheisel, J. D., Jacq, C., Johnston, M., Louis, E. J., Mewes, H. W., Murakami, Y., Philippsen, P., Tettelin, H., & Oliver, S. G. (1996). Life with 6000 Genes conveniently among the different interna- Old Questions and New Answers The genome . At the beginning of the se- of its more complex relatives in the eukary- *cerevisiae* has been completely sequenced *Schizosaccharomyces pombe* indicate. *Science*, *274*(October), 546–567.

Gómez-Herreros, F., De Miguel-Jiménez, L., Millán-Zambrano, G., Peñate, X., Delgado-Ramos, L., Muñoz-Centeno, M. C., & Chávez, S. (2012). One step back

before moving forward: Regulation of transcription elongation by arrest and backtracking. *FEBS Letters*, *586*(18), 2820–2825. https://doi.org/10.1016/j.febslet.2012.07.030

Görnemann, J., Kotovic, K. M., Hujer, K., & Neugebauer, K. M. (2005). Cotranscriptional spliceosome assembly occurs in a stepwise fashion and requires the cap binding complex. *Molecular Cell*, *19*(1), 53–63. https://doi.org/10.1016/j.molcel.2005.05.007

Grewal, S. I. S. (2010). RNAi-dependent formation of heterochromatin and its diverse functions. *Current Opinion in Genetics and Development*, *20*(2), 134–141. https://doi.org/10.1016/j.gde.2010.02.003

Grewal, S. I. S., & Jia, S. (2007). Heterochromatin revisited. *Nature Reviews Genetics*, *8*(1), 35–46. https://doi.org/10.1038/nrg2008

Grunstein, M., & Gasser, S. M. (2013). Epigenetics in Saccharomyces cerevisiae. *Cold Spring Harbor Perspectives in Biology*, *5*(7). https://doi.org/10.1101/cshperspect.a017491

Gudipati, R. K., Villa, T., Boulay, J., & Libri, D. (2008). Phosphorylation of the RNA polymerase II C-terminal domain dictates transcription termination choice. *Nature Structural and Molecular Biology*, *15*(8), 786–794. https://doi.org/10.1038/nsmb.1460

Hammell, C. M., Gross, S., Zenklusen, D., Heath, C. V., Stutz, F., Moore, C., & Cole, C. N. (2002). Coupling of Termination, 3′ Processing, and mRNA Export. In *Molecular and Cellular Biology* (Vol. 22, Issue 18, pp. 6441–6457). https://doi.org/10.1128/mcb.22.18.6441-6457.2002

Hantsche, M., & Cramer, P. (2017). Conserved RNA polymerase II initiation complex structure. *Current Opinion in Structural Biology*, *47*, 17–22. https://doi.org/10.1016/j.sbi.2017.03.013

Harigaya, Y., Tanaka, H., Yamanaka, S., Tanaka, K., Watanabe, Y., Tsutsumi, C., Chikashige, Y., Hiraoka, Y., Yamashita, A., & Yamamoto, M. (2006). Selective elimination of messenger RNA prevents an incidence of untimely meiosis. *Nature*, *442*(7098), 45–50. https://doi.org/10.1038/nature04881

Harlen, K. M., Trotta, K. L., Smith, E. E., Mosaheb, M. M., Fuchs, S. M., & Churchman, L. S. (2016). Comprehensive RNA Polymerase II Interactomes Reveal Distinct and Varied Roles for Each Phospho-CTD Residue. *Cell Reports*, *15*(10), 2147–2158. https://doi.org/10.1016/j.celrep.2016.05.010

Harris, M. A., Rutherford, K. M., Hayles, J., Lock, A., Bähler, J., Oliver, S. G., Mata, J., & Wood, V. (2022). Fission stories: using PomBase to understand *Schizosaccharomyces pombe* biology. *Genetics*, *220*(4), 1–7. https://doi.org/10.1093/GENETICS/IYAB222

Hartley, P. D., & Madhani, H. D. (2009). Mechanisms that Specify Promoter Nucleosome Location and Identity. *Cell*, *137*(3), 445–458. https://doi.org/10.1016/j.cell.2009.02.043

Hautbergue, G. M., Hung, M. L., Golovanov, A. P., Lian, L. Y., & Wilson, S. A. (2008). Mutually exclusive interactions drive handover of mRNA from export adaptors to TAP. *Proceedings of the National Academy of Sciences of the United States of*

America, *105*(13), 5154–5159. https://doi.org/10.1073/pnas.0709167105

Heath, C. G., Viphakone, N., & Wilson, S. A. (2016). The role of TREX in gene expression and disease. *Biochemical Journal*, *473*(19), 2911–2935. https://doi.org/10.1042/BCJ20160010

Heerma van Voss, M. R., van Diest, P. J., & Raman, V. (2017). Targeting RNA helicases in cancer: The translation trap. *Biochimica et Biophysica Acta - Reviews on Cancer*, *1868*(2), 510–520. https://doi.org/10.1016/j.bbcan.2017.09.006

Heo, D. H., Yoo, I., Kong, J., Lidschreiber, M., Mayer, A., Choi, B. Y., Hahn, Y., Cramer, P., Buratowski, S., & Kim, M. (2013). The RNA polymerase 2 C-terminal domain-interacting domain of yeast Nrd1 contributes to the choice of termination pathway and couples to RNA processing by the nuclear exosome. *Journal of Biological Chemistry*, *288*(51), 36676–36690. https://doi.org/10.1074/jbc.M113.508267

Herzel, L., Straube, K., & Neugebauer, K. M. (2018). Long-read sequencing of nascent RNA reveals coupling among RNA processing events. *Genome Research*, *28*(7), 1008–1019. https://doi.org/10.1101/gr.232025.117

Hilbert, M., Karow, A. R., & Klostermeier, D. (2009). The mechanism of ATP-dependent RNA unwinding by DEAD box proteins. *Biological Chemistry*, *390*(12), 1237–1250. https://doi.org/10.1515/BC.2009.135

Hilleren, P., & Parker, R. (2001). Defects in the mRNA export factors Rat7p, Gle1p, Mex67p, and Rat8p cause hyperadenylation during 3′-end formation of nascent transcripts. *Rna*, *7*(5), 753–764. https://doi.org/10.1017/S1355838201010147

Hilleren, Patricia, McCarthy, T., Rosbash, M., Parker, R., & Jensen, T. H. (2001). Quality control of mRNA 3′-end processing is linked to the nuclear exosome. In *Nature* (Vol. 413, Issue 6855, pp. 538–542). https://doi.org/10.1038/35097110

Hirai, H., & Ohta, K. (2023). Comparative Research: Regulatory Mechanisms of Ribosomal Gene Transcription in *Saccharomyces cerevisiae* and *Schizosaccharomyces pombe*. *Biomolecules*, *13*(2). https://doi.org/10.3390/biom13020288

Hirling, H., Scheffner, M., Restle, T., & Stahl, H. (1989). RNA helicase activity associated with the human p68 protein. *Nature*, *339*(6225), 562–564. https://doi.org/10.1038/339562a0

Hobson, D. J., Wei, W., Steinmetz, L. M., & Svejstrup, J. Q. (2012). RNA Polymerase II Collision Interrupts Convergent Transcription. *Molecular Cell*, *48*(3), 365–374. https://doi.org/10.1016/j.molcel.2012.08.027

Hoffman, C. S., & Winston, F. (1987). A ten-minute DNA preparation from yeast efficiently releases autonomous plasmids for transformaion of *Escherichia coli*. *Gene*, *57*(2–3), 267–272. https://doi.org/10.1016/0378-1119(87)90131-4

Hoffman, C. S., Wood, V., & Fantes, P. A. (2015). An ancient yeast for young geneticists: A primer on the *Schizosaccharomyces pombe* model system. *Genetics*, *201*(2), 403–423. https://doi.org/10.1534/genetics.115.181503

Hollingworth, D., Noble, C. G., Taylor, I. A., & Ramos, A. (2006). RNA polymerase II CTD phosphopeptides compete with RNA for the interaction with Pcf11. *Rna*, *12*(4), 555–560. https://doi.org/10.1261/rna.2304506

Hondele, M., Sachdev, R., Heinrich, S., Wang, J., Vallotton, P., Fontoura, B. M. A., & Weis, K. (2019). DEAD-box ATPases are global regulators of phase-separated organelles. *Nature*, *573*(7772), 144–148. https://doi.org/10.1038/s41586-019-1502-y

Hoskins, A. A., & Moore, M. J. (2012). The spliceosome: A flexible, reversible macromolecular machine. *Trends in Biochemical Sciences*, *37*(5), 179–188. https://doi.org/10.1016/j.tibs.2012.02.009

Hsin, J. P., & Manley, J. L. (2012). The RNA polymerase II CTD coordinates transcription and RNA processing. *Genes and Development*, *26*(19), 2119–2137. https://doi.org/10.1101/gad.200303.112

Huang, Y., Gattoni, R., Stévenin, J., & Steitz, J. A. (2003). SR splicing factors serve as adapter proteins for TAP-dependent mRNA export. *Molecular Cell*, *11*(3), 837–843. https://doi.org/10.1016/S1097-2765(03)00089-3

Huang, Y. J., Acton, T. B., & Montelione, G. T. (2014). DisMeta: A meta server for construct design and optimization. *Methods in Molecular Biology*, *1091*, 3–16. https://doi.org/10.1007/978-1-62703-691-7_1

Hung, M. L., Hautbergue, G. M., Snijders, A. P. L., Dickman, M. J., & Wilson, S. A. (2010). Arginine methylation of REF/ALY promotes efficient handover of mRNA to TAP/NXF1. *Nucleic Acids Research*, *38*(10), 3351–3361. https://doi.org/10.1093/nar/gkq033

I.Barta and R.Iggo. (1995). *Autoregulation of expression of the yeast Dbp2p DEAD-box protein is mediated sequences in the conserved DBP2 intron* (pp. 3800–3808). EMBO.

Ideue, T., Azad, A. K., Yoshida, J. I., Matsusaka, T., Yanagida, M., Ohshima, Y., & Tani, T. (2004). The nucleolus is involved in mRNA export from the nucleus in fission yeast. *Journal of Cell Science*, *117*(14), 2887–2895. https://doi.org/10.1242/jcs.01155

Ietswaart, R., Smalec, B. M., Xu, A., Choquet, K., McShane, E., Jowhar, Z. M., Guegler, C. K., Baxter-Koenigs, A. R., West, E. R., Fu, B. X. H., Gilbert, L., Floor, S. N., & Churchman, L. S. (2024). Genome-wide quantification of RNA flow across subcellular compartments reveals determinants of the mammalian transcript life cycle. *Molecular Cell*, *84*(14), 2765-2784.e16. https://doi.org/10.1016/j.molcel.2024.06.008

Inada, B. M. and M. (2018). Co-transcriptional mRNA Processing in Eukaryotes. In *Molecular Life Sciences*. https://doi.org/10.1007/978-1-4614-1531-2_41

Izaurralde, E., Lewis, J., McGuigan, C., Jankowska, M., Darzynkiewicz, E., & Mattaj, I. W. (1994). A nuclear cap binding protein complex involved in pre-mRNA splicing. *Cell*, *78*(4), 657–668. https://doi.org/10.1016/0092-8674(94)90530-4

Jalal, C., Uhlmann-Schiffler, H., & Stahl, H. (2007). Redundant role of DEAD box proteins p68 (Ddx5) and p72/p82 (Ddx17) in ribosome biogenesis and cell proliferation. *Nucleic Acids Research*, *35*(11), 3590–3601. https://doi.org/10.1093/nar/gkm058

Jalili, V., Afgan, E., Gu, Q., Clements, D., Blankenberg, D., Goecks, J., Taylor, J., & Nekrutenko, A. (2021). The Galaxy platform for accessible, reproducible and

collaborative biomedical analyses: 2020 update. *Nucleic Acids Research*, *48*(W1), W395–W402. https://doi.org/10.1093/NAR/GKAA434

Jänicke, A., Vancuylenberg, J., Boag, P. R., Traven, A., & Beilharz, T. H. (2012). ePAT: A simple method to tag adenylated RNA to measure poly(A)-tail length and other 3′ RACE applications. *Rna*, *18*(6), 1289–1295. https://doi.org/10.1261/rna.031898.111

Janknecht, R. (2010). DEAD-box proteins and tumor promoters. *Am J Transl Res*, *2*(3), 223–234.

Jankowsky, E. (2011). RNA helicases at work: Binding and rearranging. *Trends in Biochemical Sciences*, *36*(1), 19–29. https://doi.org/10.1016/j.tibs.2010.07.008

Jankowsky, E., & Bowers, H. (2006). Remodeling of ribonucleoprotein complexes with DExH/D RNA helicases. *Nucleic Acids Research*, *34*(15), 4181–4188. https://doi.org/10.1093/nar/gkl410

Jankowsky, E., & Fairman, M. E. (2007). RNA helicases - one fold for many functions. *Current Opinion in Structural Biology*, *17*(3), 316–324. https://doi.org/10.1016/j.sbi.2007.05.007

Jarmoskaite, I., & Russell, R. (2014). RNA helicase proteins as chaperones and remodelers. *Annual Review of Biochemistry*, *83*, 697–725. https://doi.org/10.1146/annurev-biochem-060713-035546

Jensen, T. H., Patricio, K., McCarthy, T., & Rosbash, M. (2001). A block to mRNA nuclear export in S. cerevisiae leads to hyperadenylation of transcripts that accumulate at the site of transcription. *Molecular Cell*, *7*(4), 887–898. https://doi.org/10.1016/S1097-2765(01)00232-5

Jeong, K., Ryu, I., Park, J., Hwang, H. J., Ha, H., Park, Y., Oh, S. T., & Kim, Y. K. (2019). Staufen1 and UPF1 exert opposite actions on the replacement of the nuclear cap-binding complex by eIF4E at the 5' end of mRNAs. *Nucleic Acids Research*, *47*(17), 9313–9328. https://doi.org/10.1093/nar/gkz643

Jia, H., Wang, X., Liu, F., Guenther, U. P., Srinivasan, S., Anderson, J. T., & Jankowsky, E. (2011). The RNA helicase Mtr4p modulates polyadenylation in the TRAMP complex. *Cell*, *145*(6), 890–901. https://doi.org/10.1016/j.cell.2011.05.010

Jimenez, A., Tipper, D. J., & Davies, J. (1973). Mode of action of thiolutin, an inhibitor of macromolecular synthesis in *Saccharomyces cerevisiae*. *Antimicrobial Agents and Chemotherapy*, *3*(6), 729–738. https://doi.org/10.1128/AAC.3.6.729

Jimeno, S., Rondón, A. G., Luna, R., & Aguilera, A. (2002). The yeast THO complex and mRNA export factors link RNA metabolism with transcription and genome instability. *EMBO Journal*, *21*(13), 3526–3535. https://doi.org/10.1093/emboj/cdf335

Johnson, Sara A., Kim, H., Erickson, B., & Bentley, D. L. (2010). The export factor Yra1 modulates mRNA 3′ end processing. In *Nature Structural and Molecular Biology* (Vol. 18, Issue 10, pp. 1164–1171). https://doi.org/10.1038/nsmb.2126

Johnson, Sara Ann, Cubberley, G., & Bentley, D. L. (2009). Cotranscriptional Recruitment of the mRNA Export Factor Yra1 by Direct Interaction with the 3′ End

Processing Factor Pcf11. *Molecular Cell*, *33*(2), 215–226. https://doi.org/10.1016/j.molcel.2008.12.007

Kaida, D., Berg, M. G., Younis, I., Kasim, M., Singh, L. N., Wan, L., & Dreyfuss, G. (2010). U1 snRNP protects pre-mRNAs from premature cleavage and polyadenylation. *Nature*, *468*(7324), 664–668. https://doi.org/10.1038/nature09479

Kar, A., Fushimi, K., Zhou, X., Ray, P., Shi, C., Chen, X., Liu, Z., Chen, S., & Wu, J. Y. (2011). RNA Helicase p68 (DDX5) Regulates tau Exon 10 Splicing by Modulating a Stem-Loop Structure at the 5′ Splice Site . *Molecular and Cellular Biology*, *31*(9), 1812–1821. https://doi.org/10.1128/mcb.01149-10

Katahira, J., Inoue, H., Hurt, E., & Yoneda, Y. (2009). Adaptor Aly and co-adaptor Thoc5 function in the Tap-p15-mediated nuclear export of HSP70 mRNA. *EMBO Journal*, *28*(5), 556–567. https://doi.org/10.1038/emboj.2009.5

Katahira, J., Sträßer, K., Podtelejnikov, A., Mann, M., Jung, J. U., & Hurt, E. (1999). The Mex67p-mediated nuclear mRNA export pathway is conserved from yeast to human. *EMBO Journal*, *18*(9), 2593–2609. https://doi.org/10.1093/emboj/18.9.2593

Kecman, T., Heo, D. H., & Vasiljeva, L. (2018). Profiling RNA Polymerase II Phosphorylation Genome-Wide in Fission Yeast. In *Methods in Enzymology* (1st ed., Vol. 612). Elsevier Inc. https://doi.org/10.1016/bs.mie.2018.07.009

Kecman, T., Kuś, K., Heo, D. H., Duckett, K., Birot, A., Liberatori, S., Mohammed, S., Geis-Asteggiante, L., Robinson, C. V., & Vasiljeva, L. (2018). Elongation/Termination Factor Exchange Mediated by PP1 Phosphatase Orchestrates Transcription Termination. *Cell Reports*, *25*(1), 259-269.e5. https://doi.org/10.1016/j.celrep.2018.09.007

Kelly, S. M., & Corbett, A. H. (2009). Messenger RNA export from the nucleus: A series of molecular wardrobe changes. *Traffic*, *10*(9), 1199–1208. https://doi.org/10.1111/j.1600-0854.2009.00944.x

Kervestin, S., & Jacobson, A. (2012). NMD: A multifaceted response to premature translational termination. *Nature Reviews Molecular Cell Biology*, *13*(11), 700–712. https://doi.org/10.1038/nrm3454

Kilchert, C., Kecman, T., Priest, E., Hester, S., Aydin, E., Kus, K., Rossbach, O., Castello, A., Mohammed, S., & Vasiljeva, L. (2020). System-wide analyses of the fission yeast poly(A)+RNA interactome reveal insights into organization and function of RNA-protein complexes. *Genome Research*, *30*(7), 1012–1026. https://doi.org/10.1101/gr.257006.119

Kilchert, C., Sträßer, K., Kunetsky, V., & Änkö, M. L. (2019). From parts lists to functional significance—RNA–protein interactions in gene regulation. *Wiley Interdisciplinary Reviews: RNA*, *October*, 1–20. https://doi.org/10.1002/wrna.1582

Kilchert, C., Wittmann, S., Passoni, M., Shah, S., Granneman, S., & Vasiljeva, L. (2015). Regulation of mRNA Levels by Decay-Promoting Introns that Recruit the Exosome Specificity Factor Mmi1. *Cell Reports*, *13*(11), 2504–2515. https://doi.org/10.1016/j.celrep.2015.11.026

Kim, M., Krogan, N. J., Vasiljeva, L., Rando, O. J., Nedea, E., Greenblatt, J. F., &

Buratowski, S. (2004). The yeast Rat1 exonuclease promotes transcription termination by RNA polymerase II. *Nature*, *432*(7016), 517–522. https://doi.org/10.1038/nature03041

Kim, M., Vasiljeva, L., Rando, O. J., Zhelkovsky, A., Moore, C., & Buratowski, S. (2006). Distinct Pathways for snoRNA and mRNA Termination. *Molecular Cell*, *24*(5), 723–734. https://doi.org/10.1016/j.molcel.2006.11.011

Kistler, A. L., & Guthrie, C. (2001). Deletion of MUD2, the yeast homolog of U2AF65, can bypass the requirement for Sub2, an essential spliceosomal ATPase. *Genes and Development*, *15*(1), 42–49. https://doi.org/10.1101/gad.851301

Klama, S., Hirsch, A. G., Schneider, U. M., Zander, G., Seel, A., & Krebber, H. (2022). A guard protein mediated quality control mechanism monitors 5'-capping of pre-mRNAs. *Nucleic Acids Research*, *50*(19), 11301–11314. https://doi.org/10.1093/nar/gkac952

Köhler, A., & Hurt, E. (2007). Exporting RNA from the nucleus to the cytoplasm. *Nature Reviews Molecular Cell Biology*, *8*(10), 761–773. https://doi.org/10.1038/nrm2255

Kölbel, K., Ihling, C., Bellmann-Sickert, K., Neundorf, I., Beck-Sickinger, A. G., Sinz, A., Kühn, U., & Wahle, E. (2009). Type I arginine methyltransferases PRMT1 and PRMT-3 act distributively. *Journal of Biological Chemistry*, *284*(13), 8274–8282. https://doi.org/10.1074/jbc.M809547200

Komarnitsky, P., Cho, E. J., & Buratowski, S. (2000). Different phosphorylated forms of RNA polymerase II and associated mRNA processing factors during transcription. *Genes and Development*, *14*(19), 2452–2460. https://doi.org/10.1101/gad.824700

Kouranti, I., Mclean, J. R., Feoktistova, A., Liang, P., Johnson, A. E., Roberts-Galbraith, R. H., & Gould, K. L. (2010). A global census of fission yeast deubiquitinating enzyme localization and interaction networks reveals distinct compartmentalization profiles and overlapping functions in endocytosis and polarity. *PLoS Biology*, *8*(9). https://doi.org/10.1371/journal.pbio.1000471

Krishnan, V., & Zeichner, S. L. (2004). Alterations in the expression of DEAD-box and other RNA binding proteins during HIV-1 replication. *Retrovirology*, *1*, 1–5. https://doi.org/10.1186/1742-4690-1-42

Kyburz, A., Friedlein, A., Langen, H., & Keller, W. (2006). Direct Interactions between Subunits of CPSF and the U2 snRNP Contribute to the Coupling of Pre-mRNA 3′ End Processing and Splicing. In *Molecular Cell* (Vol. 23, Issue 2, pp. 195–205). https://doi.org/10.1016/j.molcel.2006.05.037

LaCava, J., Houseley, J., Saveanu, C., Petfalski, E., Thompson, E., Jacquier, A., & Tollervey, D. (2005). RNA degradation by the exosome is promoted by a nuclear polyadenylation complex. *Cell*, *121*(5), 713–724. https://doi.org/10.1016/j.cell.2005.04.029

Laemmli, U. K. (1970). 227680a0. *Nature*, *227*, 680–685.

Lahudkar, S., Shukla, A., Bajwa, P., Durairaj, G., Stanojevic, N., & Bhaumik, S. R. (2011). The mRNA cap-binding complex stimulates the formation of pre-initiation complex at the promoter via its interaction with Mot1p in vivo. *Nucleic Acids Research*, *39*(6), 2188–2209. https://doi.org/10.1093/nar/gkq1029

Lai, Y. H., Choudhary, K., Cloutier, S. C., Xing, Z., Aviran, S., & Tran, E. J. (2019). Genome-wide discovery of DEAD-Box RNA helicase targets reveals RNA structural remodeling in transcription termination. *Genetics*, *212*(1), 153–174. https://doi.org/10.1534/genetics.119.302058

Langmead, B., & Salzberg, S. L. (2012). Fast gapped-read alignment with Bowtie 2. *Nature Methods*, *9*(4), 357–359. https://doi.org/10.1038/nmeth.1923

Larochelle, M., Robert, M. A., Hébert, J. N., Liu, X., Matteau, D., Rodrigue, S., Tian, B., Jacques, P. É., & Bachand, F. (2018). Common mechanism of transcription termination at coding and noncoding RNA genes in fission yeast. *Nature Communications*, *9*(1). https://doi.org/10.1038/s41467-018-06546-x

Lawrence, M., Gentleman, R., & Carey, V. (2009). rtracklayer: An R package for interfacing with genome browsers. *Bioinformatics*, *25*(14), 1841–1842. https://doi.org/10.1093/bioinformatics/btp328

Lawrence, M., Huber, W., Pagès, H., Aboyoun, P., Carlson, M., Gentleman, R., Morgan, M. T., & Carey, V. J. (2013). Software for Computing and Annotating Genomic Ranges. *PLoS Computational Biology*, *9*(8), 1–10. https://doi.org/10.1371/journal.pcbi.1003118

Le Hir, H., Izaurralde, E., Maquat, L. E., & Moore, M. J. (2000). The spliceosome deposits multiple proteins 20-24 nucleotides upstream of mRNA exon-exon junctions. *EMBO Journal*, *19*(24), 6860–6869. https://doi.org/10.1093/emboj/19.24.6860

Ledoux, S., & Guthrie, C. (2011a). Regulation of the Dbp5 ATPase cycle in mRNP remodeling at the nuclear pore: A lively new paradigm for DEAD-box proteins. *Genes and Development*, *25*(11), 1109–1114. https://doi.org/10.1101/gad.2062611

Ledoux, S., & Guthrie, C. (2011b). Regulation of the Dbp5 ATPase cycle in mRNP remodeling at the nuclear pore: A lively new paradigm for DEAD-box proteins. *Genes and Development*, *25*(11), 1109–1114. https://doi.org/10.1101/gad.2062611

Lee, E. S., Smith, H. W., Wolf, E. J., Guvenek, A., Wang, Y. E., Emili, A., Tian, B., & Palazzo, A. F. (2022). ZFC3H1 and U1-70K promote the nuclear retention of mRNAs with 5′ splice site motifs within nuclear speckles. *Rna*, *28*(6), 878–894. https://doi.org/10.1261/rna.079104.122

Lee, N. N., Chalamcharla, V. R., Reyes-Turcu, F., Mehta, S., Zofall, M., Balachandran, V., Dhakshnamoorthy, J., Taneja, N., Yamanaka, S., Zhou, M., & Grewal, S. I. S. (2013). XMtr4-like protein coordinates nuclear RNA processing for heterochromatin assembly and for telomere maintenance. *Cell*, *155*(5), 1061. https://doi.org/10.1016/j.cell.2013.10.027

Lee, S. Y., Hung, S., Esnault, C., Pathak, R., Johnson, K. R., Bankole, O., Yamashita, A., Zhang, H., & Levin, H. L. (2020). Dense Transposon Integration Reveals Essential Cleavage and Polyadenylation Factors Promote Heterochromatin Formation. *Cell Reports*, *30*(8), 2686-2698.e8. https://doi.org/10.1016/j.celrep.2020.01.094

Lei Li, Ken Roy, Sachin Katyal, Xuejun Sun, Stacey Bleoo, and R. G. (2006). Dynamic

Nature of Cleavage Bodies and Their Spatial Relationship to DDX1 Bodies, Cajal Bodies, and Gems Lei. *Molecular Biology of the Cell*, *17*(March), 1126–1140. https://doi.org/10.1091/mbc.E05

Leitão, A. L., Costa, M. C., & Enguita, F. J. (2015). Open accessunzippers, resolvers and sensors: A structural and functional biochemistry tale of RNA helicases. In *International Journal of Molecular Sciences* (Vol. 16, Issue 2, pp. 2269–2293). MDPI AG. https://doi.org/10.3390/ijms16022269

Lemay, J. F., & Bachand, F. (2015). Fail-safe transcription termination: Because one is never enough. *RNA Biology*, *12*(9), 927–932. https://doi.org/10.1080/15476286.2015.1073433

Lemay, J. F., Marguerat, S., Larochelle, M., Liu, X., van Nues, R., Hunyadkürti, J., Hoque, M., Tian, B., Granneman, S., Bähler, J., & Bachand, F. (2016). The Nrd1-like protein Seb1 coordinates cotranscriptional 3′ end processing and polyadenylation site selection. *Genes and Development*, *30*(13), 1558–1572. https://doi.org/10.1101/gad.280222.116

Lemieux, C., Marguerat, S., Lafontaine, J., Barbezier, N., Bähler, J., & Bachand, F. (2011). A Pre-mRNA degradation pathway that selectively targets intron-containing genes requires the nuclear poly(A)-binding protein. *Molecular Cell*, *44*(1), 108–119. https://doi.org/10.1016/j.molcel.2011.06.035

Li, F., Ling, X., Chakraborty, S., Fountzilas, C., Wang, J., Jamroze, A., Liu, X., Kalinski, P., & Tang, D. G. (2023). Role of the DEAD-box RNA helicase DDX5 (p68) in cancer DNA repair, immune suppression, cancer metabolic control, virus infection promotion, and human microbiome (microbiota) negative influence. *Journal of Experimental and Clinical Cancer Research*, *42*(1), 1–26. https://doi.org/10.1186/s13046-023-02787-x

Li, H., Handsaker, B., Wysoker, A., Fennell, T., Ruan, J., Homer, N., Marth, G., Abecasis, G., & Durbin, R. (2009). The Sequence Alignment/Map format and SAMtools. *Bioinformatics*, *25*(16), 2078–2079. https://doi.org/10.1093/bioinformatics/btp352

Liang, L., Diehl-Jones, W., & Lasko, P. (1994). Localization of vasa protein to the Drosophila pole plasm is independent of its RNA-binding and helicase activities. *Development*, *120*(5), 1201–1211. https://doi.org/10.1242/dev.120.5.1201

Libri, D., Graziani, N., Saguez, C., & Boulay, J. (2001). Multiple roles for the yeast SUB2/yUAP56 gene in splicing. *Genes and Development*, *15*(1), 36–41. https://doi.org/10.1101/gad.852101

Lin, C., Yang, L., Yang, J. J., Huang, Y., & Liu, Z.-R. (2005). ATPase/Helicase Activities of p68 RNA Helicase Are Required for Pre-mRNA Splicing but Not for Assembly of the Spliceosome. *Molecular and Cellular Biology*, *25*(17), 7484–7493. https://doi.org/10.1128/mcb.25.17.7484-7493.2005

Linder, P., & Fuller-Pace, F. V. (2013). Looking back on the birth of DEAD-box RNA helicases. *Biochimica et Biophysica Acta - Gene Regulatory Mechanisms*, *1829*(8), 750–755. https://doi.org/10.1016/j.bbagrm.2013.03.007

Linder, P., & Jankowsky, E. (2011). From unwinding to clamping ĝ€" the DEAD box RNA helicase family. *Nature Reviews Molecular Cell Biology*, *12*(8), 505–516.

https://doi.org/10.1038/nrm3154

Linder, P., & Lasko, P. (2006). Bent out of Shape: RNA Unwinding by the DEAD-Box Helicase Vasa. *Cell*, *125*(2), 219–221. https://doi.org/10.1016/j.cell.2006.03.030

Lipp, J. J., Marvin, M. C., Shokat, K. M., & Guthrie, C. (2015). SR protein kinases promote splicing of nonconsensus introns. *Nature Structural and Molecular Biology*, *22*(8), 611–617. https://doi.org/10.1038/nsmb.3057

Liu, F., Putnam, A. A., & Jankowsky, E. (2014). DEAD-box helicases form nucleotide-dependent, long-lived complexes with RNA. *Biochemistry*, *53*(2), 423–433. https://doi.org/10.1021/bi401540q

Liu, F., Putnam, A., & Jankowsky, E. (2008). ATP hydrolysis is required for DEAD-box protein recycling but not for duplex unwinding. *Proceedings of the National Academy of Sciences of the United States of America*, *105*(51), 20209–20214. https://doi.org/10.1073/pnas.0811115106

Logan, J., Falck-Pedersen, E., Darnell, J. E., & Shenk, T. (1987). A poly(A) addition site and a downstream termination region are required for efficient cessation of transcription by RNA polymerase II in the mouse beta maj-globin gene. *Proceedings of the National Academy of Sciences of the United States of America*, *84*(23), 8306–8310. https://doi.org/10.1073/pnas.84.23.8306

Lorch, Y., & Kornberg, R. D. (2017). Chromatin-remodeling for transcription. *Quarterly Reviews of Biophysics*, *50*, 1–15. https://doi.org/10.1017/S003358351700004X

Lorsch, J. R., & Herschlag, D. (1998). The DEAD box protein eIF4A. 2. A cycle of nucleotide and RNA-dependent conformational changes. *Biochemistry*, *37*(8), 2194–2206. https://doi.org/10.1021/bi9724319

Love, M. I., Huber, W., & Anders, S. (2014). Moderated estimation of fold change and dispersion for RNA-seq data with DESeq2. *Genome Biology*, *15*(12), 1–21. https://doi.org/10.1186/s13059-014-0550-8

Lubas, M., Andersen, P. R., Schein, A., Dziembowski, A., Kudla, G., & Jensen, T. H. (2015). The human nuclear exosome targeting complex is loaded onto newly synthesized RNA to direct early ribonucleolysis. *Cell Reports*, *10*(2), 178–192. https://doi.org/10.1016/j.celrep.2014.12.026

Lund, M. K., & Guthrie, C. (2005). The DEAD-box protein Dbp5p is required to dissociate Mex67p from exported mRNPs at the nuclear rim. *Molecular Cell*, *20*(4), 645–651. https://doi.org/10.1016/j.molcel.2005.10.005

Luo, M. J., & Reed, R. (1999). Splicing is required for rapid and efficient mRNA export in metazoans. *Proceedings of the National Academy of Sciences of the United States of America*, *96*(26), 14937–14942. https://doi.org/10.1073/pnas.96.26.14937

Luo, M. J., Zhou, Z., Magni, K., Christoforides, C., Rappsilber, J., Mann, M., & Reed, R. (2001). Pre-mrna splicing and mRNA export linked by direct interactions between UAP56 and aly. *Nature*, *413*(6856), 644–647. https://doi.org/10.1038/35098106

Luo, W., Johnson, A. W., & Bentley, D. L. (2006). The role of Rat1 in coupling mRNA 3′-end processing to transcription termination: Implications for a unified allosteric-

torpedo model. *Genes and Development*, *20*(8), 954–965. https://doi.org/10.1101/gad.1409106

Lykke-Andersen, S., Žumer, K., Molska, E. Š., Rouvière, J. O., Wu, G., Demel, C., Schwalb, B., Schmid, M., Cramer, P., & Jensen, T. H. (2021). Integrator is a genome-wide attenuator of non-productive transcription. *Molecular Cell*, *81*(3), 514-529.e6. https://doi.org/10.1016/j.molcel.2020.12.014

Ma, W. K., Cloutier, S. C., & Tran, E. J. (2013). The DEAD-box protein Dbp2 functions with the RNA-binding protein Yra1 to promote mRNP assembly. *Journal of Molecular Biology*, *425*(20), 3824–3838. https://doi.org/10.1016/j.jmb.2013.05.016

Ma, W. K., Paudel, B. P., Xing, Z., Sabath, I. G., Rueda, D., & Tran, E. J. (2016). Recruitment, Duplex Unwinding and Protein-Mediated Inhibition of the Dead-Box RNA Helicase Dbp2 at Actively Transcribed Chromatin. *Journal of Molecular Biology*, *428*(6), 1091–1106. https://doi.org/10.1016/j.jmb.2016.02.005

Mallam, A. L., Sidote, D. J., & Lambowitz, A. M. (2014). Molecular insights into RNA and DNA helicase evolution from the determinants of specificity for a DEAD-box RNA helicase. *ELife*, *3*, e04630. https://doi.org/10.7554/eLife.04630

Marblestone, J. G., Edavettal, S. C., Lim, Y., Lim, P., Zuo, X., & Butt, T. R. (2006). Comparison of SUMO fusion technology with traditional gene fusion systems: Enhanced expression and solubility with SUMO. *Protein Science*, *15*(1), 182–189. https://doi.org/10.1110/ps.051812706

Martín Caballero, L., Capella, M., Barrales, R. R., Dobrev, N., van Emden, T., Hirano, Y., Suma Sreechakram, V. N., Fischer-Burkart, S., Kinugasa, Y., Nevers, A., Rougemaille, M., Sinning, I., Fischer, T., Hiraoka, Y., & Braun, S. (2022). The inner nuclear membrane protein Lem2 coordinates RNA degradation at the nuclear periphery. *Nature Structural and Molecular Biology*, *29*(9), 910–921. https://doi.org/10.1038/s41594-022-00831-6

Martin, F. J., Amode, M. R., Aneja, A., Austine-Orimoloye, O., Azov, A. G., Barnes, I., Becker, A., Bennett, R., Berry, A., Bhai, J., Bhurji, S. K., Bignell, A., Boddu, S., Branco Lins, P. R., Brooks, L., Ramaraju, S. B., Charkhchi, M., Cockburn, A., Da Rin Fiorretto, L., … Flicek, P. (2023). Ensembl 2023. *Nucleic Acids Research*, *51*(1 D), D933–D941. https://doi.org/10.1093/nar/gkac958

Martinez-Rucobo, F. W., & Cramer, P. (2013). Structural basis of transcription elongation. *Biochimica et Biophysica Acta - Gene Regulatory Mechanisms*, *1829*(1), 9–19. https://doi.org/10.1016/j.bbagrm.2012.09.002

Masuda, S., Das, R., Cheng, H., Hurt, E., Dorman, N., & Reed, R. (2005). Recruitment of the human TREX complex to mRNA during splicing. *Genes and Development*, *19*(13), 1512–1517. https://doi.org/10.1101/gad.1302205

Mata, J. (2013). Genome-wide mapping of polyadenylation sites in fission yeast reveals widespread alternative polyadenylation. *RNA Biology*, *10*(8), 1407–1414. https://doi.org/10.4161/rna.25758

Matsuyama, A., Shirai, A., Yashiroda, Y., Kamata, A., Horinouchi, S., & Yoshida, M. (2004). pDUAL, a multipurpose, multicopy vector capable of chromosomal integration in fission yeast. *Yeast*, *21*(15), 1289–1305.

https://doi.org/10.1002/yea.1181

Maundrell, K. (1990). nmt1 of fission yeast: A highly transcribed gene completely repressed by thiamine. *Journal of Biological Chemistry*, *265*(19), 10857–10864. https://doi.org/10.1016/s0021-9258(19)38525-4

Mayer, A., Heidemann, M., Lidschreiber, M., Schreieck, A., Sun, M., Hintermair, C., Kremmer, E., Eick, D., & Cramer, P. (2012). CTD Tyrosine phosphorylation impairs termination factor recruitment to RNA polymerase II. *Science*, *336*(6089), 1723–1725. https://doi.org/10.1126/science.1219651

Mayer, A., Lidschreiber, M., Siebert, M., Leike, K., Söding, J., & Cramer, P. (2010). Uniform transitions of the general RNA polymerase II transcription complex. *Nature Structural and Molecular Biology*, *17*(10), 1272–1278. https://doi.org/10.1038/nsmb.1903

Mayer, A., Schreieck, A., Lidschreiber, M., Leike, K., Martin, D. E., & Cramer, P. (2012). The Spt5 C-Terminal Region Recruits Yeast 3′ RNA Cleavage Factor I. *Molecular and Cellular Biology*, *32*(7), 1321–1331. https://doi.org/10.1128/mcb.06310-11

McCracken, S., Fong, N., Rosonina, E., Yankulov, K., Brothers, G., Siderovski, D., Hessel, A., Foster, S., Shuman, S., & Bentley, D. L. (1997). 5'-Capping enzymes are targeted to pre-mRNA by binding to the phosphorylated carboxy-terminal domain of RNA polymerase II. *Genes and Development*, *11*(24), 3306–3318. https://doi.org/10.1101/gad.11.24.3306

Mehta, M., Braberg, H., Wang, S., Lozsa, A., Shales, M., Solache, A., Krogan, N. J., & Keogh, M. C. (2010). Individual lysine acetylations on the N terminus of *Saccharomyces cerevisiae* H2A.Z are highly but not differentially regulated. *Journal of Biological Chemistry*, *285*(51), 39855–39865. https://doi.org/10.1074/jbc.M110.185967

Meinhart, A., & Cramer, P. (2004). Recognition of RNA polymerase II carboxy-terminal domain by 3′-RNA-processing factors. *Nature*, *430*(6996), 223–226. https://doi.org/10.1038/nature02679

Meola, N., Domanski, M., Karadoulama, E., Chen, Y., Gentil, C., Pultz, D., Vitting-Seerup, K., Lykke-Andersen, S., Andersen, J. S., Sandelin, A., & Jensen, T. H. (2016). Identification of a Nuclear Exosome Decay Pathway for Processed Transcripts. *Molecular Cell*, *64*(3), 520–533. https://doi.org/10.1016/j.molcel.2016.09.025

Mersaoui, S. Y., Yu, Z., Coulombe, Y., Karam, M., Busatto, F. F., Masson, J., & Richard, S. (2019). Arginine methylation of the DDX 5 helicase RGG / RG motif by PRMT 5 regulates resolution of RNA:DNA hybrids . *The EMBO Journal*, *38*(15), 1–20. https://doi.org/10.15252/embj.2018100986

Michl-Holzinger, P., Obermeyer, S., Markusch, H., Pfab, A., Ettner, A., Bruckmann, A., Babl, S., Längst, G., Schwartz, U., Tvardovskiy, A., Jensen, O. N., Osakabe, A., Berger, F., & Grasser, K. D. (2022). Phosphorylation of the FACT histone chaperone subunit SPT16 affects chromatin at RNA polymerase II transcriptional start sites in Arabidopsis. *Nucleic Acids Research*, *50*(9), 5014–5028. https://doi.org/10.1093/nar/gkac293

Minvielle-Sebastia, L., Winsor, B., Bonneaud, N., & Lacroute, F. (1991). Mutations in

the Yeast RNA14 and RNA15 Genes Result in an Abnormal mRNA Decay Rate; Sequence Analysis Reveals an RNA-Binding Domain in the RNA15 Protein . *Molecular and Cellular Biology*, *11*(6), 3075–3087. https://doi.org/10.1128/mcb.11.6.3075-3087.1991

Mischo, H. E., & Proudfoot, N. J. (2013). Disengaging polymerase: Terminating RNA polymerase II transcription in budding yeast. In *Biochimica et Biophysica Acta - Gene Regulatory Mechanisms* (Vol. 1829, Issue 1, pp. 174–185). https://doi.org/10.1016/j.bbagrm.2012.10.003

Mitchell, A. L., Attwood, T. K., Babbitt, P. C., Blum, M., Bork, P., Bridge, A., Brown, S. D., Chang, H. Y., El-Gebali, S., Fraser, M. I., Gough, J., Haft, D. R., Huang, H., Letunic, I., Lopez, R., Luciani, A., Madeira, F., Marchler-Bauer, A., Mi, H., … Finn, R. D. (2019). InterPro in 2019: Improving coverage, classification and access to protein sequence annotations. *Nucleic Acids Research*, *47*(D1), D351–D360. https://doi.org/10.1093/nar/gky1100

Mitchell, S. F., & Parker, R. (2014). Principles and Properties of Eukaryotic mRNPs. *Molecular Cell*, *54*(4), 547–558. https://doi.org/10.1016/j.molcel.2014.04.033

Mitschka, S., & Mayr, C. (2022). Context-specific regulation and function of mRNA alternative polyadenylation. *Nature Reviews Molecular Cell Biology*, *23*(12), 779–796. https://doi.org/10.1038/s41580-022-00507-5

Moazed, D. (2001). Common themes in mechanisms of gene silencing. *Molecular Cell*, *8*(3), 489–498. https://doi.org/10.1016/S1097-2765(01)00340-9

Monahan, B. J., Villén, J., Marguerat, S., Bähler, J., Gygi, S. P., & Winston, F. (2008). Fission yeast SWI/SNF and RSC complexes show compositional and functional differences from budding yeast. *Nature Structural and Molecular Biology*, *15*(8), 873–880. https://doi.org/10.1038/nsmb.1452

Montpetit, B., Thomsen, N. D., Helmke, K. J., Seeliger, M. A., Berger, J. M., & Weis, K. (2011). A conserved mechanism of DEAD-box ATPase activation by nucleoporins and InsP6 in mRNA export. *Nature*, *472*(7342), 238–244. https://doi.org/10.1038/nature09862

Mooney, S. M., Goel, A., D'Assoro, A. B., Salisbury, J. L., & Janknecht, R. (2010). Pleiotropic effects of p300-mediated acetylation on p68 and p72 RNA helicase. *Journal of Biological Chemistry*, *285*(40), 30443–30452. https://doi.org/10.1074/jbc.M110.143792

Moore, M. J., & Proudfoot, N. J. (2009). Pre-mRNA Processing Reaches Back toTranscription and Ahead to Translation. *Cell*, *136*(4), 688–700. https://doi.org/10.1016/j.cell.2009.02.001

Moore, M. S. J. and M. J. (2003). Pre-mRNA Splicing: Awash in a Sea of Proteins. *Molecular Cell*, *12*, 442–445. https://doi.org/10.1016/B978-0-12-374984-0.01205-5

Moreno, S., Klar, A., & Nurse, P. (1991). Molecular genetic analysis of fission yeast *Schizosaccharomyces pombe*. *Methods in Enzymology*, *194*(C), 795–823. https://doi.org/10.1016/0076-6879(91)94059-L

Motamedi, M. R., & Andre Verdel. (2004). Two RNAi Complexes, RITS and RDRC, Physically Interact and Localize to Noncoding Centromeric RNAs Mohammad.

Cell, *119*(5), 603–614. https://doi.org/10.1016/j.cell.2004.11.034

Moteki, S., & Price, D. (2002). Functional Coupling of Capping and Transcription of mRNA IP experiments in budding yeast demonstrated that Ceg1 and Cet1 crosslink to promoter regions of tran-scribed genes (Komarnitsky et al., 2000) and that muta. *Molecular Cell*, *10*, 599–609.

Mouaikel, J., Causse, S. Z., Rougemaille, M., Daubenton-Carafa, Y., Blugeon, C., Lemoine, S., Devaux, F., Darzacq, X., & Libri, D. (2013). High-Frequency Promoter Firing Links THO Complex Function to Heavy Chromatin Formation. *Cell Reports*, *5*(4), 1082–1094. https://doi.org/10.1016/j.celrep.2013.10.013

Müller-McNicoll, M., Botti, V., de Jesus Domingues, A. M., Brandl, H., Schwich, O. D., Steiner, M. C., Curk, T., Poser, I., Zarnack, K., & Neugebauer, K. M. (2016). SR proteins are NXF1 adaptors that link alternative RNA processing to mRNA export. *Genes and Development*, *30*(5), 553–566. https://doi.org/10.1101/gad.276477.115

Murthy, K. G. K., & Manley, J. L. (1992). Characterization of the multisubunit cleavage-polyadenylation specificity factor from calf thymus. *Journal of Biological Chemistry*, *267*(21), 14804–14811. https://doi.org/10.1016/s0021-9258(18)42111-4

Nakayama, J., Rice, J. C., Strahl, B. D., Allis, C. D., & Grewal, S. I. S. (2001). Role of histone H3 lysine 9 methylation in epigenetic control of heterochromatin assembly. *Science*, *292*(5514), 110–113. https://doi.org/10.1126/science.1060118

Narita, T., Yung, T. M. C., Yamamoto, J., Tsuboi, Y., Tanabe, H., Tanaka, K., Yamaguchi, Y., & Handa, H. (2007). NELF Interacts with CBC and Participates in 3′ End Processing of Replication-Dependent Histone mRNAs. *Molecular Cell*, *26*(3), 349–365. https://doi.org/10.1016/j.molcel.2007.04.011

Nechaev, S., & Adelman, K. (2011). Pol II waiting in the starting gates: Regulating the transition from transcription initiation into productive elongation. *Biochimica et Biophysica Acta - Gene Regulatory Mechanisms*, *1809*(1), 34–45. https://doi.org/10.1016/j.bbagrm.2010.11.001

Nesic, D., Cheng, J., & Maquat, L. E. (1993). Sequences Within the Last Intron function in RNA 3'-End Formation in Cultured Cells. *Molecular and Cellular Biology*, *13*(6), 3359–3369. https://doi.org/10.1128/mcb.13.6.3359-3369.1993

Nielsen, K. H., Chamieh, H., Andersen, C. B. F., Fredslund, F., Hamborg, K., Le Hir, H., & Andersen, G. R. (2009). Mechanism of ATP turnover inhibition in the EJC. *Rna*, *15*(1), 67–75. https://doi.org/10.1261/rna.1283109

Niwa, M., & Berget, S. M. (1991). Mutation of the AAUAAA polyadenylation signal depresses in vitro splicing of proximal but not distal introns. *Genes and Development*, *5*(11), 2086–2095. https://doi.org/10.1101/gad.5.11.2086

Niwa, M., Rose, S. D., & Berget, S. M. (1990). In vitro polyadenylation is stimulated by the presence of an upstream intron. *Genes and Development*, *4*(9), 1552–1559. https://doi.org/10.1101/gad.4.9.1552

Nojima, T., Gomes, T., Grosso, A. R. F., Kimura, H., Dye, M. J., Dhir, S., Carmo-Fonseca, M., & Proudfoot, N. J. (2015). Mammalian NET-seq reveals genome-wide nascent transcription coupled to RNA processing. *Cell*, *161*(3), 526–540.

https://doi.org/10.1016/j.cell.2015.03.027

Nojima, T., Hirose, T., Kimura, H., & Hagiwara, M. (2007). The interaction between cap-binding complex and RNA export factor is required for intronless mRNA export. *Journal of Biological Chemistry*, *282*(21), 15645–15651. https://doi.org/10.1074/jbc.M700629200

Nosella, M. L., & Forman-Kay, J. D. (2021). Phosphorylation-dependent regulation of messenger RNA transcription, processing and translation within biomolecular condensates. *Current Opinion in Cell Biology*, *69*, 30–40. https://doi.org/10.1016/j.ceb.2020.12.007

Nousch, M., Techritz, N., Hampel, D., Millonigg, S., & Eckmann, C. R. (2013). The Ccr4-Not deadenylase complex constitutes the main poly(A) removal activity in C. elegans. *Journal of Cell Science*, *126*(18), 4274–4285. https://doi.org/10.1242/jcs.132936

O'Reilly, D., Kuznetsova, O. V., Laitem, C., Zaborowska, J., Dienstbier, M., & Murphy, S. (2014). Human snRNA genes use polyadenylation factors to promote efficient transcription termination. *Nucleic Acids Research*, *42*(1), 264–275. https://doi.org/10.1093/nar/gkt892

Osman, S., & Cramer, P. (2020). Structural Biology of RNA Polymerase II Transcription: 20 Years on. *Annual Review of Cell and Developmental Biology*, *36*, 1–34. https://doi.org/10.1146/annurev-cellbio-042020-021954

Ozdilek, B. A., Thompson, V. F., Ahmed, N. S., White, C. I., Batey, R. T., & Schwartz, J. C. (2017). Intrinsically disordered RGG/RG domains mediate degenerate specificity in RNA binding. *Nucleic Acids Research*, *45*(13), 7984–7996. https://doi.org/10.1093/nar/gkx460

Palazzo, A. F., Qiu, Y., & Kang, Y. M. (2024). mRNA nuclear export : how mRNA identity features distinguish functional RNAs from junk transcripts junk transcripts. *RNA Biology*, *21*(1), 1–12. https://doi.org/10.1080/15476286.2023.2293339

Pancevac, C., Goldstone, D. C., Ramos, A., & Taylor, I. A. (2010). Structure of the Rna15 RRM-RNA complex reveals the molecular basis of GU specificity in transcriptional 3'-end processing factors. *Nucleic Acids Research*, *38*(9), 3119–3132. https://doi.org/10.1093/nar/gkq002

Parker, R., Siliciano, P. G., & Guthrie, C. (1987). Recognition of the TACTAAC box during mRNA splicing in yeast involves base pairing to the U2-like snRNA. *Cell*, *49*(2), 229–239. https://doi.org/10.1016/0092-8674(87)90564-2

Parua, P. K., Booth, G. T., Sansó, M., Benjamin, B., Tanny, J. C., Lis, J. T., & Fisher, R. P. (2018). A Cdk9-PP1 switch regulates the elongation-termination transition of RNA polymerase II. *Nature*, *558*(7710), 460–464. https://doi.org/10.1038/s41586-018-0214-z

Passmore, L. A., & Coller, J. (2022). Roles of mRNA poly(A) tails in regulation of eukaryotic gene expression. *Nature Reviews Molecular Cell Biology*, *23*(2), 93–106. https://doi.org/10.1038/s41580-021-00417-y

Pause, A., & Sonenberg, N. (1992). Mutational analysis of a DEAD box RNA helicase: The mammalian translation initiation factor eIF-4A. *EMBO Journal*, *11*(7), 2643–2654. https://doi.org/10.1002/j.1460-2075.1992.tb05330.x

Pavri, R., Zhu, B., Li, G., Trojer, P., Mandal, S., Shilatifard, A., & Reinberg, D. (2006). Histone H2B Monoubiquitination Functions Cooperatively with FACT to Regulate Elongation by RNA Polymerase II. *Cell*, *125*(4), 703–717. https://doi.org/10.1016/j.cell.2006.04.029

Peña, Á., Gewartowski, K., Mroczek, S., Cuéllar, J., Szykowska, A., Prokop, A., Czarnocki-Cieciura, M., Piwowarski, J., Tous, C., Aguilera, A., Carrascosa, J. L., Valpuesta, J. M., & Dziembowski, A. (2012). Architecture and nucleic acids recognition mechanism of the THO complex, an mRNP assembly factor. *EMBO Journal*, *31*(6), 1605–1616. https://doi.org/10.1038/emboj.2012.10

Peng, J., Zhu, Y., Milton, J. T., & Price, D. H. (1998). Identification of multiple cyclin subunits of human P-TEFb. *Genes and Development*, *12*(5), 755–762. https://doi.org/10.1101/gad.12.5.755

Pérez-Cãadillas, J. M. (2006). Grabbing the message: Structural basis of mRNA 3′UTR recognition by Hrp1. *EMBO Journal*, *25*(13), 3167–3178. https://doi.org/10.1038/sj.emboj.7601190

Perreault, A., Lemieux, C., & Bachand, F. (2007). Regulation of the nuclear poly(A)-binding protein by arginine methylation in fission yeast. *Journal of Biological Chemistry*, *282*(10), 7552–7562. https://doi.org/10.1074/jbc.M610512200

Perriman, R., Barta, I., Voeltz, G. K., Abelsont, J., & Ares, M. (2003). ATP requirement for Prp5p function is determined by Cus2p and the structure of U2 small nuclear RNA. *Proceedings of the National Academy of Sciences of the United States of America*, *100*(SUPPL. 2), 13857–13862. https://doi.org/10.1073/pnas.2036312100

Pinto, P. A. B., Henriques, T., Freitas, M. O., Martins, T., Domingues, R. G., Wyrzykowska, P. S., Coelho, P. A., Carmo, A. M., Sunkel, C. E., Proudfoot, N. J., & Moreira, A. (2011). RNA polymerase II kinetics in polo polyadenylation signal selection. *EMBO Journal*, *30*(12), 2431–2444. https://doi.org/10.1038/emboj.2011.156

Porrua, O., Boudvillain, M., & Libri, D. (2016). Transcription Termination: Variations on Common Themes. In *Trends in Genetics* (Vol. 32, Issue 8, pp. 508–522). Elsevier Ltd. https://doi.org/10.1016/j.tig.2016.05.007

Porrua, O., & Libri, D. (2013). RNA quality control in the nucleus: The Angels' share of RNA. *Biochimica et Biophysica Acta - Gene Regulatory Mechanisms*, *1829*(6–7), 604–611. https://doi.org/10.1016/j.bbagrm.2013.02.012

Porrua, O., & Libri, D. (2015). Transcription termination and the control of the transcriptome: Why, where and how to stop. *Nature Reviews Molecular Cell Biology*, *16*(3), 190–202. https://doi.org/10.1038/nrm3943

Pryor, A., Tung, L., Yang, Z., Kapadia, F., Chang, T. H., & Johnson, L. F. (2004). Growth-regulated expression and G0-specific turover of the mRNA that encodes URH49, a mammalian DExH/D box protein that is highly related to the mRNA export protein UAP56. *Nucleic Acids Research*, *32*(6), 1857–1865. https://doi.org/10.1093/nar/gkh347

Pühringer, T., Hohmann, U., Fin, L., Pacheco-Fiallos, B., Schellhaas, U., Brennecke, J., & Plaschka, C. (2020). Structure of the human core transcription-export

complex reveals a hub for multivalent interactions. *ELife*, *9*, 1–65. https://doi.org/10.7554/eLife.61503

Putnam, A. A., & Jankowsky, E. (2013a). AMP sensing by DEAD-box RNA helicases. *Journal of Molecular Biology*, *425*(20), 3839–3845. https://doi.org/10.1016/j.jmb.2013.05.006

Putnam, A. A., & Jankowsky, E. (2013b). DEAD-box helicases as integrators of RNA, nucleotide and protein binding. *Biochimica et Biophysica Acta - Gene Regulatory Mechanisms*, *1829*(8), 884–893. https://doi.org/10.1016/j.bbagrm.2013.02.002

Pyle, A. M. (2008). Translocation and unwinding mechanisms of RNA and DNA helicases. *Annual Review of Biophysics*, *37*, 317–336. https://doi.org/10.1146/annurev.biophys.37.032807.125908

Qiu, C., Arora, P., Malik, I., Laperuta, A. J., Pavlovic, E. M., Ugochukwu, S., Naik, M., & Kaplan, C. D. (2024). Thiolutin has complex effects in vivo but is a direct inhibitor of RNA polymerase II in vitro . *Nucleic Acids Research*, 1–19. https://doi.org/10.1093/nar/gkad1258

Qu, X., Lykke-Andersen, S., Nasser, T., Saguez, C., Bertrand, E., Jensen, T. H., & Moore, C. (2009). Assembly of an Export-Competent mRNP Is Needed for Efficient Release of the 3′-End Processing Complex after Polyadenylation. *Molecular and Cellular Biology*, *29*(19), 5327–5338. https://doi.org/10.1128/mcb.00468-09

Qualmann, B., & Kessels, M. M. (2021). The role of protein arginine methylation as post-translational modification on actin cytoskeletal components in neuronal structure and function. *Cells*, *10*(5). https://doi.org/10.3390/cells10051079

Ramanathan, A., Robb, G. B., & Chan, S. H. (2016). mRNA capping: Biological functions and applications. *Nucleic Acids Research*, *44*(16), 7511–7526. https://doi.org/10.1093/nar/gkw551

Reed, R., & Cheng, H. (2005). TREX, SR proteins and export of mRNA. *Current Opinion in Cell Biology*, *17*(3), 269–273. https://doi.org/10.1016/j.ceb.2005.04.011

Reed, R., & Hurt, E. (2002). A conserved mRNA export machinery coupled to pre-mRNA splicing. *Cell*, *108*(4), 523–531. https://doi.org/10.1016/S0092-8674(02)00627-X

Reimer, K. A., Mimoso, C. A., Adelman, K., & Neugebauer, K. M. (2021). Co-transcriptional splicing regulates 3′ end cleavage during mammalian erythropoiesis. *Molecular Cell*, *81*(5), 998-1012.e7. https://doi.org/10.1016/j.molcel.2020.12.018

Richard, P., & Manley, J. L. (2009). Transcription termination by nuclear RNA polymerases. *Genes and Development*, *23*(11), 1247–1269. https://doi.org/10.1101/gad.1792809

Robinson, J. T., Thorvaldsdottir, H., Turner, D., & Mesirov, J. P. (2023). igv.js: an embeddable JavaScript implementation of the Integrative Genomics Viewer (IGV). *Bioinformatics (Oxford, England)*, *39*(1), 23–24. https://doi.org/10.1093/bioinformatics/btac830

Robinson, J. T., Thorvaldsdóttir, H., Wenger, A. M., Zehir, A., & Mesirov, J. P. (2017).

Variant review with the integrative genomics viewer. *Cancer Research*, *77*(21), e31–e34. https://doi.org/10.1158/0008-5472.CAN-17-0337

Robinson, J. T., Thorvaldsdóttir, H., Winckler, W., Guttman, M., Lander, E. S., Getz, G., & Mesirov, J. P. (2011). Integrative genomics viewer. *Nature Biotechnology*, *29*(1), 24–26. https://doi.org/10.1038/nbt.1754

Rocak, S., & Linder, P. (2004). Dead-box proteins: The driving forces behind RNA metabolism. *Nature Reviews Molecular Cell Biology*, *5*(3), 232–241. https://doi.org/10.1038/nrm1335

Rodrigues, J. P. (2001). REF proteins mediate the export of spliced and unspliced mRNAs from the nucleus. *Proceedings of the National Academy of Sciences*, *98*(3), 1030–1035. https://doi.org/10.1073/pnas.031586198

Rodríguez-Molina, J. B., West, S., & Passmore, L. A. (2023). Knowing when to stop: Transcription termination on protein-coding genes by eukaryotic RNAPII. *Molecular Cell*, *83*(3), 404–415. https://doi.org/10.1016/j.molcel.2022.12.021

Rogers, G. W., Richter, N. J., Lima, W. F., & Merrick, W. C. (2001). Modulation of the Helicase Activity of eIF4A by eIF4B, eIF4H, and eIF4F. *Journal of Biological Chemistry*, *276*(33), 30914–30922. https://doi.org/10.1074/jbc.M100157200

Rossow, K. L., & Janknecht, R. (2003). Synergism between p68 RNA helicase and the transcriptional coactivators CBP and p300. *Oncogene*, *22*(1), 151–156. https://doi.org/10.1038/sj.onc.1206067

Rougemaille, M., Dieppois, G., Kisseleva-Romanova, E., Gudipati, R. K., Lemoine, S., Blugeon, C., Boulay, J., Jensen, T. H., Stutz, F., Devaux, F., & Libri, D. (2008). THO/Sub2p Functions to Coordinate 3′-End Processing with Gene-Nuclear Pore Association. In *Cell* (Vol. 135, Issue 2, pp. 308–321). https://doi.org/10.1016/j.cell.2008.08.005

Rougemaille, M., Gudipati, R. K., Olesen, J. R., Thomsen, R., Seraphin, B., Libri, D., & Jensen, T. H. (2007). Dissecting mechanisms of nuclear mRNA surveillance in THO/sub2 complex mutants. *EMBO Journal*, *26*(9), 2317–2326. https://doi.org/10.1038/sj.emboj.7601669

Rozen, F., Edery, I., Meerovitch, K., Dever, T. E., Merrick, W. C., & Sonenberg, N. (1990). Bidirectional RNA helicase activity of eucaryotic translation initiation factors 4A and 4F. *Molecular and Cellular Biology*, *10*(3), 1134–1144. https://doi.org/10.1128/mcb.10.3.1134

Ruepp, M.-D., Chiara Aringhieri, Silvia Vivarelli, S. C., & Simona Paro, Daniel Schumperli, and S. M. L. B. (2009). Mammalian pre-mRNA 3' End Processing Factor CF Im68 Functions in mRNA Export. *Molecular Biology of the Cell*, *20*, 5211–5223. https://doi.org/10.1091/mbc.e09-05-0389

Russell, P., & Nurse, P. (1986). *Schizosaccharomyces pombe* and *saccharomyces cerevisiae:* A look at yeasts divided. *Cell*, *45*(6), 781–782. https://doi.org/10.1016/0092-8674(86)90550-7

Saavedra, C., Tuug, K. S., Amberg, D. C., Hopper, A. K., & Cole, C. N. (1996). Regulation of mRNA export in response to stress in *Saccharomyces cerevisiae*. *Genes and Development*, *10*(13), 1608–1620. https://doi.org/10.1101/gad.10.13.1608

Sadowski, M., Dichtl, B., Hübner, W., & Keller, W. (2003). Independent functions of yeast Pcf11p in pre-mRNA 3′ end processing and in transcription termination. In *EMBO Journal* (Vol. 22, Issue 9, pp. 2167–2177). https://doi.org/10.1093/emboj/cdg200

Saldi, T., Cortazar, M. A., Sheridan, R. M., & Bentley, D. L. (2016). Coupling of RNA Polymerase II Transcription Elongation with Pre-mRNA Splicing. *Journal of Molecular Biology*, *428*(12), 2623–2635. https://doi.org/10.1016/j.jmb.2016.04.017

Salzman, D. W., Shubert-Coleman, J., & Furneaux, H. (2007). P68 RNA helicase unwinds the human let-7 microRNA precursor duplex and is required for let-7-directed silencing of gene expression. *Journal of Biological Chemistry*, *282*(45), 32773–32779. https://doi.org/10.1074/jbc.M705054200

Sami, A. A., Arabia, S., Sarker, R. H., & Islam, T. (2021). Deciphering the role of helicases and translocases: A multifunctional gene family safeguarding plants from diverse environmental adversities. *Current Plant Biology*, *26*, 100204. https://doi.org/10.1016/j.cpb.2021.100204

Sansó, M., & Fisher, R. P. (2013). Pause, play, repeat: CDKs push RNAP II's buttons. *Transcription*, *4*(4), 146–152. https://doi.org/10.4161/trns.25146

Sarkar, M., & Ghosh, M. K. (2016). DEAD box RNA helicases: Crucial regulators of gene expression and oncogenesis. *Frontiers in Bioscience - Landmark*, *21*(2), 225–250. https://doi.org/10.2741/4386

Saunders, A., Werner, J., Andrulis, E. D., Nakayama, T., Hirose, S., Reinberg, D., & Lis, J. T. (2003). Tracking FACT and the RNA polymerase II elongation complex through chromatin in vivo. *Science*, *301*(5636), 1094–1096. https://doi.org/10.1126/science.1085712

Schindelin, J., Arganda-Carreras, I., Frise, E., Kaynig, V., Longair, M., Pietzsch, T., Preibisch, S., Rueden, C., Saalfeld, S., Schmid, B., Tinevez, J. Y., White, D. J., Hartenstein, V., Eliceiri, K., Tomancak, P., & Cardona, A. (2012). Fiji: An open-source platform for biological-image analysis. *Nature Methods*, *9*(7), 676–682. https://doi.org/10.1038/nmeth.2019

Schlackow, M., Marguerat, S., Proudfoot, N. J., Ḧahler, J., Erban, R., & Gullerova, M. (2013). Genome-wide analysis of poly(A) site selection in *Schizosaccharomyces pombe*. *Rna*, *19*(12), 1617–1631. https://doi.org/10.1261/rna.040675.113

Schul, W., Groenhout, B., Koberna, K., Takagaki, Y., Jenny, A., Manders, E. M. M., Raška, I., Van Driel, R., & De Jong, L. (1996). The RNA 3′ cleavage factors CstF 64 kDa and CPSF 100 kDa are concentrated in nuclear domains closely associated with coiled bodies and newly synthesized RNA. *EMBO Journal*, *15*(11), 2883–2892. https://doi.org/10.1002/j.1460-2075.1996.tb00649.x

Schwer, B. (2001). A new twist on RNA helicases: DExH/D box proteins as RNPases. *Nature Structural Biology*, *8*(2), 113–116. https://doi.org/10.1038/84091

Schwer, Beate, & Shuman, S. (2011). Deciphering the RNA Polymerase II CTD Code in Fission Yeast. *Molecular Cell*, *43*(2), 311–318. https://doi.org/10.1016/j.molcel.2011.05.024

Sengoku, T., Nureki, O., Nakamura, A., Kobayashi, S., & Yokoyama, S. (2006).

Structural Basis for RNA Unwinding by the DEAD-Box Protein Drosophila Vasa. *Cell*, *125*(2), 287–300. https://doi.org/10.1016/j.cell.2006.01.054

Sevim Ozgur, Gretel Buchwald, Sebastian Falk, Sutapa Chakrabarti, J. R. P. and E. C. (2015). The FEBS Journal - 2015 - Ozgur - The conformational plasticity of eukaryotic RNA-dependent ATPases.pdf. *850 FEBS Journal*, *282*, 850–863. https://doi.org/doi:10.1111/febs.13198

Shandilya, J., & Roberts, S. G. E. (2012). The transcription cycle in eukaryotes: From productive initiation to RNA polymerase II recycling. *Biochimica et Biophysica Acta - Gene Regulatory Mechanisms*, *1819*(5), 391–400. https://doi.org/10.1016/j.bbagrm.2012.01.010

Shatkin, A. J., & Manley, J. L. (2000). The ends of the affair: Capping and polyadenylation. *Nature Structural Biology*, *7*(10), 838–842. https://doi.org/10.1038/79583

Shi, M., Zhang, H., Wu, X., He, Z., Wang, L., Yin, S., Tian, B., Li, G., & Cheng, H. (2017). ALYREF mainly binds to the 5′ and the 3′ regions of the mRNA in vivo. *Nucleic Acids Research*, *45*(16), 9640–9653. https://doi.org/10.1093/nar/gkx597

Shi, Y., Chan, S., & Martinez-Santibañez, G. (2009). An up-close look at the pre-mRNA 3'-end processing complex. *RNA Biology*, *6*(5), 522–525. https://doi.org/10.4161/rna.6.5.9554

Shi, Y., Di Giammartino, D. C., Taylor, D., Sarkeshik, A., Rice, W. J., Yates, J. R., Frank, J., & Manley, J. L. (2009). Molecular Architecture of the Human Pre-mRNA 3′ Processing Complex. In *Molecular Cell* (Vol. 33, Issue 3, pp. 365–376). https://doi.org/10.1016/j.molcel.2008.12.028

Shi, Y., & Manley, J. L. (2015). The end of the message: Multiple protein–RNA interactions define the mRNA polyadenylation site. *Genes and Development*, *29*(9), 889–897. https://doi.org/10.1101/gad.261974.115

Shichino, Y., Otsubo, Y., Yamamoto, M., & Yamashita, A. (2020). Meiotic gene silencing complex MTREC/NURS recruits the nuclear exosome to YTH-RNA-binding protein Mmi1. *PLoS Genetics*, *16*(2), 1–19. https://doi.org/10.1371/journal.pgen.1008598

Shimada, A., Dohke, K., Sadaie, M., Shinmyozu, K., Nakayama, J. I., Urano, T., & Murakami, Y. (2009). Phosphorylation of Swi6/HP1 regulates transcriptional gene silencing at heterochromatin. *Genes and Development*, *23*(1), 18–23. https://doi.org/10.1101/gad.1708009

Shoichet, B. K., Baase, W. A., Kuroki, R., & Matthews, B. W. (1995). A relationship between protein stability and protein function. *Proceedings of the National Academy of Sciences of the United States of America*, *92*(2), 452–456. https://doi.org/10.1073/pnas.92.2.452

Shuman, S. (2000). Structure, mechanism, and evolution of the mRNA capping apparatus. *Progress in Nucleic Acid Research and Molecular Biology*, *66*, 1–40. https://doi.org/10.1016/s0079-6603(00)66025-7

Silla, T., Karadoulama, E., Mąkosa, D., Lubas, M., & Jensen, T. H. (2018). The RNA Exosome Adaptor ZFC3H1 Functionally Competes with Nuclear Export Activity to Retain Target Transcripts. *Cell Reports*, *23*(7), 2199–2210.

https://doi.org/10.1016/j.celrep.2018.04.061

Singh, G., Pratt, G., Yeo, G. W., & Moore, M. J. (2015). The clothes make the mRNA: Past and present trends in mRNP fashion. *Annual Review of Biochemistry*, *84*, 325–354. https://doi.org/10.1146/annurev-biochem-080111-092106

Singleton, M. R., Dillingham, M. S., & Wigley, D. B. (2007). Structure and mechanism of helicases and nucleic acid translocases. *Annual Review of Biochemistry*, *76*, 23–50. https://doi.org/10.1146/annurev.biochem.76.052305.115300

Snyder, N. A., & Silva, G. M. (2021). Deubiquitinating enzymes (DUBs): Regulation, homeostasis, and oxidative stress response. *Journal of Biological Chemistry*, *297*(3), 101077. https://doi.org/10.1016/j.jbc.2021.101077

So, B. R., Di, C., Cai, Z., Venters, C. C., Guo, J., Oh, J. M., Arai, C., & Dreyfuss, G. (2019). A Complex of U1 snRNP with Cleavage and Polyadenylation Factors Controls Telescripting, Regulating mRNA Transcription in Human Cells. *Molecular Cell*, *76*(4), 590-599.e4. https://doi.org/10.1016/j.molcel.2019.08.007

Somesh, B. P., Reid, J., Liu, W. F., Søgaard, T. M. M., Erdjument-Bromage, H., Tempst, P., & Svejstrup, J. Q. (2005). Multiple mechanisms confining RNA polymerase II ubiquitylation to polymerases undergoing transcriptional arrest. *Cell*, *121*(6), 913–923. https://doi.org/10.1016/j.cell.2005.04.010

Song, Q. X., Liu, N. N., Liu, Z. X., Zhang, Y. Z., Rety, S., Hou, X. M., & Xi, X. G. (2023). Nonstructural N- and C-tails of Dbp2 confer the protein full helicase activities. *Journal of Biological Chemistry*, *299*(5), 104592. https://doi.org/10.1016/j.jbc.2023.104592

Soni, K., Sivadas, A., Horvath, A., Dobrev, N., Hayashi, R., Kiss, L., Simon, B., Wild, K., Sinning, I., & Fischer, T. (2023). Mechanistic insights into RNA surveillance by the canonical poly(A) polymerase Pla1 of the MTREC complex. *Nature Communications*, *14*(1). https://doi.org/10.1038/s41467-023-36402-6

Staley, J. P., & Guthrie, C. (1998). Mechanical devices of the spliceosome: Motors, clocks, springs, and things. *Cell*, *92*(3), 315–326. https://doi.org/10.1016/S0092-8674(00)80925-3

Staley, J. P., & Guthrie, C. (1999). An RNA switch at the 5’ splice site requires ATP and the DEAD box protein Prp28p. In *Molecular Cell* (Vol. 3, Issue 1, pp. 55–64). https://doi.org/10.1016/S1097-2765(00)80174-4

Sträßer, K., Masuda, S., Mason, P., Pfannstiel, J., Oppizzi, M., Rodriguez-Navarro, S., Rondón, A. G., Aguilera, A., Struhl, K., Reed, R., & Hurt, E. (2002). TREX is a conserved complex coupling transcription with messenger RNA export. *Nature*, *417*(6886), 304–308. https://doi.org/10.1038/nature746

Steimer, L., & Klostermeier, D. (2012). RNA helicases in infection and disease. *RNA Biology*, *9*(6), 751–771. https://doi.org/10.4161/rna.20090

Steinmetz, E. J., Conrad, N. K., Brow, D. A., & Corden, J. L. (2001). RNA-binding protein Nrd1 directs poly(A)-independent 3′-end formation of RNA polymerase II transcripts. In *Nature* (Vol. 413, Issue 6853, pp. 327–331). https://doi.org/10.1038/35095090

Steitz, J. A., Dreyfuss, G., Krainer, A. R., Lamond, A. I., Matera, A. G., & Padgett, R.

A. (2008). Where in the cell is the minor spliceosome? *Proceedings of the National Academy of Sciences of the United States of America*, *105*(25), 8485–8486. https://doi.org/10.1073/pnas.0804024105

Steitz, K. M. W. and J. A. (1993). Association with terminal exons in pre- mRNAs: a new role for the U1 snRNP. *Genes and Development*, 647–659. https://doi.org/0890-9369/93

Sträßer, K., & Hurt, E. (2001). Splicing factor Sub2p is required for nuclear mRNA export through its interaction with Yra1p. *Nature*, *413*(6856), 648–652. https://doi.org/10.1038/35098113

Stutz, F., & Izaurralde, E. (2003). The interplay of nuclear mRNP assembly, mRNA surveillance and export. *Trends in Cell Biology*, *13*(6), 319–327. https://doi.org/10.1016/S0962-8924(03)00106-5

Sugiyama, T., & Sugioka-Sugiyama, R. (2011). Red1 promotes the elimination of meiosis-specific mRNAs in vegetatively growing fission yeast. *EMBO Journal*, *30*(6), 1027–1039. https://doi.org/10.1038/emboj.2011.32

Sugiyama, T., Sugioka-Sugiyama, R., Hada, K., & Niwa, R. (2012). Rhn1, a nuclear protein, is required for suppression of meiotic mRNAs in mitotically dividing fission yeast. *PLoS ONE*, *7*(8), 1–9. https://doi.org/10.1371/journal.pone.0042962

Sugiyama, T., Wanatabe, N., Kitahata, E., Tani, T., & Sugioka-Sugiyama, R. (2013). Red5 and three nuclear pore components are essential for efficient suppression of specific mRNAs during vegetative growth of fission yeast. *Nucleic Acids Research*, *41*(13), 6674–6686. https://doi.org/10.1093/nar/gkt363

Susan McCracken, Nova Fong, Krasslmlr Yankulov, Scott Ballantyne, Guohua Pant, Jack Greenblattt, Scott D. Patterson, M. W. & D. L. B. (1997). The C-terminal domain of RNA polymerase II couples mRNA processing to transcription. *Nature*, *385*, 357–361. https://doi.org/10.1038/385357a0

Suzuki, H. I., Yamagata, K., Sugimoto, K., Iwamoto, T., Kato, S., & Miyazono, K. (2009). Modulation of microRNA processing by p53. *Nature*, *460*(7254), 529–533. https://doi.org/10.1038/nature08199

Tang, P., Yang, Y., Li, G., Huang, L., Wen, M., Ruan, W., Guo, X., Zhang, C., Zuo, X., Luo, D., Xu, Y., Fu, X. D., & Zhou, Y. (2022). Alternative polyadenylation by sequential activation of distal and proximal PolyA sites. *Nature Structural and Molecular Biology*, *29*(1), 21–31. https://doi.org/10.1038/s41594-021-00709-z

Tang, Z., Yanagida, M., & Lin, R. J. (1998). Fission yeast mitotic regulator Dsk1 is an SR protein-specific kinase. *Journal of Biological Chemistry*, *273*(10), 5963–5969. https://doi.org/10.1074/jbc.273.10.5963

Taniguchi, I., & Ohno, M. (2008). ATP-Dependent Recruitment of Export Factor Aly/REF onto Intronless mRNAs by RNA Helicase UAP56. *Molecular and Cellular Biology*, *28*(2), 601–608. https://doi.org/10.1128/mcb.01341-07

Tanner, N. K. (2003). The newly identified Q motif of DEAD box helicases is involved in adenine recognition. *Cell Cycle (Georgetown, Tex.)*, *2*(1), 18–19. https://doi.org/10.4161/cc.2.1.296

Tanner, N. K., Cordin, O., Banroques, J., Doère, M., & Linder, P. (2003). The Q motif:

A newly identified motif in DEAD box helicases may regulate ATP binding and hydrolysis. *Molecular Cell*, *11*(1), 127–138. https://doi.org/10.1016/S1097-2765(03)00006-6

Tanner, N. K., & Linder, P. (2001). DExD/H box RNA helicases: From generic motors to specific dissociation functions. *Molecular Cell*, *8*(2), 251–262. https://doi.org/10.1016/S1097-2765(01)00329-X

Taschuk, F., Tapescu, I., & Moy, R. H. (2020). DDX56 binds to chikungunya virus RNA to control infection. *mBio,* 11:e02623-20. https://doi.org/10.1128/mBio.02623-20

Tedeschi, F. A., Cloutier, S. C., Tran, E. J., & Jankowsky, E. (2018). The DEAD-box protein Dbp2p is linked to noncoding RNAs, the helicase Sen1p, and R-loops. *Rna*, *24*(12), 1693–1705. https://doi.org/10.1261/rna.067249.118

Terrone, S., Valat, J., Fontrodona, N., Giraud, G., Claude, J. B., Combe, E., Lapendry, A., Polvèche, H., Ameur, L. Ben, Duvermy, A., Modolo, L., Bernard, P., Mortreux, F., Auboeuf, D., & Bourgeois, C. F. (2022). RNA helicase-dependent gene looping impacts messenger RNA processing. *Nucleic Acids Research*, *50*(16), 9226–9246. https://doi.org/10.1093/nar/gkac717

Thandapani, P., O'Connor, T. R., Bailey, T. L., & Richard, S. (2013). Defining the RGG/RG Motif. *Molecular Cell*, *50*(5), 613–623. https://doi.org/10.1016/j.molcel.2013.05.021

Cordin, O., Tanner, N K., Doe`re, M., Linder, P., and Banroques, J. (2004). The newly discovered Q motif of DEAD-box RNA helicases regulates RNA-binding and helicase activity *The EMBO Journal,* 23: 2478 - 2487, https://doi.org/10.1038/sj.emboj.7600272

Theissen, B., Karow, A. R., Köhler, J., Gubaev, A., & Klostermeier, D. (2008). Cooperative binding of ATP and RNA induces a closed conformation in a DEAD box RNA helicase. *Proceedings of the National Academy of Sciences of the United States of America*, *105*(2), 548–553. https://doi.org/10.1073/pnas.0705488105

Thorvaldsdóttir, H., Robinson, J. T., & Mesirov, J. P. (2013). Integrative Genomics Viewer (IGV): High-performance genomics data visualization and exploration. *Briefings in Bioinformatics*, *14*(2), 178–192. https://doi.org/10.1093/bib/bbs017

Tokuriki, N., Stricher, F., Serrano, L., & Tawfik, D. S. (2008). How protein stability and new functions trade off. *PLoS Computational Biology*, *4*(2), 35–37. https://doi.org/10.1371/journal.pcbi.1000002

Tomohiro Yamazaki, Naoko Fujiwara, Hiroko Yukinaga, Miki Ebisuya, Takuya Shiki, Tomoya Kurihara, N. K., & Taiho Kambe, Masaya Nagao, Eisuke Nishida, and S. M. (2010). The Closely Related RNA helicases, UAP56 and URH49, Preferentially Form Distinct mRNA Export Machineries and Coordinately Regulate Mitotic Progression. *Molecular Biology of the Cell*, *21*, 2953–2965. https://doi.org/10.1091/mbc.E09–10–0913

Tran, E. J., Zhou, Y., Corbett, A. H., & Wente, S. R. (2007). The DEAD-Box Protein Dbp5 Controls mRNA Export by Triggering Specific RNA:Protein Remodeling Events. *Molecular Cell*, *28*(5), 850–859. https://doi.org/10.1016/j.molcel.2007.09.019

Tseng, S. S. I., Weaver, P. L., Liu, Y., Hitomi, M., Tartakoff, A. M., & Chang, T. H.

(1998). Dbp5p, a cytosolic RNA helicase, is required for poly(A)+ RNA export. *EMBO Journal*, *17*(9), 2651–2662. https://doi.org/10.1093/emboj/17.9.2651

Tudek, A., Porrua, O., Kabzinski, T., Lidschreiber, M., Kubicek, K., Fortova, A., Lacroute, F., Vanacova, S., Cramer, P., Stefl, R., & Libri, D. (2014). Molecular basis for coordinating transcription termination with noncoding RNA degradation. *Molecular Cell*, *55*(3), 467–481. https://doi.org/10.1016/j.molcel.2014.05.031

Turtola, M., Manav, C. M., Kumar, A., Tudek, A., Mroczek, S., Krawczyk, P. S., Dziembowski, A., Schmid, M., Passmore, L. A., Casanal, A., & Jensen, T. H. (2021). Three-layered control of mRNA poly(A) tail synthesis in *Saccharomyces cerevisiae*. *Genes and Development*, *35*(17–18), 1290–1303. https://doi.org/10.1101/GAD.348634.121

Vagner, S., Rüegsegger, U., Gunderson, S. I., Keller, W., & Mattaj, I. W. (2000). Position-dependent inhibition of the cleavage step of pre-mRNA 3'-end processing by U1 snRNP. *Rna*, *6*(2), 178–188. https://doi.org/10.1017/S1355838200991854

Vasiljeva, L., & Buratowski, S. (2006). Nrd1 interacts with the nuclear exosome for 3′ processing of RNA polymerase II transcripts. In *Molecular Cell* (Vol. 21, Issue 2, pp. 239–248). https://doi.org/10.1016/j.molcel.2005.11.028

Vasiljeva, L., Kim, M., Mutschler, H., Buratowski, S., & Meinhart, A. (2008). The Nrd1-Nab3-Sen1 termination complex interacts with the Ser5-phosphorylated RNA polymerase II C-terminal domain. *Nature Structural and Molecular Biology*, *15*(8), 795–804. https://doi.org/10.1038/nsmb.1468

Verdel. (2013). *RNAi-Mediated Targeting of Heterochromatin by the RITS*. *303*(October).

Vo, T. V., Dhakshnamoorthy, J., Larkin, M., Zofall, M., Thillainadesan, G., Balachandran, V., Holla, S., Wheeler, D., & Grewal, S. I. S. (2019). CPF Recruitment to Non-canonical Transcription Termination Sites Triggers Heterochromatin Assembly and Gene Silencing. *Cell Reports*, *28*(1), 267-281.e5. https://doi.org/10.1016/j.celrep.2019.05.107

Volpe, T. A., Kidner, C., Hall, I. M., Teng, G., Grewal, S. I. S., & Martienssen, R. A. (2002). Regulation of heterochromatic silencing and histone H3 lysine-9 methylation by RNAi. *Science*, *297*(5588), 1833–1837. https://doi.org/10.1126/science.1074973

Vyas, A., Freitas, A. V., Ralston, Z. A., & Tang, Z. (2021). Fission Yeast *Schizosaccharomyces pombe*: A Unicellular "Micromammal" Model Organism. *Current Protocols*, *1*(6), 1–24. https://doi.org/10.1002/cpz1.151

Wahl, M. C., Will, C. L., & Lührmann, R. (2009). The Spliceosome: Design Principles of a Dynamic RNP Machine. *Cell*, *136*(4), 701–718. https://doi.org/10.1016/j.cell.2009.02.009

Walsh, M. J., Hautbergue, G. M., & Wilson, S. A. (2010). Structure and function of mRNA export adaptors. *Biochemical Society Transactions*, *38*(1), 232–236. https://doi.org/10.1042/BST0380232

Wang, H., Gao, X., Huang, Y., Yang, J., & Liu, Z. R. (2009). P68 RNA helicase is a nucleocytoplasmic shuttling protein. *Cell Research*, *19*(12), 1388–1400. https://doi.org/10.1038/cr.2009.113

Wang, J., Han, C., Wang, J., & Peng, Q. (2023). RNA helicase DDX5-induced circPHF14 promotes gastric cancer cell progression. *Aging*, *15*(7), 2525–2540. https://doi.org/10.18632/aging.204623

Wang, Y., Fan, J., Wang, J., Zhu, Y., Xu, L., Tong, D., & Cheng, H. (2021). ZFC3H1 prevents RNA trafficking into nuclear speckles through condensation. *Nucleic Acids Research*, *49*(18), 10630–10643. https://doi.org/10.1093/nar/gkab774

Weirich, C. S., Erzberger, J. P., Flick, J. S., Berger, J. M., Thorner, J., & Weis, K. (2006). Activation of the DExD/H-box protein Dbp5 by the nuclear-pore protein Gle1 and its coactivator InsP6 is required for mRNA export. *Nature Cell Biology*, *8*(7), 668–676. https://doi.org/10.1038/ncb1424

Weis, K., & Hondele, M. (2022). The Role of DEAD-Box ATPases in Gene Expression and the Regulation of RNA-Protein Condensates. *Annual Review of Biochemistry*, *91*, 197–219. https://doi.org/10.1146/annurev-biochem-032620-105429

West, S., Gromak, N., & Proudfoot, N. J. (2004). Human 5′ → 3′ exonuclease Xm2 promotes transcription termination at co-transcriptional cleavage sites. *Nature*, *432*(7016), 522–525. https://doi.org/10.1038/nature03035

West, S., & Proudfoot, N. J. (2008). Human Pcf11 enhances degradation of RNA polymerase II-associated nascent RNA and transcriptional termination. *Nucleic Acids Research*, *36*(3), 905–914. https://doi.org/10.1093/nar/gkm1112

Wittmann, S., Renner, M., Watts, B. R., Adams, O., Huseyin, M., Baejen, C., El Omari, K., Kilchert, C., Heo, D. H., Kecman, T., Cramer, P., Grimes, J. M., & Vasiljeva, L. (2017). The conserved protein Seb1 drives transcription termination by binding RNA polymerase II and nascent RNA. *Nature Communications*, *8*. https://doi.org/10.1038/ncomms14861

Wolfgang Wende, Peter Friedhoff, and K. S. (2019). Mechanism and Regulation of Co-transcriptional mRNP Assembly and Nuclear mRNA Export. In *The Biology Function Structure and of mRNA:* (Vol. 1203, pp. 1–31). https://doi.org/10.1007/978-3-030-31434-7_4

Wong, C.-M., Qiu, H., Hu, C., Dong, J., & Hinnebusch, A. G. (2007). Yeast Cap Binding Complex Impedes Recruitment of Cleavage Factor IA to Weak Termination Sites. *Molecular and Cellular Biology*, *27*(18), 6520–6531. https://doi.org/10.1128/mcb.00733-07

Wood, V., Gwilliam, R., Rajandream, M.-A., Lyne, M., Lyne, R., Stewart, A., Sgouros, J., Peat, N., Hayles, J., Baker, S., Basham, D., Bowman, S., Brooks, K., Brown, D., Brown, S., Chillingworth, T., Churcher, C., Collins, M., Connor, R., … Nurse, P. (2003). Erratum: corrigendum: The genome sequence of *Schizosaccharomyces pombe*. *Nature*, *421*(6918), 94–94. https://doi.org/10.1038/nature01203

Wu, Guanhui, Xing, Z., Tran, E. J., & Yang, D. (2019). DDX5 helicase resolves G-quadruplex and is involved in MYC gene transcriptional activation. *Proceedings of the National Academy of Sciences of the United States of America*, *116*(41), 20453–20461. https://doi.org/10.1073/pnas.1909047116

Wu, Guifen, Schmid, M., Rib, L., Polak, P., Meola, N., Sandelin, A., & Jensen, T. H. (2020). A Two-Layered Targeting Mechanism Underlies Nuclear RNA Sorting by

the Human Exosome. *Cell Reports*, *30*(7), 2387-2401.e5. https://doi.org/10.1016/j.celrep.2020.01.068

Wyers, F., Rougemaille, M., Badis, G., Rousselle, J. C., Dufour, M. E., Boulay, J., Régnault, B., Devaux, F., Namane, A., Séraphin, B., Libri, D., & Jacquier, A. (2005). Cryptic Pol II transcripts are degraded by a nuclear quality control pathway involving a new poly(A) polymerase. *Cell*, *121*(5), 725–737. https://doi.org/10.1016/j.cell.2005.04.030

Xie, Y., & Ren, Y. (2019). Mechanisms of nuclear mRNA export: A structural perspective. *Traffic*, *20*(11), 829–840. https://doi.org/10.1111/tra.12691

Xing, Z. (2018). *WIREs RNA - 2018 - Xing - The DDX5 Dbp2 subfamily of DEAD-box RNA helicases TRAN.pdf*. Wiley Periodicals, Inc. https://doi.org/doi.org/10.1002/wrna.1519

Xing, Z., Ma, W. K., & Tran, E. J. (2019). The DDX5/Dbp2 subfamily of DEAD-box RNA helicases. *Wiley Interdisciplinary Reviews: RNA*, *10*(2), 1–17. https://doi.org/10.1002/wrna.1519

Xing, Z., Wang, S., & Tran, E. J. (2017). Characterization of the mammalian DEAD-box protein DDX5 reveals functional conservation with *S. cerevisiae* ortholog Dbp2 in transcriptional control and glucose metabolism. *Rna*, *23*(7), 1125–1138. https://doi.org/10.1261/rna.060335.116

Xu, K., Sun, S., Yan, M., Cui, J., Yang, Y., Li, W., Huang, X., Dou, L., Chen, B., Tang, W., Lan, M., Li, J., & Shen, T. (2022). DDX5 and DDX17—multifaceted proteins in the regulation of tumorigenesis and tumor progression. *Frontiers in Oncology*, *12*(August), 1–20. https://doi.org/10.3389/fonc.2022.943032

Yamaguchi, Y., Shibata, H., & Handa, H. (2013). Transcription elongation factors DSIF and NELF: Promoter-proximal pausing and beyond. *Biochimica et Biophysica Acta - Gene Regulatory Mechanisms*, *1829*(1), 98–104. https://doi.org/10.1016/j.bbagrm.2012.11.007

Yamaguchi, Y., Takagi, T., Wada, T., Yano, K., Furuya, A., Sugimoto, S., Hasegawa, J., & Handa, H. (1999). NELF, a multisubunit complex containing RD, cooperates with DSIF to repress RNA polymerase II elongation. *Cell*, *97*(1), 41–51. https://doi.org/10.1016/S0092-8674(00)80713-8

Yamamoto, J., Hagiwara, Y., Chiba, K., Isobe, T., Narita, T., Handa, H., & Yamaguchi, Y. (2014). DSIF and NELF interact with Integrator to specify the correct post-transcriptional fate of snRNA genes. *Nature Communications*, *5*, 1–10. https://doi.org/10.1038/ncomms5263

Yamanaka, S., Yamashita, A., Harigaya, Y., Iwata, R., & Yamamoto, M. (2010). Importance of polyadenylation in the selective elimination of meiotic mRNAs in growing *S. pombe* cells. *EMBO Journal*, *29*(13), 2173–2181. https://doi.org/10.1038/emboj.2010.108

Yamashita, A., Shichino, Y., Tanaka, H., Hiriart, E., Touat-Todeschini, L., Vavasseur, A., Ding, D. Q., Hiraoka, Y., Verdel, A., & Yamamoto, M. (2012). Hexanucleotide motifs mediate recruitment of the RNA elimination machinery to silent meiotic genes. *Open Biology*, *2*(MARCH). https://doi.org/10.1098/rsob.120014

Yamashita, A., Takayama, T., Iwata, R., & Yamamoto, M. (2013). A novel factor Iss10

regulates Mmi1-mediated selective elimination of meiotic transcripts. *Nucleic Acids Research*, *41*(21), 9680–9687. https://doi.org/10.1093/nar/gkt763

Yan, K. K. P., Obi, I., & Sabouri, N. (2021). The RGG domain in the C-terminus of the DEAD box helicases Dbp2 and Ded1 is necessary for G-quadruplex destabilization. *Nucleic Acids Research*, *49*(14), 8339–8354. https://doi.org/10.1093/nar/gkab620

Yanagida, M. (2002). The model unicellular eukaryote, *Schizosaccharomyces pombe*. *Genome Biology*, *3*(3), 1–4.

Yonaha, M., & Proudfoot, N. J. (2000). Transcriptional termination and coupled polyadenylation in vitro. *EMBO Journal*, *19*(14), 3770–3777. https://doi.org/10.1093/emboj/19.14.3770

Yoshida, J. I., & Tani, T. (2005). Hsp16p is required for thermotolerance in nuclear mRNA export in fission yeast *Schizosaccharomyces pombe*. *Cell Structure and Function*, *29*(5–6), 125–138. https://doi.org/10.1247/csf.29.125

Zenklusen, D., Larson, D. R., & Singer, R. H. (2008). Single-RNA counting reveals alternative modes of gene expression in yeast. *Nature Structural and Molecular Biology*, *15*(12), 1263–1271. https://doi.org/10.1038/nsmb.1514

Zenklusen, D., Vinciguerra, P., Wyss, J.-C., & Stutz, F. (2002). Stable mRNP Formation and Export Require Cotranscriptional Recruitment of the mRNA Export Factors Yra1p and Sub2p by Hpr1p. *Molecular and Cellular Biology*, *22*(23), 8241–8253. https://doi.org/10.1128/mcb.22.23.8241-8253.2002

Zhang, M., & Green, M. R. (2001). Identification and characterization of yUAP/Sub2p, a yeast homolog of the essential human pre-mRNA splicing factor hUAP56. *Genes and Development*, *15*(1), 30–35. https://doi.org/10.1101/gad.851701

Zhang, Y., Liu, L., Qiu, Q., Zhou, Q., Ding, J., Lu, Y., & Liu, P. (2021). Alternative polyadenylation: methods, mechanism, function, and role in cancer. *Journal of Experimental and Clinical Cancer Research*, *40*(1), 1–19. https://doi.org/10.1186/s13046-021-01852-7

Zhang, Z., Fu, J., & Gilmour, D. S. (2005). *CTD-dependent dismantling processing factor, Pcf11 complex by the pre-mRNA 3'-end of the RNA polymerase II elongation* (pp. 1572–1580).

Zhang, Z., & Gilmour, D. S. (2006). Pcf11 is a termination factor in Drosophila that dismantles the elongation complex by bridging the CTD of RNA polymerase II to the nascent transcript. *Molecular Cell*, *21*(1), 65–74. https://doi.org/10.1016/j.molcel.2005.11.002

Zhao, J., Hyman, L., & Moore, C. (1999). Formation of mRNA 3′ Ends in Eukaryotes: Mechanism, Regulation, and Interrelationships with Other Steps in mRNA Synthesis. *Microbiology and Molecular Biology Reviews*, *63*(2), 405–445. https://doi.org/10.1128/mmbr.63.2.405-445.1999

Zhou, Y., Zhu, J., Schermann, G., Ohle, C., Bendrin, K., Sugioka-Sugiyama, R., Sugiyama, T., & Fischer, T. (2015). The fission yeast MTREC complex targets CUTs and unspliced pre-mRNAs to the nuclear exosome. *Nature Communications*, *6*(May), 1–11. https://doi.org/10.1038/ncomms8050

Zonta, E., Bittencourt, D., Samaan, S., Germann, S., Dutertre, M., & Auboeuf, D. (2013). The RNA helicase DDX5/p68 is a key factor promoting c-fos expression at different levels from transcription to mRNA export. *Nucleic Acids Research*, *41*(1), 554–564. https://doi.org/10.1093/nar/gks1046